Cytokine receptor-like factor 3 (CRLF3): A novel regulator of platelet biogenesis and potential drug target for thrombocythaemia

Cavan Bennett

University of Cambridge

Darwin College

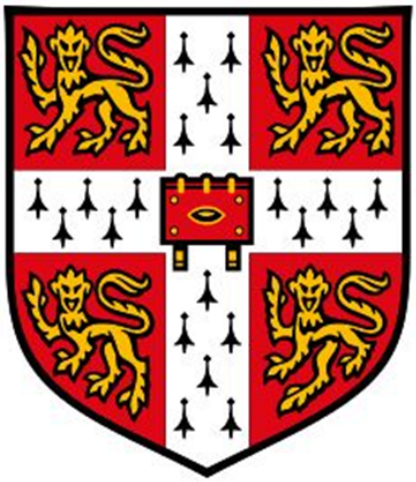

This dissertation is submitted for the degree of Doctor of Philosophy

October 2017

Cavan Bennett

Cytokine receptor-like factor 3 (CRLF3): A novel regulator of platelet biogenesis and potential drug target for thrombocythaemia

Abstract

Thrombocythaemia is defined as a circulating platelet count above $450x10^9$/L in humans. The major cause of thrombocythaemia is reactive (secondary) thrombocythaemia which occurs secondary to many conditions such as infection, cancer and inflammation. However, acquired clonal mutations in mainly Janus Kinas 2 (*JAK2*), *CALR* and *MPL* cause essential thrombocythaemia (ET). ET is a rare disease that leads to an increased risk of cardiovascular thrombotic events. Current treatment of ET uses combination of low dose aspirin (to decrease platelet function) and cytoreductive agents (to decrease thrombopoiesis). The most commonly used cytoreductive agents are hydroxyurea, anagrelide and interferon-α and all have unwanted side effects.

Cytokine receptor-like factor 3 (*CRLF3*) is a 2.4kb gene that is ubiquitously expressed throughout the haematopoietic system. Very little is known about the function of CRLF3, with only one peer reviewed journal article in the literature which shows that CRLF3 may negatively regulate the cell cycle at the G0/G1 phase. However, nothing is known about the role of CRLF3 in platelet biology. Using a *Crlf3* knockout mouse (*Crlf3*$^{-/-}$) developed by the Wellcome Trust Sanger Institute we show CRLF3's role in platelet biogenesis and how it could be used as a novel therapeutic target to treat ET.

Crlf3$^{-/-}$ mice have an isolated and sustained 25-40% decrease in platelet count compared to wildtype (WT) controls. Platelet function is unaffected as demonstrated in a range in a range of *in vitro* assays. The thrombocytopenia is a consequence of abnormalities in hematopoietic cells, as shown by bone marrow transplantations. Megakaryopoiesis is upregulated in *Crlf3*$^{-/-}$ mice and proplatelet morphology is unaffected, suggesting the thrombocytopenia is due to increased platelet clearance. Indeed, splenectomised *Crlf3*$^{-/-}$ mice show normalised platelet counts within 7 days, showing rapid splenic removal of platelets is responsible for the thrombocytopenia. Abnormal large platelet structures that resemble proplatelets shafts

(preplatelets) are abnormally present in the circulation of elderly *Crlf3*$^{-/-}$ mice. Immunohistochemistry showed increased and aberrant tubulin expression in *Crlf3*$^{-/-}$ platelets compared to WT controls, especially in the preplatelet forms. Cold induced depolymerisation of microtubules was decreased in *Crlf3*$^{-/-}$ platelets, suggestive of increased tubulin stability, however, the ratio of detyrosinated to tyrosinated tubulin was not altered.

We then crossbred *Crlf3*$^{-/-}$ mice with JAK2 V617F ET mice, to determine the effect of *Crlf3* ablation of thrombocythaemia. Crossbred mice showed restoration of platelet counts to WT values without grossly affecting platelet function or other blood lineages, providing the rational for CRLF3 as a novel therapeutic target for treatment of ET.

Finally, we aimed to resolve the crustal structure of CRLF3 and discover its interactome. To this end, we were able to resolve the crystal structure of a C-terminal portion of the full length protein containing the predicted fibronectin type III domain. To shed light on the interactome of CRLF3, endogenous *CRLF3* was tagged with a tandem affinity purification (TAP) tag using CRISPR/Cas9 technology in induced pluripotent stem cells (iPSCs). We have been able to produce megakaryocytes from these TAP-tagged iPSCs by forward programming. However, as yet we have not been able to generate enough MKs to have adequate material to perform immunoprecipitation assays. Therefore, the interactome of CRLF3 in MKs remains unknown.

In conclusion, we identified a mechanism by which *Crlf3* controls platelet biogenesis. Slowed maturation of *Crlf3*$^{-/-}$ preplatelets in the peripheral circulation potentially due to increased structural stability leads to rapid removal of these immature forms by the spleen and therefore a decrease in platelet count. The isolated effect on platelet numbers and normalisation of platelet count in ET mice deficient of *Crlf3* provides the rational for further study on CRLF3 drug targeting as a novel therapeutic strategy for ET.

This dissertation is the result of my own work and includes nothing which is the outcome of work done in collaboration except as declared in the Preface and specified in the text. It is not substantially the same as any that I have submitted, or, is being concurrently submitted for a degree or diploma or other qualification at the University of Cambridge or any other University or similar institution except as declared in the Preface and specified in the text. I further state that no substantial part of my dissertation has already been submitted, or, is being concurrently submitted for any such degree, diploma or other qualification at the University of Cambridge or any other University or similar institution except as declared in the Preface and specified in the text. It does not exceed the prescribed word limit for the relevant Degree Committee.

Acknowledgements

First and foremost, I would like to thank my PhD supervisor Dr Cedric Ghevaert. I am eternally thankful to Cedric for taking a chance on me and employing me as a Research Assistant soon after finishing my undergraduate degree in 2010. The knowledge and experience I have gained over the last 7 years in his lab has been invaluable. Without his knowledge and unwavering belief in my abilities I would not be where I am today.

I would like to thank all the past and present members of the Ghevaert lab; Maria, Tom, Amanda D, Amanda E, José, Annett, Holly, Dan, Amie, Harriet, Wardiya, Meera, Wing, Nilly, Catherine, Guénaëlle and Laura. Each and every one has helped me in their own way, passing on knowledge and experience and most importantly making life in the lab enjoyable. A special thank you to Holly for reading and re-reading draft versions of this thesis and for that undesirable task I am extremely grateful.

I would also like to thank all the collaborators near and far that have contributed to the research in this PhD. José Guerrero for his expertise in platelet biology and performing plasma TPO assays. The Wellcome Trust Sanger Institute for creating the *Crlf3* mutant mice and staff at CBS for looking after mice. Bernhard Neiswandt and the members of his group for their hospitality during my visit to Würzburg, especially Simon Stritt who performed various experiments for me and Ayesha Baig who perform *in vivo* proplatelet experiments. Tina Hamilton and Dean Pask for having the patience and time to teach me all manner of things mouse related and for irradiating mice and performing tail vein injections. My secondary supervisor Randy Read and his lab members Yahui Yan and Richard Mifsud for helping me with crystallisation experiments and for resolving the tertiary structure of CRLF3. Staff at the NIHR Cambridge BRC Cell Phenotyping Hub for cell sorting. Renet Feret, Marco Chiapello and Mike Deery for all things mass spectrometry related. Karen Hoffmeister and Silvia Giannini for western blots of platelet galactose.

I would like to thank all my friends who are there for me when times are hard and help keep me sane. To the 8BL, thanks for being you, not changing during the last 10 years and most importantly, the best nights out none of us can remember. No matter what happens in life, I know you lads are there for me. To Ryan, Alan and Bust, thanks for making the first 2 years of

my PhD incredible down Mill Road. Also, massive thanks for picking me up at my lowest. To the homeboys, thanks for everything you have done for me in life. Without all of you life would be a lot harder.

I would like to say a special thanks to Kirsty, without whom this PhD would have been much more of a struggle. Thank you for everything you do for me, listening to my problems, being my biggest supporter, standing by my side when times are hard and most importantly trying to understand my work. I appreciate everything you have done and all the sacrifices you have made to allow me to continue with an academic career.

I would like to say a massive thank you to my family. Thank you to Mum and Dad for all your help financially and emotionally, both of which have allowed me to pursue my many academic endeavors. Thank you for accepting I have 'no common sense' and pretending to understand what I do at work. Thank you to Nathan and Megan for keeping me grounded, having lengthy 'debates' with me about anything and failing to accept academia is a real career.

Finally, I would like to dedicate this thesis to my grandparents. Nan and Grandad, you are both an inspiration to me. Your hard work and unrelenting love is admirable. Grandad, your words 'more power to your elbow', gave me strength to complete this thesis when times were hard!

Table of contents

Table of Figures

Table of Tables

Abbreviations

3D	three dimension
ACD	acid citrate dextrose solution
ACTN1	actinin 1 (α-actinin)
ADF	actin depolymerising factor
Akt	protein kinase B
AML1	acute myeloid leukemia 1
AMR	Ashwell-Morell receptor
AP2	adaptor protein 2
ASGPR	asialoglycoprotein receptor
AWERB	Animal Welfare and Ethical Review Body
Bad	Bcl-2-associated death promoter
BAK	Bcl-2-antagonist/killer
BAX	Bcl-2-associated X
BCA	bicinchoninic acid
BCL-2	B-cell lymphoma 2
Bcl-xL	B-cell lymphoma-extra large
BFU-MK	burst forming unit - megakaryocyte
BMP4	Bone morphogenetic protein 4
bp	base pair
BPD	Bleeding, thrombotic and Platelet Disorders project
BSA	bovine serum albumin
BSS	Bernard-Soulier syndrome
CALR	calreticulin
Cas9	CRISPR associated protein 9
CBB	calmodulin binding buffer
CBFβ	core-binding factor subunit beta
CBL	Casitas B-lineage Lymphoma
CBP	calmodulin binding peptide
CDC42	Cell division control protein 42
cDNA	complementary DNA

CFU-MK	colony forming unit - megakaryocyte
CIP4	CDC42 interacting protein 4
c-Kit	CD117
CLP	common lymphoid progenitor
CMP	common myeloid progenitor
COX-1	cyclooxygenase 1
CR3	compliment receptor 3
CRISPR	Clustered Regularly Interspaced Short Palindromic Repeat
CRLF3	cytokine receptor-like factor 3
CRP	collagen related peptide
DAD	diaphanous autoregulatory domain
DAG	diglyceride
DAPI	4',6-diamidino-2-phenylindole
DIAPH1	diaphanous-related formin 1
DID	diaphanous inhibitory domain
DIW	deionised water
DMEM	Dulbecco's modified Eagle medium
DMS	demarcation membrane system
DMSO	dimethyl sulfoxide
DNA	deoxyribose nucleic acid
DOCK	dedicator of cytokin
DTT	dithiothreitol
DVT	Deep vein thrombosis
E	embryonic day
E8	Essential 8 medium
EB	erythroblast
ECT2	epithelial cell transforming 2
EDTA	ethylenediaminetetraacetic acid
EGTA	ethylene glycol-bis(2-aminoethylether)-N,N,N',N'-tetraacetic acid
ELISA	enzyme-linked immunosorbent assay
EPO	erythropoietin
Erg-1	Early growth factor-1

ERK	extracellular signal-regulated kinase
ES	embryonic stem
ET	essential thrombocythaemia
ETS	E26 transformation-specific
ExAC	Exome Aggregation Consortium
FACS	fluorescent-activated cell sorting
F-actin	filamentous actin
FBS	foetal bovine serum
Fc	fragment, crystallisable
FGF2	fibroblast growth factor 2
FLAG	DYKDDDDK (where D=aspartic acid, Y=tyrosine, and K=lysine)
FLI1	friend leukemia integration 1
FLNA	filamin A
FN3	fibronectin type III
FOG1	friend of GATA1
G1	Gap 1
G2	Gap 2
GABPα	GA-binding protein alpha chain
G-actin	globular actin
GAPDH	glyceraldehyde 3-phosphate dehydrogenase
gDNA	genomic DNA
GDP	guanine diphosphate
GEF	guanine exchange factor
GEF-H1	Rho guanine nucleotide exchange factor 2
GFP	green fluorescent protein
GlcNAc	N-acetylglucosamine
Glu-tubulin	detyrosinated tubulin
GM-CSF	granulocyte-macrophage colony-stimulating factor
GMP	granulocyte-macrophage progenitor
GP	glycoprotein
GPCR	G-protein coupled receptor
GPRP	Gly-Pro-Arg-Pro
GPS	gray platelet syndrome

Grb2	growth factor receptor-bound protein 2
GSK-3β	glycogen synthase kinase 3 beta
GST	Glutathione-*S*-transferase
GTP	guanine triphosphate
H&E	Haemotoxylin and Eosin
HBS	HEPES buffered saline
HEPES	4-(2-hydroxyethyl)-1-piperazineethanesulfonic acid
Hg	mercury
Hgb	haemoglobin
HIF-1	hypoxia inducing factor-1
HipSci	human induced pluripotent stem cell initiative
HMGB-1	high motility group box-1
HPLC	high-performance liquid chromatography
HSC	haematopoietic stem cell
ID	identification number
IFN	interferon
IgG	Immunoglobulin G
IL	interlukin
IP_3	inositol 1,4,5-triphosphate
iPSC	induced pluipotent stem cell
IPTG	isopropul-1-thio-β-D-galactopyranoside
ITP	idiopathic or immune thrombocytopenic purpura
IVC	inferior vena cava
JAK2	Janus kinase 2
JAM	junctional adhesion molecule
JH1	JAK2 tyrosine kinase domain
JH2	JAK2 pseudokinase domain
KO	knockout
LIF	leukaemia inhibitory factor
LNK	lymphocyte adapter protein
loxP	locus of X-over P1
LRCH	leucine-rich repeat and calponin homology domain-containing

LT	long term
LYN	Lck/Yes novel tyrosine kinase
Mac-1	macrophage receptor 1
MAPK	mitogen-activated protein kinase
MCL-1	myeloid cell leukemia 1
MCV	Mean corpuscular volume
mDia1	diaphanous-related formin 1
MEK	mitogen-induced extracellular kinase
MEP	megakaryocyte/erythrocyte progenitor
MFI	Mean fluorescence intensity
MK	megakaryocyte
MKB	megakaryoblast
MOI	multiplicity of infection
MPF	mitosis promoting factor
MPL	myeloproliferative leukemia protein
MPN	myeloproliferative neoplasms
MPO	myeloperoxidase
MPV	mean platelet volume
mRNA	messenger ribonucleic acid
MVB	multivesicular body
MYH9	myosin, heavy chain 9
NBEAL2	neurobeachin-like 2
NE	neutrophil elastase
neo	neomycin
NET	neutrophil extracellular trap
NF-κB	nuclear factor- κB
NF1	neurofibromatosis type 1
NHS-Biotin	biotin N-hydroxysuccinimide ester
NK	natural killer
NMMHC-IIA	nonmuscle myosin heavy chain IIA
NO	nitric oxide
NOX	NAPDH oxidase
N-WASp	neuronal Wiskott-Aldrich Syndrome protein

OCS	open canalicular system
PAD4	peptidylarginine deiminase 4
PAI-1	plasminogen activator inhibitor-1
PAK2	p21-activated kinase 2
PAR	protease-activated receptor
PBE	PBS/BSA/EDTA
PBS	phosphate buffered saline
PCR	polymerase chain reaction
PEG	polyethylene glycol
pen/strep	penicillin/streptomycin
PFA	paraformaldehyde
Pfn	profilin 1
PGE_1	Prostaglandin E_1
PGI_2	prostaglandin I_2
PHD	propyl hydroxylase
PHOX	phagocytic oxidase
PI3K	phosphoinositol-3 kinase
PIP4Kα	PI-5-P-4 kinase α
pIpC	polyinosinic-polycytidylic acid
PIPES	piperazine-N,N-bis-2- ethanesulfonic acid
PLC	phospholipase C
PMF	primary myelofibrosis
PRP	Platelet rich plasma
PS	phosphatidylserine
PSGL-1	P-selectin ligand 1
PV	polycythaemia vera
PVDF	polyvinylidene fluoride
qPCR	quantitative polymerase chain reaction
RAGE	receptor for advanced glycation endproducts
Raf-1	RAF proto-oncogene serine/threonine-protein kinase
RBC	red blood cell
RhoA	Ras homolog gene family, member A

RNA	ribonucleic acid
ROS	reactive oxygen species
RT	room temperature
RUNX1	Runt-related transcription factor 1
S phase	synthesis phase
S1P	Shingosine-1-phosphate
S1pr1	Sphingosine-1-phosphate receptor 1
SAD	single anomalous diffraction
SCF	stem cell factor
SEM	scanning electron microscopy
sgRNA	single-guide RNA
shRNA	short hairpin ribonucleic acid
SLAM	signalling lymphocyte activation molecule
SOCS	supressor of cytokine signalling
SOS	Son of Sevenless
Src	Proto-oncogene tyrosine-protein kinase Src
ST	short term
St3gal4	st3 beta-galactoside alpha-2,3-sialyltransferase 4
STAT	signal transducer and activator of transcription
TAP	tandem affinity purification
TEM	transmission electron microscopy
TEV	Tobacco etch virus
TF	Tissue factor
TGF-β	transforming growth factor beta
TPM	Tropomyosin
TPO	thrombopoietin
TUBB1	β_1-tubulin
TxA2	Thromboxane A_2
Tyk2	TYK2 tyrosine kinase 2
Tyr	tyrosine
Tyr-tubulin	tyrosinated tubulin
VTN-N	truncated vitronectin
vWF	von Willebrand factor

WAS	Wiskott-Aldrich syndrome
WASp	Wiskott-Aldrich syndrome protein
WAVE	Wiskott-Aldrich syndrom protein family verprolin homolog
WBC	white blood cell
WIP	WASp-interacting protein
WT	wildtype
WTSI	Wellcome Trust Sanger Institute

Abstract

Thrombocythaemia is defined as a circulating platelet count above $450x10^9$/L in humans. The major cause of thrombocythaemia is reactive (secondary) thrombocythaemia which occurs secondary to many conditions such as infection, cancer and inflammation. However, acquired clonal mutations in mainly Janus Kinas 2 (*JAK2*), *CALR* and *MPL* cause essential thrombocythaemia (ET). ET is a rare disease that leads to an increased risk of cardiovascular thrombotic events. Current treatment of ET uses combination of low dose aspirin (to decrease platelet function) and cytoreductive agents (to decrease thrombopoiesis). The most commonly used cytoreductive agents are hydroxyurea, anagrelide and interferon-α and all have unwanted side effects.

Cytokine receptor-like factor 3 (*CRLF3*) is a 2.4kb gene that is ubiquitously expressed throughout the haematopoietic system. Very little is known about the function of CRLF3, with only one peer reviewed journal article in the literature which shows that CRLF3 may negatively regulate the cell cycle at the G0/G1 phase. However, nothing is known about the role of CRLF3 in platelet biology. Using a *Crlf3* knockout mouse (*Crlf3*$^{-/-}$) developed by the Wellcome Trust Sanger Institute we show CRLF3's role in platelet biogenesis and how it could be used as a novel therapeutic target to treat ET.

Crlf3$^{-/-}$ mice have an isolated and sustained 25-40% decrease in platelet count compared to wildtype (WT) controls. Platelet function is unaffected as demonstrated in a range in a range of *in vitro* assays. The thrombocytopenia is a consequence of abnormalities in hematopoietic cells, as shown by bone marrow transplantations. Megakaryopoiesis is upregulated in *Crlf3*$^{-/-}$ mice and proplatelet morphology is unaffected, suggesting the thrombocytopenia is due to increased platelet clearance. Indeed, splenectomised *Crlf3*$^{-/-}$ mice show normalised platelet counts within 7 days, showing rapid splenic removal of platelets is responsible for the thrombocytopenia. Abnormal large platelet structures that resemble proplatelets shafts (preplatelets) are abnormally present in the circulation of elderly *Crlf3*$^{-/-}$ mice. Immunohistochemistry showed increased and aberrant tubulin expression in *Crlf3*$^{-/-}$ platelets compared to WT controls, especially in the preplatelet forms. Cold induced depolymerisation of microtubules was decreased in *Crlf3*$^{-/-}$ platelets, suggestive of increased tubulin stability, however, the ratio of detyrosinated to tyrosinated tubulin was not altered.

We then crossbred *Crlf3*$^{-/-}$ mice with JAK2 V617F ET mice, to determine the effect of *Crlf3* ablation of thrombocythaemia. Crossbred mice showed restoration of platelet counts to WT values without grossly affecting platelet function or other blood lineages, providing the rational for CRLF3 as a novel therapeutic target for treatment of ET.

Finally, we aimed to resolve the crystal structure of CRLF3 and discover its interactome. To this end, we were able to resolve the crystal structure of a C-terminal portion of the full length protein containing the predicted fibronectin type III domain. To shed light on the interactome of CRLF3, endogenous *CRLF3* was tagged with a tandem affinity purification (TAP) tag using CRISPR/Cas9 technology in induced pluripotent stem cells (iPSCs). We have been able to produce megakaryocytes from these TAP-tagged iPSCs by forward programming. However, as yet we have not been able to generate enough MKs to have adequate material to perform immunoprecipitation assays. Therefore, the interactome of CRLF3 in MKs remains unknown.

In conclusion, we identified a mechanism by which *Crlf3* controls platelet biogenesis. Slowed maturation of *Crlf3*$^{-/-}$ preplatelets in the peripheral circulation potentially due to increased structural stability leads to rapid removal of these immature forms by the spleen and therefore a decrease in platelet count. The isolated effect on platelet numbers and normalisation of platelet count in ET mice deficient of *Crlf3* provides the rational for further study on CRLF3 drug targeting as a novel therapeutic strategy for ET.

1

Introduction

1.1 Overview of haematopoiesis

Haematopoiesis is essential for the generation of all the mature cells of haematopoietic system. Defects in haematopoiesis can result in life threatening illnesses including blood cancer and bleeding disorders.

All the cells in the blood lineage are produced by cellular differentiation of the most naïve cell in the haematopoietic system, the haematopoietic stem cell (HSC) (fig. 1.1). HSCs can be separated into two distinct populations: long term (LT) and short term (ST). Although both LT- and ST-HSCs are able to produce all other haematopoietic cells, only LT-HSCs are able to maintain long term regeneration of the tissue through their ability to self-renew (Orkin and Zon, 2008). HSCs are characterised by their lack of mature lineage markers, namely: CD2, CD3, CD14, CD16, CD19, CD24, CD56, CD66b, GlyA (termed '*Lin*-') (Bryder et al., 2006; Laurenti and Dick, 2012).

Differentiation of HSCs results in a number of multipotent progenitors that can in turn differentiate to produce all the mature cells of the haematopoietic system. Differentiation of HSCs results in the common lymphoid progenitor (CLP) and the common myeloid progenitor (CMP). CLPs can further differentiate into mature natural killer (NK) cells, B lymphocytes and T lymphocytes. CMPs however differentiate into two progenitor cells, the granulocyte-macrophage progenitor (GMP) and the megakaryocyte/erythrocyte progenitor (MEP); however there is evidence that the MEP can arise directly from HSCs without the need for a CMP intermediate (Adolfsson et al., 2005). GMPs give rise to mature neutrophils, eosinophils, mast cells and monocytes/macrophages. MEP differentiation results in two committed progenitor cells, namely erythroblasts (EBs) and megakaryoblasts (MKBs). EBs mature into erythrocytes and MKBs mature into megakaryocytes (MKs) which eventually give rise to platelets (Bryder et al., 2006; Chang et al., 2007).

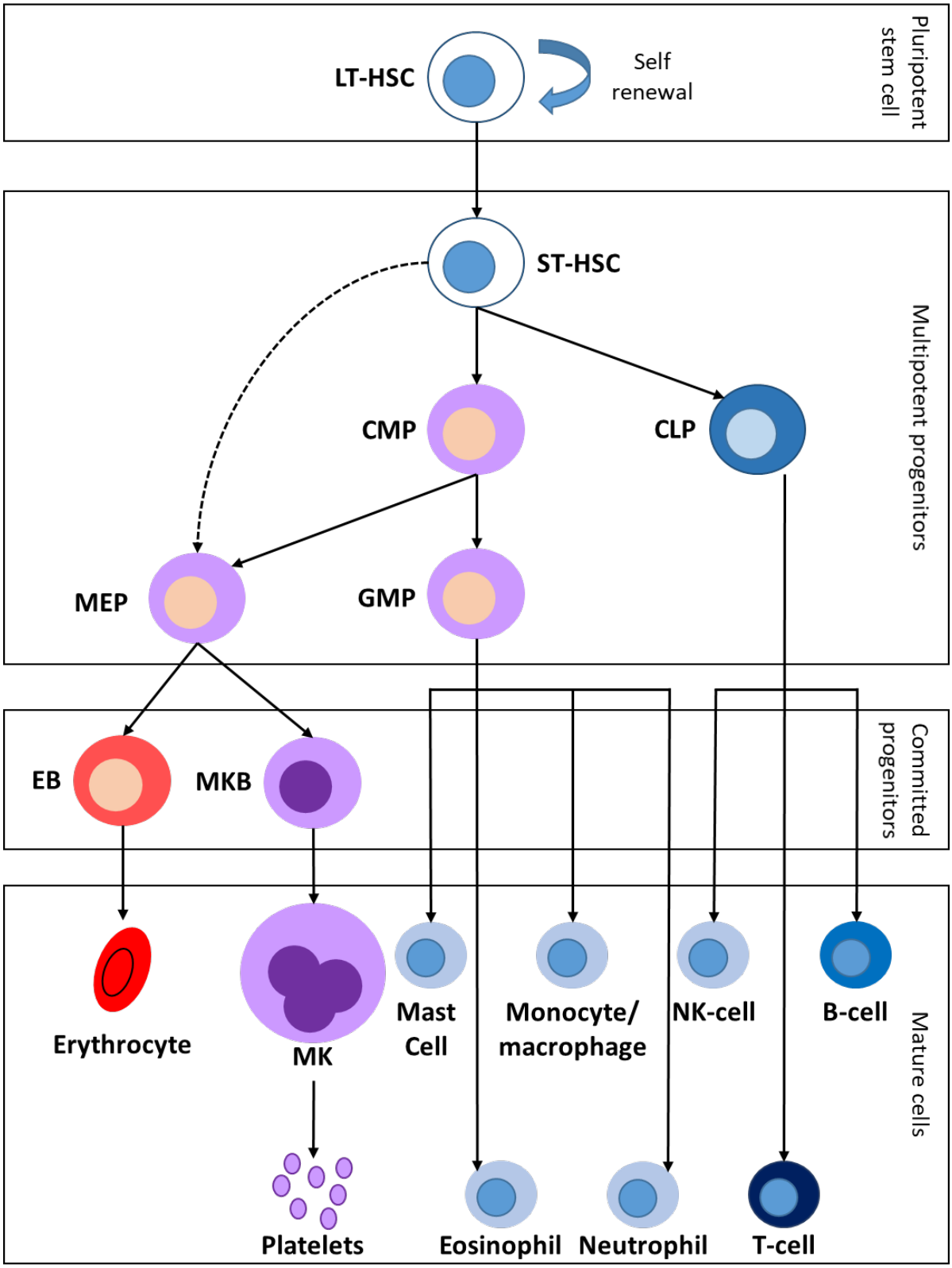

Figure 1.1 – Schematic representation of the haematopoietic tree. LT-HSC = long term-haematopoietic stem cell; ST-HSC = short term-haematopoietic stem cell; CMP = common myeloid progenitor; CLP = common lymphoid progenitor; GMP = granulocyte-macrophage progenitor; MEP = megakaryocyte/erythrocyte progenitor; EB = erythroblast; MKB = megakaryoblast and MK = megakaryocyte

1.2 Megakaryocyte maturation

As described above, MKs originate from a bipotent progenitor cell, the MEP. The transcriptional regulation that directs passage through the erythroid or MK lineage from the MEP is not fully understood. Cells that enter the MK lineage first differentiate into the highly proliferative burst-forming unit (BFU-MK) and then into the less proliferative colony-forming unit (CFU-MK). BFU-MKs are able to produce 40-500 megakaryocytes in specific *in vitro* conditions, whereas CFU-MKs produce colonies of 3-50 megakaryocytes in *in vitro* colony forming assays (Briddell et al., 1989; Long et al., 1985). Maturation of CFU-MKs gives promegakaryoblasts, the first MK precursor to be recognised in bone marrow. Promegakaryoblasts become megakaryoblasts (Stage I MKs). Megakaryoblasts are small (10-15µm), immature 2/4N MKs and retain the ability to proliferate. They have high nuclear: cytoplasm ratio and lack organelles characteristic of a mature MK (i.e. α- and dense-granules). Stage I MKs become Stage II MKs (promegakaryocytes) when α- and dense-granules and the demarcation membrane system (DMS) begin to form. Stage III and IV MKs represent mature MKs. Mature MKs are non-proliferative, large, polyploid cells that contain a large multilobular nucleus. Stage III and IV MKs are separated based on three cytoplasmic regions. The marginal zone contains numerous micro-vesicles and is predominant at stage III but smaller at stage IV. The middle zone contains α- and dense-granules and DMS. The middle zone contains some cytoplasm in stage III but is full of cytoplasm in stage IV. Finally, the perinuclear zone contains organelles such as mitochondria and endoplasmic reticulum and is present at stage III but missing at stage IV (Ru et al., 2016)

MK maturation is monitored by expression of MK and platelet specific surface glycoproteins such as GPIIb/IIIa (integrin $\alpha_{IIb}\beta_3$ or CD41/CD61; the fibrinogen receptor) and the GPIb-V-IX complex (GPIba, GPIbb, GPIX and GPV or CD42a, b, c and d; the von Willebrand factor (vWF) receptor). Although CD41 is not truly MK specific, expression is found throughout haematopoietic progenitors, the MK lineage and mast cells, expression increases along the MK lineage. Co-expression of CD41 with CD42 (GPIb) is currently thought to be specific of the MK lineage. Expression of CD42 and CD61 appear at the later stages of differentiation and are therefore used to identify mature MKs (fig. 1.2) (Chang et al., 2007).

Proteins contained within α-granules, such as platelet factor 4 (PF4), vWF, thrombospondin and coagulation factor V and proteins involved in proplatelet formation (β_1-tubulin) are also used as indicators of the later stages of MK development (Chang et al., 2007).

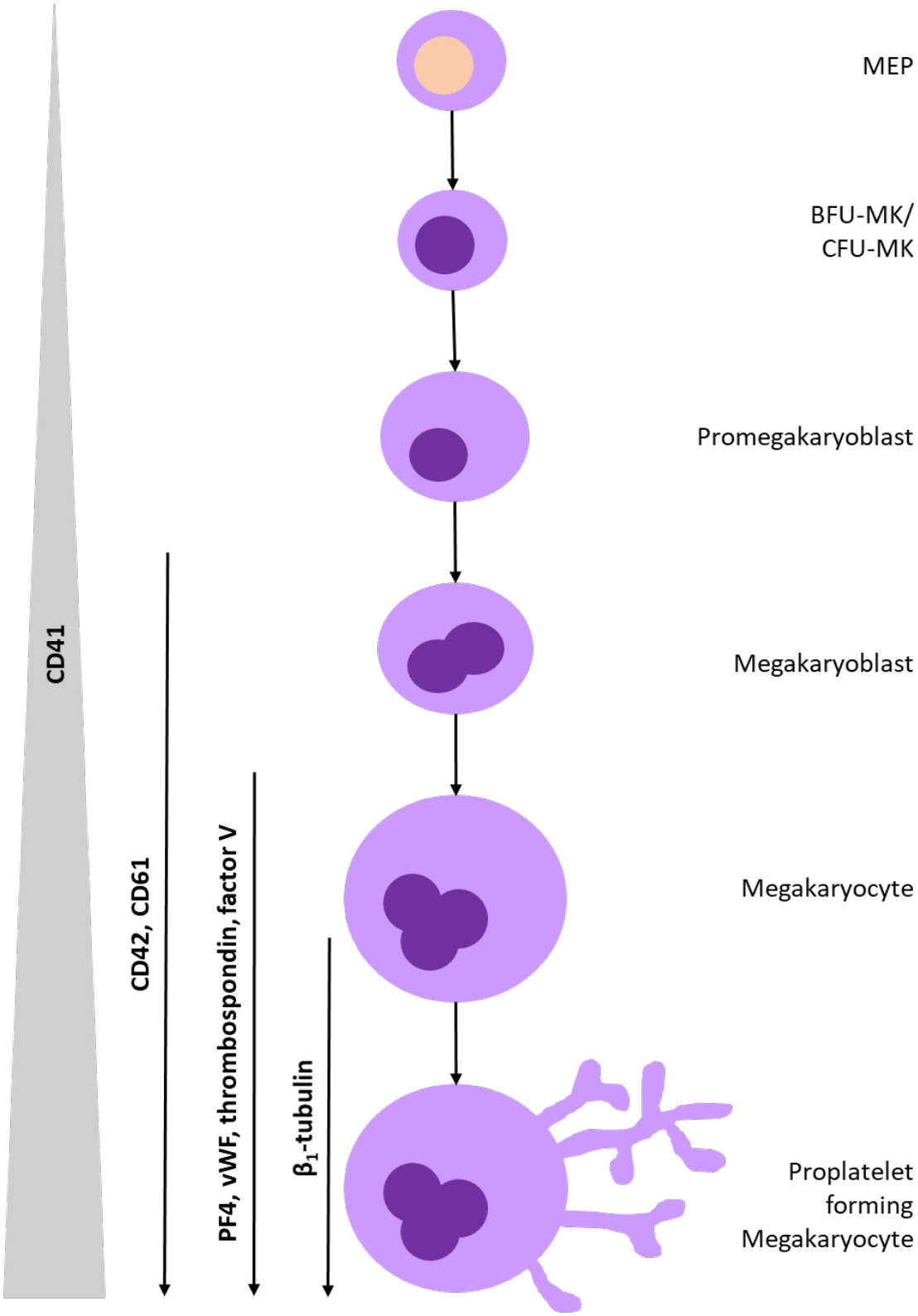

Figure 1.2 – Schematic representation of megakaryocyte maturation. MEP = megakaryocyte/erythrocyte progenitor; BFU-MK = burst-forming unit-megakaryocyte and CFU-MK = colony forming unit-megakaryocyte.

1.3 Transcriptional regulation of megakaryopoiesis

Transcription factors are proteins that bind to specific regions of DNA termed motifs. Once bound, transcription factors are able to recruit transcriptional machinery and/or inhibitory proteins to the promotor region of specific genes, thus promoting or inhibiting the expression of those genes. The cell and time specific combination of transcription factors provide a robust mechanism for the genetic regulation of a cell. Although the role and combinations of transcription factors in megakaryopoiesis is not fully understood, below is an overview of the known essential transcription factors (summarised in Table 1.1).

GATA1 and FOG1 (ZFPM1)

Murine studies have revealed that GATA1 is essential for proper megakaryopoiesis. Homozygous null mutations of *Gata1* in mice causes embryonic lethality due to anaemia (Fujiwara et al., 1996). A haematopoietic lineage conditional knockout (KO) results in MKs with decreased ploidy and excessive proliferation. Induction of cyclin–D1 in these KO mice restored ploidy levels, however terminal differentiation was still altered (Shivdasani et al., 1997). Furthermore, Moreau *et al* (2016) showed MKs could be generated from human induced pluripotent stem cells (iPSCs) by transducing with recombinant GATA1, TAL1 and FLI1 (Moreau et al., 2016).

Friend of GATA1 (FOG1; also called ZFPM1) does not bind to DNA but binds GATA1. Murine *Fog1* KOs die of severe anaemia midway through embryonic development as per *Gata1* KO mice. However, unlike *Gata1* KOs MKs fail to develop and platelet production was absent in *Fog1* KO mice, suggesting an independent role of FOG1 in MK development and thrombopoiesis (Tsang et al., 1998).

SCL (TAL1)

In 1995 Shivdasani *et al* and Robb *et al* showed the essential role of *Scl* (also known as *Tal1*) in haematopoiesis. Both groups developed KO mice that showed lethality at day E9.5. Interestingly, these KO mice had a complete absence of haematopoiesis (Robb et al., 1995; Shivdasani et al., 1995). More recently, Hall *et al* developed a haematopoietic specific

conditional *Scl* KO mouse. This conditional KO had perturbed megakaryopoiesis and erythropoiesis with a loss of early progenitors. Platelet counts and haematocrit were also reduced in these mice (Hall et al., 2003).

RUNX1 (AML1)

RUNX1 (also known as AML1) functions as a heterodimeric complex with its cofactor, CBFβ. It is essential for the emergence of HSCs during embryogenesis and therefore *Runx1* KO mice are embryonically lethal. Deletion of *Runx1* from the adult haematopoietic system using a conditional murine knockout showed decreased maturation of MKs. Conditional *Runx1* knockout mice have decreased platelet counts and an accumulation of immature MK progenitor cells within the bone marrow, similar to what was seen in the conditional *Gata1* KO mouse (Tijssen and Ghevaert, 2013).

FLI1 and GABPα

FLI1, GABPα and ETV6 are part of the E26 transformation-specific (ETS) family, which is one of the largest families of transcription factors. All ETS proteins contain a helix-loop-helix DNA binding (ETS) domain and many ETS factors have a role in megakaryopoiesis. FLI1 is essential for MK development and has been shown to negatively regulate erythropoiesis whilst positively regulating megakaryopoiesis. *Fli1* homozygous null mice die at approximately E11.5 due to cerebral bleeding and show dysmegakaryopoiesis that resembles that seen in patients with Jacobsen Syndrome (Hart et al., 2000). Jacobsen Syndrome, also known as 11q deletion disorder, results in decreased platelet counts amongst many other symptoms.

FLI1 potentially acts in tandem with GABPα in MKs. As MKs mature, the ratio of FLI1: GAPBα increases, this is consistent with the observation that GABPα regulates the expression of early MK genes where FLI1 regulates both early and late MK genes (Pang et al., 2006).

ETV6 (TEL)

ETV6 (also called TEL) can inhibit the activity of FLI1 at the transcriptional and biological levels (Kwiatkowski et al., 2000). The level of TEL expression is important for maintenance of

megakaryopoiesis. Overexpression of TEL in cell line causes inhibition of MK genes and the generation of an erythroid phenotype (Sakurai et al., 2003). In contrast, GATA1-Cre mediated conditional deletion of *Tel* in the MK-erythroid lineage had no effect on red cell population but caused a 50% decrease in platelet count (Hock et al., 2004).

TF	**Expression within haematopoietic system**	**Function/Role in haematopoiesis**
GATA1	Expressed in platelets, MKs, EBs and eosinophils. Low level of expression in basophils.	Recognise [5'-(A/T)GATA(A/G)-3'] motifs and are able to bind cofactors which increase DNA binding stability. Essential for proper megakaryopoiesis.
FOG1 (ZFPM1)	Low levels of expression in platelets, MKs, EBs and eosinophils.	Roles in MK development and thrombopoiesis. Binds GATA1 allowing the formation of a complex with the nucleosome remodelling and deacetylase (NURD). The formation of the GATA1/FOG1/NURD complex allows efficient regulation of gene transcription.
SCL (TAL1)	Expression limited to platelets, MKs, EBs and basophils. Very high in platelet, high in MKs and EBs and lower in basophils.	Essential for proper haematopoiesis. Knockout mice show perturbed megakaryopoiesis and erythropoiesis.
RUNX1 (AML1)	Low levels of expression in all haematopoietic cells, except basophils and platelets that have high expression.	Essential for the emergence of HSCs during embryogenesis. In adult system required for proper maturation of MKs. Forms a heterodimeric complex CBFβ, which causes increased DNA binding and stability.
FLI1	Platelets have high expression and all other haematopoietic cells have medium to low expression levels.	Essential for MK development, by regulating the expression of both early and late MK genes. It also negatively regulates erythropoiesis whilst positively regulates megakaryopoiesis.

GABPα	Lowly expressed in all haematopoietic cells.	Regulates the expression of early MK genes.
ETV6 (TEL)	Lowly expressed in all haematopoietic cells, except neutrophils, monocytes, basophils, eosinophils and platelets which have higher expression.	Binds to and inhibits the activity of FLI1. Level of TEL expression is important for maintenance of megakaryopoiesis, with overexpression leading to erythroid phenotype and ablation causing thrombocytopenia.

Table 1.1 – Summary of expression and function/role of the key transcription factors involved in megakaryopoiesis. TF= Transcription factor. Expression data from Chen *et al* (2014). Function/role of TFs reviewed in Tijssen *et al* (2016)

1.4 Thrombopoietin signalling in megakaryopoiesis

The main driver of megakaryopoiesis is the cytokine thrombopoietin (TPO) binding to its receptor c-Mpl. TPO was discovered in 1994 (Bartley et al., 1994; Lok et al., 1994; Sohma et al., 1994) after the discovery of its receptor c-Mpl in 1992 (Vigon et al., 1992). However, TPO was known to exist long before this. In 1958 Cserhati, Tanos and Kelemen first coined the term TPO and postulated its role in platelet production (Cserhati et al., 1958; Kelemen et al., 1958).

Once recombinant TPO was made available, it was shown to be the main regulator of megakaryopoiesis and platelet production. Kaushansky *et al* showed that addition of TPO to whole bone marrow cells was enough to produce polyploid MK containing colonies. When TPO was added to cultures containing interlukin-3 (IL-3) or c-Kit, proteins known to drive MK proliferation, very large MK colonies were observed. At later stages of maturation, TPO was shown to increase MK size and ploidy (Kaushansky et al., 1994).

TPO is produced mainly in the liver, but the bone marrow, kidney and smooth muscle cells have also been shown to express TPO mRNA (Hitchcock and Kaushansky, 2014; Kile, 2015; Sungaran et al., 1997). In 2015, Grozovsky *et al* showed that the production of TPO is in part determined by clearance of platelets by the spleen. As platelets age they lose sialic acid from

their surface exposing galatacose oligosaccharide chains. These glatacose chains are recognised by the Ashwell-Morell receptor (AMR) on the vascular surface of hepatocytes stimulating platelet removal and TPO production (fig. 1.3) (Grozovsky et al., 2015a).

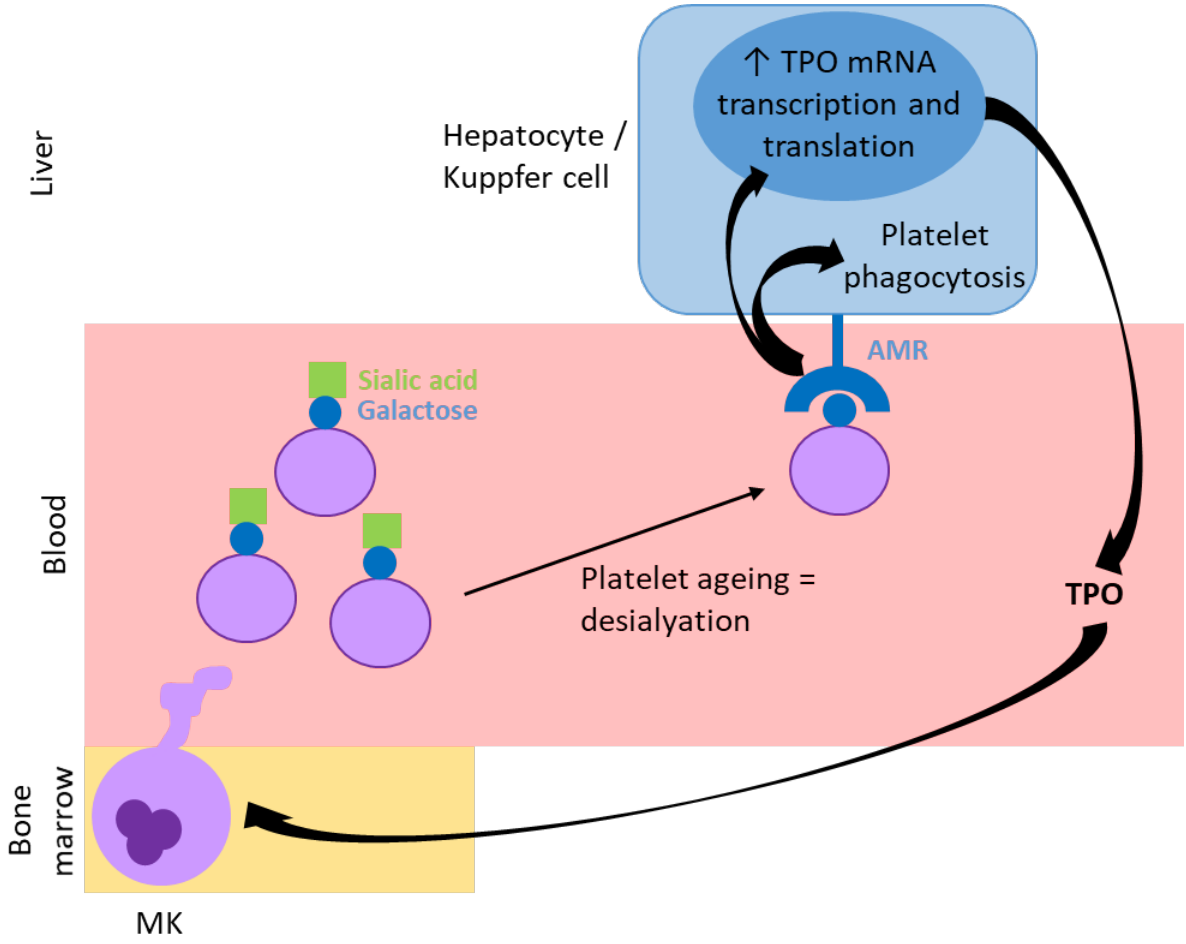

Figure 1.3 – Schematic representation of platelet clearance and thrombopoietin production by liver cells. Newly produced platelets have sialic acid coated surfaces, as they age sialic acid is lost revealing galactose. Galactose molecules are recognised by the Ashwell-Morell receptor (AMR) on hepatocytes and Kuppfer cells, which results in platelet removal (phagocytosis) and thrombopoietin (TPO) production. Increased plasma TPO levels stimulate megakaryopoiesis and the generation of more platelets.

TPO acts by binding to the extracellular domain of c-Mpl. c-Mpl does not have intrinsic kinase activity, its signalling relies on the tyrosine kinase Janus kinase 2 (JAK2) which is bound to the cytoplasmic region of c-Mpl. Binding of TPO to c-Mpl induces dimerisation of the c-Mpl receptor, which brings the JAK2 proteins close enough to become activated through trans-autophosphorylation (Geddis, 2010; Kaushansky, 2016). Following activation of JAK2, multiple signalling pathways become activated, including the signal transducer and activator of transcription (STAT) pathway via direct phosphorylation of STAT 1, 3, 5a and 5b (fig. 1.4). Once

phosphorylated these STAT proteins promote the transcription of genes involved in cell cycle such as cyclin-D1, p21 and Bcl-xL by forming dimers and translocating to the nucleus where they bind STAT-responsive transcriptional elements. JAK2 phosphorylation also causes the small GTPase Ras to become activated. JAK2 phosphorylation is known to phosphorylate c-Mpl at tyrosine (Tyr) 625 and 630. Phosphorylation of Tyr625 allows the binding of the adaptor protein Shc which subsequently leads to the assembly of a complex containing Grb2 and the guanine nucleotide exchange factor SOS. SOS then activates Ras by facilitating the exchange of GDP for GTP. Activated Ras is able to initiate signalling through two important pathways, namely the mitogen-activated protein kinase (MAPK) and phosphoinositol-3 kinase (PI3K) pathways (Geddis, 2010).

TPO induced MAPK signalling has been shown to be important in megakaryocyte differentiation from progenitor cells (Fichelson et al., 1999). Activated Ras in turn activates Raf-1, mitogen-induced extracellular kinase (MEK) and finally ERK (MAPK) 1/2. Once avtivated ERK 1/2 enter the nucleus and activate key transcription factors including Jun and Fos (Geddis, 2010). Although the canonical activation of Ras in TPO mediated signalling relies on phosphorylation of c-Mpl Tyr625, MAPK activation, although significantly reduced, is still seen in c-Mpl mutant mice that lack Tyr625 (Luoh et al., 2000). This suggests that the MAPK pathway can be activated through another mechanism. One possibility is through the Grb2/SOS complex recruited to phosphorylated JAK2 (Brizzi et al., 1996).

TPO induced PI3K signalling is essential for megakaryopoiesis as inhibition of the PI3K pathway in megakaryocyte progenitors results in cell cycle arrest (Geddis et al., 2001). Activated Ras has been shown to contribute to the activation of PI3K (Kodaki et al., 1994). Activated PI3K phosphorylates the serine/threonine Akt which can activate Bad, Forkhead, the transcription factor FOXO3a and glycogen synthase kinase 3 beta (GSK-3β) promoting survival and proliferation of megakaryocytic cells (Geddis, 2010).

TPO signalling is tightly controlled and defects in the control mechanisms can lead to myeloproliferative neoplasms amongst other diseases. Two main auto-regulation mechanisms are known to exist: internalisation and degradation of c-Mpl and activation of negative regulators. TPO-stimulation results in rapid internalisation of c-Mpl caused by association of Adaptor protein 2 (AP2) which drives clathrin formation and endocytosis. Once

internalised, c-Mpl is subjected to lysosomal and proteasomal degradation, the latter via ubiquitination of activated c-Mpl (Hitchcock and Kaushansky, 2014).

As well as degrading c-Mpl, TPO signalling leads to activation of negative regulators. Activation of the JAK/STAT pathway induces transcription of the suppressor of cytokine signalling (SOCS) family. SOCS1 and 3 bind directly to JAK2 inhibiting its activity (Croker et al., 2008; Geddis et al., 2002). The Src kinase family member, LYN, has been shown to negatively regulate TPO-induced ERK1/2 signalling. Also the adaptor protein LNK regulates the TPO-induced activation of STAT5 and ERK1/2 (Hitchcock and Kaushansky, 2014).

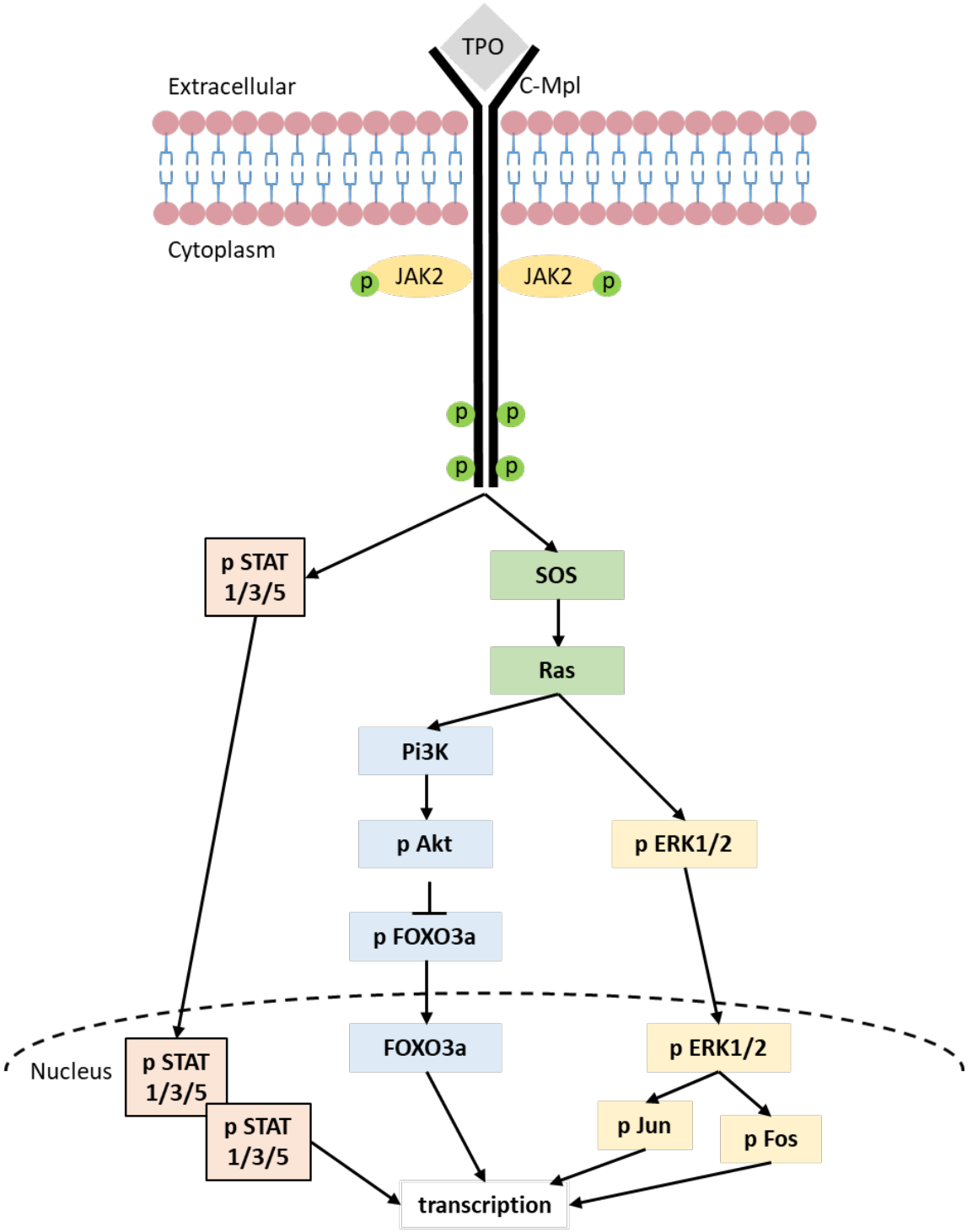

Figure 1.4 – Schematic representation of TPO induced signalling

1.5 TPO free megakaryopoiesis

Ablation of either TPO or c-Mpl in mice results in a 90% decrease in platelet counts and bone marrow MK numbers, indicating the importance of TPO on megakaryopoiesis. The mice in these studies were healthy and despite having only a platelet count 10% that of wildtype animals' spontaneous haemorrhage was not observed (Bunting et al., 1997; Gurney et al., 1994). This suggests that other regulators of megakaryopoiesis exist and are sufficient to maintain haemostasis in the absence of TPO. A number of cytokines could be responsible for this residual megakaryopoiesis and platelet formation. The most likely candidates to promote the residual megakaryopoiesis are Interleukin-6 (IL-6) and other IL-6 family members such as IL-11 and leukaemia inhibitory factor (LIF), as this family of proteins have been shown to stimulate megakaryopoiesis *in vitro*. This family of proteins are able to bind to and signal through gp130 proteins. Gp130 is ubiquitously expressed and binding causes activation of the JAK/STAT and MAPK pathways, therefore promoting megakaryopoiesis (Burstein et al., 1992; Sasaki et al., 1995; Zheng et al., 2008). Other candidates include IL-3 which can promote proliferation of CFU-MKs and cause maturation of MK nuclei; and stem cell factor (SCF) which can enhance the effects of IL-3 and granulocyte-macrophage colony-stimulating factor (GM-CSF) on the formation of BFU-MK colonies (Zheng et al., 2008).

1.6 Megakaryocyte maturation

As briefly mentioned in section 1.1.3, when MKs mature they become polyploid and develop a DMS. As well as developing these defining features, MKs migrate from the osteoblastic to vascular niche within the bone marrow. This section will discuss each feature of MKs maturation in detail.

1.6.1 Endomitosis and polyploidisation

During maturation MKs become polyploid through a process of DNA replication without cell division, termed endomitosis (fig. 1.5). This process results in very large cells with a polyploid nucleus. The number of endomitotic cycles a MK undergoes can vary from 2-7 with ploidy as large as 256N. However, most MKs undergo 3 rounds of endomitosis resulting in 16N MKs.

Polyploidisation of MKs results in a functional gene amplification which likely increases protein synthesis in-line with increased cell size to aid platelet production (Raslova et al., 2003).

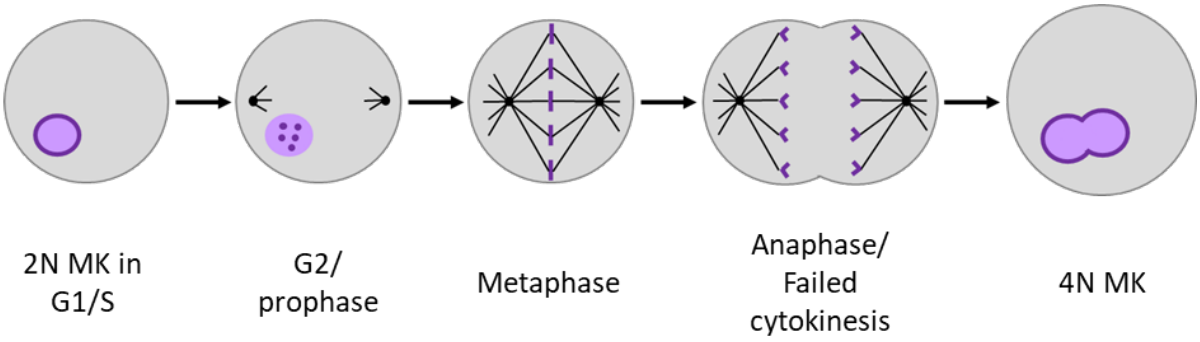

Figure 1.5 – Schematic representation of endomitosis. Diploid megakaryocytes (MKs) progress through S phase and enter mitosis. Anaphase initiates with separation of sister chromatids and formation of the cleavage furrow. However, for reasons as yet not fully understood, cytokinesis fails and the cleavage furrow regresses resulting in a 4N MK that re-enters G1.

During the first cycle of endomitosis, diploid MK progenitors enter a short G1 phase, followed by a 6-7 hour S phase allowing DNA replication. Following a short G2 phase, the cell undergoes prophase with chromatin condensation, rupture of the nuclear envelope and formation of an unusual spherical mitotic spindle. Metaphase is normal with correct attachment of mitotic spindles to chromatids and alignment of the chromatids equidistance from the two spindle poles. Anaphase starts correctly with the movement of sister chromatids to their respective poles, formation of the midzone (a network of antiparallel microtubules that forms between the separating chromosomes) and initiation of cleavage furrows. However, despite significant ingression of the cleavage furrows, they eventually regress, leading to failure of cytokinesis. The 2 daughter cells then move back and reassemble into a single cell. A nuclear envelope then forms around both sets of sister chromatids, creating a larger single lobed nucleus (in the majority of cases, single cells with multiple nuclei also been noted *in vitro*) and doubling the number of copies of chromosomes. Cells then re-enter G1 and undergo the process of endomitosis again. Interestingly, in MKs with higher ploidy, ingression of cleavage furrows is less pronounced than in immature MKs (Geddis et al., 2007; Lordier et al., 2008).

The biological reasons for the failure of cytokinesis in MKs is still not fully understood, however, it has been the focus of several laboratories. One family of proteins that have been implicated in endomitosis is the cyclins. Mitosis promoting factor (MPF) is formed of a complex

between cyclin B1 and Cdc2. MPF has a kinase activity required for the cell to enter mitosis. In human and mouse cell lines it has been shown that Cdc2 is inactive and cyclin B1 is absent during endomitosis. However, studies using *in vitro* megakaryocytes oppose this view (Datta et al., 1996; Zhang et al., 1996). E-type cyclins have also been shown to have a role in endomitosis. Geng *et al*, showed a decrease in ploidy compared to controls of *in vitro* cultured mouse MKs from cyclin E KO mice. This suggests cyclin E is required for normal endomitosis of mouse megakaryocytes, at least in vitro (Geng et al., 2003).

Another protein that has been implicated in polyploidisation of MKs is the GTPase RhoA. Conditional RhoA knockout mice develop larger MKs with higher ploidy than controls (Suzuki et al., 2013). RhoA usually accumulates in the cleavage furrow of mitotic cells where it promotes the assembly and contraction of the actomyosin ring which is essential for proper cytokinesis. However, during endomitosis RhoA activity and F-actin are markedly decreased and myosin IIA is not recruited to the contractile ring causing cytokinesis to fail (Gao et al., 2012; Lordier et al., 2008). The decreased RhoA activity during endomitosis seems to be attributed to a decrease in two guanine exchange factors (GEFs) needed for RhoA activation. The GEFs GEF-H1 and ECT2 are downregulated during MK polyploidisation. GEF-H1 downregulation appears to be essential for the transition from immature 2N cells to 4N, whereas ECT2 must be downregulated beyond the 4N stage (Gao et al., 2012).

Other molecules that may have an effect on MK endomitosis and polyploidisation include transforming growth factor beta (TGF-β) and p21-activated kinase 2 (PAK2). Recently, it was shown that a competitive inhibitor of TGF-β could dramatically increase the ploidy of cultured human cord blood derived MKs, suggesting TGF-β signalling could have an effect on endomitosis. However, surprisingly, only 1 TGF-β inhibitor gave this result out of a number of inhibitors that were tested in the study (Huang et al., 2016).

Kosoff *et al* showed *Pak2* knockout mice (*Pak2*$^{-/-}$*)* have a marked increase in ploidy level and diameter of megakaryocytes in their bone marrow. Indeed, treatment of mice with an inhibitor of *Pak2* increased ploidy of bone marrow MKs. Phosphorylation of cofilin was reduced in *Pak2*$^{-/-}$ MKs. Cofilin is active in its un-phosphorylated state and acts to sever actin filaments. This may partly explain the decrease in F-actin during endomitosis mentioned previously. Similar to this, Aurora A/B/C phosphorylation was decreased in *Pak2*$^{-/-}$. Aurora A

regulates microtubule dynamics and is a negative regulator of polyploidisation (Kosoff et al., 2015).

1.6.2 Demarcation membrane system

As MKs mature, they develop a network of membrane channels composed of flattened cisternae and tubules unique to MKs that is termed the demarcation membrane system (DMS). Development of the DMS starts in promegakaryocytes but it becomes most noticeable in mature MKs where it dominates the entire cytoplasm except from a thin layer at the cortex. Electron microscopy revealed that the DMS is formed from tubular invaginations of the plasma membrane and that the entirety of the DMS is in contact with the extracellular space (Behnke, 1968).

The DMS originates from folding of the plasma membranes that resembles cleavage furrow formation at defined locations, forming a perinuclear pre-DMS. Membrane is then added to this pre-DMS by Golgi-dervied vesicles and the transfer of lipids mediated by the endoplasmic reticulum, extending the pre-DMS into its mature form (Eckly et al., 2014).

It was originally hypothesised that the DMS formed 'platelet territories' within the cytoplasm, however the currently hypothesis is that the DMS serves as a reservoir for proplatelet production. This current hypothesis is derived from the fact that proteins that affect DMS formation also affect proplatelet formation. CDC42 interacting protein 4 (CIP4) is an F-BAR protein that binds to membrane phospholipids via its BAR domain and causes membrane tubulation. It also interacts with the Wiskott-Aldrich syndrome protein (WASp). *Cip4* knockout (*Cip4*$^{-/-}$) mice have severely reduced or missing DMS in bone marrow MKs and *in vitro* cultured *Cip4*$^{-/-}$ MKs show decreased proplatelet production (Chen et al., 2013a).

PI-4,5-P_2 (a phospholipid) is usually confined to the plasma membrane. However, in MKs, PI-4,5-P_2 is found in the DMS and within close proximity to PI-5-P-4 kinase α (PIP4Kα). Activation of PI-4,5-P_2 by PIP4Kα can promote actin polymerisation by activating Rho-like GTPases and WASp family proteins. PI-4,5-P_2 signalling from these GTPases to the ARP2/3 complex (which promotes actin filamentation) is mediated through members of the WASp family. Loss of PIPK4α expression by short hairpin (sh) RNA in murine MKs led to impairment of the DMS and

proplatelet formation. However, negative regulation of all WASp family proteins (WASp, N-WASp and WAVE) showed decreased proplatelet formation but no effect on DMS formation, suggesting WASp proteins do not affect DMS formation (Schulze et al., 2006). Recently, a study using *in vitro* cultured human MKs showed that N-WASp but not WASp is involved in formation of DMS and proplatelet formation. When N-WASp expression was reduced using shRNA DMS development was affected causing dilation of the DMS and proplatelet formation was decrease. Interestingly, N-WASp is expressed at much lower levels than WASp in MKs, but expression increases as MKs mature (Palazzo et al., 2016).

Despite N-WASp and CIP4 being involved with CDC42 (WASp family proteins are effectors of CDC42), CDC42 itself is dispensable for proper DMS formation. Despite a dominant negative form of CDC42 displaying decreased proplatelet formation, no effect on the DMS was observed (Palazzo et al., 2016).

Mutations in GPIb-V-IX the vWF receptor complex result in Bernard-Soulier syndrome (BSS), a rare bleeding disorder characterised by macrothrombocytopenia. MKs from patients with BSS and from GPIbα knockout mice show impaired DMS development (Dutting et al., 2017; Poujol et al., 2002).

1.6.3 MK migration

Haematopoiesis starts in the osteoblastic niche of the bone marrow. Most LT-HSCs found in close contact to osteoblasts and osteoclasts, which secrete many factors required for HSC maintenance. The main extracellular matrix component of the osteoblastic niche is fibrillar collagen type I. *In vitro* studies have shown that collagen type I significantly inhibits proplatelet formation, therefore preventing the early release of proplatelets (and platelets) into the osteoblastic niche by MKs. MKs, like platelets, express two main collagen receptors GPVI and integrin $\alpha_2\beta_1$. Collagen type I induced proplatelet inhibition mainly depends on its interaction with integrin $\alpha_2\beta_1$ (Sabri et al., 2004).

In contrast, the extracellular matrix of the vascular niche, which surrounds the bone marrow arterioles, capillaries and venous sinusoids, is replete with vWF, fibrinogen and fibronectin (Machlus and Italiano, 2013). All three of these extracellular matrix proteins are important in

the productions of platelets. Fibrinogen has been shown to promote proplatelet formation (the precursor to platelet production, see section 1.7.1) *in vitro*. Fibrinogen induced proplatelet formation is mediated via signalling through the major fibrinogen receptor on MKs, $\alpha_{IIb}\beta_3$. This is known as blocking the fibrinogen receptor on MKs with $\alpha_{IIb}\beta_3$ antagonists prevented proplatelet formation (Larson and Watson, 2006). Interestingly, $\alpha_{IIb}\beta_3$ is expressed on MKs early during their development, however it only becomes functionally active as MKs mature; thus preventing premature proplatelet release (Eto et al., 2002).

As mentioned in section 1.6.2 mutations in GPIb-V-IX result in BSS. MKs from BSS patients show impaired proplatelet formation *in vivo* (Balduini et al., 2011), linking binding of vWF to MKs in the control of platelet size and numbers. Finally, fibronectin is important in MK development, promoting both differentiation and proliferation, as well as proplatelet formation. Proplatelet formation in MKs is enhanced by the binding of fibronectin to very late antigen 4 and 5 (VLA-4 and VLA-5) on MKs and subsequent activation of the MAPK pathway (Matsunaga et al., 2012).

The migration of MKs from the osteoblastic niche to the vascular niche is mainly driven by the cytokine stromal derived growth factor 1α (SDF-1α (or CXCL12)). Unlike other blood vessels, bone marrow residing sinusoids are devoid of pericytes but are instead surrounded by specialised CXCl12-abudant reticular (CAR) cells. CAR cells secrete SDF-1α therefore creating a gradient of SDF-1α between the osteoblastic and vascular niches (Psaila et al., 2012; Sugiyama et al., 2006). Binding of SDF-1α by its receptor on MKs, CXCR4, is responsible for the migration of MKs towards sinusoids (Avecilla et al., 2004). When MKs are on a fibronectin matrix, as is abundant in the vascular niche, directional movement towards the SDF-1α gradient is dependent on Src family kinases (SFKs), Syk kinase and phospholipase C γ2 (PLCγ2) signalling downstream of the fibronectin receptor integrin $\alpha_{IIb}\beta_3$. Mazharian *et al*, showed that *in vitro* cultured MKs were unable to migrate towards an SDF-1α gradient when treated with either SFKs or Syk inhibitors or an $\alpha_{IIb}\beta_3$ antagonist. This is because SFKs and Syk inhibitors prevented MKs from spreading, a prerequisite for cell motility, on fibronectin surfaces (Mazharian et al., 2010). The initial movement out of the osteoblastic niche, where fibronectin is not present, and into the vascular niche may be mediate through another pathway. In 2013, Abbonante *et al*, described a novel collagen receptor expressed by human MKs, discoidin domain receptor 1 (DDR1). They showed that binding of DDR1 to collagen type 1 facilitated

MK migration as migration was severely decreased when a DDR1 blocking molecule was added to MKs. Similarly to MK motility on fibronectin, DDR1 induced migration involves Syk signalling. Binding of DDR1 to fibrillar collagen causes phosphorylation and increased enzyme activity of the SH2 domain-containing phosphatase SHP1, which in turn dephosphorylates Syk allowing MK migration along collagen type 1 fibrils (Abbonante et al., 2013).

1.7 Platelets

Platelets are small (2-4μm) anucleated discoid cells that are derived from MKs mainly in the bone marrow but also in the spleen and lungs. Recent data suggests that as much as 50% of platelet formation occurs in the lungs of mice (Lefrancais et al., 2017); although, this has yet to be confirmed experimentally. The first description of platelets in scientific literature was by William Osler in 1873. Osler described platelet as single disc like cells in the blood that are able to aggregate. However, he was unsure if these disc like cells were normal blood components or from an exogenous source (Osler, 1873). In 1882, Giulio Bizzozero was the first to attribute platelets in haemostasis. He noted that platelets adhered to vascular lesions and to each other to form a thrombus (Mazzarello et al., 2001; Norris and Neale, 1882).

Since the discovery of platelets, they have attracted much scientific interest due to the involvement in a multitude of physiological processes. Not only do they participate in normal haemostasis and wound healing, they have been shown to have roles in tumour metastasis (Leblanc and Peyruchaud, 2016), inflammation (Semple et al., 2011), bacterial infection (Deppermann and Kubes, 2016) and tissue repair and regeneration (Gawaz and Vogel, 2013).

1.7.1 Platelet formation and the proplatelet theory

The mechanism by which platelets are generated have been of scientific interest since the early 20th century. Wright was the first to indicate that platelets derive from MKs in 1906, but it was not until 1955 that there was indisputable evidence of this link between platelets and MKs (Humphrey, 1955; Wright, 1906).

Originally it was believed platelets were generated by fragmentation of MK cytoplasm along DMS fracture lines between ‘platelet territories’. The majority of evidence now dismisses this

in support of the proplatelet theory of platelet biogenesis in which long cytoplasmic protrusions extend from MKs into the bone marrow sinusoids. This theory is supported by the fact that: *in vitro* proplatelet formation produces platelets that are functionally and structurally similar to blood platelets (Choi et al., 1995); many species of mammals have been shown to produce proplatelets (Choi et al., 1995; Handagama et al., 1987; Junt et al., 2007); and mutations that cause a decrease/loss of proplatelet formation also result in a decreased platelet count (Chen et al., 2013a; Palazzo et al., 2016). However, in 2015 Nishimura *et al* presented evidence that rapid rupture of MKs may be responsible for the generation of platelets during times of acute platelet need. This MK rupture is believed to be driven by interleukin-1α (IL-1α) rather than by TPO as in steady state platelet biogenesis (Nishimura et al., 2015).

The proplatelet theory, established by Becker and De Bruyn, postulates that MKs produce pseudopod like cytoplasmic extensions in the bone marrow that extend into the sinusoids and later fragment to produce single platelets (fig. 1.6) (Becker and De Bruyn, 1976). The cytoplasmic extensions, which are believed to be an intermediate structure in the transition from MKs to platelets, have a 'beads-on-a-string' structure with numerous platelet sized swelling tethered together by thin cytoplasmic bridges. Before proplatelet formation occurs, the DMS polarises to one pole of the MK. Proplatelet formation starts with the erosion of MK cytoplasm at the pole where the DMS has polarised and the formation of thick extensions from this pole. These thick protrusions extend over 4-10 hours into thin 2-4µm tubes which bend, branch and develop platelet sized swellings to give the stereotypical proplatelet shape. Proplatelet formation uses almost all of the MKs cytoplasm and intracellular component and once completed the MK is left as a naked nuclei (Italiano et al., 1999).

Directional control of proplatelets into the lumen of bone marrow sinusoids has recently been attributed to crosstalk between GPIbα/CDC42 and RhoA signalling in MKs. Mutation of the ectodomain of Gp1bα or deletion of CDC42 in mouse MKs located MKs further from bone marrow sinusoids. This suggests activation of CDC42 downstream of GP1bα signalling acts as a positive regulator to locate MKs to the sinusoids. In stark contrast, ablation of RhoA led to an increase of MKs in the lumen of sinusoids, suggesting RhoA signalling acts as a negative regulator of MK guidance to the sinusoids. Once located at the vascular interface of sinusoids, polarisation of the DMS is needed for MKs to produce proplatelets. DMS polarisation is

associated with CDC42 activation. Mice with mutated Gp1bα had decreased CDC42 activation, showing the importance of CDC42 activation via GP1bα for DMS polarisation. RhoA knockout mice had increased CDC42 activity at the polarised DMS, suggesting RhoA controls DMS polarisation by limiting CDC42 activity (Dutting et al., 2017).

Shingosine 1 phosphate (S1P) and its receptor on MKs (S1pr1) have also been shown to act as regulators of directional proplatelet formation and release. S1P circulates in the blood and because of the location of MKs at the vascular interface of bone marrow sinusoids, MKs are subjected to a gradient of S1P. This S1P gradient is thought to guide proplatelet formation into the sinusoid lumen. Mice lacking S1P show abnormal formation and shedding of proplatelets in the extravascular space of the bone marrow (Zhang et al., 2012). S1pr1 is a G-protein coupled receptor (GPCR; see section 1.7.4.2 for details), but the exact signalling pathway involved in the directional control of proplatelet formation by S1P-S1pr1 is not known. In other cell types, activation of S1P-S1pr1 leads to signalling via different pathways which in turn causes a range of different downstream effects. For example, activation of the P13K-Akt signalling pathway leads to increased survival of lymphocytes, whereas activation of Ras-ERK1/2 signalling pathway causes immune cell proliferation (Mazharian and Senis, 2016).

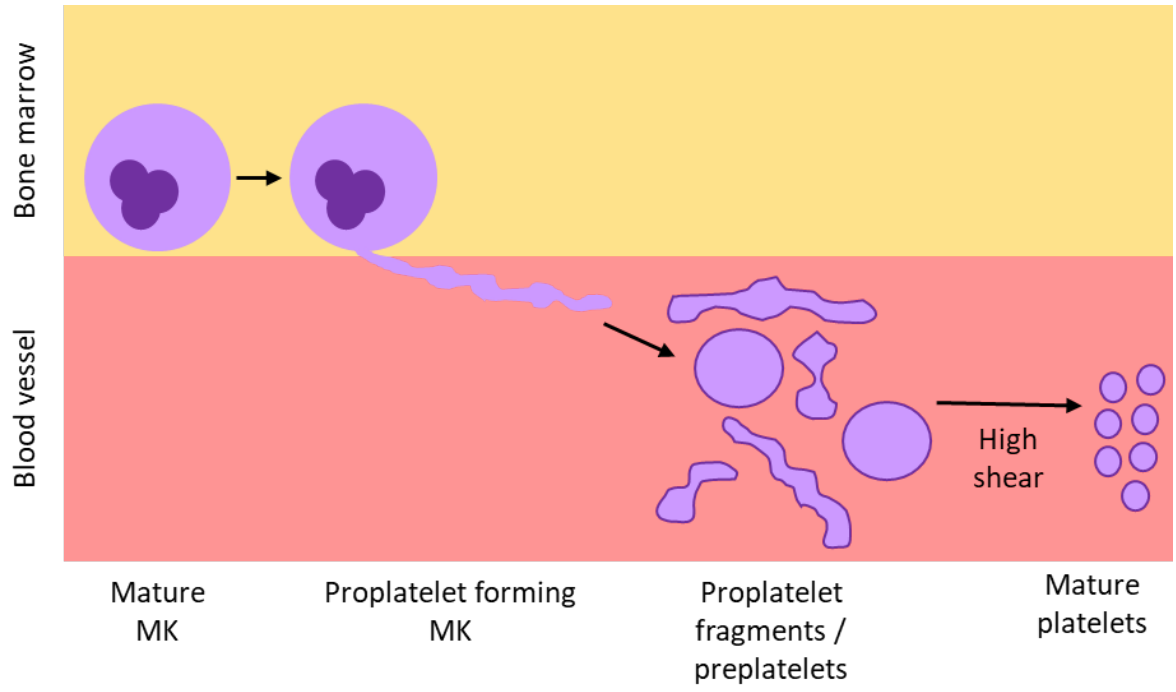

Figure 1.6 – Schematic representation of proplatelet formation, preplatelet release and platelet maturation.

1.7.1.1 Microtubules

Proplatelet formation is driven mainly by MK cytoskeletal proteins. The main cytoskeletal proteins involved in this process are microtubules, actin and spectrin. Microtubules serve to power proplatelet elongation and allow transport of organelles and granules along proplatelets. Microtubules are hollow tubes, 24nm in diameter, composed of polymerised αβ tubulin dimers. β-tubulin has GTPase activity and addition of tubulin heterodimers activates the GTPase, locking the β-tubulins in a GDP bound state. Microtubules are polar molecules due to the orientation of the heterodimers. The end of a microtubule that terminates with an α-tubulin protein (minus end) is much more stable than the plus end, which terminates in a β-tubulin protein. Therefore, microtubule elongation and retraction happens mainly at the plus end. To help prevent depolymerisation, the β-tubulins at the end of the microtubules form a GTP cap (Parker et al, 2014). It has been shown that β_1-tubulin is especially important for proper thrombopoiesis. β_1-tubulin expression is restricted to platelets and mature MKs and ablation of β_1-tubulin in the mouse leads to thrombocytopenia due to defective proplatelet formation (Schwer et al., 2001).

In immature MKs, microtubules extend from the cell centre to the cortex in a starburst like pattern. During the initial stages of proplatelet formation when thick pseudopodia are forming, cortex and membrane associated microtubules merge into thick bundles positioned just the plasma membrane of these pseudopodia. Elongation of the pseudopodia into proplatelets, at a rate of 1µm/min (*in vitro*, but up to 30µm/min *in vivo*), is driven by continuous polymerisation of thick bundles of microtubules at a rate of ~10µm/min. As the proplatelet extends it narrows and the bundles of microtubules thin out, with thick bundles seen near the cell body of the MK and bundles of approximately seven microtubules at the proplatelet tip. At the proplatelet tips, microtubules coil 8-12 times to form a tear drop shaped loop and then proceed to re-enter the shaft of the proplatelet. This microtubule coil, which is a defining feature of mature platelets, is only seen in the bulbs at the end of proplatelet tips suggesting that only these bulbs will form mature platelets (Italiano et al., 1999; Patel et al., 2005).

The fact that microtubule assembly rates are approximately 10 times faster than proplatelet elongation rates *in vitro* suggests that these processes are not tightly linked. Indeed,

proplatelet elongation is still observed when microtubule assembly is chemically blocked (Patel et al., 2005). Proplatelet elongation has been attributed to microtubule sliding control by dynein. Dynein is a minus end microtubule motor protein that concentrates along microtubules in proplatelets. Inhibition of dynein in proplatelet forming MKs prevented elongation of the proplatelet shafts (Bender et al., 2015). These experiments reveal that dynein-mediated microtubule sliding actually provides the power for proplatelet elongation.

A second function served by microtubules in proplatelets is to facilitate the transport of organelles, granules and membrane from the MK body to the nascent platelets at the proplatelet tips. Organelles are able to travel bi-directionally along proplatelet shafts until they are captured in the proplatelet tips. This movement of organelles is not affected by inhibitors of actin filament, suggesting it is a microtubule based mechanism. Richardson *et al* have postulated a twofold microtubule based mechanism of organelle transport in proplatelets. Firstly, organelles and granules translocate bidirectionally along microtubules likely facilitated by kinesin. Kinesin is a microtubule motor protein that walks along microtubule filaments towards the plus end, powered by the hydrolysis of ATP. The bidirectional movement is permitted due to the mixed polarity of microtubules in proplatelets. Secondly, indirectly moving in a 'piggy back' fashion as microtubules slide bidirectionally to one another powered by dynein (Richardson et al., 2005).

1.7.1.2 Actin

Actin is a 42 kDa protein that exists in two forms: a monomeric form, known as globular (G-) actin, and a polymerised form called filamentous (F-) actin. Although actin is dispensable for proplatelet formation, it is vital for proplatelet bending and bifurcation. As nascent platelets are believed to arise from the proplatelet tips, amplification of these tips is important process of proplatelet formation. Proplatelet tip amplification is caused by proplatelet shafts being bent into sharp kinks that then bend back on themselves, forming a loop in the microtubule bundle. This new microtubule loop then elongates forming a new proplatelet shaft branching from the original proplatelet. The branching process of proplatelet tip amplification has been shown to be driven by actin. MKs exposed to actin depolymerising agents are able to produce proplatelets but they are devoid of branching and contain few swellings (Italiano et al., 1999).

How actin causes this branching process in proplatelets is still unclear, however several actin binding proteins have been suggested to play a role.

One possibility is that non-muscle myosin II powers this branching process. Mutations in *MYH9*, the gene encoding non-muscle myosin heavy chain-A, results in *MYH9*-related diseases including May-Hegglin anomaly and the Sebastin, Fechtner, and Epstein syndromes. These four autosomal dominant diseases result in macrothrombocytopenia and can be distinguished from each other by the combination of associated clinical and laboratory signs. Fechtner syndrome is associated with Döhle-like leukocyte inclusions as well as sensorineural deafness, cataracts, and nephritis. Epstein syndrome is similar to Fetchner syndrome and is associated with sensorineural deafness and nephritis, but patients do nto present cataracts or Döhle-like leukocyte inclusions. Both May-Hegglin anomaly and Seastin syndrome are associated with Döhle-like leukocyte inclusions and lack sensorineural deafness, cataracts, and nephritis. These diseases are distinguished by ultrastructure analysis of the leukocyte inclusions. Leukocyte inclusions of May-Hegglin anomaly are composed of cytoplasm surrounding parallel microfilaments with clustered ribosomes, in Sebastian syndrome the inclusions are composed of highly dispersed microfilaments with few ribosomes (Ma and Key, 2009; Rodriguez et al., 2013). *MYH9*-related diseases are characterised by macrothrombocytopenia. Analysis of proplatelet formation in MKs cultured from patients with *MYH9*-related diseases showed decreased proplatelet formation, which could be rescued with a myosin II inhibitor (Chen et al., 2013b). However, cultured murine MKs from mice with *Myh9* deleted were able to branch and bifurcate (Eckly et al., 2009).

Other actin binding proteins involved in the proplatelet forming process include: filamin A, cofilin-1 and profilin1. Filamin A cross links actin filaments, anchors membrane receptors and promotes high angle branching of actin filaments. Mice with conditional deletion of Filamin A in the MK and platelet have severe macrothrombocytopenia but proplatelets were able to branch normally (Begonja et al., 2011).

Cofilin-1 is a F-actin severing protein, along with actin depolymerising factor (ADF) and cofilin-2, and promotes the disassembly of actin filaments. Conditional cofilin-1 knockout of the MK and platelet lineage in mice results in a 60-80% decrease in platelet count associated with increased platelet size. Surprisingly, ADF knockout mice have normal platelet counts. ADF and

cofilin-1 deletion virtually abolishes platelet formation with platelet counts below 5% that of controls (Bender et al., 2010). Profilin1 binds to monomeric G-actin accelerating the nucleotide-exchange from ADP to ATP and consequently promoting actin filament elongation. Ablation of Profilin1 in the MK and platelet lineage of mice results in microthrombocytopenia and premature release of platelets into the extravascular space of the bone marrow. This phenotype recapitulated those seen in Wiskott-Aldrich syndrome in which the WASp protein is mutated (Bender et al., 2014). These results suggest cytoskeletal dynamics and actin filament turnover are critical for platelet production.

1.7.1.3 Spectrin

Spectrin is a cytoskeletal protein that lines the intracellular side of the plasma membrane and is important for membrane integrity. α- and β-spectrin monomers associate laterally to form a heterodimer. Dimers then associate head to head to form a tetramer. Association of tetramers in an end to end fashion with actin filaments creates triangular pores. Platelets contain approximately 2,000 spectrin molecules that form a network that coats the cytoplasmic surface of the open canalicular system (OCS) and the plasma membrane.

Electron microscopy of proplatelet forming MKs shows proplatelets contain a spectrin based cytoskeleton similar to that of platelets. Cultured murine MKs expressing a spectrin-tetramer disrupting peptide showed severely impaired proplatelet formation. Also, addition of this disrupting peptide to proplatelet forming MKs disrupted proplatelet morphology, causing massive swelling (Patel-Hett et al., 2011). These results show the importance of spectrin in proplatelet formation and preservation of proplatelet structure.

1.7.2 Release of preplatelets and platelet maturation in the periphery

Intravital microscopy in mice has allowed proplatelet formation and platelet release to be visualised *in vivo*. Surprisingly, proplatelet fragments released into the circulation are much larger than mature platelets (Junt et al., 2007; Zhang et al., 2012). The shedding of these large proplatelet fragments from proplatelet shafts is reliant on S1pr1 signalling as S1pr1 knockout mice rarely shed proplatelets fragments *in vivo* (Zhang et al., 2012).

The released proplatelet fragments generally resemble proplatelet shafts with a bead-on-a-string morphology. Fission of these large proplatelet fragments results in smaller fragments termed preplatelets. The fission occurs by thinning and eventually snapping of the connections between bulbous swellings at a constriction site resembling a cleavage furrow. Once the fission has taken place the fragmented ends retract toward their daughter cells. Preplatelets are giant platelets (3-10µm diameter discoid cells) that have a cortical microtubule band and contain platelet organelles. Preplatelets are thought to be intermediates between proplatelets fragments and mature platelets and can reversibly change between resembling barbells and giant platelets by forces generated by twisting of microtubules. By injection of pre-labelled *in vitro* cultured proplatelet fragments/preplatelets into mice it was shown that preplatelet fission results in the formation of mature platelets (Thon et al., 2012a; Thon et al., 2010). This generation of mature platelets from proplatelet fragments and preplatelets is accelerated by shear stress *in vitro* (Thon et al., 2010). This compliments the observation that proplatelet fragments/preplatelets are more concentrated in pre-pulmonary vessels compared to post-pulmonary vessels in rats (Handagama et al., 1987). Myosin IIA has also been implicated in the fission of preplatelet to mature platelets. Phosphorylation of myosin IIA leads to inactivation and has been shown to decrease during thrombopoiesis with threefold more phosphorylation in MKs than platelets. Dephosphorylation of myosin IIA causes assembly of myosin filaments that interact with actin filaments and contributes to membrane integrity and cell division. Shear induced activation of myosin IIA is important for the fission of preplatelets into platelets as pharmacological inhibition of myosin IIA with blebstatin in platelets results in decreased fission of proplatelets (Spinler et al., 2015).

Although preplatelets are present in the blood of healthy humans (Behnke and Forer, 1998), they are rarely recorded. This is possibly due to blood smears generally being performed on EDTA treated blood. EDTA treatment can cause platelet sphering and condensation of platelets, preventing preplatelets from being seen on blood smears (the same is true for heparin treatment.). However, when human blood is treated with sodium citrate, preplatelets are readily observed on blood smears (Thon et al., 2012a). Nevertheless, the effects of different anticoagulants on murine preplatelets have not been tested, so cannot be assumed.

The ability of mature platelets to create progeny has also recently been shown (Schwertz et al., 2010). The process in which this occurs is remarkably similar to the formation of proplatelets and fission of preplatelets into mature platelets. The molecular mechanisms behind the formation of cytoskeletal projections and production of progeny is unknown, however one possibility is that platelets maintain a preplatelet like phenotype allowing them to divide further upon maturation.

1.7.3 Morphology

As mentioned in section 1.7.1.1, resting platelets contain a marginal microtubule coil, which is a defining feature of platelets. The coil is comprised of multiple microtubules with mixed polarity that form a band that circulates the periphery 8-12 times (Patel-Hett et al., 2008). The coil is responsible for maintaining the discoid shape of resting platelets. Depolymerisation of microtubules with pharmaceutical agents or by chilling platelets at 4^{o}C causes loss of the stereotypical discoid shape. The plasma membrane and OCS are also supported by an actin-spectrin based scaffold. The OCS is a tubular network of invaginations of the plasma membrane that acts as a reservoir of membrane for platelet spreading upon activation and facilitates in the uptake and release of granule proteins (White and Clawson, 1980). Platelets contain approximately 2,000 spectrin molecules that attach to the 2-5,000 actin filaments in a triangular lattice fashion to create a cytoskeletal scaffold. Actin filaments are also crosslinked by proteins such as filamin and α-actinin to create a rigid network.

The resting platelet can be divided into three distinct zones. 1) The peripheral zone which is responsible for platelet adhesion and aggregation. This zone comprises a glycoprotein coat, the platelet membrane containing receptors for agonists and the cytoskeleton. 2) The sol-gel zone which is responsible for contraction and support of microtubules and contains the tubules of the OCS. 3) The organelle zone which contains all the platelet organelles such as α- and dense granules, lysosomes and mitochondria (Cimmino and Golino, 2013).

1.7.3.1 Granules

A significant proportion of the total platelet volume is filled by secretory granules. Platelets contain four main types of secretory granules, α- and dense granules, lysosomes and the

recently described T-granules, which are critical to normal platelet function.

α-Granules

α-Granules are the most abundant platelet granule with roughly 50-80 per platelet, ranging in size from 200-500nm and totalling approximately 10% of the platelet volume. Genesis of α-granules begins in MKs but continues in platelets. In MKs, small vesicles that contain newly synthesised proteins, such as vWF, bud off from the trans-Golgi network and travel to multivesicular bodies (MVBs). Other α-granule proteins, for example fibrinogen, can be delivered to MVBs after endocytosis by the plasma membrane. MVBs are endosomal structures that serve as an intermediate stage of granule production and sort endocytosed and newly synthesised vesicles. Immature α-granules are then transported along proplatelets where they become trapped in the terminal tips. Maturation of α-granules continues in the peripheral circulation by endocytosis of platelet plasma membrane in a clathrin dependant manner (Blair and Flaumenhaft, 2009; Heijnen et al., 1998).

α-Granules contain over 300 proteins involved in a multitude of processes. Many of the proteins are involved in haemostasis and coagulation (for example, vWF and fibrinogen). α-Granules also contain several membrane receptors including GPIIb/IIIa and P-Selectin and small vesicles known as exosomes (Blair and Flaumenhaft, 2009).

Mutations in the scaffolding protein NBEAL2 result in gray platelet syndrome (GPS), a rare bleeding disorder. GPS patients have macrothrombocytopenia with platelets appearing grey due to their lack of α-granules. *Nbeal2* knockout mice which have a GPS phenotype show protection against cancer metastasis, revealing the importance of α-granules in cancer metastasis (Guerrero et al., 2014).

Dense-granules

Dense granules are the second major secretory granule in platelets (3 to 8 per platelets) and are so named because of their dark appearance in electron microscopy. Dense granules are formed in a similar fashion to α-granules with MVBs as an intermediate. However, platelet storage pool diseases affecting dense granules, such as Hermansky-Pudlak syndrome, show

normal α-granule formation but defective dense granules, suggesting formation of the two granules are distinct (Blair and Flaumenhaft, 2009; Heijnen and van der Sluijs, 2015; Youssefian and Cramer, 2000).

Dense granules contain a variety of proteins involved in haemostasis including serotonin, ADP, ATP, calcium, magnesium as well as membrane proteins such as GPIb and P-Selectin (Israels et al., 1992; Youssefian and Cramer, 2000).

Lysosomes

Platelet lysosomes have a role in digestion of phagocytic and cytosolic components and as such contain degrading enzymes such as proteases, hydrolases and glycosidases. The may also have roles in extracellular functions such as degradation of extracellular matrix and facilitating receptor cleavage (Heijnen and van der Sluijs, 2015).

T-granules

T-granules are a novel secretory granule found in platelets that were first described in 2012 (Thon et al., 2012b). They have a tubular morphology and contain protein disulphide isomerase (PDI). PDI has been shown to be released from activated platelets and is critical for proper thrombus formation in mice (Cho et al., 2008).

1.7.4 Role in thrombus formation at sites of vascular injury

The primary role of platelets is to maintain haemostasis by forming platelet plugs at sites of vascular injury. Circulating platelets are maintained in a resting state mainly by the actions of endothelial cells that line the blood vessels. Endothelial cells act as a physical barrier between platelets and the activating subendothelial extracellular matrix and also secrete platelet inhibiting factors such as nitric oxide (NO), prostaglandin I_2 (PGI_2) and ectonucleotidase CD39 (Furie and Furie, 2008; Rumbaut and Thiagarajan, 2010).

The formation of the platelet clot at sites of exposed endothelial extracelluar matrix requires a series of coordinated sequential events. Firstly, platelets must adhered to sites of vascular

injury (tethering and stable adhesion). Adherence of platelets leads to platelet activation which causes the release of numerous soluble factors that recruit and activate addition platelets (platelet activation and aggregation). Finally, the platelet aggregate undergoes a final stabilisation step to form an effective thrombus that stops blood loss (clot stabilisation) (fig. 1.7). This process of thrombus formation must be tightly controlled, as uncontrolled thrombosis can cause vessel blockade and tissue ischaemia that can lead to major events such as myocardial infarction and stroke.

1.7.4.1 Tethering and stable adhesion

Vessel injury leads to exposure of platelets to the subendothelial matrix. Platelets adhere to either exposed fibrilar collagen or von Willebrand factor (vWF) multimers (that have bound to the exposed collagen via their A3 (and possibly A1) domain (Cruz et al., 1995)) depending on shear rates. At low venous shear rates (<200 s^{-1}) platelets bind to collagen, however at arterial (>500 s^{-1}) and arteriolar shear rates (1,000 – 1,800 s^{-1}) platelets bind to vWF (Fogelson and Neeves, 2015; Furie and Furie, 2008).

Collagen/GPVI or integrin $\alpha_2\beta_1$ adhesion

Stable adhesion of platelets to the exposed matrix is brought about by binding to fibrillar collagen. At low shear rates, platelets are able to bind directly to collagen, but at high shear tethering of platelets to vWF decreases platelet speed allowing platelet/collagen interactions. The main collagen receptors expressed by platelets are GPVI and integrin $\alpha_2\beta_1$ (GPIa/IIa). Stable platelet adhesion is achieved via synergistic binding of both receptors to collagen (Rivera et al., 2009). This is evident by the fact that murine GPVI or $\alpha_2\beta_1$ knockouts have partial defect in thrombi formation whereas ablation of both GPVI and $\alpha_2\beta_1$ causes complete inhibition of thrombus formation (Sarratt et al., 2005).

1.7.4.2 Platelet activation and aggregation

Stable adhesion of platelets to exposed fibrillar collagen leads to activation of platelets and the release of a multitude of factors that in turn recruit further platelets causing aggregation.

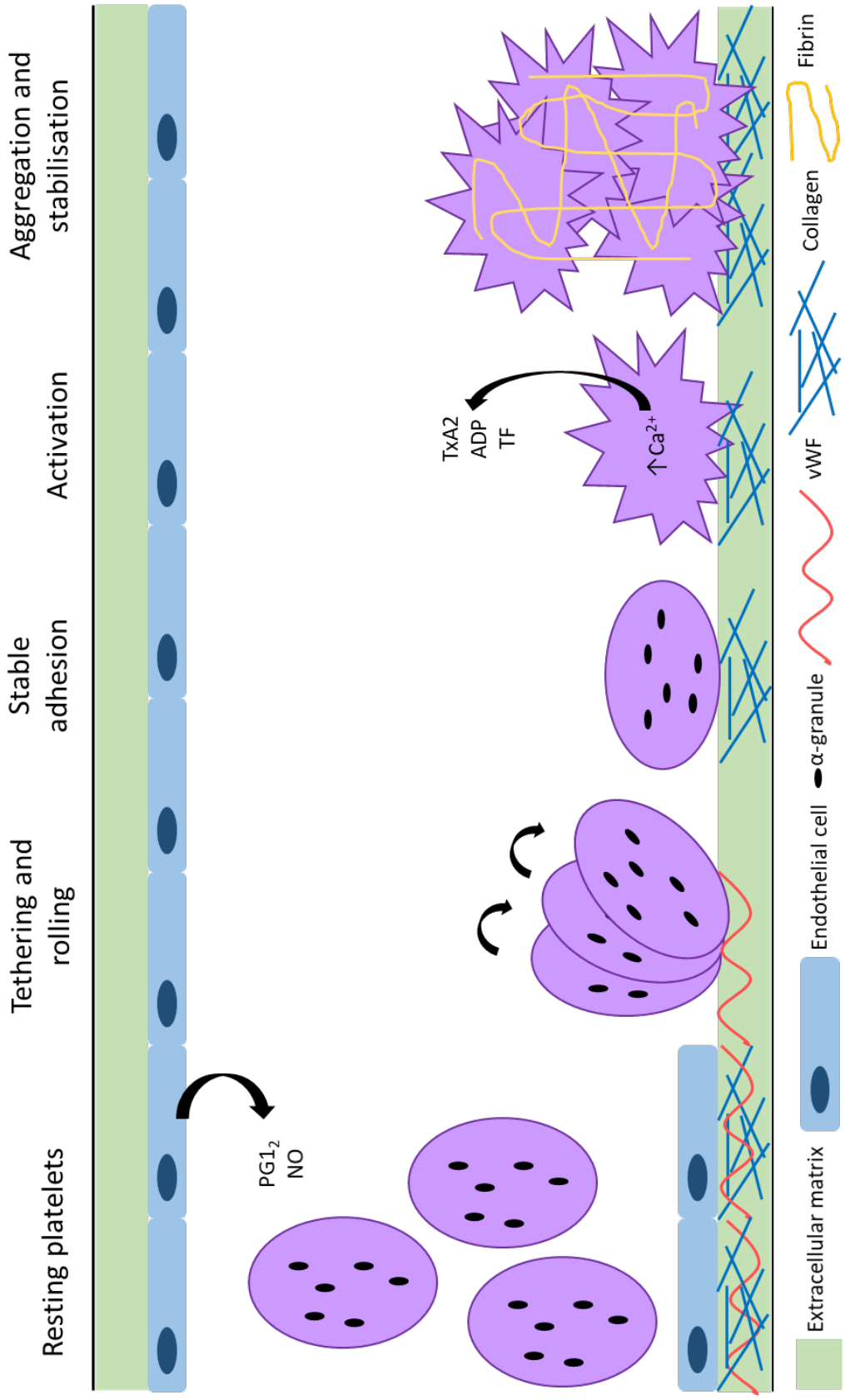

Figure 1.7 – Schematic representation of platelet activation and thrombus formation at sites of vascular injury. Platelets are maintained in their resting state by endothelial cells. Upon exposure of the extracellular matrix, platelets tether to von Willebrand Factor (vWF) and adhere to collagen fibres. Stable adhesion of platelets causes activation and platelet degranulation. Tissue factor (TF) produces fibrin, which creates a mesh forming a stable thrombi.

Platelet activation

Platelet activation is characterised by platelet shape change and degranulation and is dependent on increased intracellular concentrations of calcium ions (Ca^{2+}). Platelet GPVI receptors are bound to the Src kinases Fyn and Lyn via their cytoplasmic tail. GPVI is also constitutively associated with a Fc receptor (FcR) γ-chain dimer that has an immunoreceptor tyrosine-based activation motif (ITAM). When GPVI binds to collagen in the exposed extracellular matrix, the Src kinases phosphorylate the ITAM sequence and initiates activation of a downstream signalling cascade. Important to the signalling is the formation of the 'signalosome' which is composed of multiple adapter and effector proteins. The signalosome activates phospholipase Cγ (PLCγ) which liberates the second messengers 1, 2 diacylglycerol (DAG) and inositol 1,4,5 triphosphate (IP_3). DAG and IP3 increase intracellular Ca^{2+} by mediating calcium influx via the plasma membrane and liberating intracellular stores, respectively, thus resulting in platelet activation. Increased Ca^{2+} and liberation of DAG also activates protein kinase C (PKC) family proteins. Activation of PKC proteins has been shown to be critical for platelet degranulation, as broad range PKC inhibitors have been shown to ablate platelet granule secretion. In contrast, PKC proteins appear to have differential effects on platelet spreading. Some isoforms (PKCβand θ) positively regulate platelet spreading on fibrinogen, whereas other isoforms (PKCδ) seem to negatively regulate filopodia formation (Harper and Poole, 2010). Binding of collagen to integrin $\alpha_2\beta_1$ triggers a similar signalling cascade to GPVI/collagen binding and results in platelet activation.

During platelet activation, platelets undergo shape change in which their morphology changes from discoid to spiny spheres. Shape change is mediated by extensive reorganisation of the cytoskeleton. Platelets also undergo degranulation, where contents of the α- and dense-granules are released into the lumen of the OCS and then into the exterior. Thromboxane A_2 (TxA2), a potent platelet activator, is also released by the plasma membrane. Increased cytosolic Ca^{2+} leads to the liberation of arachidonic acid from membrane phospholipids. Arachidonic acid is converted to TxA2 by enzymes including cyclooxygenase 1 (COX-1). Finally, platelet activation induces conformational changes and therefore activation of many membrane integrin receptors, such as integrin $\alpha_{IIb}\beta_3$.

Many factors released by the platelet granules upon activation are platelet activators themselves (ADP, TxA2, thrombin and adrenaline for example) and many of these act by binding to GPCRs. Binding of agonists to GPCRs leads to downstream activation of PLCβ which in turn releases DAG and IP_3 as per PLCγ. This local increase of platelet agonists leads recruitment of further platelets to the area of vascular injury (Rivera et al., 2009; Rumbaut and Thiagarajan, 2010).

Activated platelets are able to bind to neutrophils via interactions of P-selectin on activated platelets and P-selectin glycoprotein ligand-1 (PSGL-1) on neutrophils (Sreeramkumar et al., 2014). Once bound to platelets, neutrophils become activated by interactions of the transmembrane receptor RAGE (receptor for advanced glycation endproducts) on neutrophils with high motility group box-1 (HMGB-1) protein that is exposed on the membrane of activated platelets (Maugeri et al., 2014). Activation of neutrophils by RAGE/HMGB-1 interactions results in NETosis, the process of neutrophil extracellular trap (NET) formation. NETosis begins with the production of reactive oxygen species (ROS) by phagocytic oxidase (PHOX), which liberates the proteases neutrophil elastase (NE) from azurophilic granule membranes, potentially by ROS interactions with the protease myeloperoxidase (MPO). Once liberated, NE bind actin filaments in the cytoplasm and promotes F-actin degradation, allowing NE to enter the nucleus (Metzler et al., 2014). MPO also migrates to the nucleus after NE, where the two proteases facilitate chromatin decondensation. Chromatin decondensation is further enhanced by peptidylarginine deiminase 4 (PAD4), which catalyses the conversion of arginine residues to citrulline. After chromatin has fully decondensed, neutrophils rupture, releasing NETs which consist of extracellular chromatin fibres surrounding a backbone of histones decorated with granular and cytoplasmic proteins (Brinkmann and Zychlinsky, 2012). NETs themselves are able to bind and activate platelets, mediated by histones (Brinkmann et al., 2004), thus propagating platelet activation during thrombus formation.

Platelets can also become activated in a collagen independent manner. Tissue factor (TF) released at sites of vascular injury forms a complex with blood coagulation enzyme factor VIIa that circulates in the blood. This interaction initiates a cascade of coagulation factors that results in the formation of thrombin. Thrombin activates platelets by binding to the GPCRs protease-activated receptor (PAR) 1 and 4 (Furie and Furie, 2008).

Aggregation

Integrin $\alpha_{IIb}\beta_3$ is a fibrinogen and vWF receptor located on the plasma membrane of platelets. In resting platelets it is maintained in a low affinity state, upon platelet activation the integrin undergoes a conformational change into a high affinity state. Activated $\alpha_{IIb}\beta_3$ can bind soluble plasma fibrinogen and the fibrinogen acts as a bridge between two $\alpha_{IIb}\beta_3$ receptors on adjacent platelets. These fibrinogen bridges cause the aggregation of platelets. vWF can also substitute for fibrinogen as the bridging molecule under high shear.

Although fibrinogen/vWF bridging via $\alpha_{IIb}\beta_3$ is the most studied method of platelet aggregation, other molecules have been implicated. These include junctional adhesion molecules (JAMs), signalling lymphocyte activation molecule (SLAM) proteins and CD40 ligand (CD40L aka CD154). (Rivera et al., 2009; Rumbaut and Thiagarajan, 2010).

1.7.4.3 Clot stabilisation

The formation of a fibrin mesh within the thrombus is the last critical event in the production of a stable thrombus. Fibrin is produced by cleavage of fibrinogen by thrombin. As discussed in section 1.7.4.2, thrombin is produced by TF. As well as TF derived from vessel damage, TF is present in monocyte derived microparticles. These monocyte microparticles are captured by in the thrombus by interaction between P-selectin on activated platelets and PSGL-1 on the microparticles or trapped by NETs (Rivera et al., 2009).

The conversion of TF to thrombin is accelerated roughly 150,000-fold by the presence of plasma membrane phosphatidylserine (PS). PS is located of the cytoplasmic surface of the plasma membrane in resting platelets. However, vesicles produced by activated platelets contain PS on the plasma facing side of the membrane. This exposed PS allows efficient production of thrombin and formation of a fibrin mesh (Lentz, 2003).

1.7.5 Role in thrombus formation in the absence of vascular injury

In 1856 Rudolf Virchow proposed a triad of factors that contribute to venous thrombosis. He postulated that changes in vessels walls, changes in blood coagulability or blood stasis could

cause thrombosis. Given that the venous thrombi are rarely the result of vascular injury (Sevitt, 1974), initiation of thrombosis in veins is mainly controlled by blood stasis or changes in blood coagulation factors.

Many autopsy (Sevitt, 1974; Teviotdale and Gwynne, 1967) and phlebography (Browse and Thomas, 1974; Cotton and Clark, 1965) studies have concluded that lower limb venous valve sinuses are the major site of thrombus formation in the absence of vascular injury. This conclusion is supported by the correlation between the number of valves an individual has and the frequency of deep vein thrombosis (DVT) (Liu et al., 1986). Valve sinuses are areas in which blood undergoes prolonged periods of stasis. McLachlin *et al* showed that contrast media used in venography studies remained for an average of 27 minutes, but up to 60 minutes in the valve sinuses of lower limbs and that the stasis time was highly correlated with age (McLachlin et al., 1960). The prolonged blood stasis in lower limb valve sinuses is correlated with hypoxia in these regions. It was shown that at the bottom of canine limb valve sinuses, the region where venous thrombosis usually occurs, blood undergoes localised serve hypoxia when exposed to static flow for 2 hours. Early thrombus formation was also noted in the most hypoxic regions, implicating hypoxia with initiation of venous thrombosis (Hamer et al., 1981).

Intermittent hypoxia, as occurs at lower limb valve sinuses, results in activation of endothelial cells and leukocytes. Hypoxia is sensed by mitochondria or NADPH oxidase (NOX) leading to production of ROS. ROS accumulation leads to degranulation of Weibel-Palade bodies in endothelial cells and exposure of P- and E-selectin and vWF on their plamsa membrane. ROS also activates two important transcription factors, namely hypoxia inducing factor -1 (HIF-1) and early growth response -1 (Egr-1), via inhibition of HIF prolyl hydroxylase (PHD) or activation of nuclear factor-κB (NF- κB). Activation of HIF-1 and Erg-1 alters the transcriptional activity of endothelial cells, which leads to a prothrombotic state (decreased production of NO, increased production of plasminogen activator inhibitor-1 (PAI-1), which inhibits fibrinolysis, and potentially exposure of TF on the plasma membrane) (Bovill and van der Vliet, 2011).

Activated endothelium is able to capture platelets via vWF interactions (see 1.7.4.1) and leukocytes (mainly neutrophils and monocytes (von Bruhl et al., 2012)) and TF positive

leukocyte and platelet derived microparticles via interactions of P-selection with PSGL-1 (Mackman, 2012). Captured leukocytes become activated by hypoxia in a similar fashion to endothelial cells as above, leading to exposure of TF on their plasma membrane and release of TF positive microparticles (Bovill and van der Vliet, 2011). Leukocyte capture by P-selectin and localised exposure of TF are both critical for venous thrombosis. This is demonstrated by the fact both mice lacking P-selectin and mice with very low levels of TF are protected against thrombus formation in a model of DVT (von Bruhl et al., 2012). NETosis has also been shown to be critical for proper venous thrombosis propagation. Treatment of mice with DNase1 or heparin (which has a high affinity for histones) reduced NET formation and significantly reduced thrombus growth in a model of DVT (von Bruhl et al., 2012).

As discussed in sections 1.7.4.2 and 1.7.4.3 TF causes the generation of thrombin which convert fibrinogen to fibrin. Venous thrombi are composed of a fibrin mesh trapping a multitude of blood cells. Unlike thrombi at sites of vascular injury, venous thrombi are called red clots due to their high level of red cell content.

Although platelets do not appear to be critical for the generation of venous thrombi, there is growing evidence suggesting they contribute. For example, thrombocytosis has been shown to be a risk factor for venous thromboembolism in cancer patients (Jensvoll et al., 2014) and mice depleted of platelets had significantly reduced thrombi in a model of DVT (von Bruhl et al., 2012). Also, platelets appear to be important for the recruitment of leukocytes to venous thrombi and for the formation of NETs. Platelets are able to interact with leukocytes via numerous receptor interactions, the most common being platelet P-selectin with leukocyte PSGL-1 and platelet GPIbα with leukocyte αMβ2 integrin (Li et al., 2015). Both leukocyte numbers and NET formation were significantly reduced in a model of DVT which used mice lacking the external domain of GPIbα (von Bruhl et al., 2012).

1.7.6 Removal from circulation

After being released by MKs into the peripheral circulation platelets circulate for 8 to 10 days (in humans, 4 to 5 in mice) before being removed (Leeksma and Cohen, 1955; Machlus and Italiano, 2013). Platelet clearance mainly occurs in the spleen and liver and is controlled by several mechanisms.

One such mechanism involves signals induced by aging (senescence) of platelets. Senescent platelets lose sialic acid from plasma membrane associated receptors, exposing underlying β-galactose. This loss of sialic acid is probably due to upregulation of the sialidases, Neu1 and Neu3. Exposed galactose residues are recognised by Ashwell-Morrell receptors (AMRs), located on liver macrophages (Kupffer cells) and hepatocytes, which leads to platelet clearance (fig. 1.3). The AMR is a transmembrane heteroligomeric glycoprotein receptor composed of two ASGPR1 molecules and one ASGPR2 molecule. Studies using knockout mice revealed the importance of desialyation and the AMR in platelet clearance. *St3gal4* knockout mice, which lack the enzyme responsible for sialyation of β-galactose, have thrombocytopenia due to increased hepatic platelet clearance, whereas *Asgr2* knockout mice have increased platelet counts and half-life. Cross-breeding of these mice normalised platelet counts, proving that the AMR was responsible for recognising desialyated platelets (Grozovsky et al., 2015a; Grozovsky et al., 2015b; Sorensen et al., 2009).

Kupffer cells are also able to clear platelets via interin αMβ2 (also called CD11b, macrophage receptor 1 (Mac-1) and compliment receptor 3 (CR3)). Desialyated platelets can undergo de-galactosylation, removing the galactose residues that cap GPIbα subunits of the vWF receptor and exposing N-acetylglucosamine (GlcNAc). Exposed GlcNAc on GPIbα subunits are recognised by the αM subunit of integrin αMβ2 leading to phagocytosis and platelet clearance. De-galactosylation of platelets is rapidly increased when platelets are cooled below room temperature and cooled platelets are rapidly removed from the circulation upon transfusion. Thus, platelet transplant units are stored at room temperature and as such have a short shelf life due to the potential of bacterial contamination (Grozovsky et al., 2015b; Grozovsky et al., 2010).

Platelet lifespan has been attributed to the interplay between members of the BCL-2 family, which are regulators of the intrinsic apoptotic pathway. Deletion of the pro-survival protein BCL-X_L in mice dramatically accelerates platelet clearance, whereas ablation of the pro-apoptotic proteins BAK and BAX increased platelet half-life (Mason et al., 2007). However, other pro-survival proteins, namely BCL-2 and MCL-1, are dispensable for platelet survival as deletion in mice had no effect on platelet clearance (Debrincat et al., 2015). In nucleated cells, BCL-2 pro-survival proteins interact with BAK/BAX inhibiting their pro-apoptotic actions. In

response to pro-apoptotic signals, BH3-only pro-death proteins (e.g. BAD, BIM and BID) become activated and disrupt the interaction between BCL-2 pro-survival proteins and BAK/BAX, allowing BAK/BAX to become activated and initiate apoptosis (McArthur et al., 2018). Whether this canonical apoptotic pathway exists in platelets is yet to be fully elucidated. BAD knockout mice have increased platelet counts due to a mild but significant increase in platelet lifespan, but BIM knockout mice have no alteration in platelet count (Kelly et al., 2010). Also, whether this modest increase in platelet count and lifespan in BAD knockout mice is due to BAD actively signalling to BAK and/or BAK or due to decreased inhibition of BCL-X_L is unknown. Therefore, if BH3-only pro-death proteins are involved in the apoptotic pathway of platelets, the exact BH3-only pro-death proteins and combination in which they function are unknown. BAK/BAX-mediated apoptosis leads to the classical hallmarks of apoptosis in cells, i.e. mitochondrial damage, caspase activation, cytoplasmic condensation and PS exposure. Once platelets are apoptotic, it is presumed they are cleared by phagocytes of the mononuclear phagocyte system in both the liver and spleen (Grozovsky et al., 2015b). One may expect that desialyation of platelets triggers the intrinsic apoptosis pathway as both mechanisms lead to platelet clearance, however a clear link between platelet desialyation, platelet ageing and the triggering of platelet apoptosis remains unknown.

Platelets can also be cleared in an antibody dependant manner by macrophages primarily, but not exclusively, in the spleen. Immunoglobulin G (IgG) autoantibodies produced by the white pulp of the spleen bind to circulating platelets. The antibodies are mainly directed against the two most numerous membrane glycoproteins, namely integrin $\alpha_{IIb}\beta_3$ and the GPIbα subunit of the GPIb-V-IX complex. The slow movement of IgG bound platelets through splenic sinusoids allows association between the IgG Fc region and Fcγ receptors of macrophages. This binding initiates phagocytosis and destruction of platelets by the macrophages (Grozovsky et al., 2015b; Grozovsky et al., 2010).

The spleen acts as a filter for misshaped or irregular blood cells. This is evident as splenectomised patients are easily identified by their blood films which show red blood cells with membrane abnormalities (codocytes/target cells) and red blood cells containing remnants of nuclear material (Howell-Jolly bodies). The exact mechanism by which the spleen removes abnormal red blood cells is not known. Whether the spleen plays a role in thrombocytopenia seen in genetic disorders that cause the formation of abnormally shaped

platelets is also unknown. However, the early removal of platelets by the spleen has been implicated in twinfilin 2a knockout mice. These mice have thrombocytopenia due to the early removal of hyper-reactive platelets. Although the exact mechanism by which the spleen removes these hyper-active platelets has not been resolved, it is independent of macrophages. This is evident as macrophage depletion using clodronate liposomes had no effect on platelet counts, whereas splenectomy restored platelet counts to normal levels (Stritt et al., 2017).

1.8 Thrombocythaemia

Thrombocythaemia, also known as thrombocytosis, is defined as a circulating platelet count of above $450x10^9$/L in humans (see Table 1.2). The major cause of thrombocythaemia is reactive (secondary) thrombocythaemia which occurs secondary to many conditions such as infection, cancer and inflammation. Reactive thrombocythaemia is driven by elevated levels of cytokines that drives thrombopoiesis, for example TPO, IL-6 and IL-11 (Schafer, 2004).

1.8.1 Essential Thrombocythaemia

Thrombocythaemia due to acquired clonal mutations of HSCs is termed essential (primary) thrombocythaemia (ET). ET is a member of a family of diseases called Philadelphia chromosome negative myeloproliferative neoplasms (MPNs) along with polycythaemia vera (PV) and primary myelofibrosis (PMF). Diagnosis criteria of ET set by the World Health Organisation is one of exclusion. As well as sustained thrombocythaemia and increased bone marrow megakaryocytes, ET diagnosis is confirmed on exclusion of other MPNs, myeloid neoplasms or iron deficiency as the cause of the thrombocythaemia (Cervantes, 2011).

ET is a rare disease with a prevalence of around 30 per 100,000 people and an incidence rate of ≈2 per 100,000. The median age of diagnosis is 65 to 70 years but the age of onset is very wide (Briere, 2007).

1.8.1.1 Genetic causes

The work of many groups have identified acquired mutations that lead to an ET phenotype. The major mutations seen in ET affect the tyrosine kinase Janus Kinase 2, the endoplasmic reticulum chaperone, Calreticulin, and the TPO receptor gene *MPL*. Other genetic mutations have been elucidated, for example loss of function mutations of LNK which negatively regulates TPO/erythropoietin (EPO) signalling and mutations of CBL. Despite this work, approximately 10% of patients have ET of unknown cause (McPherson et al., 2017).

Janus Kinase 2

In 2005, four groups identified a mutation in exon 14 of *JAK2* that causes a substitution of valine for phenylalanine at amino acid 617 (JAK2 V617F), which is present in approximately 50% of ET and PMF cases and 90% of PV cases (Baxter et al., 2005; James et al., 2005; Kralovics et al., 2005; Levine et al., 2005). Allele burden is thought to determine how one mutation leads to multiple phenotypes, with lower burdens leading to ET. Most patients with PV are homozygous for JAK2 V617F whereas homozygosity is rare in ET patients (Scott et al., 2006). These results are paralleled by mouse models, where high mutant JAK2 levels caused a PV phenotype but lower mutant transgene levels resulted in an ET phenotype (Li et al., 2010; Tiedt et al., 2008).

JAK2 has two kinase domains, a canonical tyrosine kinase domain (JH1) paired in tandem with a pseudokinase domain (JH2). Under normal physiology, the JH2 interacts with and inhibits the JH1 domain in the absence of ligand binding. The JAK2 V617F mutation is located in the JH2 domain and prevents inhibition of JH1 by JH2. Therefore, JAK2 V617F causes continuous activation of JAK2 and downstream signalling independent of cytokine stimuli. However, in the heterozygous state of ET, TPO receptors are still responsive to growth factor binding and for full signalling binding is required (Spivak, 2017). Growth factor binding to JAK2 V617F bound receptors leads to increased and prolonged signalling. This upregulation of JAK2 signalling results in increased megakaryopoiesis seen by increased bone marrow MKs, increased proplatelet formation and thrombocythaemia. Beyond an increase of platelet numbers the JAK2 V617F mutation causes platelets to hyper-reactive to a range of agonists (Hobbs et al., 2013).

Calreticulin

Mutations in *CALR*, the gene that encodes calreticulin, are the second most common in MPNs. CALR has roles in glycoprotein folding and calcium homeostasis. Exome sequencing revealed that approximately 70% of ET patients with non-mutated *JAK2* carry *CALR* exon 9 mutations. *CALR* exon 9 mutations result in frameshifts producing CALR protein with a novel C-terminus with positive instead of negative charge (Klampfl et al., 2013; Nangalia et al., 2013). Mutated CALR is able to bind c-Mpl via c-Mpl's extracellular domain and chaperone it to the plasma membrane. Binding of mutant CALR to c-Mpl is presumed to causes structural changes in c-Mpl leading to activation of JAK2 and constitutive downstream signalling (Araki et al., 2016). CALR positive ET patients have a lower risk of thrombosis and increased overall survival compared to JAK2 V617F and MPL patients (McPherson et al., 2017).

MPL

Approximately 15% of JAK2 V617F negative ET patients have mutations in the *MPL* gene, mainly in exon 10 (primarily W515L/K). These mutations lead to constitutive activation of the JAK/STAT pathway seen by constitutive phosphorylation of JAK2, STAT3 and STAT5 in mutated cell lines (Pardanani et al., 2006; Pikman et al., 2006).

Platelet count	Disease		Cause/mutated gene
150-400 x10^9/L	None, normal platelet range		N/A
>450x10^9/L	Essential thrombocythaemia		JAK2 (≈50%), CALR (≈7-8%), MPL (≈35%), ≈10% unknown (McPherson et al., 2017).
	Reactive thrombocythaemia		Secondary to many conditions such as infection, cancer and inflammation, driven by elevated levels of thrombopoietic cytokines (TPO, IL-6 and IL-11) (Schafer, 2004).
<150 x10^9/L	Inherited thrombocytopenia	Thromobocytopenia associated with sitosterolaemia	ABCG5 (Berge et al., 2000)
			ABCG8 (Berge et al., 2000)
		ACTN1 related thrombocytopenia	ACTN1 (Murphy et al., 2016)
		Thrombotic thrombocytopenic purpura (TTP), Upshaw-Schulman syndrome	ADAMTS13 (Levy et al., 2001)
		ANKRD26-related thrombocytopenia	ANKRD26 (Noris et al., 2011)
		CYCS-related thrombocytopenia	CYCS (Morison et al., 2008)
		DIAPH1 related macrothrombocytopenia	DIAPH1 (Stritt et al., 2016)
		Thrombocytopenia 5 (THC5)	ETV6 (Zhang et al., 2015)
		Paris Trousseau type thrombocytopenia/Jacobsen (11q23 del)	FLI1 (Tunnacliffe et al., 1999)
		FLNA-related thrombocytopenia	FLNA (Nurden et al., 2011)
		Novel thrombocytopenia	FYB (Levin et al., 2015)
		GATA1 related disease	GATA1 (Nichols et al., 2000)
		Bernard-Soulier Syndrome (BSS)	GP1BA (Ware et al., 1990)
			GP1BB (Budarf et al., 1995)
			GP9 (Wright et al., 1993)
		GNE myopathy with congenital thrombocytopenia	GNE (Izumi et al., 2014)

		Amegakaryocytic thrombocytopenia with radio-ulnar synostosis	HOXA11 (Thompson and Nguyen, 2000)
		Glanzmann's thrombasthenia	ITGA2B (Burk et al., 1991)
			ITGB3 (Loftus et al., 1990)
		Thrombocytopenia with immunodeficiency	MKL1 (Record et al., 2015)
		Congentical amegakaryocytic thrombocytopenia	MPL (Ihara et al., 1999)
		MYH9 related disease	MYH9 (Spinler et al., 2015)
		Grey Platelet Syndrome	NBEAL2 (Gunay-Aygun et al., 2011)
		Bleeding disorder, platelet-type 19	PRKACG (Manchev et al., 2014)
		Thrombocytopenia with absent radii (TAR)	RBM8A (Albers et al., 2012)
		Familial platelet disorder and predisposition to AML	RUNX1 (Song et al., 1999)
		Novel thrombocytopenia	SLFN14 (Fletcher et al., 2015)
		Stormorken Syndrome	STIM1 (Picard et al., 2009)
		Mild novel thrombocytopenia (heterozygous)	THPO (Dasouki et al., 2013)
		TPM4-related macrothrombocytopenia	TPM4 (Pleines et al., 2017)
		TUBB1-related macrothrombocytopenia	TUBB1 (Kunishima et al., 2009)
		Von Willebrand disease type 2B	vWF (Cooney et al., 1991)
		Wiskott-Aldrich syndrome, X-linked thrombocytopenia (XLT)	WAS (Derry et al., 1994)
	Secondary thrombocytopenia		Secondary consequence in a number of diseases (cancers and infections), therapeutic treatments (chemotherapy) and autoimmunity.

Table 1.2 – Causes of thrombocythaemia and thrombocytopenia.

1.8.1.2 Treatment

The main complications of ET are arterial and venous thrombotic events. The incidence of these thrombotic complications in ET have been difficult to assess, however a review of the literature in 2005 by Elliot and Tefferi showed that arterial thrombotic events are more common than venous events. At presentation 10-25% of ET patients show major thrombosis with 80-90% of these being arterial thrombotic events. At follow up, the number of thrombotic events is similar to presentation statistics, but venous thrombotic events contributed to a greater proportion of the total thrombotic events (up to 37.5%) compared to presentation. The review by Elliot and Tefferi also highlighted that thrombotic events account for a significant proportion of deaths in ET patients, with up to 27.3% of patients ET patients dying from thrombotic events (in studies where multiple patients died) (Elliott and Tefferi, 2005). Despite this, survival rates are high in ET (80% at 15 years); and as such, the focus of therapeutic management in ET patients is primarily to prevent thrombotic events that cause significant morbidity without increasing the risk of bleeding. This is done by reducing platelet function and, in high risk patients, which make up the majority of ET patients as onset is usually above 60 years of age (see below), platelet numbers (Dombi et al., 2017). However, current therapies for high risk patients (section 1.8.1.2.1) are not platelet specific and therefore have a range of unwanted side effects.

Treatment of ET is based on the individual patient needs depending on their risk of thrombosis and/or bleeding. The three risk factors used to categorise patients into low risk and high risk are: patient's age ≥ 60 years, history of thrombosis or major bleeding and platelet count ≥ $1500x10^9$/L (Birgegard, 2016; Rumi and Cazzola, 2016).

Low risk patients are those with none of the three risk factors and receive no therapeutic treatment or low dose aspirin, depending on the genetic mutation which causes ET. All JAK2 V617F positive ET patients receive aspirin, whereas *CALR* positive, *MPL* positive and triple-negative patients may not be administered aspirin if they do not have other cardiovascular risk factors such as hypertension, diabetes or tobacco use (Rumi and Cazzola, 2016). Aspirin is used to reduce platelet function, due to its ability to inhibit COX by acetylating its active site, thus decreasing the formation of TxA2 from arachidonic acid (see section 1.1.6.5.2) (Patrignani

et al., 1982), and has been shown to reduce the incidence of venous thrombosis without increasing the risk of bleeding in JAK2 V617F positive patients (Alvarez-Larran et al., 2016).

High risk patients are those with 1-3 of the three risk factors. All high risk patients with a platelet count below $1500x10^9$/L will receive low dose aspirin, above this aspirin treatment is associated with a decrease of plasma vWF multimers and excessive bleeding times (van Genderen et al., 1997). High risk patients may also be administered cytoreductive agents.

1.8.1.2.1 Cytoreductive agents

The use of cytoreductive therapy in the treatment of high risk ET patients is dependant mainly on the patients' age. All patients over 60 years will be administered cytoreductive therapies whereas only 15 and 20% of patients are administered cytoreductive therapies if they are under 40 years or between 40-60 years, respectively. The requirement of cytoreductive therapies for patients under 60 years is based on fulfilment of 1 or both of the other two risk factors that group patients into high and low risk (Rumi and Cazzola, 2016).

The 3 main cytoreductive therapies used to treat ET are hydroxyurea, interferon-α and anagrelide.

Hydroxyurea

Hydroxyurea is used widely in the treatment of high risk ET patients as it effectively decreases platelets counts and prevents thrombotic events (Cortelazzo et al., 1995; Rumi and Cazzola, 2016). Hydroxyurea impairs DNA synthesis through inhibition of ribonucleotide reductase, which catalyses the formation of single DNA nucleotides from ribonucleotides. Impairment of DNA synthesis in MKs impedes maturation, decreasing platelet biogenesis and therefore lowering platelet counts (Tefferi et al., 2000). Impaired DNA synthesis impacts on other high turnover tissues, in particular the whole haematopoietic compartment and therefore other blood cytopenias are not uncommon.

Interferon-α

In 1957 Isaacs and Lindenmann discovered the first cytokine and named it Interferon (IFN) because of its ability to interfere with viral propagation (Isaacs and Lindenmann, 1957). The IFN-α family comprises 14 genes that encode 13 proteins. Binding of IFN-α proteins to their receptors on cell membranes (type I IFN receptors), activates receptor associated JAKs (Tyk2 and JAK1). Activation of these JAKs leads to STAT1/2 activation and translocation to the nucleus where they promote the transcription of IFN regulated genes (Kiladjian et al., 2008).

Although the exact mechanism by which IFN-α treatment decreases platelet counts in ET patients is yet to be elucidate, IFN-α has been shown to reduce the colony-forming ability of erythroid, granulocytic and megakaryocytic progenitors. Evidence from both *in vitro* and *in vivo* assays suggest IFN-α targets clonal progenitors preferentially to unaffected counterparts. Megakaryocyte biogenesis seems particularly sensitive to IFN-α treatment. IFN-α treated patients have decreased bone marrow MK numbers and MKs also have decreased size (Chott et al., 1990; Kiladjian et al., 2008).

IFN-α treatment is associated with a variety of side effects. Haematological effects include neutropenia, although this is rare in ET, and lymphopenia. Other side effects of IFN-α treatment include flu-like symptoms, fatigue, musculoskeletal pain and mood changes such as anxiety and depression (Kiladjian et al., 2008).

Anagrelide

Anagrelide was originally developed as an antiplatelet agent and its thrombocytopenic actions were observed during pre-clinical trials. It is the most platelet specific cytoreductive agent and has no effect on red or white blood cell lineage. It affects MK differentiation, decreasing MK ploidy and size but MK proliferation appears to be unaffected with normal bone marrow MK numbers. The platelet lowering action of anagrelide is mediated through its ability to decrease proplatelet formation and proplatelet complexity, possibly via phosphorylation of myosin II light chain (Birgegard, 2016; Espasandin et al., 2015)). Comparison of ET patients treated with anagrelide or hydroxyurea in combination with aspirin showed anagrelide treatment is more effective at reducing thrombotic events (Dombi et al., 2017).

The most common side effects of anagrelide treatment are tachycardia, headache, dizziness and diarrhoea and although common in the first weeks of treatment, they usually subside. Due to its tachycardic effects and worsening cardiac insufficiency in some patients, anagrelide treatment is used with caution in patients with a history of cardiac failure. Combination therapy with low dose aspirin increases the risk of haemorrhage and therefore should be used with caution in patients with previous bleeding episodes (Birgegard, 2016).

1.9 Thrombocytopenia

Thrombocytopenia is defined as a circulating platelet count below $150x10^9$/L. Thrombocytopenia is generally the consequence of decreased platelet production or increased platelet clearance. Like thrombocythaemia, thrombocytopenia can occur secondary to a number of diseases (such as cancer and infections), therapeutic treatments (such as chemotherapy) and autoimmunity, but it can also be inherited (Table 1.2).

1.9.1 Inherited causes

There are currently over 30 known genes whose mutations lead to thrombocytopenia (table 1.2). Many inherited thrombocytopenias affect cytoskeletal proteins, these will be discussed below.

MHY9-related disorders

Mutations in *MYH9* that encodes for non-muscle myosin heavy chain IIA (NMMHC-IIA) are responsible for *MYH9*-related disorders which encompass several autosomal-dominant diseases previously classified as May-Hegglin anomaly, Fechtner syndrome, Sebastian syndrome, or Epstein syndrome. All patients share the combination of macrothrombocytopenia and leukocyte inclusions (Döhle-like bodies). Despite the thrombocytopenia, platelet mass (thrombocrit) is unchanged, suggesting the thrombocytopenia is a result of terminal platelet formation in the periphery. *MYH9* mutations result in increased platelet myosin IIA phosphorylation and therefore inactivation. Increased

inactivation results in decreased fission of preplatelets, thus resulting in macrothrombocytopenia (Spinler et al., 2015).

Wiskott-Aldrich syndrome

Wiskott-Aldrich syndrome (WAS) is caused by mutations in the *WAS* gene located on chromosome X and is characterised by severe microthrombocytopenia, immunodeficiency and eczema (Derry et al., 1994). WAS protein (WASp) regulates actin assembly and prevents actin degradation in platelets by constitutive interaction with WASp-interacting protein (WIP). Interestingly, *WAS* mutated platelets have increased microtubule content, increased microtubules coils in the marginal band, altered microtubule organisation and increased microtubule stability. Surprisingly, this phenotype is recapitulated by condition megakaryocytic lineage knockout of the actin binding protein profilin 1 in mice. Profilin 1 localises to the microtubule marginal band in healthy resting platelets and re-localises to the cytoplasm upon microtubule disassembly, suggesting profilin 1 localisation is microtubule dependant. Platelets from WAS patients show mislocalisation of profilin 1, suggesting WASp modulates profilin 1 which regulates microtubule assembly (Bender et al., 2014).

Bernard-Soulier syndrome

Bernard-Soulier syndrome (BSS) is a severe bleeding disorder characterised by macrothrombocytopenia. BSS is caused by mutations in the GPIbα (Ware et al., 1990), GPIbβ (Budarf et al., 1995) or GPIX (Wright et al., 1993) subunits of the GPIb-V-IX vWF receptor complex. As discussed in section 1.1.5.2 mutations in the GPIb-V-IX complex cause reduced DMS maturation. GPIbα knockout murine MKs locate further from BM sinusoids, which may in part determine the thrombocytopenia observed in BSS (Dutting et al., 2017).

TUBB1-related thrombocytopenia

Mutations in *TUBB1* that encodes for β_1-tubulin results in macrothrombocytopenia with an absence or severely decreased marginal microtubule coil. Mutated β_1-tubulin failed to incorporate into microtubules in mouse foetal liver derived MKs, which resulted in decreased proplatelet formation with abnormal morphology (large bleb protrusions). This lack of

proplatelet formation due to decrease of microtubule formation is thought to confer the thrombocytopenia seen in patients with *TUBB1* mutations (Kunishima et al., 2009; Kunishima et al., 2014).

FLNA-related thrombocytopenia

FLNA encodes the actin cross-linking protein filamin A. Mutations in *FLNA* results in irregular sized platelets that are generally larger and rounder. *FLNA* mutant platelets have heterogeneous α-granule content with some large α-granules and murine *FlnA* knockout platelets have increased microtubules in the marginal microtubule coil. *FLNA* mutated MKs have impaired proplatelet formation and murine *FlnA* knockout proplatelets have increased tip size and increased platelet shedding. Thrombocytopenia in *FlnA* knockout mice is associated with increased platelet clearance (Begonja et al., 2011; Nurden et al., 2011).

ACTN1-related thrombocytopenia

ACTN1 encodes the rod shaped actin cross-linking protein actinin 1 (α-actinin). Currently 13 mutations in *ACTN1* have been identified and are linked with macrothrombocytopenia. *ACTN1* mutations cause disorganisation of the actin cytoskeleton in cell lines potentially due to increased binding of actinin 1 to F-actin causing increased actin bundling (Murphy et al., 2016).

TPM4-related thrombocytopenia

Tropomyosins (TPMs) form copolymers with actin filaments and have muscle and non-muscle (cytoskeletal) isoforms. Nonmuscle TPMs regulate the interaction of other actin-binding and myosin motor proteins to the actin firmaments. TPM4 is the major tropomyosin isoform present in MKs and platelets. Mutations in *TPM4* confer macrothrombocytopenia with the inclusion of large vacuoles. In human proplatelet forming MKs, TPM4 localises to proplatelets and co-localises with F-actin. Mutations in *TPM4* cause decreased proplatelet formation in human and murine MKs with aberrant morphology (decreased branching and tip size). *TPM4* mutations also effects many actin-binding proteins. Expression of both filamin A and actinin 1 are decreased in *TPM4* mutated platelets, NMMHC-IIA localisation in proplatelets is dysregulates and phosphorylation of cofilin is decreased in MKs and platelets, suggesting

increased actin turnover and indeed F-actin is decreased. This data suggest cytoskeletal defects are responsible for the macrothrombocytopenia (Pleines et al., 2017).

DIAPH1-related macrothrombocytopenia

DIAPH1 encodes diaphanous-related formin 1 (DIAPH1 or mDia1), which is known to stabilise and orientate microtubules. A heterozygous point mutation in *DIAPH1* results in a premature stop codon at amino acid 1213 (R1213*) and causes macrothrombocytopenia and hearing loss. Proplatelet formation is increased in cultured MKs in which *DIAPH1* had been knocked down by shRNA, but decreased when a constitutively active form of DIAPH1 is overexpressed, suggesting that activation of DIAPH1 inhibits proplatelet formation. DIAPH1 activation is regulated by interaction of two domains (diaphanous autoregulatory domain (DAD) and diaphanous inhibitory domain (DID)) that causes autoinhibition. DIAPH1 R1213* is likely to decrease the interaction of the DAD and DID domains and therefore decrease autoinhibition of DIAPH1. This is reflected by the fact that proplatelet formation is decreased in *in vitro* cultured MKs from patients harbouring the R1213* mutation. DIAPH1 also effects microtubule stability. DIAPH1 R1213* platelets have increased microtubules in the marginal coil compared to control and their microtubules do not disassemble at 4^{o}C. Increase tubulin stability is associated with increased detyrosinated (Glu) tubulin: tyrosinated (Tyr) tubulin ratio and DIAPH1 R1213* platelets show higher Glu-tubulin: Tyr-tubulin (Pan et al., 2014; Stritt et al., 2016).

2

Aims

As described in section 1.8.1.1, ET is caused by mutations in mainly *JAK2*, *MPL* and *CALR* and results in a chronic increase of platelet numbers. Treatment of ET patients at high risk of thrombotic and/or bleeding events relies on cytoreductive therapies that have unwanted haematological side effects (Cervantes, 2011). An ideal therapy would normalise platelet numbers whilst having minimal side effects, especially those relating to the haematopoietic system.

This thesis is split into 3 sections, with the overall aim of showing that a cytokine receptor-like factor 3 (CRLF3) could be a novel therapeutic target for the treatment of thrombocythaemia (including cases of reactive thrombocythaemia). This thesis focusses specifically on the platelet lowering effect of CRLF3 in ET as murine models of ET were freely available and have been extensively studied. We will use a *Crlf3* knockout mouse (*Crlf3*$^{-/-}$) developed by the Wellcome Trust Sanger Institute that have an isolated platelet phenotype (see section 4.1.2 for more details). In the first section of the thesis we have two main aims: firstly, to determine whether ablation of *Crlf3* results in an isolated and sustained thrombocytopenic phenotype and secondly, to determine the biological mechanisms underlying the observed thrombocytopenia.

In the second section of the thesis we cross the *Crlf3*$^{-/-}$ mice with a JAK2 V617F knock-in mouse that has a phenotype similar to that of JAK2 V617F positive ET patients (see section 5.1 for more details). The main aim of this section is to determine whether CRLF3 could be a potential novel therapeutic target for the treatment of ET.

In the final section of this thesis we look at the structure and function of CRLF3. Firstly, we aim to resolve the 3D structure of CRLF3 by X-ray crystallography. We then go on to tag endogenous *CRLF3* in human induced pluripotent stem cells (iPSCs). We forward programme these tagged iPSCs into MKs and the final aim of the thesis is to determine the interactome of CRLF3 in these MKs, which should help uncover the function of CRLF3 in MKs.

3

Materials and methods

3.1 Generation of *Crlf3* mutant mice

Generation of *Crlf3* mutant mice was performed by the Wellcome Trust Sanger Institute (WTSI) as part of an international consortium (www.knockountmouse.org) as previously reported (Ryder et al., 2013; Skarnes et al., 2011; White et al., 2013). Briefly, a mutant *Crlf3*$^{tm1a(KOMP)Wtsi}$ allele was created by insertion of a lacZ-neo cassette upstream of *Crlf3* exon 2 and loxP sites upstream and downstream of exon 2 into ES cells using standard cloning techniques (fig. 3.1A). The ES clone EPD0033_3_C11 was selected on the basis of neomycin resistance and β-galactosidase expression, confirming *Crlf3*$^{tm1a(KOMP)Wtsi}$ allele expression. Mice were generated according to standard techniques and after germline transmission of the *Crlf3*$^{tm1a(KOMP)Wtsi}$ allele, exon 2 of *Crlf3* was excised by cre-mediated recombination by crossing with *Hprt*$^{Tg(CMV-cre)Brd}$ mice, producing the mutant *Crlf3*$^{tm1b(KOMP)Wtsi}$ allele (fig. 3.1B). After confirmation of allele conversion, mice carrying the *Crlf3*$^{tm1b(KOMP)Wtsi}$ allele were backcrossed to eliminate the cre transgene, generating *Crlf3*$^{+/-}$ mice.

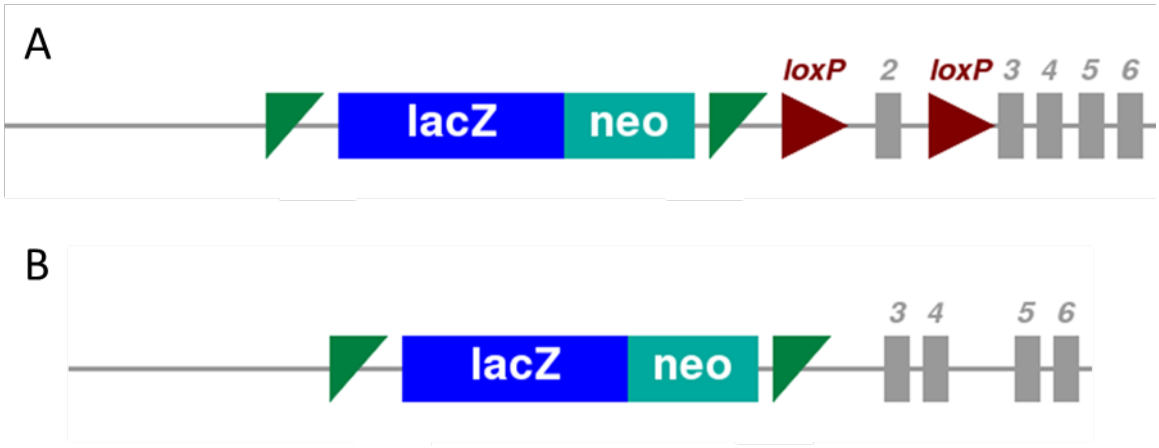

Figure 3.1 Generation of *Crlf3* mutant mice. A) Production of the mutant *Crlf3*$^{tm1a(KOMP)Wtsi}$ allele by insertion of a lacZ-neo cassette upstream of *Crlf3* exon 2 and loxP sites upstream and downstream of exon 2 in ES cells by standard cloning technique. B) Cre-recombination in mutant mice excises *Crlf3* exon 2, creating the mutant *Crlf3*$^{tm1b(KOMP)Wtsi}$ allele.

3.2 Genotyping

For *Crlf3*$^{-/-}$ and WT mice, genotyping of mice was performed by PCR of genomic (g) DNA with specific primers (table 3.1 and 3.12). gDNA was produced from mouse ear notches using PureLink Genomic DNA Mini Kit (Invitrogen). PCR products were resolved by electrophoresis on a 1.5% agarose TBE (100mM Tris base, 100mM boric acid, 2mM EDTA) gel supplemented

with 5µl/ml DNA SafeView (NBS Biologicals Ltd). *Crlf3* mutant (*Crlf3*$^{tm1b(KOMP)Wtsi}$) alleles produced bands of 159bp and wildtype alleles produced bands of 281bp.

For crossbred mice used in chapter 4, genotyping was performed as above for *Crlf3* mutant and *Crlf3* WT alleles. For *Jak2* WT, *Jak2* mutant and Mx1Cre alleles, genotyping was performed as per *Crlf3* alleles using primers described in Li et al. (2010).

Primer	Sequence (5'>3')
*Crlf3*_F	TGGATACATTGATTAGCTTGACAGA
*Crlf3*_R	AGGGGATGAGAGGGTCTTCAG
Cassette_R	TCGTGGTATCGTTATGCGCC

Table 3.1 – Primers used to genotype *Crlf3* WT and *Crlf3* mutant alleles

3.3 Mouse husbandry and regulated procedures

Mice were housed in pathogen free conditions at Central Biomedical Services (University of Cambridge, Cambridge, UK) and cared for by staff. This research has been regulated under the Animals (Scientific Procedures) Act 1986 Amendment Regulations 2012 following ethical review by the University of Cambridge Animal Welfare and Ethical Review Body (AWERB). Experiments were performed under Project Licence 70/8406 (formerly 80/2376) by trained, Personal Licence (PIL) holders. Experiments carried out at the University of Würzburg (Würzburg, Germany) in collaboration with the group of Professor Bernhard Nieswandt were approved by the district government of Lower Franconia (Bezirksregierung Unterfranken). Power analysis was performed using a Type I error rate (α) of 5% and 80% power based on the results of preliminary experiments. These analyses determined few mice (3-6 per genotype per experiment) would be required to detect significant outcomes.

3.4 Induction of mutant *Jak2* expression

Two to three day-old mice were injected subcutaneously with sterile polyinosinic-polycytidylic acid (pIpC; Sigma-Aldrich) to induce Cre recombinase expression. All mice were injected with 50µL pIpC (3mg/mL in PBS, 150µg/dose) every other day for a total of 4 injections.

3.5 Bleeding mice

Mice were bled via the tail vein or the inferior vena cava (IVC), unless otherwise stated. For tail vein bleeds, mice were heated at 38-40^{o}C for 10-15 minutes in a heat box. The tail vein of heated mice was punctured with a sterile scalpel blade and up to 200µL blood was collected in EDTA coated Microvette® tubes (Sarstedt). For IVC bleeds, mice were killed by exposure to increasing volumes of carbon dioxide. Once death had been confirmed, up to 1ml blood was withdrawn from the IVC using a 25G needle and 1ml syringe into 100µl 0.5M EDTA, 1,000U/ml heparin or acid citrate dextrose (ACD; 111mM glucose, 71mM citric acid, 116mM sodium citrate) to prevent coagulation.

3.6 Full blood counts

Full blood counts were recorded using a Scil Vet ABC animal blood analyser (Woodley), using blood collected into EDTA.

3.7 Platelet rich plasma and washed platelets

Platelet rich plasma (PRP) was made by diluting whole blood with 1.5 volumes Tyrode's buffer (134mM sodium chloride, 2.9mM potassium chloride, 0.34mM sodium phosphate dibasic, 12mM sodium bicarbonate, 20mM HEPES, 1mM magnesium chloride, 5mM glucose, pH 7.3) and centrifuging at 100*g* for 10 minutes. The top yellowish layer (PRP) was collected, being careful to avoid the white buffer coat.

Washed platelets were prepared by adding 50ng/ml Prostaglandin E_1 (PGE_1; Caymen Chemical Company) and 0.5U/ml apyrase (Sigma-Aldrich) to PRP and centrifuging at 1,000*g* for 10 minutes. The platelet pellet was resuspended in Tyrode's buffer supplemented with 50ng/ml PGE_1 and 0.5U/ml apyrase and centrifuged at 1,000*g* for 10 minutes. Washed platelets were resuspended as desired.

3.8 *In vitro* culture of bone marrow derived MKs

Tibia and femurs were removed from culled mice and stored on ice. Bone marrow was removed by flushing tibia and femurs with Dulbecco's modified Eagle medium (DMEM; PAA laboratories) supplemented with 10% BSA (Biosera), 2mM L-glutamate (PAA Laboratories) and 100U/ml penicillin/streptomycin (pen/strep; PAA Laboratories) and pelleted at 200*g* for 5 minutes. Red cells were lysed by incubation with ACK (150mM ammonium chloride, 1mM potassium bicarbonate, 0.1mM EDTA, pH 7.3) and cells pelleted again. Pelleted cells were incubated with antibodies against mouse CD11b, Ly6G, CD45R and CD16/CD32 (table 3.2 and 3.13) for 30min at 4^{o}C and leukocytes removed with magnetic beads against rat IgG (Invitrogen). Remaining cells enriched in blood progenitors were again pelleted, washed in supplemented DMEM and finally cultured in CellGRO SCGM (Cellgenix) supplemented with 100U/ml pen/strep and 50ng/mL (unless stated) recombinant murine TPO (PepreoTech) for 4-5 days at 37^{o}C under 5% CO_2 in a humidified incubator.

MKs were purified by pelleting cells at 120*g* and resuspending in 4ml PBS (PAA Laboratories). Resuspended cells were layered on to an 8ml 1.5/3% BSA gradient and resolved at 1*g* for 45 mins. The bottom 2ml MK fraction was collected, washed with PBS and pelleted at 120*g* for 5 minutes. MKs were resuspended as needed.

Antibody	Clone	Manufacturer
Biotin Rat anti-mouse CD11b	M1/70	eBioscience
Rat anti-mouse Ly-6G (Gr-1)	RB6-8C5	eBioscience
Rat anti-mouse CD16/CD32	2.4G2	BD Pharmigen
Biotin Rat anti-mouse CD45R/B220	RA3-6B2	BD Pharmigen

Table 3.2 – Antibodies used for *in vitro* culture of bone marrow derived MKs

3.9 Quantitative polymerase chain reaction

RNA was extracted from purified *in vitro* cultured MKs (section 3.8) using RNeasy plus mini Kit (Qiagen). Complementary (c) DNA was made using SuperScipt III First Strand Kit (Invitrogen) starting from 100ng total RNA and using oligo-dT as reverse transcription primers. Quantitative polymerase chain reaction (qPCR) of the murine genes *Crlf3* and *Gapdh* was carried out using specific primers that had previously been tested for optimal efficiency (table

3.3 and 3.12), Brilliant II SYBR green chemistry (Agilent Technologies) and Mx3000P Real-Time PCR system (Stratagene). The analysis of gene expression was performed by the Δ Ct method, where:

$\Delta Ct = Ct_{\text{target gene (}\textit{Crlf3}\text{)}} - Ct_{\text{housekeeping gene (}\textit{Gapdh}\text{)}}$

Relative gene expression was expressed as $2^{-\Delta Ct}$.

Primer	Sequence (5'>3')
*Crlf3*_F_qPCR	GGGTGTTCTCTACTCCAGCG
*Crlf3*_R_qPCR	GCCATTCTGCCTTTCTGCAC
*Gapdh*_F_qPCR	CCCTTAAGAGGGATGCTGCC
*Gapdh*_R_qPCR	TACGGCCAAATCCGTTCACA

Table 3.3 – Primers used for qPCR

3.10 Western blot

Purified *in vitro* cultured MKs (section 3.8) or washed platelets (section 3.7) were lysed in RIPA buffer (150mM sodium chloride, 60mM Tris pH 8.0, 0.6% w/v sodium deoxycholate, 0.1% w/v sodium dodecyl sulfate, 1% v/v NP-40). Samples were diluted 1:1 with 2x Laemmli sample buffer (125mM Tris pH 6.8, 20% v/v glycerol, 4% w/v sodium dodecyl sulfate, 10% v/v β-mercaptoethanol, 0.002% w/v bromophenol blue) and incubated at 95°C to denature proteins. Proteins were resolved on 4-12% Bis-Tris NuPAGE gradient gels (Invitrogen), transferred to PVDF membrane (Millipore) that had been soaked in 100% methanol for 5 minutes then washed in ultrapure water using a Trans-Blot SD Semi-Dry Transfer Cell (Bio-Rad) for 1 hour at 90mA. Membranes were then blocked for >2 hours in 5% non-fat milk (Sigma-Aldrich) in TBS-T (20mM Tris, 137mM sodium chloride, 0.1% Tween-20, pH 7.6) or Odyssey Blocking Buffer (LI-COR). Post block membranes were immunoblotted with primary antibodies (table 3.4 and 3.13) overnight at 4°C, then washed with TBS-T or Odyssey Blocking Buffer and then incubated with the appropriate secondary antibodies (table 3.5 and 3.13) TBS-T or Odyssey Blocking Buffer supplemented with 0.1% Tween-20 in for 1 hour at RT in the dark. Membranes were then washed with TBS-T or Odyssey Blocking Buffer supplemented with 0.1% Tween-20, before proteins were detected by enhanced chemiluminescence (HRP conjugated) or imaged with Odyssey Fc OFC-1095 version 1.0.36 imaging system (LI-COR; IRDye® 680RD and IRDye® 800CW conjugated). Expression was quantified using Image Studio Lite (https://www.licor.com/bio/products/software/image_studio_lite).

Antibody	Clone	Manufacturer
anti-β-actin produced in mouse	AC-15	Sigma-Aldrich
Rabbit anti-human CRLF3	polyclonal	Atlas antibodies
Rabbit anti-human GAPDH	14C10	Cell Signalling Technology
anti-Detyrosinated tubulin produced in rabbit	polyclonal	Millipore
anti- tyrosine tubulin produced in mouse	TUB-1 A2	Sigma-Aldrich
Biotinylated Ricinus Communis Agglutinin I (RCA-I)	n/a	Vector Laboratories
Rabbit anti-human Integrin beta 1	polyclonal	Abcam

Table 3.4 – Primary antibodies used for western blot

Antibody	Manufacturer
HRP Sheep anti-mouse IgG	GE Healthcare
HRP donkey anti-rabbit IgG	GE Healthcare
Streptavidin HRP	Cell Signalling Technology
IRDye 800CW Donkey anti-rabbit IgG	LI-COR
IRDye 800CW Goat anti-mouse IgG	LI-COR
IRDye 680LT Goat anti-rabbit IgG	LI-COR
IRDye 680LT Donkey anti-mouse IgG	LI-COR

Table 3.5 – Secondary antibodies used for western blot

3.11 Quantification of MKs in bone marrow

Tibia and humeri were removed and fixed in 10% neutral buffered formalin solution (Sigma-Aldrich) and processed by the Department of Pathology, University of Cambridge, Cambridge, UK or the Histopathology Team, WT-MRC Stem Cell Institute, University of Cambridge, Cambridge, UK as described elsewhere (Guerrero et al., 2014). Briefly, fixed tissue was embedded in paraffin and sections cut, deparaffinised and rehydrated. Sections were then stained with Haematoxylin and Eosin stain. After staining, images were acquired using an Axiovert 40 CFL microscope and AxioVision 40 version 4.8.2.0 software (both Zeiss) and MKs blindly quantified manually by myself or José Guerrero (University of Cambridge, Cambridge, UK).

3.12 Plasma thrombopoietin

Plasma thrombopoietin (TPO) assays were performed by José Guerrero (University of Cambridge, Cambridge, UK). Plasma was collected by centrifugation of whole blood

withdrawn from the IVC at 6,000rpm. Plasma TPO concentrations were determined by following the manufacturer's instructions of a commercially available ELISA kit (Mouse Thrombopoietin Quatikine ELISA Kit; R&D systems).

3.13 Ploidy analysis

Purified MKs (section 3.8) were fixed in 70% ethanol at -20^{o}C for >24h after BSA gradients. Fixed MKs were washed in PBE (0.3% BSA, 0.5mM EDTA in PBS) and then stained with fluorescently labelled antibodies against CD41 (FITC Rat anti-mouse CD41, clone MWReg30; BD Pharmigen) for 15 mins in the dark. MKs were again washed in PBE and resuspended in ploidy stain buffer (PBE supplemented with 32.5µg/mL propidium iodide, 0.025mg/mL RNase A and 0.1% v/v Tween (all Sigma-Aldrich)) and incubated at 37^{o}C for 30 mins in the dark. Ploidy of CD41^{+} events were analysed by flow cytometry using a CyAN flow cytometer and Kaluza Analysis version 1.5a software (both Beckman Coulter).

3.14 *In vitro* proplatelet formation

Purified MKs (section 3.8) were resuspended in culture medium supplemented with 100U/mL heparin sodium (Wockhardt UK Ltd) and seeded onto glass coverslips coated with 20ng/ml fibrinogen (Enzyme Research). Cells were incubated at 37^{o}C under 5% CO_2 for either 3 or 5 hours. Attached MKs were fixed with 10% neutral buffered formalin solution and washed in PBS. Fixed MKs were stained for and imaged by confocal microscopy using the 20x objective as per section 3.24 with primary antibodies against CD41 (Rat anti-mouse CD41, clone MWReg30; BioLegend), appropriate fluorescent secondary antibodies (Alexa Flour 488 Goat anti-rat IgG; Invitrogen), a fluorescently labelled F-actin probe (Alexa Flour 555 Phalloidin; Invitrogen) and the nuclear stain DAPI (Sigma-Aldrich). Proplatelet forming MKs were counted against the total number of MKs to calculate the percentage of proplatelet forming MKs using confocal microscopy. At least 460 MKs were counted for each condition.

3.15 *In vivo* proplatelet formation

In vivo proplatelet formation experiments were performed by Ayesha Baig (University of Würzburg, Würzburg, Germany). Briefly, mice were anaesthetised with triple narcotics ((Midazolam [5 µg/g body weight] (Pfizer), Medetomidine [0.5 µg/g body weight] (Roche), Fentanyl [0.05 µg/g body weight] (Janssen-Cilag))) and a 1cm incision was made along the midline to expose the frontoparietal skull while carefully avoiding damage to the bone tissue. The mouse was placed on a customized metal stage equipped with a stereotactic holder to immobilize its head. Bone marrow vasculature was visualized by injection of tetramethylrhodamine dextran (Molecular Probes) and rat anti-CD105 alexa fluor 594 (clone MJ17/18; Biolegend) (table 3.12). Platelets and MKs were antibody-stained (Alexa Flour 488 Rat anti-mouse GPIX, clone Xia.B4; Emfret Analytics) (table 3.12). Images were acquired every 5 minutes with a fluorescence microscope equipped with a 20x water objective with a numerical aperture of 0.95 and a TriM Scope II multiphoton system (LaVision BioTec), controlled by ImSpector Pro-V380 software (LaVision BioTec). Emission was detected with HQ535/50-nm and ET605/70-nm filters. A tuneable broad-band Ti:Sa laser (Chameleon, Coherent) was used at 760nm to capture Alexa F488 and rhodamine dextran fluorescence. ImageJ software (NIH) was used to generate movies.

3.16 Platelet survival

Mice were injected with 1mg biotin N-hydroxysuccinimide ester (NHS-Biotin; Sigma-Aldrich) dissolved in 250µL 20% dimethyl sulfoxide (DMSO; Sigma-Aldrich) in PBS into the tail vein (injections performed by Dean Pask). Injected and uninjected control mice were bled from the tail vein 24, 48, 72, 96 and 168 hours post injection into EDTA-coated Microvette® tubes (Sarstedt). Cells were washed and incubated with fluorescently labelled antibodies against CD41, Ter-119 and streptavidin (table 3.6 and 3.13). The percentage of biotinylated platelets at each time point was determined by flow cytometry as the percentage of $CD41^+$/$Ter\text{-}119^-$ events that were streptavidin positive.

Antibody	Clone	Manufacturer
FITC Rat anti-mouse CD41	MWReg30	BD Pharmigen
APC Streptavidin	n/a	BD Pharmigen

PE Rat anti-mouse TER-119	TER-119	BD Pharmigen

Table 3.6 – Antibodies used for platelet survival

3.17 Splenectomy

Splenectomies were performed by Simon Stritt (University of Würzburg, Würzburg, Germany). Briefly, the surgical site on anesthetized mice (triple narcotics (as per section 3.15)) was sterilely prepared and a 1cm incision was made. After the spleen was identified, blood supply was stopped by ligation of vascular pedicles and the spleen was removed. Mice were monitored for 48 hours for signs of internal bleeding and infection. After a recovery period of 6 days, platelet counts and size were followed over time by flow cytometry. Mice were then bled from the retro-orbital plexus every 7 days to determine platelet and preplatelet counts. Platelet counts were determined on a FACSCalibur (BD Biosciences) using fluorescently labelled antibodies against GPV (FITC Rat anti-mouse GPV, clone DOM2; Emfret Analytics) and GPIIbIIIa (PE Rat anti-mouse GPIIb/IIIa, Leo.F2; Emfret Analytic).

3.18 Preplatelet quantification

Method was adapted from (Thon et al., 2012a). Briefly, whole blood was diluted 1:20 in Tyrode's buffer (section 3.7) supplemented with 2U/ml heparin. Diluted blood was incubated with antibodies against GPV and GPIIb/IIIa (section 3.17). Preplatelets were determined by flow cytometry using a FACSCalibur and CellQuest™ software (BD Biosciences) as $GPV^+/GPIIbIIIa^+$ events that have larger forward /sideward scatter characteristics than normal platelets. To exclude the possibility preplatelets could be platelet microaggregates, heparinised diluted blood was incubated with antibodies against activated GPIIbIIIa (PE rat anti-mouse GPIIb/IIIa, clone JON/A; Emfret Analytics) and CD62P (FITC rat anti-mouse CD62P, clone Wug.E9; Emfret Analytics) and assessed by flow cytometry as above.

3.19 Bone Marrow Transplants

Donor mice were culled and tibia collected. Bone marrow cells were flushed into 2% foetal bovine serum (FBS; Gibco) in PBS and made into a single cell solution by repeated passes

through a 25 gauge needle then passing through a 70µm cell strainer (BD Falcon). Recipient mice were sub lethally irradiated with a split dose of 4.75Gy and injected with $5x10^6$ donor cells in 200µL 2% FBS/PBS via the tail vein (irradiation and tail vein injections performed by Dean Pask, University of Cambridge, Cambridge, UK). Irradiated mice were treated with oral antibiotics for 7 days (Bayrtil (2.5% enrofloxacin); Bayer). Mice were bled from the tail vein and full blood counts performed.

3 months post-transplant, mice were culled by cervical dislocation, tibia and femurs removed and MKs cultured as per section 3.8. Chimerism was determined by western blot of purified MKs with primary antibodies against CRLF3 and GAPDH (table 3.4 and 3.13) and appropriate secondary antibodies (table 3.5 and 3.13) following the method described in section 3.10.

3.20 Platelet surface receptor expression

ACD (section 3.5) anticoagulated whole blood was diluted 1:10 with HBS (150mM sodium chloride, 5mM potassium chloride, 1mM magnesium sulphate, 10mM HEPES, pH 7.4) and incubated with antibodies against CD41, CD61, CD42a, CD42d, CD49b, GPVI, FITC IgG or PE IgG (table 3.7 and 3.13) individually for 20 minutes. Blood was then further diluted 1:10,000 in 0.2% formyl saline (0.2% formalydehyde (Sigma-Aldrich), 0.85% sodium chloride) to fix platelets. Mean fluorescence intensity (MFI) was assessed by flow cytometry using a Gallios flow cytometer (Beckman Coulter) and Kaluza Analysis version 1.5a software. Staining of the antibodies was confirmed to be specific by gating against the appropriately labelled IgG isotype control.

Antibody	Clone	Manufacturer
PE Mouse anti-human CD42a	ALMA.16	BD Pharmigen
FITC Rat anti-mouse CD49b	Sam.G4	Emfret Analytics
FITC Rat anti-mouse GPVI	JAQ1	Emfret Analytics
FITC hamster anti-mouse CD61	2C9.G3	eBioscience
PE hamster anti-mouse CD42d	1C2	eBioscience
PE Rat anti-mouse IgG1, κ Isotype Control	n/a	BD Pharmigen
FITC Rat anti-mouse IgG1, κ Isotype Control	n/a	BD Pharmigen

Table 3.7 – Antibodies used for platelet surface receptor expression

3.21 Platelet activation

ACD (section 3.5) anticoagulated whole blood was diluted 1:10 with HBS (section 3.20) and incubated with fluorescently labelled antibodies against P-Selectin, fibrinogen and CD41 (table 3.8 and 3.13) and either no agonist, EDTA, thrombin, Gly-Pro-Arg-Pro (GPRP), ADP (all Sigma-Aldrich) or collagen related peptide (CRP; Department of Biochemistry, University of Cambridge) for 20 minutes. Blood was then further diluted 1:10,000 in 0.2% formyl saline (section 3.20) to fix platelets. P-Selectin surface expression on and fibrinogen binding to $CD41^+$ events was assessed by flow cytometry using a Gallios flow cytometer and Kaluza Analysis version 1.5a software.

Antibody	Clone	Manufacturer
APC Rat anti-mouse CD41	MWReg30	eBioscience
PE Rat anti-mouse P-selectin (CD62P)	Wug.E9	Emfret analytics
FITC Rabbit anti-human Fibrinogen	polyclonal	DakoCytomation

Table 3.8 – Antibodies used for platelet activation

3.22 Platelet spreading

Washed platelets were resuspended in Tyrode's buffer (section 3.7) at a concentration of $1x10^5$/µl and allowed to rest at 30°C for >30 minutes. 2mM Ca^{2+} and 0.01U/ml thrombin (Sigma-Aldrich) was added to the rested platelets, which were then immediately placed on a glass coverslip coated with 100ng/ml fibrinogen (Enzyme Research) and incubated at 37°C for 45 minutes. Attached platelets were fixed to the coverslip using 10% neutral buffered formalin solution. Fixed platelets were stained for and imaged by confocal microscopy as per section 3.24 with a fluorescently labelled F-actin probe (Alexa Flour 555 Phalloidin; Invitrogen). Average platelet area was determined by thresholding of F-actin expression using ImageJ software.

3.23 *In vitro* Thrombus formation

Channels of a Vena8 Fluoro+ Biochip (Cellix) were pre coated with HORM Collagen (Takeda) and subsequently blocked with Tyrode's buffer (section 3.7) supplemented with 2mM Ca^{2+}

and 0.1% w/v bovine serum albumin (BSA; Sigma-Aldrich). Tyrode's buffer supplemented with 2mM Ca^{2+} was then flowed through the channel at 400µl/min to linearize the HORM collagen. Whole blood anticoagulated in heparin was then flowed at 40µl/min (1,000s^{-1}) for 3 minutes. The channel was washed with Tyrode's buffer supplemented with 2mM Ca^{2+} to remove unbound blood cells. Five images per channel were taken using an EVOS fl microscope and an AMG camera. The area of each thrombus was measured using ImageJ software.

3.24 Platelet morphology

Blood smears were created by pushing 5µL whole blood across a microscope slide and leaving to air dry overnight. Blood smears were then stained with Rapid Romanowsky staining kit (TCS biosciences) following the manufacturer's instructions.

To assess platelet morphology by confocal microscopy, blood smears were washed with 50mM ammonium chloride to remove red cells, then remaining cells were permeabilised with PBS containing 0.1% w/v saponin and 0.2% w/v gelatin (both Sigma-Aldrich). Samples were incubated with primary antibodies against CD41 (Rat anti-mouse CD41, clone MWReg30; BioLegend) and von Willebrand Factor (vWF) (Rabbit anti-human von Willebrand Factor; DakoCytomation) in saponin-gelatin-PBS for 1 hour at room temperature. Samples were washed with saponin-gelatin-PBS before incubating with appropriate secondary antibodies (Alexa Flour 488 Goat anti-rat IgG or Alexa Flour 555 Goat anti-rabbit IgG; both Invitrogen) in saponin-gelatin-PBS for 1 hour at room temperature in the dark. Samples were again washed in saponin-gelatin-PBS before glass coverslips were mounted using hydromount (National Diagnostics) and images were acquired using a Leica Sp5 inverted confocal microscope with the 63x immersion-oil objective and the Leica LAS 2.1 software.

3.25 Electron microscopy

For transmission electron microscopy (TEM), washed platelets were resuspended in 0.85% sodium chloride (Sigma-Aldrich), diluted 1:1 with 0.4% glutaraldehyde in 0.1M sodium cacodylate pH 7.4 (gift from Cambridge Advanced Imaging Centre, University of Cambridge, Cambridge, UK) and incubated at room temperature for 2 hours. Platelets were then pelleted at 1,000*g*, resuspended in fixation buffer (2% glutaraldehyde, 2% formaldehyde, 0.05M

sodium cacodylate, pH 7.4; gift from Cambridge Advanced Imaging Centre) and incubated at 4°C for 4-6 hours. Fixed platelets were then processed by Jeremy Skepper (Cambridge Advanced Imaging Centre). Briefly, platelets were incubated serially in buffers containing 1% osmium tetroxide and 1.5% potassium ferricyanide, 1% thiocarbohydrazide, 2% osmium tetroxide and finally 2% uranyl acetate. Samples were then dehydrated in an ascending series of ethanol solutions from 50% to 100%, followed by treatment with dry acetonitrile and infiltration with Quetol epoxy resin. Sections were cut at 60nm using a diamond knife with a Leica UCT ultramicrotome. Sections were viewed using an FEI Tecnai G2 TEM and images captured with an AMT XR60B camera using Deben software.

For scanning electron microscopy (SEM), washed platelets were resuspended in 0.85% sodium chloride, diluted 1:1 with 0.4% glutaraldehyde in 0.1M sodium cacodylate pH 7.4 and incubated at room temperature for 2 hours. Platelets were then pelleted at 1,000*g*, resuspended in fixation buffer (as above) and stored at 4°C until processed. Fixed platelets were then processed by Jeremy Skepper (Cambridge Advanced Imaging Centre). Briefly, platelets were rinsed in deionised water (DIW) and incubated in 1% osmium ferricyanide for 4 days, rinsed again in DIW and incubated in 2% uranyl acetate in 0.05M Maleate buffer (pH 5.5) for 4 days at 4°C. Platelets were resuspended in DIW and attached to poly-L-lysine coated glass cover-slips for 30 minutes in a humid chamber so no air drying occurred. After unattached platelets were removed, samples were quench frozen in melting propane cooled in liquid nitrogen, then dried overnight in a Quorum K775 freeze dryer. The dry cover-slips were attached to 13mm Cambridge SEM stubs with colloidal silver DAG sputter coated with 10 nm of iridium and viewed in an FEI Verios 460L using a secondary electron detector and images were recorded as tiff files.

3.26 Platelet cytoskeleton at 37°C and 4°C

Experiments were performed by Simon Stritt (University of Würzburg, Würzburg, Germany). Briefly, PRP was prepared and adjusted to $3x10^5$ platelets/µL with Tyrode's buffer (section 3.7). PRP was incubated at 37°C or 4°C for 3 hours then attached to poly-L-lysine (Sigma-Aldrich) coated coverslips and fixed with PHEM buffer (60 mM PIPES, 25 mM HEPES, 10 mM EGTA, 2 mM magnesium chloride, pH 6.9) supplemented with 4% paraformaldehyde (PFA) and 1% IGEPAL CA-630 (both Sigma-Aldrich), stained with fluorescent antibodies against α-

tubulin (Mouse anti-α-tubulin-Alexa 488, clone B-5-1-2; Invitrogen) and a fluorescently labelled F-actin probe (phalloidin-Atto647N; Attotec) and mounted with Fluoroshield (Sigma-Aldrich). Samples were visualised using a Leica TCS SP5 confocal microscope controlled by LAS AF software (Leica Microsystems).

3.27 Cloning *Crlf3* constructs into pGEX vector

Crlf3 constructs (see section 6.4.1.1 and fig. 6.2 for details) were amplified from murine *in vitro* cultured MK cDNA by PCR using specific primers that include the BamHI or NotI restriction sites (table 3.9 and 3.12) and Platinum High Fidelity Taq Polymerase (Invitrogen) following manufacturer's instructions. PCR products were resolved on a 1.5% agarose TAE (40mM Tris, 20mM acetic acid, 1mM EDTA) gel and specific bands extracted and purified using QIAquick Gel Extraction Kit and QIAquick PCR Purification Kit (both QIAGEN). Purified PCR products were digested for 1 hour at 37°C with NotI and BamHI (both New England Biolabs). Vector pGEX-6P-2 (GE Healthcare) was also digested with NotI and BamHI then resolved on a 1.5% agarose TAE gel, the resulting open plasmid vector extracted and cleaned as above. The *Crlf3* PCR fragments were subsequently ligated into the open pGEX-6P-2 vector using T4 Ligase (New England Biolabs) following manufacturer's instructions (see fig. 6.1 for vector map). pGEX vectors containing *Crlf3* constructs were transformed into BL21-CodonPlus™-(DE3)-RP competent *E.coli* cells (Stratagene) following manufacturer's instructions.

Primer	Sequence (5'>3')
CRLF3_1_BamHI_F	ATACTGGGATCCATGAAGGGCGATGGAGCCG
CRLF3_17_BamHI_F	AAAAGGATCCGCCCGCGAGAACGTGGAG
CRLF3_34_BamHI_F	AAAAGGATCCCGGGAGGCGCAGAGGCA
CRLF3_174_BamHI_F	AAAAGGATCCCATGGAACAGTAGCTTCCCGC
CRLF3_173_NotI_R	CCCCGCGGCCGCTCACTTAAAAATGTGGTCTTTCACTATGT
CRLF3_442_NotI_R	GCGGCCGCTTACTAAAATACC

Table 3.9 – Primers used to amplify *Crlf3* constructs

3.28 Protein production

Protein from *Crlf3* constructs were produced as per Harper and Speicher Harper and Speicher (2008). Briefly, transformed BL21 cells were grown in 2xTY media at 37°C until OD_{600} reached

≈0.8. 1mM isopropul-1-thio-β-D-galactopyranoside (IPTG; Sigma-Aldrich) was added and cells were incubated at 30°C for ≥5h. Pelleted cells were lysed in PBS supplemented with 1mg/mL lysozyme (Sigma-Aldrich), 10mM magnesium chloride, 10U/mL DNase I (Sigma-Aldrich) and 1x Protease Inhibitor Cocktail (c0mplete Tablets EDTA-free; Roche). Lysed cells were spun at 10,000rpm, 40min, 4°C and supernatant containing protein stored at -80°C until needed.

3.29 Protein purification

Glutathione-*S*-transferase (GST) was removed from CRLF3 constructs by affinity chromatography using GSTrap FF 5mL columns and PreScission Protease (both GE Healthcare), following manufacturer's instructions. Remaining free GST was removed by ion exchange chromatography using HiTrap Q FF columns (GE Healthcare) following manufacturer's instructions.

3.30 Protein concentration

Protein was concentrated under centrifugation using VivaSpin 2 columns with 10kDa cut off (Sartorius Stedim Biotech) following manufacturer's instructions. Protein concentration was determined by Nanodrop or bicinchoninic acid (BCA) assay using Pierce® BCA Protein Assay Kit (both Thermo Scientific) following manufacturer's instructions.

3.31 Protein crystallisation

Crystallisation was screened by the vapour diffusion method in 96-well sitting drop plates set up with a Nanodrop Screenmaker 96+8 (Innovadyne Technologies), using drops containing 200nL protein and 200nL screening solution equilibrated with 70µL screening solution. Screen plates Structure Screen 1 and 2, PACT Premier, Stura Footprint Screen, MacroSol and JCSG-Plus (all Molecular Dimensions), Wizard 1, 2, 3 and 4 and Cryo I and II (all Emerald BioSystems) and PEG/Ion Screen and PEG/Ion 2 Screen (both Hampton Research) were used. Screen plates were kept at 20°C and imaged using a Rock Imager crystal screening system (Formulatrix).

3.32 Structural solution

Structural solution was performed by Randy Read, Yahui Yan and Richard Mifsud (University of Cambridge, Cambridge, UK). Briefly, crystals from a range of conditions were picked for X-ray diffraction and stored in 25% ethylene glycol (Hampton Research) as a cryopreservative. A number of crystals underwent heavy atom soaking before cryopreservation, which was optimised by soaking crystals with serial dilutions of the mercury heavy atom derivative thimerosal (Sigma-Aldrich) for various times. Diffraction data were recorded at Diamond Light Source beamline I04 (Didcot, UK). Diffraction data were indexed, integrated, and scaled using Mosflm (Leslie and Powell, 2007) and Aimless (Evans, 2011) via the xia2 automated data processing pipeline (Winter, 2010). The structure of CRLF3 construct 3 was determined by Hg-SAD using AutoSol-wizard (Terwilliger et al., 2009) of the PHENIX suite (Adams et al., 2010) Further refinement was then performed using Phenix.refine (Adams et al., 2010) and by manual building in Coot (Emsley et al., 2010). Molecular graphics were prepared using PyMOL version 1.5.0.4 (https://www.pymol.org/).

3.33 Maintenance and expansion of human induced pluripotent stem cells (iPSCs)

Qolg iPSCs (HipSci line HPSI1113i-qolg_3 (http://www.hipsci.org)) were maintained as colonies on truncated vitronectin (VTN-N; Thermofisher Scientific) coated tissue culture plastic plates (Corning) in Essential 8 medium (E8; Gibco) unless stated. iPSCs were fed daily with fresh E8 after removal of old medium. Near confluent cultures were split to new VTN-N coated plates by dissociation of colonies into small clumps with 0.5mM EDTA in PBS and manual scraping After 24 hours, medium was removed and replaced with E8 and cells then fed daily as above. When iPSCs were needed in single cell solution for differentiation or electroporation experiments, colonies were dissociated with TrypLE (Life technologies), pelleted at 300*g* before resuspending in E8 medium supplemented with 10μM Y-27632 (Sigma-Aldrich) to prevent apoptosis.

3.34 Tandem Affinity Purification (TAP) tagging *CRLF3* in human iPSCs by CRISPR/Cas9

CRISPR ID 1146192702 was picked from www.sanger.ac.uk/htgt/wge (Hodgkins et al., 2015), due to its close proximity to CRLF3's stop codon and having few predicted off target sites. Single-guide RNA (sgRNA) expression constructs were generated using the plasmid-based procedure as described by Ran et al. (2013). Briefly, sgRNA oligos were synthesised and cloned into the pSpCas9(BB)-2A-GFP plasmid (Adgene). This was used to transform Mix & GO *E.Coli* cells (Zymo Research), which were plated on LB agar plates supplemented with ampicillin and grown overnight at 37°C. Ampicillin resistant colonies were expanded in 2xTY media liquid cultures overnight at 37°C with shaking and sgRNA/Cas9-GFP plasmid DNA was prepared from liquid cultures using QIAprep® Spin Miniprep Kit (QIAGEN).

For the donor vector (see section 6.4.2 and fig. 6.6 for details), 1Kb gDNA homology arms upstream and downstream of CRLF3's stop codon and the TAP-tag were amplified by PCR using specific primers (table 3.10 and 3.12) and Platinum Taq DNA HiFi Polymerase (ThermoFisher Scientific) from iPSC gDNA and a plasmid containing the TAP-tag (gift from David Adams, Wellcome Trust Sanger Institue, Hinxton, UK), respectively. Vector pBS KS (Addgene) was linearized by PCR with specific primers (table 3.10 and 3.12) and Platinum Taq DNA HiFi Polymerase. Homology arms and the TAP-tag were then cloned into pBS KS by Gibson assembly using a commercial kit (Gibson Assembly Cloning Kit; New England Biosciences). Donor vector DNA was then transformed into XL-10 Gold ultra-competent *E.coli* (Straragene) following manufacturer's instructions. Transformed *E. coli* were plated on LB agar plates supplemented with ampicillin and grown overnight at 37°C. Ampicillin resistant colonies were expanded in 2xTY media liquid cultures overnight at 37°C with shaking and TAP-tag donor vector DNA was prepared from liquid cultures using QIAprep® Spin Miniprep Kit.

sgRNA/Cas9-GFP plasmid and TAP-tag donor vector DNA were introduced into Qolg iPSC's in a single cell solution by nucleofection using Amaxa Human Stem Cell Nucleofector Kit 2 and an Amaxa Nucleofector II (both Lonza), following manufacturer's instructions. 48 hours after nucleofection, cells were sorted based on GFP expression by flow assisted cell sorting (cell sorting performed by staff of the NIHR Cambridge BRC Cell Phenotyping Hub, University of

Cambridge, Cambridge, UK). GFP positive iPSCs were seeded individually to laminin (Biolamina) coated 96 well tissue culture plates and maintained in E8 medium supplemented with 100U/ml pen/strep for 5 days then E8 medium until needed.

Primer	Sequence (5'>3')
CRLF3_5'_hom arm_F	CTCTAGAACTAGTGGATCCCATTTTGTGGTGTTGGCTGGGCAC
CRLF3_5'_hom arm_R	CGCCTCTTCTCCATGCTTCCAAACACTAACACTTTCCATCCAGGATAGA
CRLF3_3'_hom arm_F	ACAAAGACGATGACGACAAGTTCAGGGTCTAACGTAGCTGTCCT
CRLF3_3'_hom arm_R	ACGGTATCGATAAGCTTGATCATATTACATACATATGAAATGGCTAACA CTGCTG
Vector_F	TTTCATATGTATGTAATATGATCAAGCTTATCGATACCGTCGAC
Vector_R	CCCAGCCAACACCACAAAATGGGATCCACTAGTTCTAGAGCGG
TAP_tag_F	GATGGAAAGTGTTAGTGTTTGGAAGCATGGAGAAGAGGCG
TAP_tag_R	CAGCTACGTTAGACCCTGAACTTGTCGTCATCGTCTTTGTAGTCA

Table 3.10 – Primers used for creation of TAP-tag donor vector

3.35 TOPO TA cloning to screen *CRLF3* in iPSC lines

CRLF3 was amplified from cDNA from iPSC lines BobC and Qolg (cDNA gifted by Amanda Evans, University of Cambridge, Cambridge UK) by PCR using specific primers (table 3.11 and 3.12) and Platinum Taq DNA HiFi Polymerase. PCR products were resolved by electrophoresis on 0.8% agarose TBE (section 3.2) gels and specific bands cut out. DNA was extracted from gel using QIAquick gel extraction kit (Qiagen). *CRLF3* fragments were cloned into TOPO vector and subsequently transformed into One Shot TOP 10 competent *E. coli* using TOPO TA cloning kit (ThermoFisher Scientific), following manufacturer's instructions. Transformed *E. coli* were plated on LB agar plates supplemented with ampicillin and grown overnight at 37^{o}C. Ampicillin resistant colonies were expanded in 2xTY media liquid cultures overnight at 37^{o}C with shaking and TOPO vector DNA containing the inserted *CRLF3* was prepared from liquid cultures using QIAprep® Spin Miniprep Kit.

Primer	Sequence (5'>3')
CRLF3_TOPO_F	GGAACCCGCGCTAGGTTTCG
CRLF3_TOPO_R	CATCTAAAACACTAACACTTTCCATCCAGGA

Table 3.11 – Primers used for TOPO TA cloning

3.36 TAP-tag expression in iPSCs by flow cytometry

To screen for genetically modified iPSC clones, untagged and TAP-tagged iPSCs were detached from cultured plates with TrypLE and pelleted (section 3.33). Cells were then fixed and permeabilised using a commercial kit (FIX & PERM™ Cell Permeabilization Kit; Life Technologies) following manufacturer's instructions and then incubated with fluorescently labelled antibodies against the TAP-tag (FITC anti-FLAG M2 produced in mouse, clone M2; Sigma-Aldrich) or an IgG control (FITC mouse IgG1 κ isotype control; BD Pharmigen) . Stained samples were washed once in PBE (section 3.13) then resuspended in PBE and analysed by flow cytometry using a Gallios flow cytometer and Kaluza Analysis version 1.5a software.

3.37 CRLF3 interactome in iPSCs

$9x10^6$ iPSCs were dissociated to a single cell solution, washed 3 times in PBS then snap frozen and stored at -80^oC until needed. Frozen pellets were then lysed in lysis buffer (10mM Tris hydrochloride, 150mM sodium chloride, 0.1% NP-40), centrifuged at 13,000rpm for 15 minutes and lysates collected. Proteins interacting with TAP-tagged CRLF3 were then collected by incubating the lysates with magnetic beads (Dynal protein G; Invitrogen) coated with anti-FLAG antibody (anti-FLAG M2 produced in mouse, clone M2; Sigma-Aldrich) before collecting the beads. Beads where then washed 3 times in lysis buffer and then twice in TEV buffer (10mM Tris hydrochloride, 150mM sodium chloride, 0.1% NP-40, 0.5mM EDTA, 1mM Dithiothreitol) to remove unbound proteins. Bead bound proteins were then dissociated by incubation with 100U AcTEV protease (Invitrogen) in TEV buffer before collection of the eluates. The eluates were then diluted in calmodulin binding buffer (CBB; 10mM Tris-HCl, 150mM sodium chloride, 1mM magnesium acetate, 1mM Imidazole, 2mM calcium chloride, 10mM β-mercaptoethanol, 0.1% NP-40) before interacting proteins were further purified by incubation of the diluted eluates with calmodulin binding peptide (CBP) affinity resin (Agilent), pelleting and removal of the supernatant. CBP resin was then washed 3 times with CBB before incubation in calmodulin elution buffer (10mM Tris-HCl, 150mM sodium chloride, 0.02% NP-40, 1mM magnesium acetate, 1mM Imidazole, 20mM EGTA, 10mM β-mercaptoethanol) to dissociate bound proteins, which were collected in the eluates after pelleting of the CBP resin. The eluates were then snap frozen and stored at -80^oC until mass spectrometry was

performed. Mass spectrometry and LC-MS/MS analysis was performed by Renata Feret, Marco Chiapello and Mike Deery (Cambridge Centre for Proteomics, University of Cambridge, Cambridge, UK). Briefly, samples were mixed with SDS loading buffer and run on 12% SDS PAGE gel in order to remove MS incompatible detergents. Samples were only run till a dye front was about 2cm below the well. Gel was stained with coomassie blue colloidal stain and each lane cut into 4 equal pieces. Each piece was finely chopped and transferred to 0.5ml Eppendorf tube and was treated as individual MS sample. The gel pieces were distained by washing with 50% acetonitrile, 50% ammonium bicarbonate followed by wash with HPLC water. Distained samples were then treated with 100% acetonitrile, air dried and reduced with 10mM DTT in 100mM ammonium bicarbonate for 1 hour at 37^{O}C. The DTT solution was removed and replaced with 55mM iodoacetamide in 100mM ammonium bicarbonate and incubated for 45 minutes at RT in darkness. Samples were then washed with 50% ammonium bicarbonate, 50% acetonitrile followed by addition of 100% acetonitrile. Acetonitrile was removed and samples dried again, before resuspending in a 1:200 solution of trypsin in 50mM ammonium bicarbonate and incubating overnight at 37^{o}C.

LC-MS/MS analysis

Post-trypsin digestion, the supernatant was pipetted into a sample vial and loaded onto an autosampler for automated LC-MS/MS analysis.

All LC-MS/MS experiments were performed using a Dionex Ultimate 3000 RSLC nanoUPLC system and a Q Exactive Orbitrap mass spectrometer (both Thermo Fisher Scientific). Separation of peptides was performed by reverse-phase chromatography at a flow rate of 300nL/min and a Thermo Scientific reverse-phase nano Easy-spray column (Thermo Scientific PepMap C18, 2μm particle size, 100Å pore size, 75nm i.d. x 50cm length). Peptides were loaded onto a pre-column (Thermo Scientific PepMap 100 C18, 5μm particle size, 100Å pore size, 300nm i.d. x 5mm length) from the Ultimate 3000 autosampler with 0.1% formic acid for 3 minutes at a flow rate of 10nL/min. After this period, the column valve was switched to allow elution of peptides from the pre-column onto the analytical column. Solvent A was water + 0.1% formic acid and solvent B was 80% acetonitrile, 20% water + 0.1% formic acid. The linear gradient employed was 2-40% B in 30 minutes.

The LC eluent was sprayed into the mass spectrometer by means of an Easy-Spray source (ThermoFisher Scientific). All *m/z* values of eluting ions were measured in an Orbitrap mass analyzer, set at a resolution of 70000 and was scanned between *m/z* 380-1500. Data dependent scans (Top 20) were employed to automatically isolate and generate fragment ions by higher energy collisional dissociation (HCD, NCE:25%) in the HCD collision cell and measurement of the resulting fragment ions was performed in the Orbitrap analyser, set at a resolution of 17500. Singly charged ions and ions with unassigned charge states were excluded from being selected for MS/MS and a dynamic exclusion window of 20 seconds was employed.

Post-run, the data was processed using Protein Discoverer (version 2.1., Thermo Scientific). Briefly, all MS/MS data were converted to mgf files and the files were then submitted to the Mascot search algorithm (Matrix Science) and searched against the UniProt human database (UniProt_Human201701 201701, 70956 sequences; 23911858 residues) and a common contaminant sequences (115 sequences, 38274 residues). Variable modifications of oxidation (M), deamidation (NQ) and carbamidomethyl were applied. The peptide and fragment mass tolerances were set to 5ppm and 0.1 Da, respectively. A significance threshold value of $p<0.05$ and a peptide cut-off score of 20 were also applied.

3.38 Forward programming

Forward programming of iPSCs to MKs was carried out following the method of Moreau et al. (2016). Briefly, near confluent (50-80%) untagged and TAP-tagged iPSC cultures were dissociated to single cells and seeded onto vitronectin coated 6 well tissue culture plates at 125,000 cells per well. After 24 hours, cells were washed once with PBS then transduced with GATA1, FLI1 and TAL1 lentiviral vectors (MOI 20, Vectalys) suspended in transduction medium (AE6 media (DMEM/F12 (Gibco), 0.05% sodium bicarbonate (Gibco), 64mg/L L-Ascorbic acid (Sigma), 20mg/L Insulin, 11mg/L Transferrin, 13.4µg/L Selenium (all ThermoFisher Scientific)) supplemented with 20ng/ml FGF2, 10ng/ml BMP4 (both Bio-Techne) and 10µg/ml protamine sulphate (Sigma-Aldrich)). 24 hours after transduction, the medium was removed, cells were washed with PBS and mesoderm media was added (AE6 media supplemented with 20ng/ml FGF2 and 10ng/ml BMP4). 24 hours later, mesoderm medium was removed, cells were washed in PBS and MK medium (CellGRO SCGM (CellGenix) supplemented with 20ng/ml TPO

(Bio-Techne) and 50ng/ml SCF (Gibco)) was added. 9 days after transduction, cells were split using TrypLE and further maintained as suspension cultures in MK medium up to 25 days post transduction.

3.39 Localisation of CRLF3 in proplatelet forming forward programmed MKs

Forward programmed MKs were pelleted and resuspended in RPMI (Gibco). $1.5x10^5$ MKs were seeded onto glass coverslips coated with 100ng/ml fibrinogen (Enzyme Research) and incubated at 37°C under 5% CO_2 for 24-48 hours until proplatelets were observed. MKs attached to the coverslips were fixed with 10% neutral buffered formalin and washed in PBS. Fixed MKs were stained for and imaged by confocal microscopy as per section 3.24 with primary antibodies against the TAP-tag (anti-FLAG M2 produced in mouse, clone M2; Sigma-Aldrich) and appropriate secondary antibodies (Alexa Flour 488 Goat anti-mouse IgG; Invitrogen) and the nuclear stain DAPI.

3.40 Statistics

Statistical significance between 2 experimental groups was analysed using an unpaired 2-tailed Student's *t* test with correction for multiple comparisons using the Holm-Sidak method where appropriate or a two-way analysis of variance (ANOVA) using Tukey's or Sidak's correction for multiple comparisons (as stated). When more than 2 experimental groups were compared, data were analysed using a one- or two-way ANOVA using Tukey's correction for multiple comparisons (Prism 7; GraphPad Software). *P* values less than 0.05 were considered as statistically significant. **p*<0.05; ***p*<0.01; ****p*<0.005. Data are represented as mean ± s.d.

Primer	Sequence (5'>3')	Section referred to in
*Crlf3*_F	TGGATACATTGATTAGCTTGACAGA	3.2 and 4.4.1
*Crlf3*_R	AGGGGATGAGAGGGTCTTCAG	3.2 and 4.4.1
Cassette_R	TCGTGGTATCGTTATGCGCC	3.2 and 4.4.1
*Crlf3*_F_qPCR	GGGTGTTCTCTACTCCAGCG	3.9
*Crlf3*_R_qPCR	GCCATTCTGCCTTTCTGCAC	3.9
*Gapdh*_F_qPCR	CCCTTAAGAGGGATGCTGCC	3.9
*Gapdh*_R_qPCR	TACGGCCAAATCCGTTCACA	3.9
CRLF3_1_BamHI_F	ATACTGGGATCCATGAAGGGCGATGGAGCCG	3.27 and 6.4.1
CRLF3_17_BamHI_F	AAAAGGATCCGCCCGCGAGAACGTGGAG	3.27 and 6.4.1
CRLF3_34_BamHI_F	AAAAGGATCCCGGGAGGCGCAGAGGCA	3.27 and 6.4.1
CRLF3_174_BamHI_F	AAAAGGATCCCATGGAACAGTAGCTTCCCGC	3.27 and 6.4.1
CRLF3_173_NotI_R	CCCCGCGGCCGCTCACTTAAAAATGTGGTCTTTCACTATGT	3.27 and 6.4.1
CRLF3_442_NotI_R	GCGGCCGCTTACTAAAATACC	3.27 and 6.4.1
M13_F	GTAAAACGACGGCCAG	6.4.2
M13_R	CAGGAAACAGCTATGAC	6.4.2
CRLF3_5'_homarm_F	CTCTAGAACTAGTGGATCCCATTTTGTGGTGTTGGCTGGGCAC	3.34
CRLF3_5'_homarm_R	CGCCTCTTCTCCATGCTTCCAAACACTAACACTTTCCATCCAGGATAGA	3.34
CRLF3_3'_homarm_F	ACAAAGACGATGACGACAAGTTCAGGGTCTAACGTAGCTGTCCT	3.34
CRLF3_3'_homarm_R	ACGGTATCGATAAGCTTGATCATATTACATACATATGAAATGGCTAACACTGCTG	3.34
Vector_F	TTTCATATGTATGTAATATGATCAAGCTTATCGATACCGTCGAC	3.34

Vector_R	CCCAGCCAACACCACAAAATGGGATCCACTAGTTCTAGAGCGG	3.34
TAP_tag_F	GATGGAAAGTGTTAGTGTTTGGAAGCATGGAGAAGAGGCG	3.34
TAP_tag_R	CAGCTACGTTAGACCCTGAACTTGTCGTCATCGTCTTTGTAGTCA	3.34
iPSC_DV_Seq_TAP_F	GGAAGCATGGAGAAGAGGC	6.4.2
iPSC_DV_Seq_3'HA_R	CATATTACATACATATGAAATGGCTAACACTG	6.4.2
CRLF3_TOPO_F	GGAACCCGCGCTAGGTTTCG	3.35 and 6.4.2
CRLF3_TOPO_R	CATCTAAAACACTAACACTTTCCATCCAGGA	3.35 and 6.4.2

Table 3.12 – List of all primers used

Antibody	Clone	Manufacturer	Section used in	Dilution/ concentration
Biotin Rat anti-mouse CD11b	M1/70	eBioscience	3.8	1:250
Rat anti-mouse Ly-6G (Gr-1)	RB6-8C5	eBioscience	3.8	1:250
Rat anti-mouse CD16/CD32	2.4G2	BD Pharmigen	3.8	1:250
Biotin Rat anti-mouse CD45R/B220	RA3-6B2	BD Pharmigen	3.8	1:250
anti-β-actin produced in mouse	AC-15	Sigma-Aldrich	3.10	1:1,000
Rabbit anti-human CRLF3	polyclonal	Atlas antibodies	3.10	1:1,000
Rabbit anti-human GAPDH	14C10	Cell Signalling Technology	3.10	1:1,000
HRP Sheep anti-mouse IgG	n/a	GE Healthcare	3.10	1:10,000
HRP donkey anti-rabbit IgG	n/a	GE Healthcare	3.10	1:10,000
anti-Detyrosinated tubulin produced in rabbit	polyclonal	Millipore	3.10	1:1,000
anti- tyrosine tubulin produced in mouse	TUB-1 A2	Sigma-Aldrich	3.10	1:1,000
Biotinylad Ricinus Communis Agglutinin I (RCA-I)	n/a	Vector Laboratories	3.10	1:1,000
Rabbit anti-human Integrin beta 1	polyclonal	Abcam	3.10	1:1,000
Streptavidin HRP	n/a	Cell Signalling Technology	3.10	1:10,000
IRDye 800CW Donkey anti-rabbit IgG	n/a	LI-COR	3.10	1:15,000
IRDye 800CW Goat anti-mouse IgG	n/a	LI-COR	3.10	1:15,000
IRDye 680LT Goat anti-rabbit IgG	n/a	LI-COR	3.10	1:15,000
IRDye 680LT Donkey anti-mouse IgG	n/a	LI-COR	3.10	1:15,000
FITC Rat anti-mouse CD41	MWReg30	BD Pharmigen	3.13, 3.16, 3.20	1:50
Rat anti-mouse CD41	MWReg30	BioLegend	3.14, 3.24	1:200
Alexa Flour 488 Goat anti-rat IgG	n/a	Invitrogen	3.14, 3.24	1:1,000
Alexa Fluor 594 Rat anti-mouse CD105	MJ7/18	BioLegend	3.15	0.4 µg/g
Alexa Flour 488 Rat anti-mouse GPIX	Xia.B4	Emfret Analytics	3.15	0.6 µg/g
APC Streptavidin	n/a	BD Pharmigen	3.16	1:100
PE Rat anti-mouse TER-119	TER-119	BD Pharmigen	3.16	1:50

FITC Rat anti-mouse GPV	DOM2	Emfret Analytics	3.17, 3.18	1:10
PE Rat anti-mouse GPIIb/IIIa	Leo.F2	Emfret Analytics	3.17, 3.18	1:10
PE Rat anti-mouse GPIIb/IIIa	JON/A	Emfret Analytics	3.18	1:10
FITC rat anti-mouse CD62P	Wug.E9	Emfret Analytics	3.18	1:10
PE Mouse anti-human CD42a	ALMA.16	BD Pharmigen	3.20	1:25
FITC Rat anti-mouse CD49b	Sam.G4	Emfret Analytics	3.20	1:25
FITC Rat anti-mouse GPVI	JAQ1	Emfret Analytics	3.20	1:25
FITC hamster anti-mouse CD61	2C9.G3	eBioscience	3.20	1:25
PE hamster anti-mouse CD42d	1C2	eBioscience	3.20	1:25
PE Rat anti-mouse IgG1, κ Isotype Control	n/a	BD Pharmigen	3.20	1:25
FITC Rat anti-mouse IgG1, κ Isotype Control	n/a	BD Pharmigen	3.20, 3.36	1:25
APC Rat anti-mouse CD41	MWReg30	eBioscience	3.21	1:25
PE Rat anti-mouse P-selectin (CD62P)	Wug.E9	Emfret analytics	3.21	1:10
FITC Rabbit anti-human Fibrinogen	polyclonal	DakoCytomation	3.21	1:25
Rabbit anti-human von Willebrand Factor	polyclonal	DakoCytomation	3.24	1:50
Alexa Flour 555 Goat anti-rabbit IgG	n/a	Invitrogen	3.24	1:1,000
Mouse anti-α-tubulin-Alexa 488	B-5-1-2	Invitrogen	3.26	1:150
FITC anti-FLAG M2 produced in mouse	M2	Sigma-Aldrich	3.36	1:25
anti-FLAG M2 produced in mouse	M2	Sigma-Aldrich	3.37, 3.39	1:10, 1:200
Alexa Flour 488 Goat anti-mouse IgG	n/a	Invitrogen	3.39	1:1,000

Table 3.13 – List of all antibodies used

4

Results 1

Phenotyping of *Crlf3*$^{-/-}$ mice and biological mechanisms for thrombocytopenia

4.1 Introduction

4.1.1 Cytokine receptor-like factor 3

Cytokine receptor-like factor 3 (*CRLF3*) also known as *CYTOR4, CREME9, FRWS, P48* and *P48.2* is a 2.4kb gene locate in the neurofibromatosis type 1 (NF1) microdeletion region on the q arm of chromosome 17 (chromosome 11 in mice). The NF1 microdeletion region encompasses 13 genes (*CRLF3, C17orf41, C17orf42, CENTA2, RNF135, OMG, EVI2B, EVI2A, RAB11FIP4, C17orf79, UTP6, SUZ12* and *LRRC37B*) and mutations in this region cause NF1 (5-10% of cases are due to deletions). NF1 is a common genetic condition with an incidence rate of 1:3,000, which causes tumors to grow along the nervous system (neurofibromas) along with a multitude of other symptoms. Individuals with deletions are more likely to have facial dysmorphism, learning disability, congenital heart defects and high numbers of neurofibromas (Douglas et al., 2007).

CRLF3 is ubiquitously expressed throughout the haematopoietic system (fig 4.1). CRLF3 has two protein coding isoforms, the longer of which contains 442 amino acids and a shorter transcript containing 118 amino acids. In mice the longer isoform contains 442 amino acids is 93% homologous to the human longer isoform. The shorter isoform contains 334 amino acid and is missing exon 7 of longer transcript. However, expression within the haematopoietic system is almost exclusive to the longer transcript (fig. 4.2) (Chen et al., 2014). CRLF3 has been shown to be localised mainly in the cytoplasm of cell lines. This localisation of CRLF3 was deciphered by transfection of labelled CRLF3 into a range of human and monkey cell lines (Yang et al., 2009).

Very little is known about the function of CRLF3. To date there has only been one published peer-reviewed journal article on mammalian CRLF3, which implicated CRLF3 as a potential negative regulator of cell cycle at the G0/G1 phase (Yang et al., 2009). Overexpression of CRLF3 in the human cell line HEK293T caused G0/G1 arrest with fewer cells entering S phase. This cell cycle arrest was mediated by increased phosphorylation of STAT3 leading to upregulation of cyclin D1, cyclin D3 and p27. Conversely, repressing *CRLF3* expression with specific small interfering RNA reduced the G0/G1 cell population. CRLF3's full interactome is yet to be discovered, however, CRLF3 has been shown to interact with DOCK6, DOCK7 DOCK8, LRCH1,

LRCH2 and LRCH3 (Couzens et al., 2013). DOCK6, 7 and 8 are atypical guanine exchange factors for the cytoskeletal-associated guanosine triphosphate Rac. LRCH family proteins contain a calponin homology domain that mediates interactions with actin filaments.

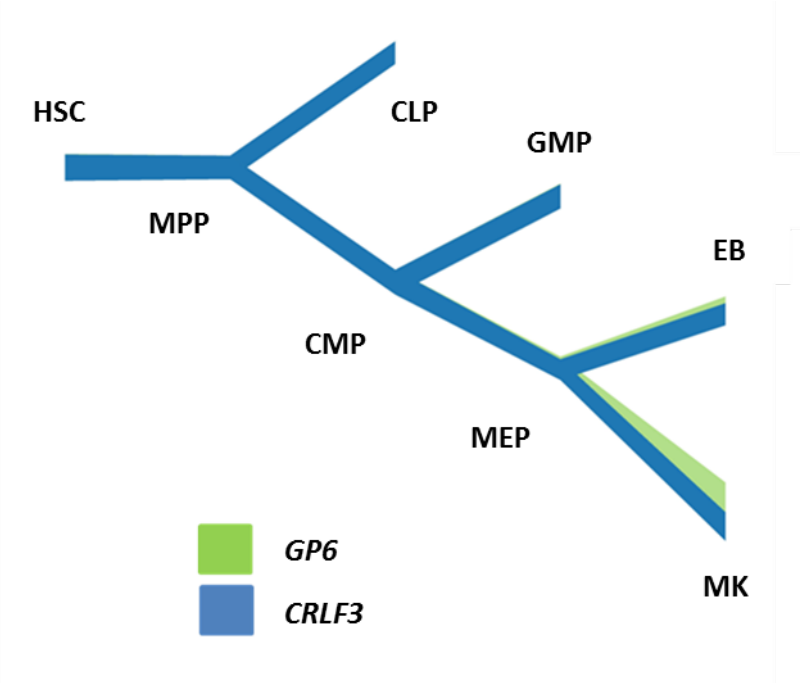

Figure 4.1 – *CRLF3* expression in haematopoietic cells. *CRLF3* (blue) is expressed throughout the haematopoietic system, whereas *GP6* (green) expression is limited mainly to MKs. Thickness of line represents level of expression. HSC = haematopoietic stem cell; MPP = multi-potent progenitor CMP = common myeloid progenitor; CLP = common lymphoid progenitor; GMP = granulocyte-macrophage progenitor; MEP = megakaryocyte/erythrocyte progenitor; EB = erythroblast and MK = megakaryocyte. Data from Chen et al. (2014).

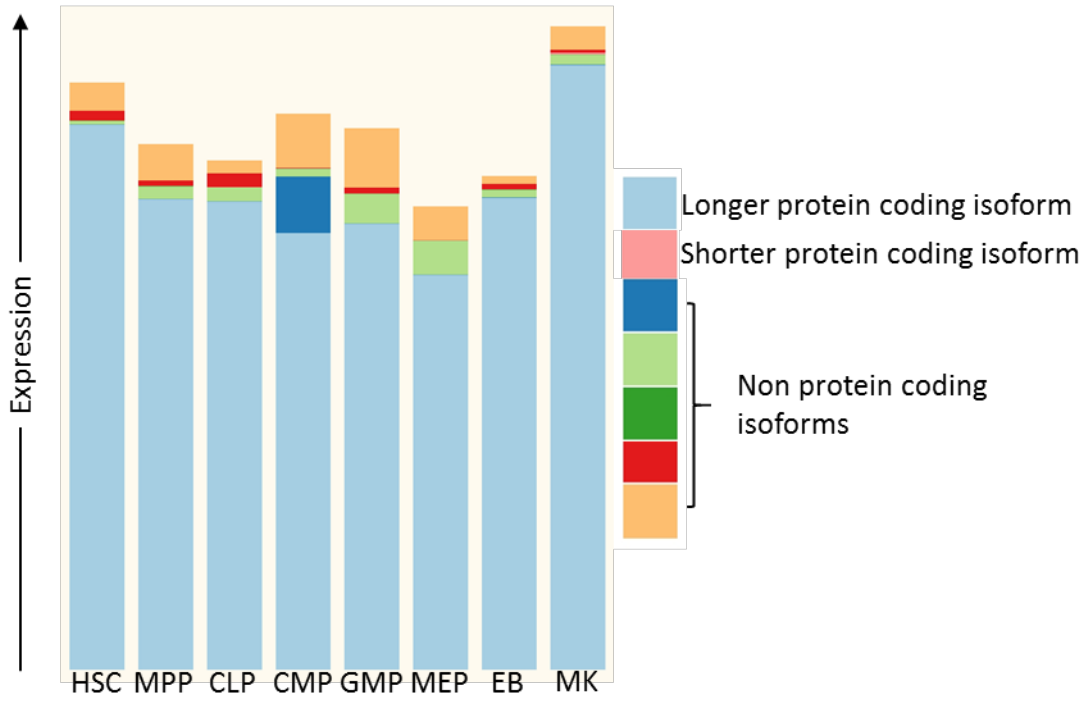

Figure 4.2– Expression of *CRLF3* transcripts in the haematopoietic system. HSC = haematopoietic stem cell; MPP = multi-potent progenitor CMP = common myeloid progenitor; CLP = common lymphoid progenitor; GMP = granulocyte-macrophage progenitor; MEP = megakaryocyte/erythrocyte progenitor; EB = erythroblast and MK = megakaryocyte. Data from Chen et al. (2014).

4.1.2 *Crlf3* knockout mice

An international collaborative consortium (International Mouse Phenotyping Consortium, www.mousephenotype.org) was established to knockout each gene in the mouse genome individually and phenotype any effect in the mouse progeny. As part of this consortium, the Wellcome Trust Sanger Institute (Hinxton, UK) developed a *Crlf3* knockout mouse (Crlf3$^{tm1b(KOMP)Wtsi}$, see section 3.1 for details). Pipeline phenotyping of 9-16 week old mice revealed effects limited to the blood system. Circulating magnesium levels were decreased ($p=6.164x10^{-5}$), however both male (2.23 mg/dl) and female (2.46 mg/dl) *Crlf3*$^{-/-}$ magnesium levels were within the normal range of 2.20-2.67mg/dl (https://www.mousephenotype.org/data/); suggesting biological effects of this decrease would be minimal. Mean corpuscular volume (MCV), which is a measure of the average volume of a red blood cell, was also decreased ($p=0.023$ females and $1.321x10^{-7}$ males). Again both male (48.9 fl) and female (49.1 fl) *Crlf3*$^{-/-}$ MCV were within the normal range (48.8-50.6 fl) suggesting a minimal biological effect. Finally, *Crlf3*$^{-/-}$ mice had thrombocytopenia with platelet counts decreased 30-40% compared to WT controls ($p=9.969x10^{-11}$). The average

platelet counts for both males ($960x10^6$/ml) and females ($742x10^6$/ml) was outside of the normal range of 1058 – 1481 suggesting *Crlf3* has a real biological influence on platelet numbers.

Chronic thrombocytopenia generally results from either decreased platelet production or increased platelet destruction. Decreased platelet production is evident in patients with *TUBB1*-, *TPM4*- and *DIAPH1*-related thrombocytopenias. In the case of these particular genes, proplatelet formation has been shown to be impaired *in vitro* (Kunishima et al., 2014; Pleines et al., 2017; Stritt et al., 2016). In the case of *TPM4*, platelet lifespan was shown to be unaffected in *Tpm4* mutated mice (Pleines et al., 2017).

Increased platelet clearance is seen in *FLNA*-related thrombocytopenia. Begonja *et al*, demonstrated that mice with conditional inactivation of *Flna* in the MK lineage had upregulated megakaryopoiesis and thrombopoiesis, with normal proplatelet formation, showing platelet formation was unaffected. However, platelet clearance was rapidly increased in these mice mediated by macrophages (Begonja et al., 2011).

However, this over simplified generalisation is not always true. In some chronic thrombocytopenias, both increased platelet destruction and decreased platelet production occur together. For example, it is likely that patients with Wilkott-Aldrich syndrome (WAS) experience increased destruction and decreased production of platelets. Knockout mice of two proteins implicated in the development of WAS, namely, profilin 1 ($Pfn1^{-/-}$) and *WASp* ($WASp^{-/-}$) have decreased platelet lifespans (Bender et al., 2014; Falet et al., 2009), showing increased platelet destruction. In the case of $Pfn1^{-/-}$ this platelet clearance was mediated by macrophages. Both $Pfn1^{-/-}$ and $WASp^{-/-}$ mice show aberrant proplatelet formation and platelet release into the bone marrow space (Bender et al., 2014; Sabri et al., 2006), suggesting that platelet production is also affected.

This dual effect on platelets is also seen in patients with idiopathic or immune thrombocytopenic purpura (ITP). ITP can be acute, often following an infection, or chronic and causes a characteristic purpuric rash and increases the tendency to bleed. Platelet destruction is mediated by the production of IgG autoantibodies against platelet specific glycoproteins (usually GPIIb-IIIa and Ib-IX). Platelets bound with autoantibodies are phagocytosed by the

mononuclear phagocyte system primarily in the spleen but also in the liver and bone marrow. There is also evidence that the autoantibodies affect the production of MKs and platelets, thus contributing to the thrombocytopenia by decreasing platelet production (Cooper and Bussel, 2006).

4.2 Chapter hypotheses and aims

We hypothesise that ablation of *Crlf3* will cause isolated and maintained thrombocytopenia in mice. We hypothesise that the thrombocytopenia is likely caused by excessive removal of platelets by the spleen. Therefore, there are two main aims of this chapter, firstly, to determine whether ablation of *Crlf3* results in long term sustained and isolated thrombocytopenia. The second aim is to determine the biological consequences of *Crlf3* ablation that result in thrombocytopenia.

4.3 Chapter overview

Firstly, this chapter will show that ablation of *Crlf3* in mice results in sustained isolated thrombocytopenia. Secondly, we go on to show that *Crlf3*$^{-/-}$ mice have upregulated megakaryopoiesis and proplatelet formation both *in vitro* and *in vivo*. However, we show terminal maturation of preplatelets in the peripheral circulation is defective possibly due to increased microtubule stability. Finally, we show that rapid removal of a proportion of preplatelets is the cause of the thrombocytopenia in *Crlf3*$^{-/-}$ mice.

4.4 Results

4.4.1 Confirmation of genotype

We received *Crlf3* heterozygous (*Crlf3*$^{+/-}$) mice from the Wellcome Trust Sanger Institute, in which a LacZ-neo cassette is inserted into *Crlf3* and exon 2 is excised. These mice were bred together to produce *Crlf3*$^{-/-}$, *Crlf3*$^{+/-}$ and *Crlf3*$^{+/+}$ (WT) mice. This thesis chapter will only concern *Crlf3*$^{-/-}$ and WT mice. Firstly, we wanted to confirm the genotype of the mice. DNA isolated from ear notches taken for identification were used in PCR reactions with specific primers

(table 3.1 and 3.12). The PCR was designed to amplify both a 281bp portion of *Crlf3* that is only present on unaffected alleles and a 159bp that incorporates the inserted cassette and therefore will only be amplified if a mutated allele is present. *Crlf3*$^{-/-}$ and WT mice were easily identified based on the presence or absence of the 281bp and 159bp bands (fig. 4.3A). We then wanted to confirm the ablation of *Crlf3* from the cells of interest, MKs and platelets. Messenger RNA from *in vitro* cultured MKs is almost completely ablated in *Crlf3*$^{-/-}$ mice (fig. 4.3B). Finally, we checked for the presence of CRLF3 from *in vitro* cultured MKs (fig. 4.3C) and platelets isolated from whole blood (fig. 4.3D) by western blot. *Crlf3*$^{-/-}$ mice have minimal expression, or complete absence, of CRLF3 in MKs and platelets.

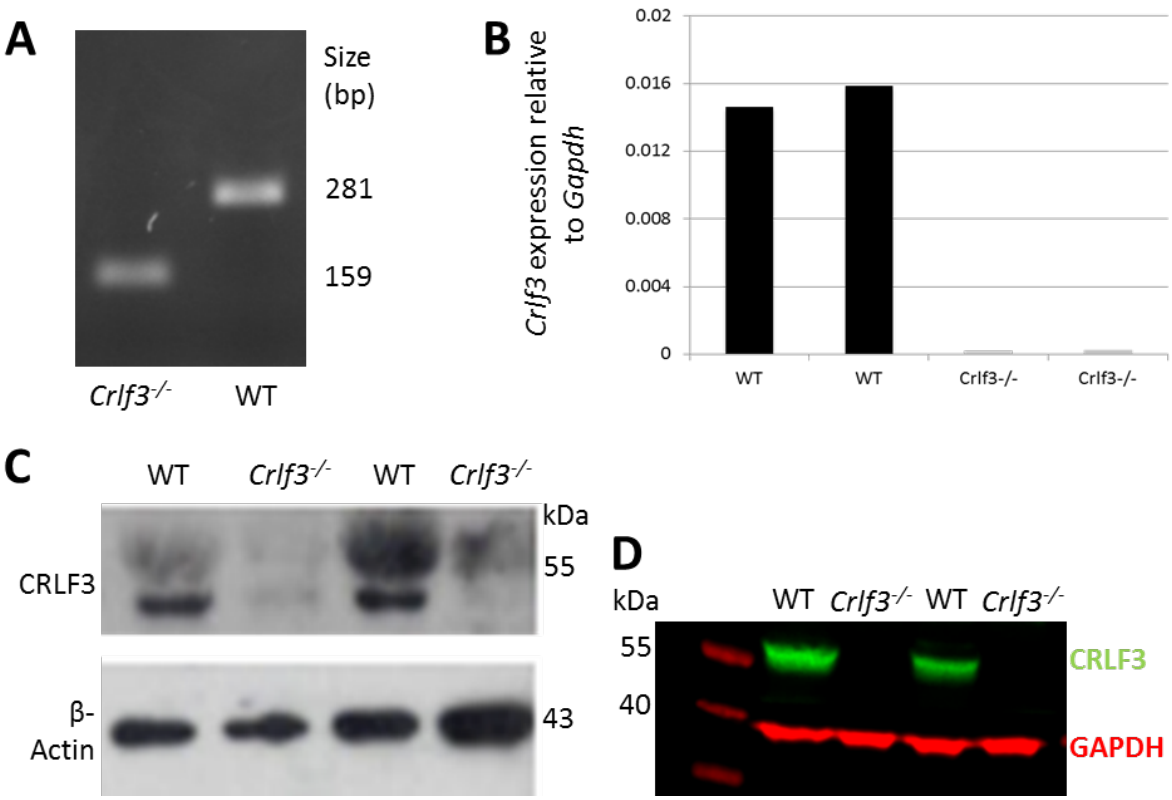

Figure 4.3 – Genotyping of *Crlf3*$^{-/-}$ and WT mice. (A) Genomic DNA amplified by PCR using specific primers, resolved on a 1.5% agarose TBE gel to determine DNA fragment size. (B) Expression of *Crlf3* relative to *Gapdh* determined by Q-PCR of WT (black) and *Crlf3*$^{-/-}$ (grey) cDNA isolated from *in vitro* cultured MKs. Western blot of *in vitro* cultured MK (C) and platelet (D) lysates using specific antibodies against CRLF3, β-actin and GAPDH.

4.4.2 Sustained and isolated thrombocytopenia

To determine the effect of *Crlf3* ablation on blood cells during aging, *Crlf3*$^{-/-}$ and WT mice were bled from the tail vein or inferior vena cava into EDTA at young (12-20 weeks), middle

(21-40 weeks) and old (>52 weeks) age time points. Full blood counts were determined using an automated haemocytometer. In essence, the 12-20 week time point should recapitulate the results of the pipeline phenotyping done by the Wellcome Trust Sanger Institute. Indeed, platelet counts are reduced 38.5% in males and 38.6% in females (p<0.005 in both cases) (fig. 4.4 and table 4.1). However, MCV was unaffected in both male and female *Crlf3*$^{-/-}$ mice (p=0.999 for both sexes; data not shown).

Male								
		Plt (10^3/μL)	MPV (fL)	Hgb (g/dL)	RBC (10^6/μL)	WBC (10^3/μL)	Age (weeks)	*n*
12-20 weeks	WT	1423.90 (250.92)	5.01 (0.38)	14.51 (1.16)	10.32 (1.38)	11.15 (2.64)	15.34 (2.93)	10
	Crlf3$^{-/-}$	875.14 (170.18)	5.19 (0.37)	13.51 (1.42)	9.46 (1.48)	13.56 (5.71)	15.55 (3.38)	7
	p value	***	ns	ns	ns	ns	ns	
21-40 weeks	WT	1581.50 (225.07)	4.83 (0.32)	13.08 (1.77)	9.65 (1.43)	8.95 (2.20)	30.79 (5.92)	10
	Crlf3$^{-/-}$	1079.00 (202.56)	5.02 (0.22)	13.08 (1.23)	9.17 (0.80)	8.38 (1.06)	27.31 (4.15)	5
	p value	***	ns	ns	ns	ns	ns	
>52 weeks	WT	1513.50 (443.97)	5.30 (0.42)	13.86 (0.75)	10.34 (1.03)	10.53 (3.18)	65.39 (13.21)	12
	Crlf3$^{-/-}$	1132.30 (383.60)	5.21 (0.60)	12.43 (1.44)	9.11 (1.52)	12.30 (3.36)	64.94 (14.43)	23
	p value	***	ns	ns	ns	ns	ns	
Female								
		Plt (10^3/μL)	MPV (fL)	Hgb (g/dL)	RBC (10^6/μL)	WBC (10^3/μL)	Age (weeks)	*n*
12-20 weeks	WT	1116.60 (261.33)	4.96 (0.09)	15.72 (2.33)	10.21 (1.70)	7.80 (1.44)	16.82 (2.90)	5
	Crlf3$^{-/-}$	685.80 (105.11)	5.08 (0.15)	15.02 (1.58)	9.68 (1.23)	7.40 (3.46)	14.83 (2.39)	5
	p value	***	ns	ns	ns	ns	ns	
21-40 weeks	WT	1034.80 (133.04)	4.96 (0.09)	13.42 (0.97)	8.71 (0.75)	6.86 (1.34)	27.14 (4.30)	5
	Crlf3$^{-/-}$	771.00 (134.04)	5.13 (0.14)	13.83 (1.03)	9.04 (0.60)	5.70 (1.38)	25.86 (4.69)	6
	p value	***	ns	ns	ns	ns	ns	
>52 weeks	WT	1323.91 (242.01)	5.50 (0.64)	13.47 (1.73)	9.57 (1.65)	6.18 (0.95)	69.01 (14.56)	11
	Crlf3$^{-/-}$	771.07 (156.33)	5.41 (0.38)	13.24 (1.33)	8.95 (1.36)	7.96 (3.47)	64.98 (15.00)	15
	p value	***	ns	ns	ns	ns	ns	

Table 4.1 – Effect of *Crlf3* ablation on blood lineages at different mice ages. Full blood counts determined by an automated haemocytometer on EDTA anticoagulated venous blood taken from male and female young (12-20 weeks), middle aged (21-40 weeks) and old (>52 weeks) mice. Data represents mean (SD). Unpaired 2-tailed Student's *t* test with correction for multiple comparisons using the Holm-Sidak method. *** denotes p<0.005.

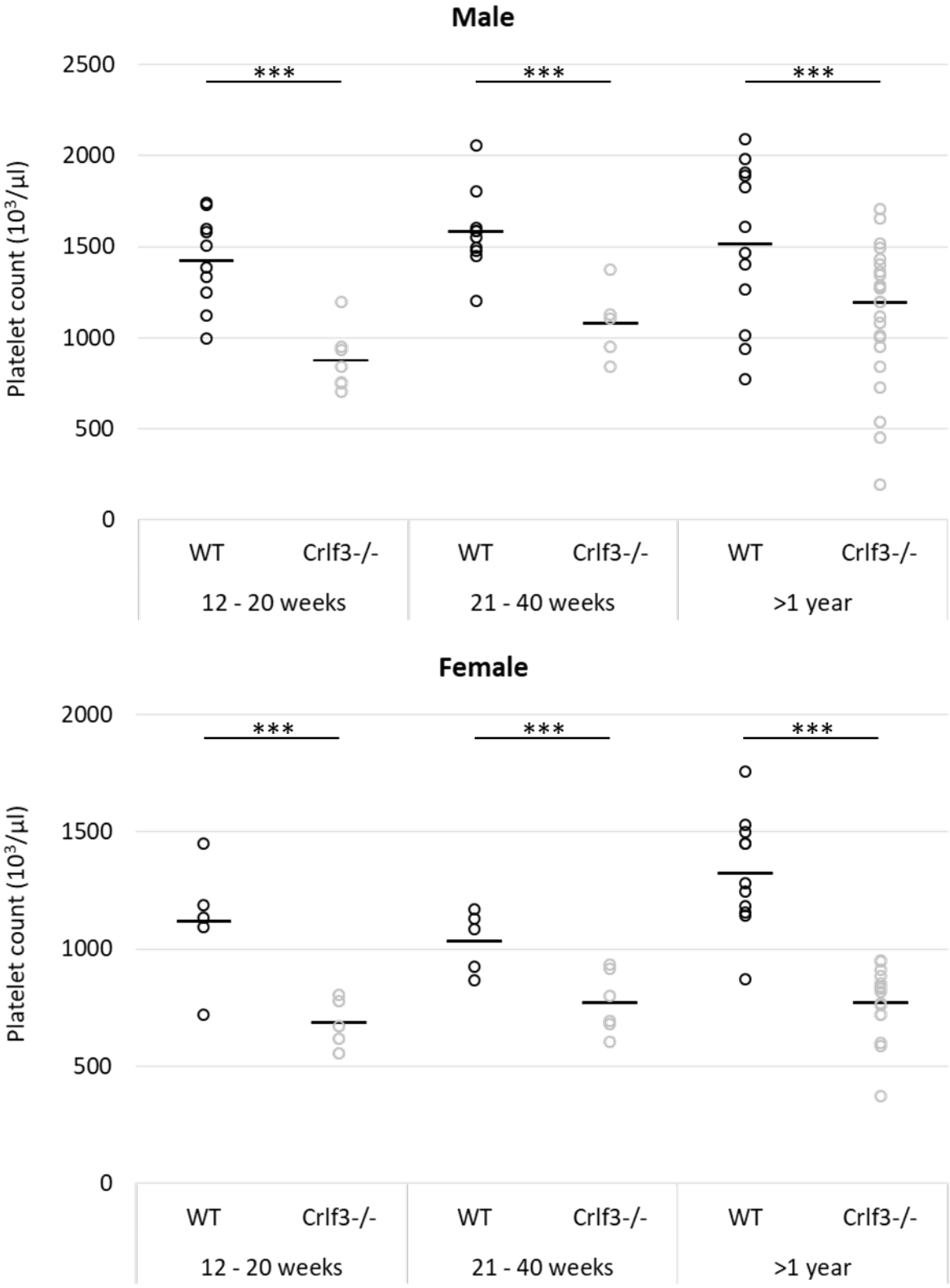

Figure 4.4 – Sustained thrombocytopenia in *Crlf3*$^{-/-}$ mice. Platelet counts determined by an automated haemocytometer on EDTA anticoagulated venous blood taken from male (*n*=5-23) and female (*n*=5-15) young (12-20 weeks), middle aged (21-40 weeks) and old (>52 weeks) mice. Unpaired 2-tailed Student's *t* test with correction for multiple comparisons using the Holm-Sidak method. *** denotes $p<0.005$.

4.4.3 Platelet production is unaffected

As previously mentioned in section 4.1.2, chronic thrombocytopenia is either a result of increased platelet clearance, decreased platelet production or a combination of both. To determine if ablation of *Crlf3* results in decreased platelet production, we firstly determined whether megakaryopoiesis and thrombopoiesis were affected in *Crlf3*$^{-/-}$ mice. Megakaryopoiesis was assessed by counting the number of bone marrow residing MKs in fixed bone samples. Unexpectedly, MK numbers are increased in *Crlf3*$^{-/-}$ mice compared to WT controls (MKs per high power field at 12 months of age 12.65 ± 1.03 *Crlf3*$^{-/-}$ vs 8.90 ± 2.51 WT, p=0.021, fig. 4.5). The main driver of megakaryopoiesis is the cytokine TPO. Therefore, we assessed the plasma concentration of TPO using a commercially available ELISA kit (experiments performed by José Guerrero, University of Cambridge, Cambridge, UK). The plasma TPO concentration was unaltered in *Crlf3*$^{-/-}$ mice compared to WT controls (201.3 ± 56.1 pg/ml *Crlf3*$^{-/-}$ vs 253.3 ± 136.3 pg/ml, p=0.448; fig. 4.6), suggesting that increased megakaryopoiesis is not due to increased TPO levels. We then assessed whether bone marrow residing MK precursor cells from *Crlf3*$^{-/-}$ animals are intrinsically primed to become MKs. To test this, *Crlf3*$^{-/-}$ or WT bone marrow cells were cultured in culture medium supplemented with 5ng/ml TPO for 5 days, after which the percentage of CD41 positive cells was assessed by flow cytometry. Interestingly, cultures from *Crlf3*$^{-/-}$ bone marrow cells produced a significantly larger percentage of CD41 positive cells compared to cultures from control WT bone marrow cells (fig. 4.7). This suggests that MK progenitor cells are intrinsically primed towards the MK lineage in *Crlf3*$^{-/-}$ mice.

Next, we wanted to determine whether ablation of *Crlf3* has an effect on MK maturation. One feature of MK maturation is polyploidisation. *In vitro* cultured MKs were fixed and stained with propidium iodide and assessed for ploidy level by flow cytometry. We observed no differences in the level of polyploidy in MKs cultured from *Crlf3*$^{-/-}$ bone marrow compared to control cultured WT MKs (fig. 4.8); suggesting that *Crlf3* does not influence maturation of MKs.

Platelets are mainly produced in the bone marrow from cytoplasmic protrusions produced by MKs (proplatelets). Therefore, we wanted to check whether the ability of MKs to produce proplatelets, and therefore platelets, was effected by ablation of *Crlf3*. Mature *in vitro* cultured MKs were purified by BSA gradient and seeded onto fibrinogen coated coverslips,

then incubated at 37°C for 3 or 5 hours to produce proplatelets. As can be seen in figure 4.9 *Crlf3*$^{-/-}$ MKs are able to produce proplatelets that are similar in appearance to WT MKs. Although at 3 hours there is no difference in proplatelet formation between *Crlf3*$^{-/-}$ and WT MKs (373/1111 *Crlf3*$^{-/-}$ MKs imaged v 263/911 WT; p=0.290; fig. 4.9), fragmentation of proplatelets appears to be upregulated in *Crlf3*$^{-/-}$ MKs. Indeed, between 3 and 5 hours in WT MKs, proplatelet formation appears to be increasing with a trend towards increased MKs forming proplatelets at 5 hours (p=0.088; fig. 4.9), but the total number of MKs is relatively unchanged (882 total MKs imaged v 911 MKs at 3 hours). Conversely, in *Crlf3*$^{-/-}$ MKs the trend is towards decreased MKs forming proplatelets at 5 hours (p=0.120; fig. 4.9), probably due to the most mature *Crlf3*$^{-/-}$ MKs being completely fragmented by this time point, leaving only less mature MKs to be counted. This is evident as the total number of MKs imaged at the 5 hours is dramatically reduced in the *Crlf3*$^{-/-}$ samples (464 total MKs imaged v 1111 MKs at 3 hours). Proplatelet formation is increased in WT MKs compared to *Crlf3*$^{-/-}$ MKs at 5 hours (123/464 *Crlf3*$^{-/-}$ MKs analysed v 459/882 WT; p=0.035; fig. 4.9) further suggesting that proplatelet formation is increasing from 3 to 5 hours in WT MKs but decreasing in *Crlf3*$^{-/-}$ MKs.

Proplatelet formation was also studied *in vivo* using two-photon intravital microscopy of the bone marrow. MKs from *Crlf3*$^{-/-}$ mice produced proplatelets into the bone marrow sinusoids similarly to that of MKs from WT mice (supplementary video 1 and 2) (*in vivo* proplatelet formation experiments performed by Ayesha Baig, University of Würzburg, Würzburg, Germany). Taken together, these data suggest that platelet production is not impaired in *Crlf3*$^{-/-}$ mice and decreased platelet production is not the reason for the observed thrombocytopenia.

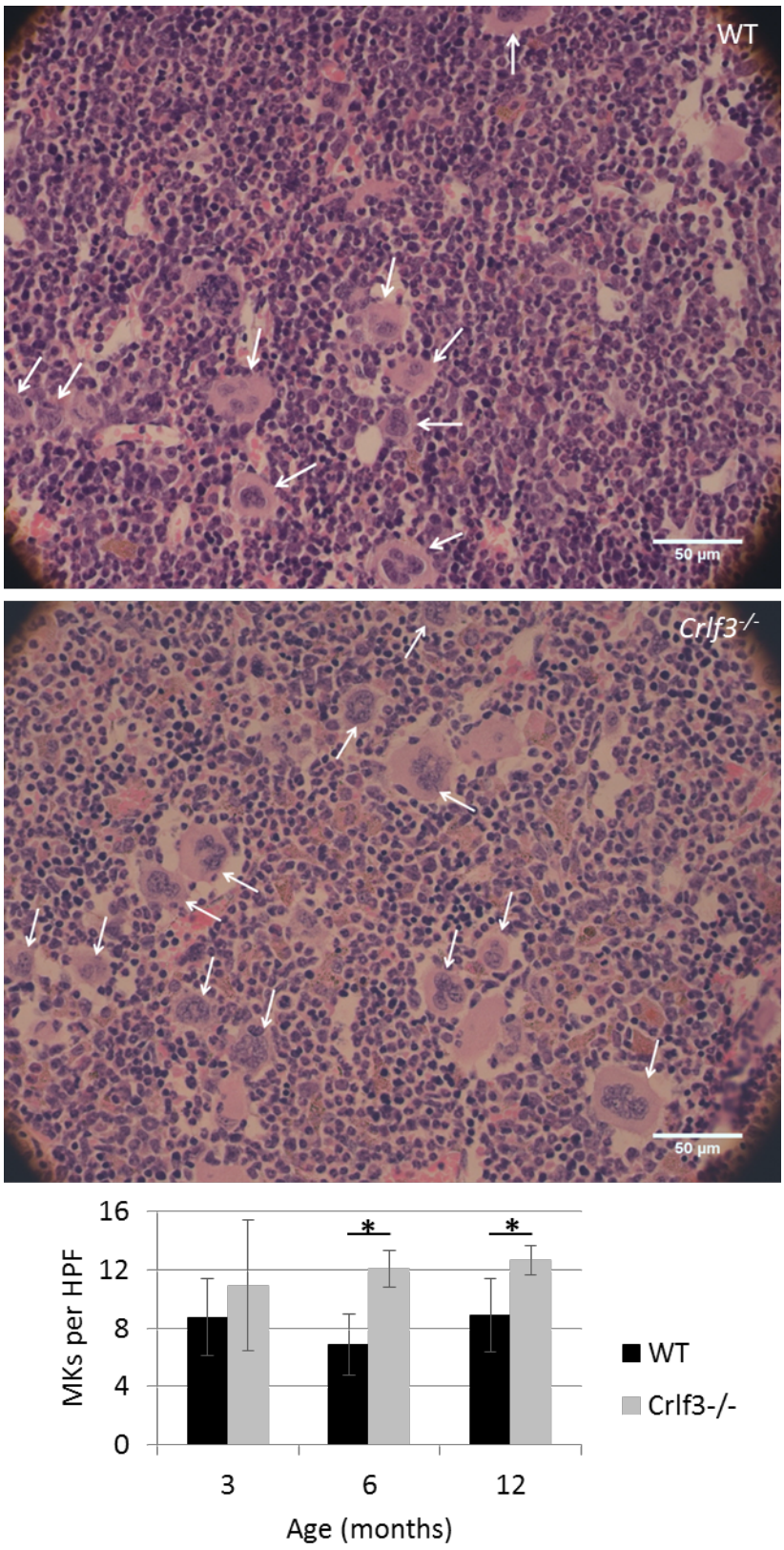

Figure 4.5 – Megakaryopoiesis is upregulated in *Crlf3*$^{-/-}$ mice. H&E staining performed on fixed and sectioned mice tibias. MKs quantified blinded by manual counting for WT (black) and *Crlf3*$^{-/-}$ (grey) images (high power field (HPF)). Images are representative of 12 month old *Crlf3*$^{-/-}$ and WT mice and white arrow heads point to MKs. Scale bars are 50µm. Data represents mean ± SD (*n*=3-6). Unpaired 2-tailed Student's *t* test with correction for multiple comparisons using the Holm-Sidak method. * denotes $p<0.05$.

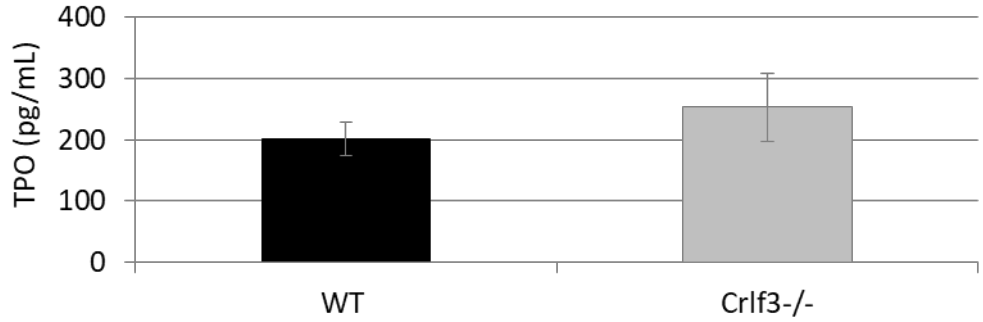

Figure 4.6 – Plasma TPO levels are unaltered in *Crlf3*$^{-/-}$ mice. Plasma thrombopoietin (TPO) concentration determined by ELISA for WT (black) and *Crlf3-/-* (grey) mice. Data represents mean ± SD (*n*=5-6). Unpaired 2-tailed Student's *t* test.

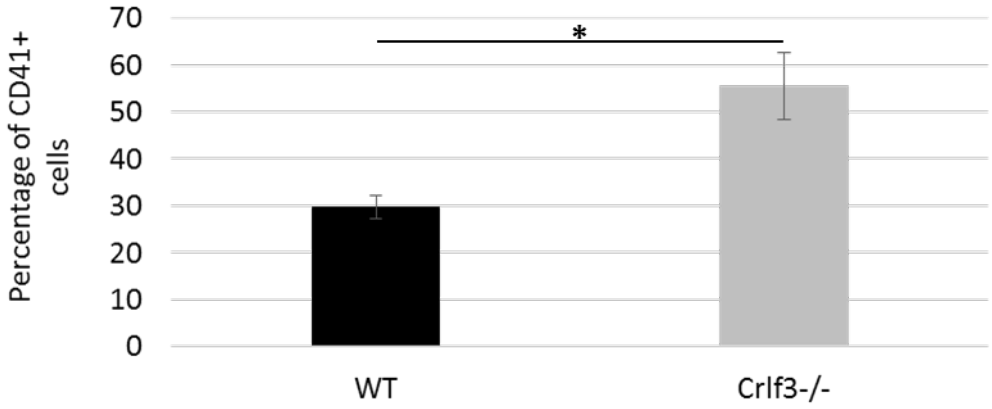

Figure 4.7 – *Crlf3*$^{-/-}$ progenitors are primed to form MKs. Flow cytometry analysis of CD41+ WT (black) and *Crlf3*$^{-/-}$ (grey) cells after culture of bone marrow cells for 5 days in defined conditions using specific antibodies against CD41. Data represents mean ± SD (*n*= 3). Unpaired 2-tailed Student's *t* test; * denotes $p<0.05$.

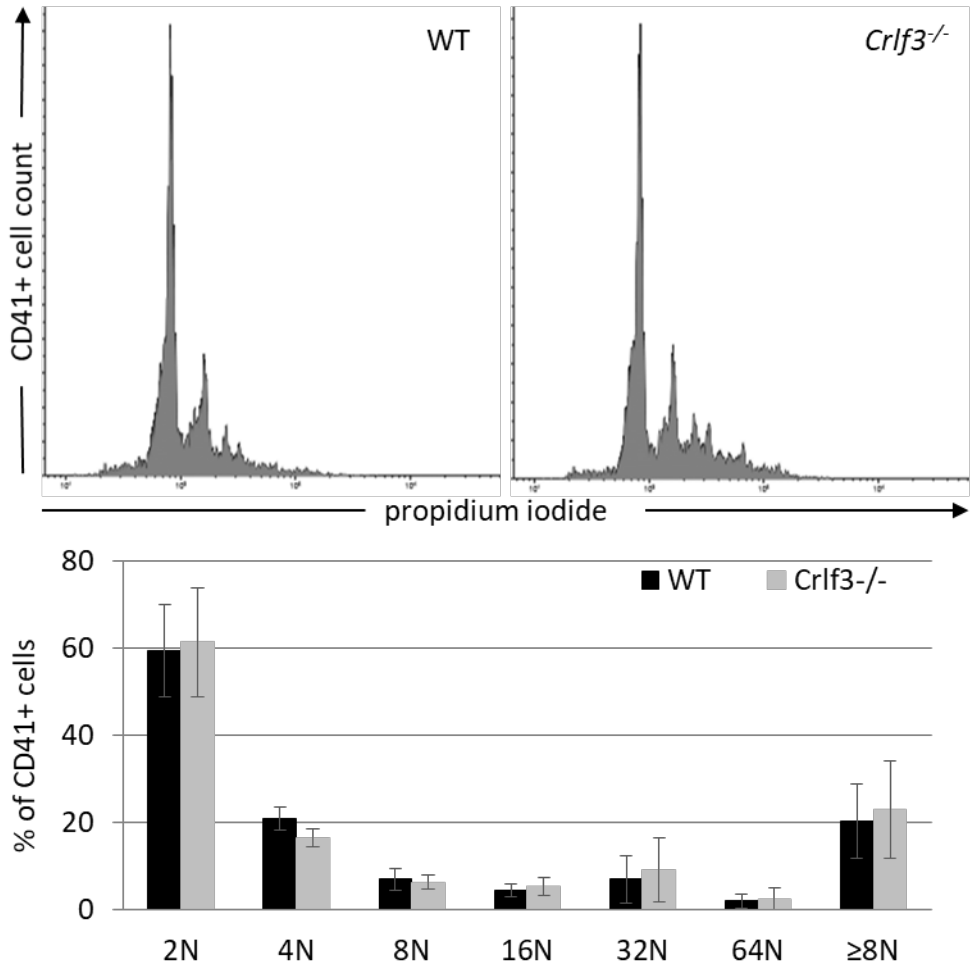

Figure 4.8 MK polyploidisation is unaffected by ablation of *Crlf3*. *In vitro* cultured WT (black) and *Crlf3*$^{-/-}$ (grey) MKs fixed and stained with propidium iodide and analysed by flow cytometry using specific antibodies against CD41 to assess polyploidisation. Ploidy profiles are representative of 5 mice per genotype. Data represents mean ± SD (*n*=5). Unpaired 2-tailed Student's *t* test with correction for multiple comparisons using the Holm-Sidak method.

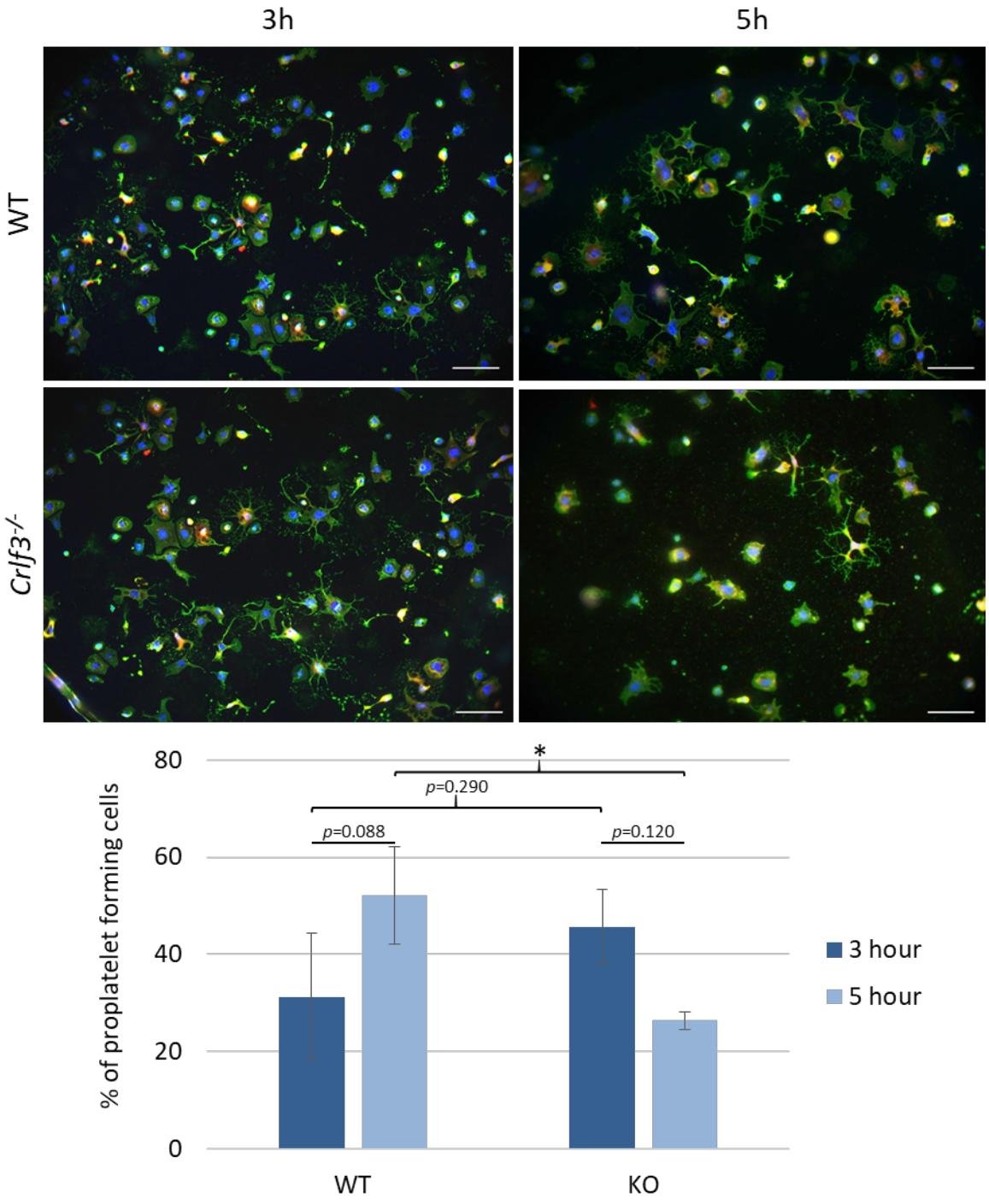

Figure 4.9 Proplatelet fragmentation occurs faster in *Crlf3*$^{-/-}$ MKs. *In vitro* cultured MKs were seeded onto fibrinogen coated coverslips and incubated at 37°C for 3 or 5 hours to induce proplatelet formation. Samples were fixed, stained with specific antibodies against CD41 (green), a fluorescently labelled F-actin probe (red) and the nuclear stain DAPI (blue), and imaged by confocal microscopy. Percentage of proplatelet forming MKs was determined for WT and *Crlf3*$^{-/-}$ MKs as the percentage of proplatelet forming MKs compared to total number of MKs per image. At least 460 MKs were counted in each condition. Images are representative of 5 images taken for 3 mice per genotype. Scale bars are 50µm. Data represents mean ± SD (n=3). Two-way ANOVA with Tukey's correction for multiple comparisons. * denotes p<0.05.

4.4.4 Increased platelet clearance in *Crlf3*$^{-/-}$ mice causes thrombocytopenia

As decreased platelet production was not the cause of the thrombocytopenia in *Crlf3*$^{-/-}$ mice, we next looked at platelet clearance. First we assessed platelet survival *in vivo* by injecting biotin into the bloodstream, thus labelling all blood cells. The removal of biotin bound platelets over time was then determined by flow cytometry, using 24 hours post biotin injection as baseline biotin labelling (100%). Surprisingly, we observed no difference in platelet survival between *Crlf3*$^{-/-}$ and WT platelets (fig. 4.10A). This result suggests that if platelets are being cleared from the circulation it must happen rapidly, within the first 24 hours of release into the bone marrow sinusoids.

We then looked at clearance by the liver, despite there being no difference in TPO levels in *Crlf3*$^{-/-}$ mice, as this is one of the major sites of platelet removal. Exposed terminal galactose residues on platelets are recognised by Ashwell-Morell receptors on liver hepatocytes and Kupffer cells and leads to platelet phagocytosis and production of TPO. Therefore, we assessed the level of terminal galactose exposure on platelets by western blot (experiments performed by Silvia Giannini and Karin Hoffmeister, Brigham and Women's Hospital, Boston, USA). *Crlf3*$^{-/-}$ platelets have a slight increase in terminal galactose exposure compared to WT controls (fig. 4.10B), suggesting platelet phagocytosis by the liver may play a role in the thrombocytopenia. However, this small increase is unlikely to cause a chronic 30-40% decrease in platelets counts.

We then turned our attention to clearance by the spleen. Splenomegaly was observed in 2 out of 11 old (>52 week old) *Crlf3*$^{-/-}$ mice (fig. 4.11A), suggesting the spleen may be removing platelets from the circulation. To assess whether platelet removal by the spleen was responsible for the thrombocytopenia in *Crlf3*$^{-/-}$ mice, we splenectomised *Crlf3*$^{-/-}$ and WT mice (splenectomies and subsequent orbital bleeds and flow cytometry performed by Simon Stritt, University of Würzburg, Würzburg, Germany). As can be seen in figure 4.11B, removal of the spleen increases platelet counts in WT mice showing that the spleen is responsible for a portion of platelet removal under normal physiology. Interestingly, splenic removal in *Crlf3*$^{-/-}$ mice not only increased the platelet count but actually normalised it to WT values within 7 days. This data suggests that rapid removal of a portion of newly formed platelets by the spleen is the cause of thrombocytopenia in *Crlf3*$^{-/-}$ mice.

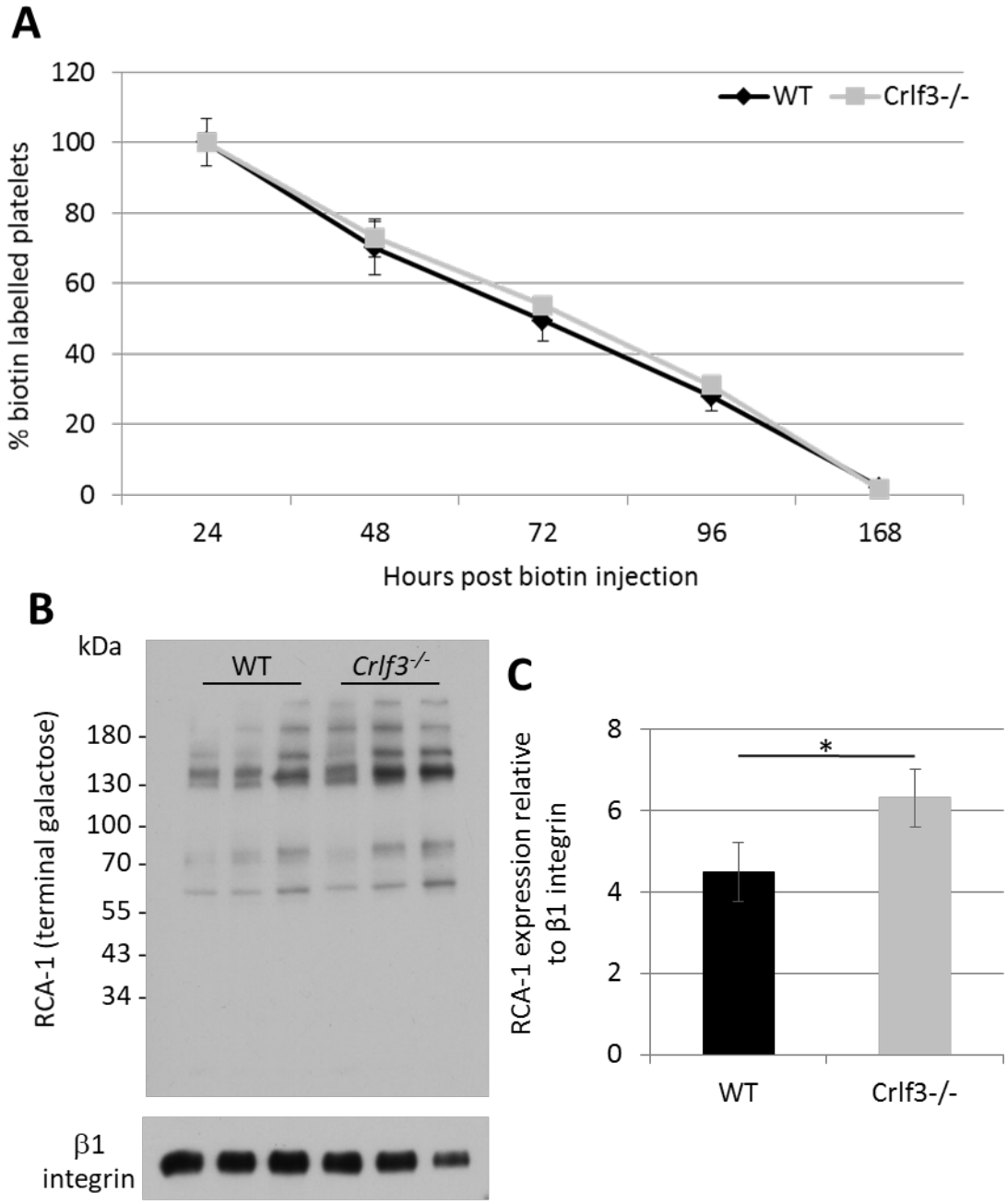

Figure 4.10 – Platelet clearance occurs within the first 24 hours of release and facilitated partly by the spleen. (A) WT (black) and *Crlf3*$^{-/-}$ (grey) mice injected with 1mg NHS-biotin. Blood withdrawn 24, 48, 72, 96 and 168 hours post injection was labelled with specific antibodies against CD41, Ter119 and streptavidin and the percentage of streptavidin positive platelets (CD41^{+}/Ter119^{-}) determined by flow cytometry. Percentage of streptavidin positive platelets at 24 hours represents 100% biotin bound platelets (*n*=5). (B) Western blot of washed platelet lysates using specific antibodies against terminal galactose (RCA-1) and β1 integrin. (C) Expression of RCA-1 relative to β1 integrin determined from western blot (B) using Image Studio Lite (*n*=3). Data represents mean ± SD. (A) Two-way repeated measures (RM) ANOVA with Sidak's correction for multiple comparisons; (C) Unpaired 2-tailed Student's *t* test. * denotes $p<0.05$.

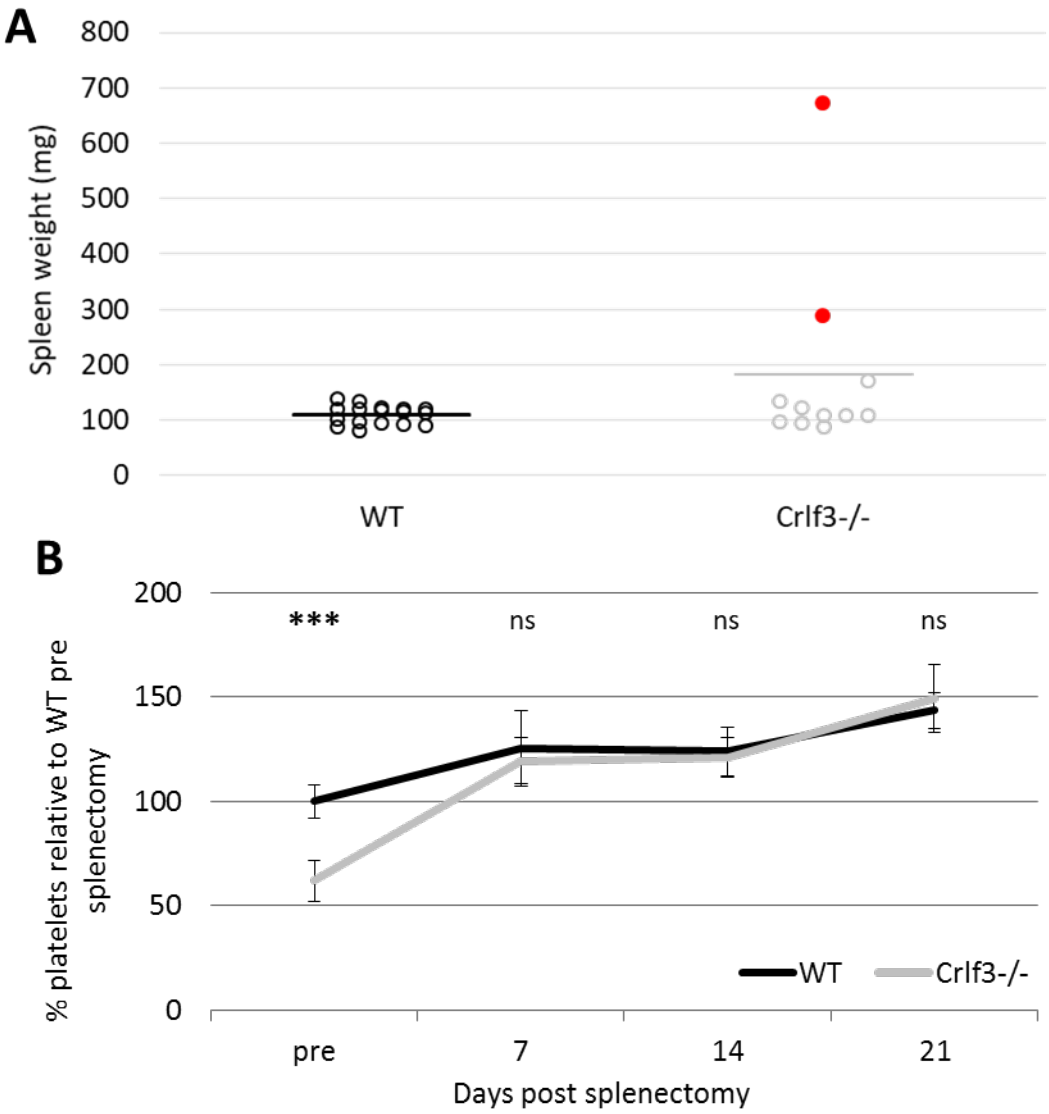

Figure 4.11 – Thrombocytopenia in *Crlf3*$^{-/-}$ mice is driven by splenic clearance. (A) Spleen weights of WT (black) and *Crlf3*$^{-/-}$ (grey) old (>52 week old) mice. Red data points show observed splenomegaly (*n*=11-17). (B) Splenectomises performed on WT (black) and *Crlf3*$^{-/-}$ (grey) mice and platelet counts determined by flow cytometry on venous blood (*n*=4-5). Data represents mean ± SD. (A) Unpaired 2-tailed Student's *t* test; (B) two-way ANOVA with Sidak's correction for multiple comparisons. *** and ns denote $p<0.005$ and not significant, respectively.

4.4.5 Platelet clearance driven by haematopoietic compartment but not due to platelet activation/aggregation defects

We sought to determine whether ablation of *Crlf3* causes defects intrinsically to the platelets or extrinsically to the platelet environment. To assess this we performed bone marrow transplants, transplanting 5 million bone marrow cells from WT and *Crlf3*$^{-/-}$ donors to WT and *Crlf3*$^{-/-}$ sub-lethally irradiated recipients. Results suggest that the defect leading to splenic removal of platelets is isolated to the haematopoietic compartment, as WT recipients that receive *Crlf3*$^{-/-}$ bone marrow cells show a 59% decrease in platelet counts 3 months after transplantation (fig. 4.12A). In contrast, the platelet counts of *Crlf3*$^{-/-}$ mice transplanted with WT bone marrow cells recover to WT levels. Interestingly, restoration of platelet counts in *Crlf3*$^{-/-}$ mice transplanted with WT bone marrow and thrombocytopenia in WT mice transplanted with *Crf3*$^{-/-}$ bone marrow occurred despite incomplete chimerism (fig. 4.12B).

Next, we determined whether *Crlf3* ablation causes defects in the ability of platelets to activate and aggregate, defects that may target platelets for removal. First, we looked at the major platelet surface receptors by flow cytometry. *Crlf3*$^{-/-}$ platelets did not show altered expression of the fibrinogen receptor integrins CD41 (integrin α_{IIb}, GPIIb) and CD61 (integrin β_3, GPIIIa), the vWF receptor glycoproteins CD42d (GPV) and CD42a (GPIX) and the collagen receptor glycoproteins CD49b (integrin α_2, GPIa) and GPVI, compared to WT platelets (fig. 4.13A).

Then we assessed platelet activation in response to a range of agonists *in vitro* by flow cytometry. The ability of platelets to activate was assessed by α-granule secretion (P-selectin surface expression) and fibrinogen binding (which requires activation of integrin $\alpha_{IIb}\beta_3$ (CD41/61, GPIIb/IIIa)). Platelet activation is unaffected by removal of CRLF3, as *Crlf3*$^{-/-}$ platelets were able to activate similarly to WT platelets when stimulated with a range of agonists (fig. 4.13B).

Upon activation, platelets change shape and spread which requires re-organisation of the cytoskeleton. We assessed the ability of *Crlf3*$^{-/-}$ platelets to spread on fibrinogen-coated coverslips. We observed no difference in the mean platelet area of spread platelets between *Crlf3*$^{-/-}$ and WT spread platelets (fig. 4.14A), suggesting *Crlf3*$^{-/-}$ platelets are able to reorganise

their cytoskeleton and change shape upon activation. Finally, we looked at the ability of *Crlf3*$^{-/-}$ platelets to form stable thrombi under shear conditions *in vitro*, by flowing whole *Crlf3*$^{-/-}$ or WT blood over fibrillar collagen at arteriolar shear rates. Thrombi area was the same for *Crlf3*$^{-/-}$ and WT blood (fig. 4.14B). These data suggest ablation of *Crlf3* does not affect the primary haemostatic function of platelets and therefore, defects of platelet aggregation/activation are not responsible for platelet clearance by the spleen.

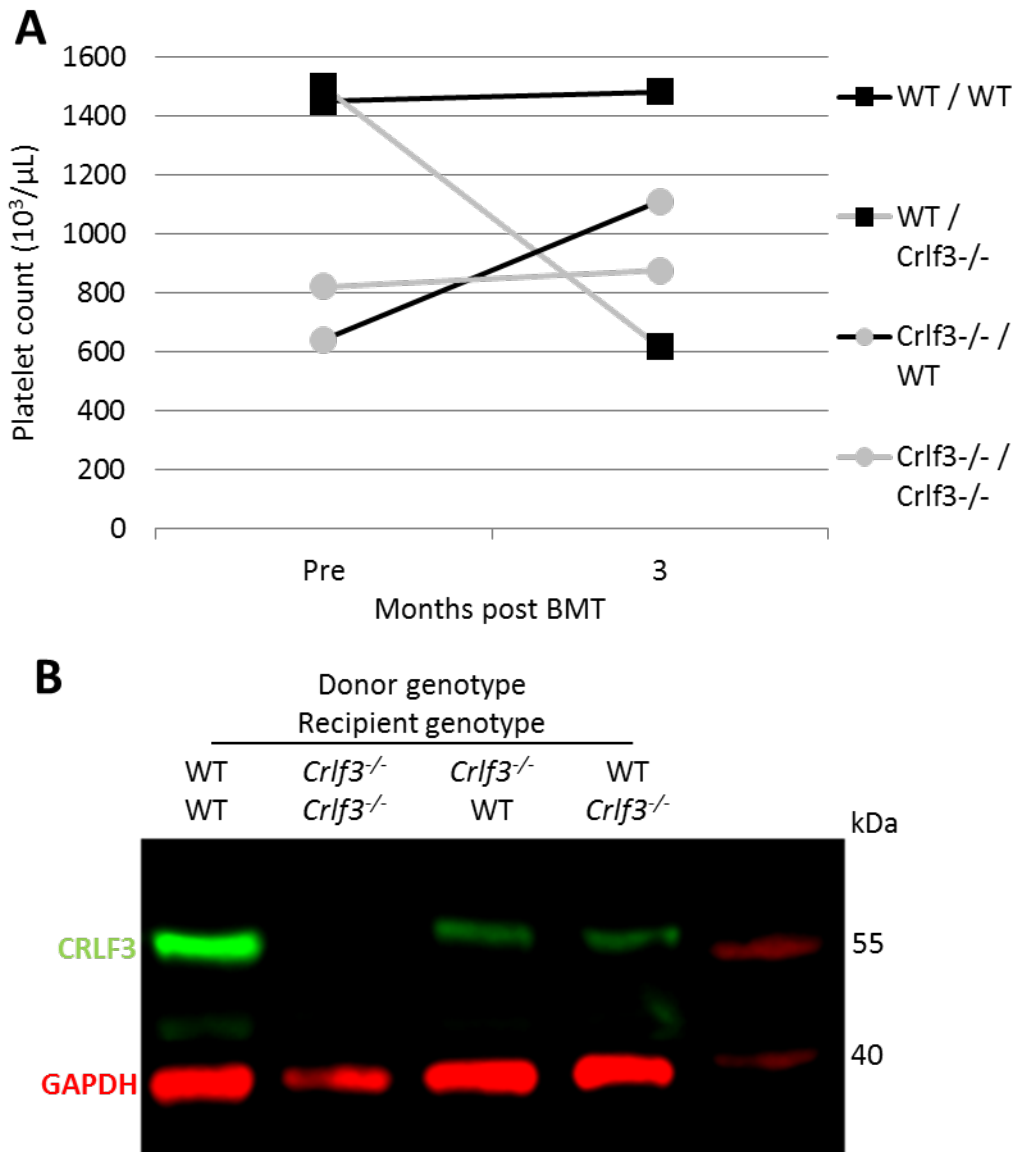

Figure 4.12 – Defects in the haematopoietic compartment cause thrombocytopenia in *Crlf3*$^{-/-}$ mice. (A) Sub lethally irradiated WT (black square) and *Crlf3*$^{-/-}$ (grey circle) recipient mice transplanted with WT (black lines) or *Crlf3*$^{-/-}$ (grey lines) bone marrow cells. Data represents mean (*n*=1-2). (B) Western blot of *in vitro* cultured MK lysates using specific antibodies against CRLF3 and GAPDH.

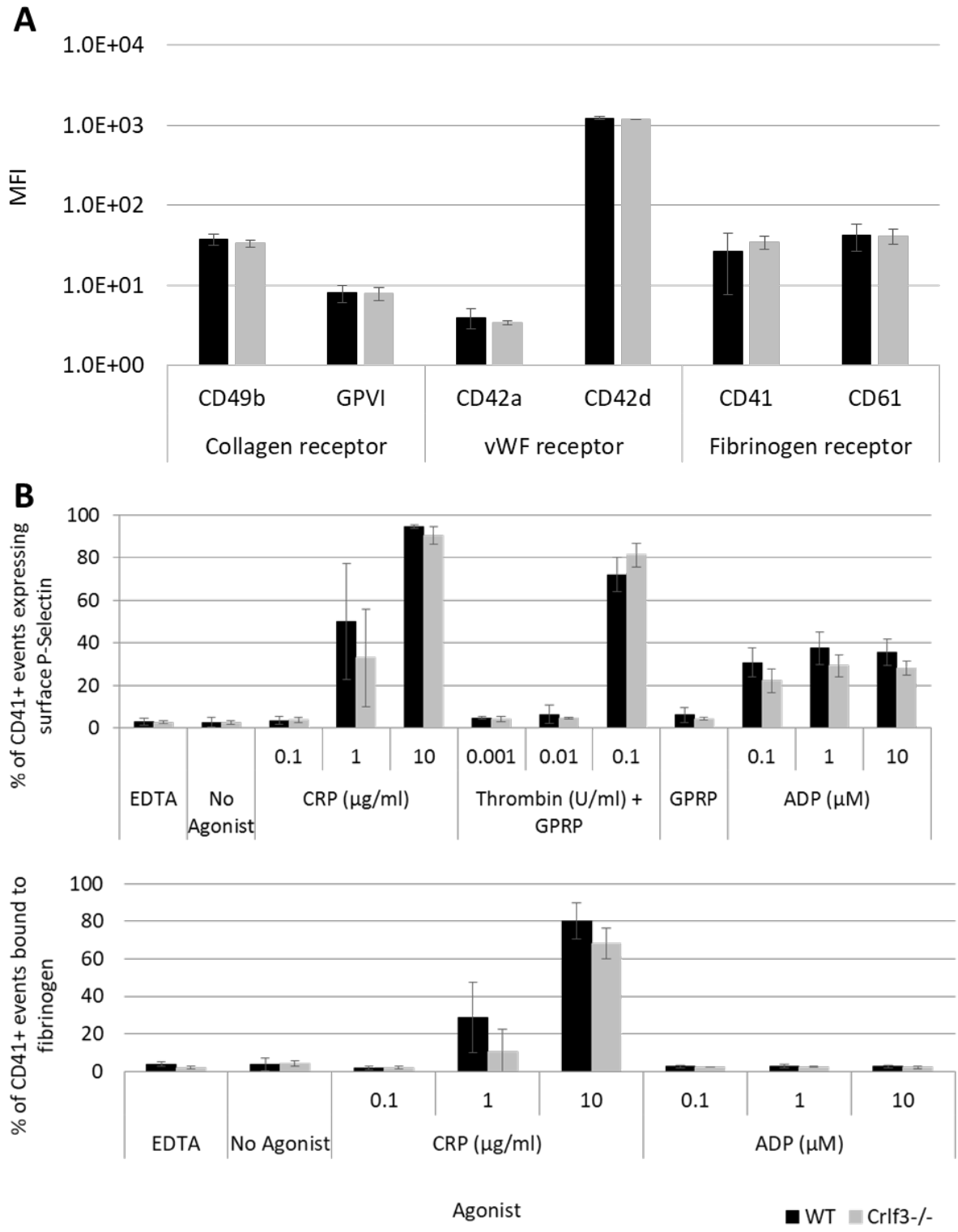

Figure 4.13 – platelet activation is unaffected in *Crlf3*$^{-/-}$ mice. (A) WT (black) and *Crlf3*$^{-/-}$ (grey) whole blood incubated with specific antibodies against CD41, CD61, CD42d, CD42a, CD49b and GPVI and assessed by flow cytometry, gating on platelet sized events (*n*=3). MFI denotes mean fluorescent intensity. (B) WT (black) and *Crlf3*$^{-/-}$ (grey) whole blood incubated with specific antibodies against CD41, P-Selectin and fibrinogen with or without addition of agonists. Percentage of CD41^{+} events expressing surface P-selectin (top panel) or bound to fibrinogen (bottom panel) was determined by flow cytometry (*n*=3). Data represents mean ± SD. Unpaired 2-tailed Student's *t* test with correction for multiple comparisons using the Holm-Sidak method.

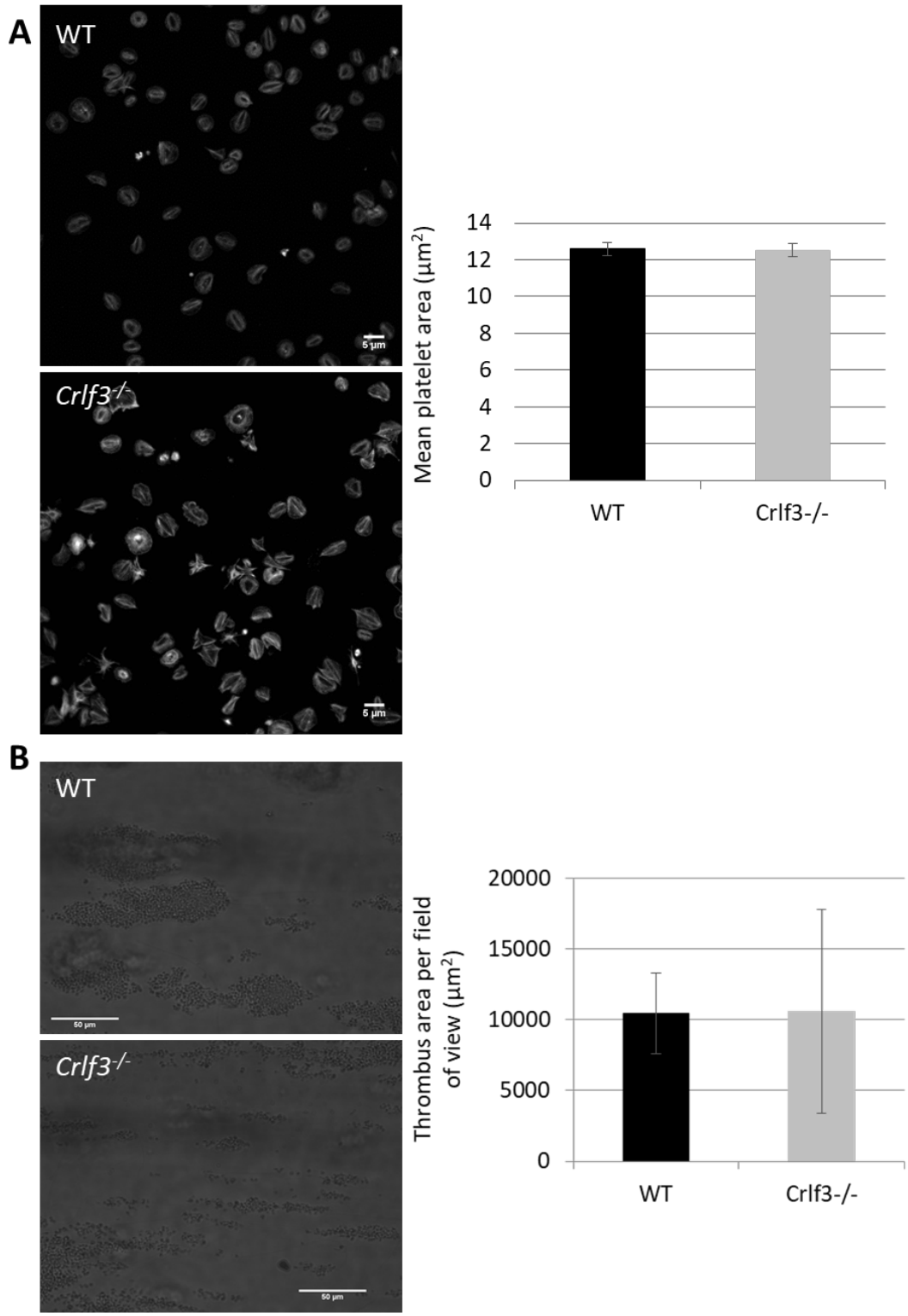

Figure 4.14 - *Crlf3*$^{-/-}$ platelets can form stable thrombi under arteriolar shear. (A) WT (black) and *Crlf3*$^{-/-}$ (grey) washed platelets seeded onto fibrinogen coated coverslips and incubated for 30 mins at 37°C. Fixed samples stained with a fluorescently labelled F-actin probed and imaged by fluorescent microscopy. Platelet area determined by thresholding images on F-actin staining using ImageJ. Images representative of 5 images taken per mouse (*n*=3). Scale bars are 5µm. (B) Heparinised whole blood flowed over fibrillar collagen and imaged by light microscopy. Thrombus area for WT (black) and *Crlf3*$^{-/-}$ (grey) mice determined by manually measuring the size of each thrombi using ImageJ. Images representative of 10 images taken per mouse (*n*=3). Scale bars are 50µm. Data represents mean ± SD. Unpaired 2-tailed Student's *t* test.

4.4.6 Ineffective thrombopoiesis

Rapid Romanowsky staining of blood smears made using EDTA anticoagulated blood of old (>52 weeks) *Crlf3*$^{-/-}$ mice revealed proplatelet like fragments (from now on termed preplatelets) in the peripheral circulation (fig. 4.15A). Although preplatelets are known to exist in the peripheral circulation of WT mice, they are not seen on blood smears when EDTA is used as an anticoagulant possibly due to the sphering effect of EDTA (Thon et al., 2012a); indeed, blood smears from old WT mice did not show preplatelets. Therefore, by observing preplatelets in *Crlf3*$^{-/-}$ blood smears made with blood anticoagulated using EDTA, it suggests there is a real difference structure and/or stability of *Crlf3*$^{-/-}$ preplatelets. To confirm the observed preplatelets were indeed proplatelet like fragments, *Crlf3*$^{-/-}$ blood smears were stained with fluorescently labelled antibodies against CD41 and vWF. The preplatelets are CD41 positive and have a granular staining of vWF reminiscent of proplatelets (vWF is packaged into immature α-granules in proplatelets) (fig. 4.15B), confirming the preplatelets are indeed fragments of proplatelets. Washed platelets from old *Crlf3*$^{-/-}$ mice were then fixed and prepared for transmission and scanning electron microscopy (TEM and SEM, respectively). Preplatelets with the stereotypical beads-on-a-string morphology of proplatelets were seen by both TEM and SEM (fig. 4.15C and D, respectively).

In normal conditions, large proplatelet fragments undergo fission into smaller fragments which again fragment to become mature platelets. This process is facilitated by the high shear of the peripheral circulation. The presence of large preplatelets in the peripheral circulation of *Crlf3*$^{-/-}$ mice suggests a defect in the final maturation process of platelets, which we have termed ineffective thrombopoiesis. As removal of the spleen was able to normalise platelet counts in *Crlf3*$^{-/-}$ mice, we looked at the effect of splenic removal on preplatelet numbers. To this end, we assessed the level of preplatelets in the peripheral circulation of young mice pre and post splenectomy by flow cytometry (experiments performed by Simon Stritt, University of Würzburg, Würzburg, Germany). Before splenectomy, preplatelets were observed in both WT and *Crlf3*$^{-/-}$ blood, consistent with previous observations that preplatelets exist in the peripheral circulation. However, *Crlf3*$^{-/-}$ mice had significantly more preplatelets in their peripheral circulation than WT mice (p=0.002; fig. 4.15E), suggesting the release of preplatelets is upregulated or fission of preplatelets to mature platelets is decreased. Post splenectomy, WT mice experience a small increase in platelet count (fig. 411B), which is

accompanied by a small increase in the number of preplatelets. WT preplatelets are able to mature very quickly in the peripheral circulation and therefore the removal of the spleen only increases the number of circulating preplatelets by a small margin (the few that would otherwise be cleared by the spleen). In the *Crlf3*$^{-/-}$ mice however, preplatelet counts remain stable or slightly decrease after splenectomy despite a large increase and normalisation of platelet counts. The normalisation of platelet counts without an increase in circulating preplatelets suggests that without the spleen, *Crlf3*$^{-/-}$ preplatelets are able to undergo fission and form mature platelets thus normalising platelet counts.

Of note, the preplatelets recorded by flow cytometry are unlikely to be platelet microaggregates as events with forward/side scatter characteristics of preplatelets (i.e. larger than mature platelets) do not show activated GPIIb/IIIa or P-selectin surface exposure, which are indicative of platelet activation and needed for platelet aggregation (fig. 4.15F).

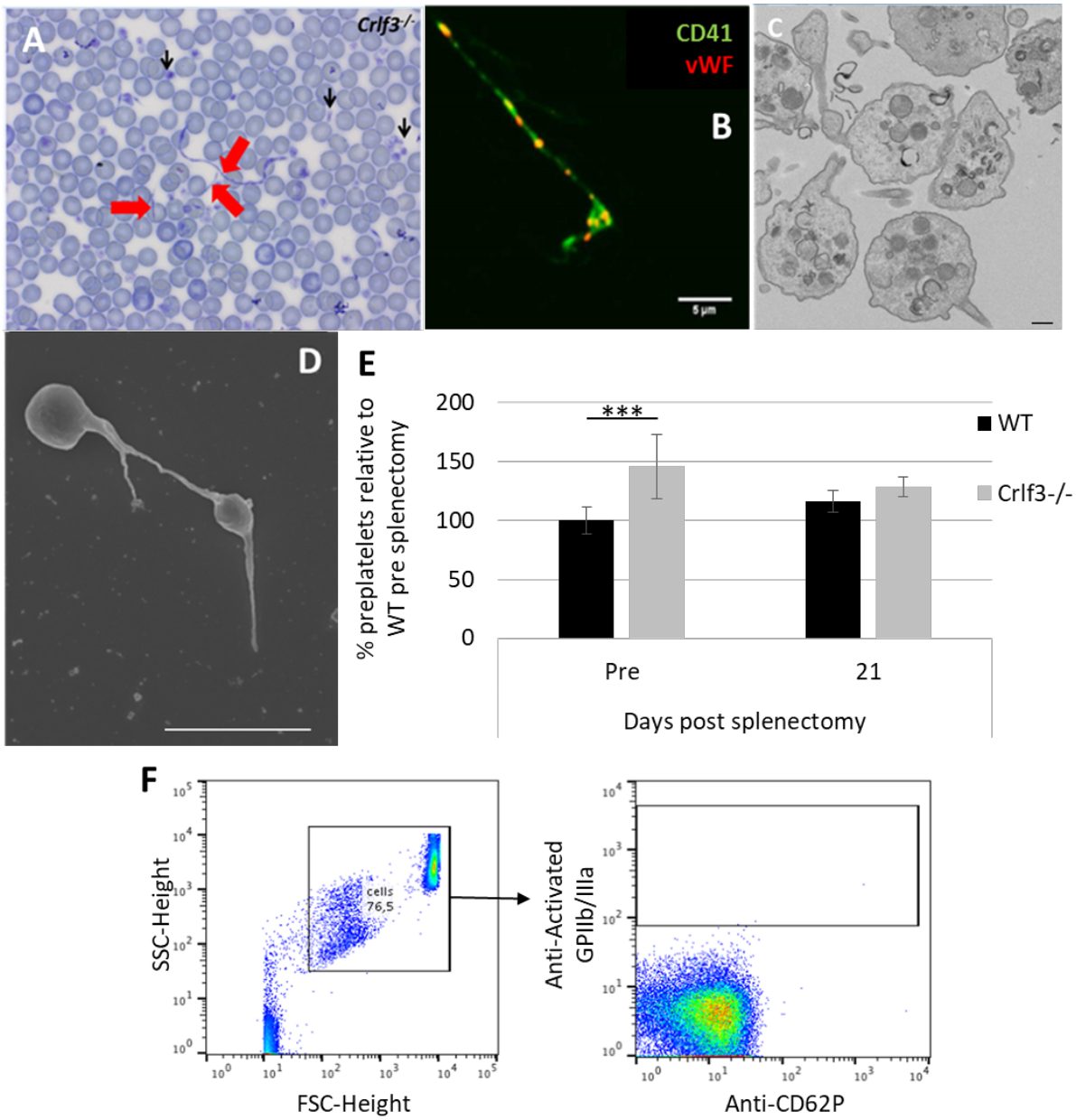

Figure 4.15 – Large preplatelet are retained in the peripheral circulation of old *Crlf3*$^{-/-}$ mice. (A) Blood smear from EDTA anticoagulated whole blood of an old *Crlf3*$^{-/-}$ mouse. Red arrow heads point to preplatelets, black arrow heads point to mature round platelets. (B) *Crlf3*$^{-/-}$ blood smear stained with specific antibodies against CD41 (green) and vWF (red) and imaged by confocal microscopy. Washed platelets from old *Crlf3*$^{-/-}$ mice fixed and prepared for transmission (C) and scanning (D) electron microscopy. (E) WT (black) and *Crlf3*$^{-/-}$ (grey) mice were splenectomised. Heparinised venous blood incubated with specific antibodies against GPV and GPIIbIIIa. Percentage of preplatelets determined by flow cytometry as GPV^{+}/GPIIbIIIa^{+} events with larger forward scatter/side scatter than mature platelets (*n*=4-5). (F) Heparinised venous blood incubated with specific antibodies against activated GPIIb/IIIa and CD62P and assessed by flow cytometry, to rule out the possibility that preplatelets are platelet microaggregates. Scale bars are 10µm (A), 5µm (B and D) and 500nm (C). Data represents mean ± SD. Two-way ANOVA with Tukey's correction for multiple comparisons. *** denotes p<0.005.

4.4.7 *Crlf3*$^{-/-}$ platelets have increased microtubule stability

As evidence has pointed to impaired maturation of preplatelets in the peripheral circulation, we looked at the major cytoskeletal proteins actin and tubulin in *Crlf3*$^{-/-}$ platelets, as these proteins are the major drivers of proplatelet formation. *Crlf3*$^{-/-}$ and WT washed platelets were fixed, permeabilised and allowed to adhere to poly-L-lysine coated coverslips in their resting state. Staining of resting WT platelets maintained at 37^{o}C with fluorescent antibodies against α-tubulin and a fluorescently labelled F-actin probe showed a stereotypical cytoplasmic actin staining with a well-defined marginal microtubule coil (fig. 4.16A and B). Although many *Crlf3*$^{-/-}$ platelets stained similarly to WT platelets, some platelets had disorganised and/or increased tubulin expression (fig. 4.16C and D). This abnormal tubulin staining is reminiscent of that seen in platelets from profilin 1 knockout mice and WAS patients (Bender et al., 2014) and patients with DIAPH1-related macrothrombocytopenia (Stritt et al., 2016). Profilin 1 knockout and DIAPH1 mutant platelets were shown to have increased microtubule stability, so we tested whether microtubule stability was affected in *Crlf3*$^{-/-}$ platelets. Washed platelets were incubated at 4^{o}C to induce microtubule depolymerisation and then fixed, permeabilised and allowed to adhere to poly-L-lysine coverslips. As was expected, the majority of WT platelets were able to fully depolymerise their marginal microtubule coil, resulting in abolished tubulin staining (fig. 4.16E, F and I). However, significantly more *Crlf3*$^{-/-}$ platelets did not undergo microtubule depolymerisation, retaining their marginal microtubule coil (41.01% *Crlf3*$^{-/-}$ vs 13.43% WT, p=8.4x10^{-5}, fig. 4.16G, H and I), suggesting microtubule stability is increased in *Crlf3*$^{-/-}$ platelets (Platelet fixation staining and image acquisition performed by Simon Stritt, University of Würzburg, Würzburg, Germany).

Dynamic microtubules are characterised by tyrosinated α-tubulin (Tyr-tubulin), whereas stable microtubules are associated with detyrosination (Glu-tubulin). The ratio between Glu- and Tyr-tubulin can be used as an indicator of the degree of microtubule stability (Pan et al., 2014; Stritt et al., 2016). Surprisingly, we found no difference in the ratio of Glu-tubulin to Tyr-tubulin expression in resting *Crlf3*$^{-/-}$ platelets compared to WT controls (fig. 4.16J and K).

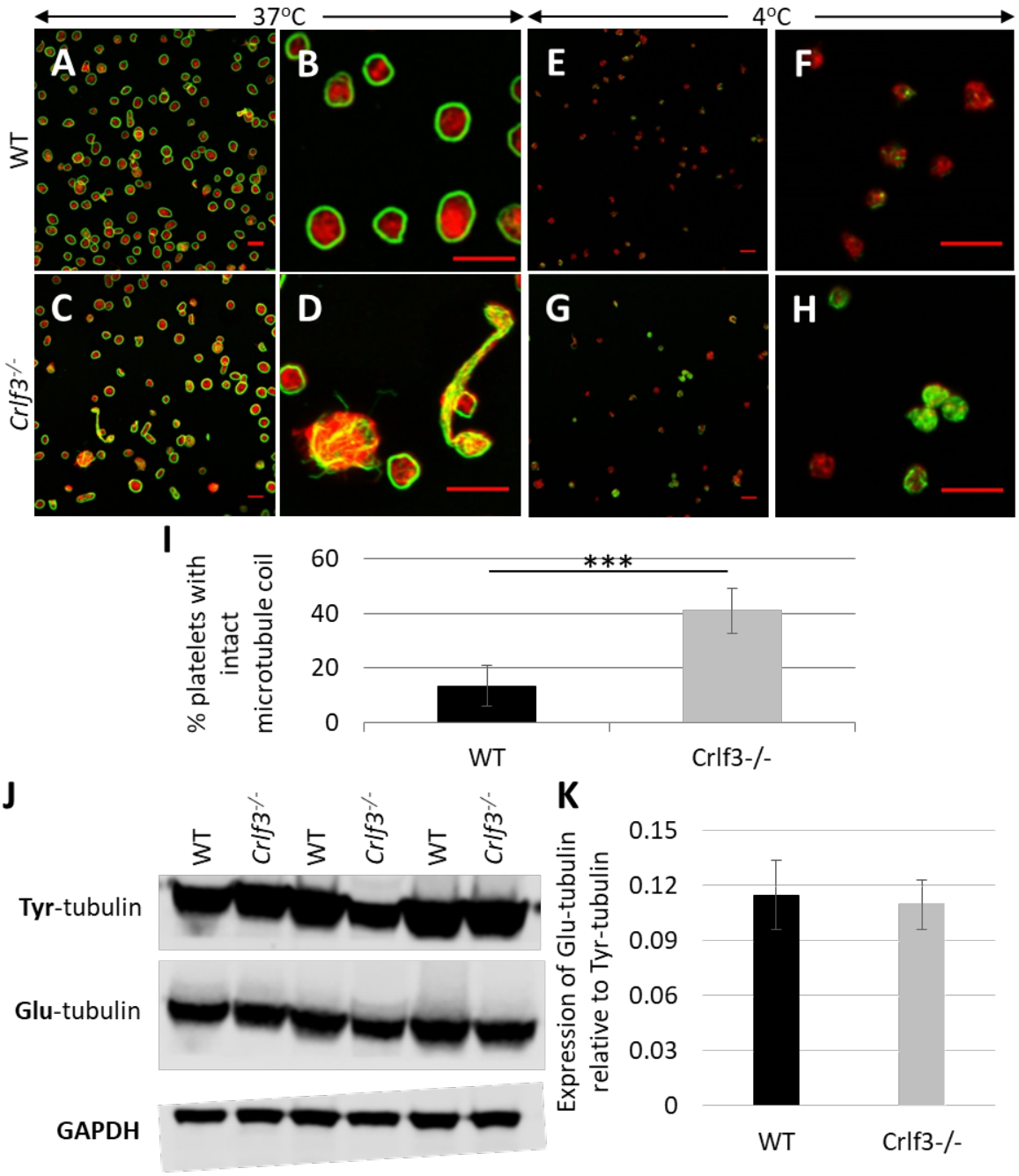

Figure 4.16 – Aberrant tubulin expression and possibly increased microtubule stability in *Crlf3*$^{-/-}$ platelets. Washed platelets maintained at 37°C (WT - A and B and *Crlf3*$^{-/-}$ - C and D) or stored at 4°C for 3 hours (WT - E and F and *Crlf3*$^{-/-}$ - G and H) adhered to poly-L-lysine coated coverslips and stained with specific antibodies against α-tubulin (green) and a fluorescently labelled F-actin probe (red). Scale bars are 5µm. (I) Platelets with intact microtubule coils after incubation at 4°C were determined by manual counting of 5 images for WT (black) and *Crlf3*$^{-/-}$ (grey) mice (*n*=4). (J) Western blot of washed platelet lysates using specific antibodies against tyrosinated (Tyr) tubulin, detyrosinated (Glu) tubulin and GAPDH. (K) Expression of Tyr- and Glu-tubulin determined from western blot (J) using Image Studio Lite (*n*=3). Data represents mean ± SD. Unpaired 2-tailed Student's *t* test.

4.5 Chapter conclusions

There were two main aims of this chapter, to show that the isolated thrombocytopenia in *Crlf3*$^{-/-}$ mice is sustained throughout life and to uncover the biological mechanisms in which ablation of *Crlf3* results in thrombocytopenia.

Isolated thrombocytopenia

Performing automated full blood counts on venous blood of *Crlf3*$^{-/-}$ and WT control mice at young (≤20 weeks), middle (21-40 weeks) and old (≥52 weeks) age time points revealed that *Crlf3* induced thrombocytopenia is maintained throughout life. Ablation of *Crlf3* effects the formation of platelets very specifically. The degree of thrombocytopenia varies over time, but there is a 25-39% decrease in platelet count in male mice and 26-42% decrease in female mice compared to aged matched WT controls (fig 4.4 and table 4.1). Surprisingly, the MPV is unchanged in *Crlf3*$^{-/-}$ mice (table 4.1). Most inherited thrombocytopenias are associated with increased MPV (gray platelet syndrome (Guerrero et al., 2014), Bernard-Soullier syndrome (Dutting et al., 2017) and Wiskott-Aldrich syndrome (Bender et al., 2014)). The normal MPV recorded in *Crlf3*$^{-/-}$ mice is probably due to the mechanism by which the automated haemocytometer defines platelets. As *Crlf3*$^{-/-}$ results in large proplatelet fragments (preplatelets) in the peripheral circulation (fig. 4.15A-D), MPV should be increased. However, these preplatelets will not be recorded as platelets by the haemocytometer and therefore the MPV will only be determined by mature round platelets.

In our hands, no other blood lineage was affected by *Crlf3* ablation despite MCV being recorded as significantly decreased in pipeline phenotyping done by the Wellcome Trust Sanger Institute.

Biological consequences of *Crlf3* ablation

Ablation of *Crlf3* appears to affect the final maturation step of platelets in the peripheral circulation, rather than release of platelets. Megakaryopoiesis is upregulated in *Crlf3*$^{-/-}$ mice (fig. 4.5) and MK maturation is unaffected *in vitro* (fig. 4.8). *Crlf3*$^{-/-}$ MKs are also able to produce proplatelets with similar morphology to WT proplatelets both *in vitro* (fig. 4.9) and *in vivo*

(supplementary videos 1 and 2), all data that suggests production of platelets from MKs is not affected. Under normal physiology, preplatelets released by proplatelet shafts into the bone marrow sinusoids rapidly undergo fission into mature platelets in the high shear of the peripheral circulation. However, *Crlf3*$^{-/-}$ mice contain large preplatelets in the peripheral circulation (fig. 4.15A-D), and *Crlf3*$^{-/-}$ mice have increased preplatelets in the peripheral circulation compared to WT control mice (fig. 4.15E), suggesting that fission of *Crlf3*$^{-/-}$ preplatelets is decreased. Although the exact mechanism for decreased fission of *Crlf3*$^{-/-}$ preplatelets has not been discovered, we were able to show that *Crlf3*$^{-/-}$ platelets have disorganised tubulin expression especially in the preplatelet forms (fig. 4.16A-D). The disorganised tubulin expression is similar to that seen in the platelets of patients with WAS and DIAPH1-related macrothrombocytopenia and in profilin 1 knockout mice (Bender et al., 2014; Stritt et al., 2016). In all cases, abnormal tubulin expression confers to increased tubulin stability. In concordance with this, depolymerisation of the microtubules is decreased in *Crlf3*$^{-/-}$ platelets incubated at 4^{o}C (fig. 4.16E-I). However, we did not observe an increase in the ratio of detyrosinated (Glu-) tubulin to tyrosinated (Tyr-) tubulin (fig. 4.16J-K). Therefore, whether increased tubulin stabilisation is the cause of decreased preplatelet fission is yet to be resolved.

The thrombocytopenia in *Crlf3*$^{-/-}$ mice can be attributed to rapid splenic removal of preplatelets from the circulation. Studies on platelet lifespan show the removal of platelets must happen within the first 24 hours of release from MKs as post 24 hours, platelet lifespan is comparable to WT platelets (fig. 4.10A). In splenectomised WT mice we observe a small increase in the platelet count (fig. 4.11B) accompanied by a small increase in the number of preplatelets (fig. 4.15E). WT preplatelets are known to mature very quickly in the circulation and therefore the removal of the spleen only increases the number of circulating preplatelets by a small margin (the few that would otherwise be cleared by the spleen). However, *Crlf3*$^{-/-}$ preplatelets mature a lot slower, which is evidenced by large preplatelets observed in the peripheral circulation (fig. 4.15A-D). The decrease rate of maturation of *Crlf3*$^{-/-}$ preplatelets is possibly due to increased tubulin stability (fig. 4.15E-I). As a consequence of the decreased preplatelet maturation in *Crlf3*$^{-/-}$ mice a much larger proportion of the preplatelets released by MKs are removed by the spleen before giving rise to mature platelets. This leads to thrombocytopenia. In response the bone marrow is stimulated to compensate by producing more MKs (as evidence in fig. 4.5). Once the spleen is removed, *Crlf3*$^{-/-}$ preplatelets are allowed

to mature into platelets thereby correcting the platelet count (fig. 4.11B). It is likely that the positive feed-back loop to the bone marrow disappears and preplatelet production from MKs is decreased. This is likely why we observe a slight decrease of preplatelets in the peripheral circulation after splenectomy in *Crlf3*$^{-/-}$ mice (fig. 4.15E), because production by the bone marrow has now reached a steady state comparable to that seen in the WT animals.

In spite of mild thrombocytopenia and abnormal tubulin expression in platelets, *Crlf3* ablation does not affect the ability of platelets to perform their primary haemostatic function. *Crlf3*$^{-/-}$ platelets express the major surface receptors required for platelet tethering, activation and aggregation/thrombus formation similarly to WT platelets (fig. 4.13A) and *Crlf3*$^{-/-}$ platelets activate appropriately in response to a range of agonists (fig. 4.13B). During the process of activation, platelets undergo shape change mediated by reorganisation of their cytoskeleton. Interestingly, despite aberrant tubulin expression and reduced cold induced microtubule depolymerisation, *Crlf3*$^{-/-}$ platelets are able to spread comparably to WT platelets when seeded onto fibrinogen (fig. 4.14A). This suggests reorganisation of tubulin and actin is unaffected at room temperature in *Crlf3*$^{-/-}$ platelets. In agreement with this, the size of thrombi produced by *Crlf3*$^{-/-}$ whole blood flowed over fibrillar collagen at arteriolar shear rates was similar to that of WT blood (fig. 4.14B).

5

Results 2

CRLF3 as a novel therapeutic target for the treatment of essential thrombocythaemia

5.1 Introduction

Essential thrombocythaemia (ET) is a rare disease that results in circulating platelet counts above $450x10^9$/L, caused by acquired clonal mutations mainly in *JAK2, CALR or MPL*. ET is a member of a group of diseases termed myeloproliferative neoplasms (MPN) along with polycythaemia vera (PV, increased red blood cells) and primary myelofibrosis (PMF, bone marrow fibrosis and extramedullary haematopoiesis). Treatment of ET is based on an individual needs and currently uses combination therapy of low dose aspirin to reduce platelet function and cytoreductive agents to reduce MK and platelet content. The cytoreductive agents have a range cardiovascular and haematological side effects and are therefore not suitable and/or tolerated by some patients (Cervantes, 2011; Rumi and Cazzola, 2016). An ideal therapy would specifically decrease platelet counts whilst having minimal side effects, especially those affecting the haematological and cardiovascular systems.

A gain of function mutation in *JAK2* (JAK2 V617F) is present in the majority of PV cases and approximately 50-60% of ET and PMF cases, therefore it has been studied in the most detail (Baxter et al., 2005; James et al., 2005; Kralovics et al., 2005; Levine et al., 2005). It is unknown exactly how this single point mutation can lead to different diseases, but mutant allele dose has been suggested as most patients with PV have clones homozygous for the JAK2 V617F mutation, although this is rare in ET (Scott et al., 2006). This mutation allele dose theory is backed up by evidence from a multitude of murine models developed to study the role of JAK2 V617F in ET. Retroviral transduction of bone marrow with mutant JAK2 V617F containing vectors and subsequent transplantations leads to overexpression of mutant JAK2 relative to WT JAK2. Mice induced in this way show a PV phenotype with a marked increase in haematocrit (Lacout et al., 2006; Wernig et al., 2006). Also, transgenic mice generated using a human BAC containing a 5' portion of JAK2 and retrofitted with a 3' cDNA fragment containing the rest of JAK2 with the V617F mutation displayed varying phenotypes based on mutant JAK2 copy number. When these transgenic mice were crossed with VavCre mice, relatively few transgene copies were retained and mice displayed an ET phenotype, whereas, when crossed with Mx1Cre mice multiple transgene copies were retained and a more PV phenotype was observed (Tiedt et al., 2008).

Despite the VavCre model described above providing a model of ET, there are some differences to phenotype of JAK2 V617F positive ET seen in humans. Firstly, platelet counts were drastically increased in VavCre mice whereas JAK2 V617F patients have mild thrombocythaemia, secondly splenomegaly was observed readily in VavCre mice where it is rare in patients and finally, haemoglobin levels where unaffected whereas they are mildly but significantly increased in patients (Cervantes, 2011; Tiedt et al., 2008). In 2010, Li *et al* developed an inducible (Mx1Cre) knock-in JAK2 V617F mutant heterozygous mouse (*Jak2*$^{fl/+}$ Cre^{+}). They inserted a floxed minigene together with mutant human JAK2 V617F cDNA into the translation start site of exon 2. Removal of the minigene by Cre-mediated recombination results in expression of mutant *JAK2* under the control of endogenous mouse *Jak2* locus. As such, expression levels of murine *Jak2* and mutant human *JAK2* are similar and there is no increase in total JAK2 in mutant mice. *Jak2*$^{fl/+}$ Cre^{+} mice have an ET phenotype similar to that seen in JAK2 V617F positive patients. They have a mild thrombocythaemia, slightly increased haemoglobin level and splenomegaly is rarely seen. MK hyperplasia is also seen in *Jak2*$^{fl/+}$ Cre^{+} mice and is a feature of ET (Cervantes, 2011; Li et al., 2010). Using this mouse model, it was shown that JAK2 V617F mutant platelets are hyper-reactive to a range of agonists, show increased spreading on fibrinogen and form larger thrombi under pathological shear conditions. This hyper-reactive state of mutant platelets may increase the chance of arterial and venous thrombotic events, which are the major causes of morbidity and mortality in ET patients (Hobbs et al., 2013).

5.2 Chapter hypotheses and aims

We hypothesise that CRLF3 could be a novel therapeutic target for the treatment of thrombocythaemia, with inhibitors against CRLF3 specifically decreasing platelet counts. Therefore, we aim to show a normalisation of platelet counts in ET mice crossbred with *Crlf3*$^{-/-}$ mice. We also aim to show that the decrease of platelet counts is isolated in an ET setting.

5.3 Chapter overview

This chapter will show how *Crlf3*$^{-/-}$ mice were cross bred with JAK2 V617F ET mice to allow assessment of whether CRLF3 could be a therapeutic target for the treatment of ET. We show

that ablation of *Crlf3* in an ET setting restores platelet counts to WT levels, the prerequisite for CRLF3 as a therapeutic target. We also show that other abnormalities associated with ET (MK hyperplasia and platelet hyper-reactivity) are unchanged after ablation of *Crlf3*.

5.4 Results

5.4.1 Breeding strategy

To assess how ablation of *Crlf3* affects the phenotype of ET (increased platelet counts, MK hyperplasia and increased platelet reactivity), we crossbred *Crlf3*$^{-/-}$ mice with knock-in JAK2 V617F mutant mice (*Jak2*$^{fl/+}$ Cre^{+}) that have an ET phenotype (fig. 5.1). Pups derived from these mating's were all heterozygous for *Crlf3*, could carry WT *Jak2* alleles (*Jak2*$^{+/+}$) or be heterozygous for the mutant *Jak2* allele (*Jak*$^{fl/+}$) and could carry an allele for Mx1Cre or not (Cre^{+} or Cre^{-}, respectively). At approximately 8 weeks old, *Crlf3* heterozygous *Jak2*$^{fl/+}$ Cre^{+} mice were crossbred with *Crlf3* heterozygous *Jak2*$^{+/+}$ Cre^{-} mice (or *Jak2*$^{fl/+}$ Cre^{-} mated with *Jak2*$^{+/+}$ Cre^{+}). Pups from these mating's could have one, both or neither *Crlf3* allele deleted (*Crlf3*$^{+/-}$, *Crlf3*$^{-/-}$ and *Crlf3*$^{+/+}$, respectively). As per the previous mating's, pups could also could carry WT *Jak2* alleles or be heterozygous for the mutant *Jak2* allele and could carry an allele for Mx1Cre or not. Of the 12 possible genotypes, we were only interested in *Crlf3*$^{+/+}$ *Jak2*$^{+/+}$ Cre^{+}, *Crlf3*$^{-/-}$ *Jak2*$^{+/+}$ Cre^{+}, *Crlf3*$^{+/+}$ *Jak2*$^{fl/+}$ Cre^{+} and *Crlf3*$^{-/-}$ *Jak2*$^{fl/+}$ Cre^{+} mice (henceforth termed WT (Cre), *Crlf3*$^{-/-}$ (Cre), ET and ET x *Crlf3*$^{-/-}$, respectively). All pups were injected with sterile polyinosinic-polycytidylic acid prior to genotyping to induce the expression of the mutant *Jak2* in ET and ET x *Crlf3*$^{-/-}$ mice and to control for any effect of interferon induction.

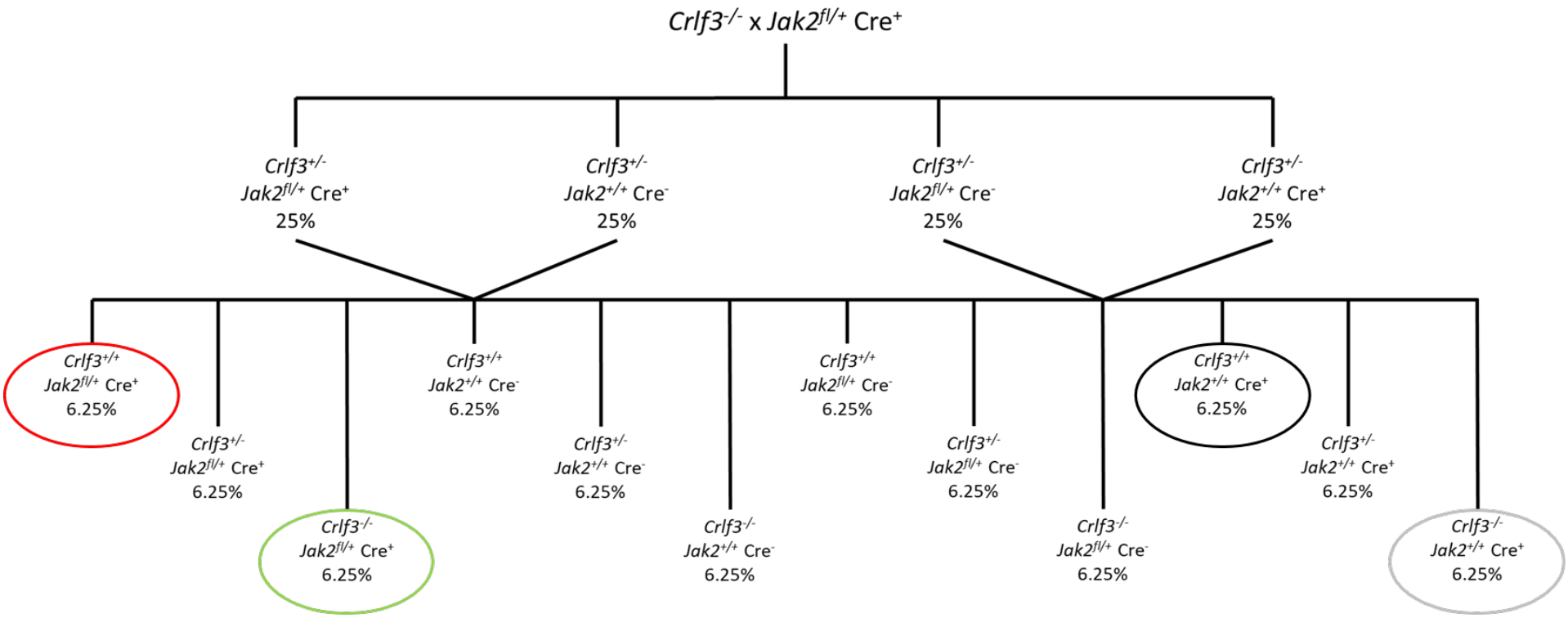

Figure 5.1 – Breeding strategy to create ET mice with *Crlf3* ablated. *Crlf3*$^{-/-}$ mice were crossbred with JAK2 V617F mice generating *Crlf3* heterozygous intermediates, which were cross bred again to generated lines of interest. Genotypes of interest are circled (black = WT (Cre); grey = *Crlf3*$^{-/-}$ (Cre); red = ET and green = ET x *Crlf3*$^{-/-}$).

5.4.2 Ablation of *Crlf3* restores platelet counts in ET mice

To determine the effect of ablation of CRLF3 on the haematopoietic lineage of crossbred mice, full blood counts were performed on venous blood from young (0-20 week old) and old (>48 weeks old) female mice. Only female mice were used for full blood counts, as the isolated thrombocytopenia seen in uncrossed *Crlf3*$^{-/-}$ mice was similar between males and females (fig. 4.3 and table 4.1) and maintaining female animals for long periods is much more cost effective as female mice are able to be combined to reduce cage numbers, whereas male mice cannot. Platelet counts tended to be lower in *Crlf3*$^{-/-}$ (Cre) mice compared to WT (Cre) controls (686 ± 222 x10^3/µl *Crlf3*$^{-/-}$ (Cre) vs 875 ± 306 x10^3/µl WT (Cre) in young mice and 712 ± 227 x10^3/µl *Crlf3*$^{-/-}$ (Cre) vs 1030 ± 426 x10^3/µl WT (Cre) in old mice, fig. 5.2 and table 5.1). As would be expected, ET mice have increased platelet counts compared to WT (Cre) controls. However, statistical significance is reached when comparing platelet counts of ET and *Crlf3*$^{-/-}$ (Cre) mice (p<0.005 for both young and old mice, fig. 5.2 and table 5.1), suggesting *Crlf3*$^{-/-}$ (Cre) mice have platelet counts lower than WT (Cre) mice and ET mice have higher platelet counts than WT (Cre) mice. Interestingly, ET x *Crlf3*$^{-/-}$ mice have platelet counts similar to WT (Cre) mice (879 ± 229 x10^3/µl ET x *Crlf3*$^{-/-}$ vs 875 ± 306 x10^3/µl WT (Cre) in young mice and 789 ± 294 x10^3/µl ET x *Crlf3*$^{-/-}$ vs 1030 ± 426 x10^3/µl WT (Cre) in old mice; p>0.999 and p=0.460 for young and old mice, respectively; fig. 5.2 and table 5.1) showing that ablation of *Crlf3* normalises platelet counts in ET mice.

Importantly, ablation of *Crlf3* in ET mice does not lead to dysregulation of any other blood lineage irrespective of age (table 5.1). This confirms the isolated effect of CRLF3 on platelet production and suggests therapeutics that target CRLF3 may have less side effects than current cytoreductive agents.

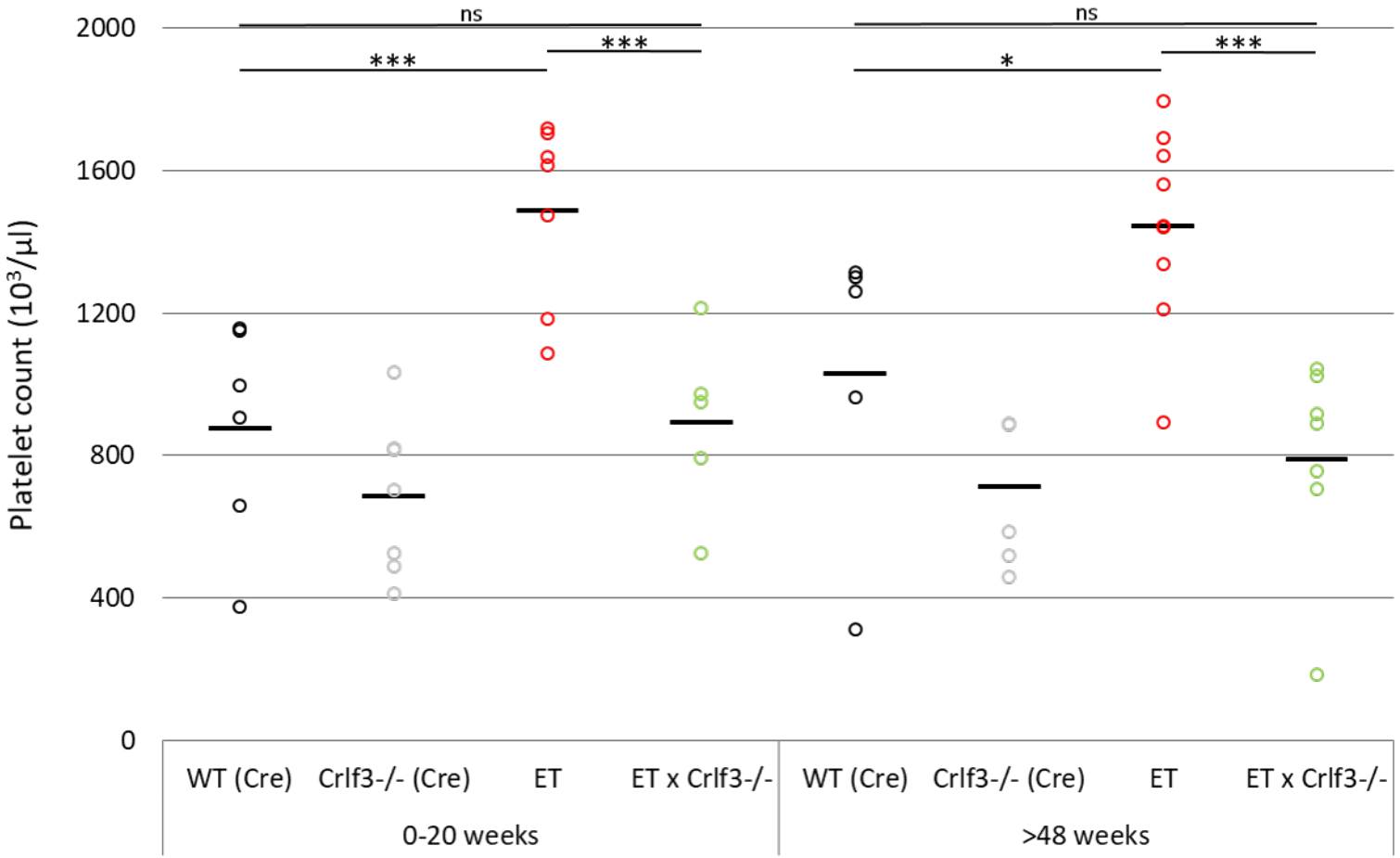

Figure 5.2 – Ablation of *Crlf3* normalises platelet counts in ET mice. Platelet counts determined using an automated haemocytometer on EDTA anticoagulated venous blood withdrawn from young (0-20 weeks; *n*=6-7) and old (>48 weeks; *n*=5-9) female WT (Cre) (black), *Crlf3*$^{-/-}$ (Cre) (grey), ET (red) and ET x *Crlf3*$^{-/-}$ (green) mice. Two-way ANOVA with Tukey's correction for multiple comparisons; ns, * and *** denote not significant, $p<0.05$ and $p<0.005$, respectively.

0-20 week old mice								
		Plt (10^3/μL)	**MPV (fL)**	**Hgb (g/dL)**	**RBC (10^6/μL)**	**WBC (10^3/μL)**	**Age (weeks)**	***n***
	WT (Cre)	875.00 (305.95)	5.62 (0.26)	14.52 (0.75)	10.52 (0.54)	10.37 (4.24)	10.21 (3.46)	6
	Crlf3 $^{-/-}$ **(Cre)**	686.29 (222.19)	5.71 (0.32)	13.63 (1.48)	9.98 (1.22)	8.90 (2.93)	9.49 (3.38)	7
	ET	1488.71 (255.17)	5.64 (0.36)	14.79 (0.94)	10.68 (0.63)	10.16 (2.27)	12.53 (4.79)	7
	ET x *Crlf3* $^{-/-}$	879.17 (228.67)	5.83 (0.53)	14.78 (1.54)	10.93 (1.27)	11.42 (2.35)	12.31 (4.24)	6
Statistical significance	WT (Cre) vs *Crlf3* $^{-/-}$ (Cre)	ns	ns	ns	ns	ns	ns	
	WT (Cre) vs ET	***	ns	ns	ns	ns	ns	
	WT (Cre) vs ET x *Crlf3* $^{-/-}$	ns	ns	ns	ns	ns	ns	
	Crlf3 $^{-/-}$ (Cre) vs ET	***	ns	ns	ns	ns	ns	
	Crlf3 $^{-/-}$ (Cre) vs ET x *Crlf3* $^{-/-}$	ns	ns	ns	ns	ns	ns	
	ET vs ET x *Crlf3* $^{-/-}$	***	ns	ns	ns	ns	ns	
>48 week old mice								
		Plt (10^3/μL)	**MPV (fL)**	**Hgb (g/dL)**	**RBC (10^6/μL)**	**WBC (10^3/μL)**	**Age (weeks)**	***n***
	WT (Cre)	1030.40 (425.87)	5.46 (0.52)	13.90 (1.19)	10.24 (0.41)	12.42 (4.13)	57.86 (7.77)	5
	Crlf3 $^{-/-}$ **(Cre)**	712.43 (227.21)	5.31 (0.59)	13.54 (1.77)	9.55(1.42)	8.00 (2.06)	65.74 (8.17)	7
	ET	1445.78 (275.61)	5.30 (0.47)	13.58 (1.33)	10.23 (1.05)	9.27 (3.01)	68.06 (11.05)	9
	ET x *Crlf3* $^{-/-}$	789.29 (293.88)	5.26 (049)	14.87 (2.05)	11.04 (1.53)	9.33 (1.73)	70.84 (14.99)	7
Statistical significance	WT (Cre) vs *Crlf3* $^{-/-}$ (Cre)	ns	ns	ns	ns	ns	ns	
	WT (Cre) vs ET	*	ns	ns	ns	ns	ns	
	WT (Cre) vs ET x *Crlf3* $^{-/-}$	ns	ns	ns	ns	ns	ns	
	Crlf3 $^{-/-}$ (Cre) vs ET	***	ns	ns	ns	ns	ns	
	Crlf3 $^{-/-}$ (Cre) vs ET x *Crlf3* $^{-/-}$	ns	ns	ns	ns	ns	ns	
	ET vs ET x *Crlf3* $^{-/-}$	***	ns	ns	ns	ns	ns	

Table 5.1 – Full blood counts in crossbred female mice. Full blood counts determined using an automated haemocytometer on EDTA anticoagulated venous blood withdrawn from young (0-20 week old; *n*=6-7) and old (>48 week old; *n*=5-9) female WT (Cre), *Crlf3*$^{-/-}$ (Cre), ET and ET x *Crlf3*$^{-/-}$ mice. Data represents mean (SD). Two-way ANOVA with Tukey's correction for multiple comparisons; ns, * and *** denote not significant, $p<0.05$ and $p<0.005$, respectively.

5.4.3 Platelet reactivity and MK hyperplasia not increased

JAK2 V617F positive ET is associated with MK hyperplasia and increased platelet reactivity as well as the classical increase in platelet numbers, as discussed in section 5.1. To determine whether ablation of *Crlf3* has any effect on these other features of ET, we assessed platelet activation and thrombus formation *in vitro* and observed MK numbers in the bone marrow of crossbred mice.

Mice tibia were fixed and sectioned and MKs counted after H&E staining. Unexpectedly, we observed similar numbers of bone marrow residing MKs in all genotypes (fig. 5.3). In section 4.4.3 we showed upregulation of megakaryopoiesis in *Crlf3*$^{-/-}$ mice compared to WT controls, so we would have expected to see an increase in MKs in *Crlf3*$^{-/-}$ (Cre) mice compared to WT (Cre) controls. Also, the JAK2 V617F positive ET mice used here are known to have increased

bone marrow residing MKs (Li et al., 2010), which was not seen by us. Although no increased in MK numbers was observed in ET x *Crlf3*$^{-/-}$ mice compared to ET mice, suggesting that inhibitors of CRLF3 may not exacerbate the MK hyperplasia associated with ET, we must take into consideration that the phenotype of *Crlf3*$^{-/-}$ and ET mice was not recapitulated with regards to MK hyperplasia.

We did not expect to observe any difference in the ability of platelets to activate and form thrombi between *Crlf3*$^{-/-}$ (Cre) and WT (Cre) controls, as no differences were reported in section 4.4.5. Indeed, no difference were observed in the ability of platelets to degranulate and bind fibrinogen in response to a range of agonists (fig. 5.4), undergo shape change (fig. 5.5A) or form stable thrombi under arteriolar shear conditions (fig 5.5B).

However, we expected ET platelets to be hyperactive. Contrary to this, we saw no difference in activation of ET platelets compared to WT (Cre) platelets in response to a range of agonists (fig. 5.4), spreading on fibrinogen was not exacerbated (fig. 5.5A) and thrombi area was not increased (fig 5.5B).

Finally, we wanted to observe any effect caused by ablation of *Crlf3* in ET mice. Platelet activation was not grossly affected; ET x *Crlf3*$^{-/-}$ platelets were able to express P-selectin on their surface and bind fibrinogen to the same degree as WT (Cre) and ET platelets in response to all agonists tested, with the exception of medium concentrations of CRP where activation was decreased compared to WT (Cre) (fig. 5.4). Similarly, platelet spreading and thrombus formation under pathological shear were not affected in ET x *Crlf3*$^{-/-}$ platelets. ET x *Crlf3*$^{-/-}$ platelets also formed stable thrombi under shear conditions and thrombus area was not different to that formed by WT (Cre) or ET platelets (fig 5.5B). These data suggest that CRLF3 does not grossly affect platelet activation and thrombus formation. However, we cannot interpret the effect of ablation of *Crlf3* on platelet hyperactivity that is a feature of JAK2 V617F positive ET, as we were unable to recapitulate this platelet hyperactivity in our crossbred ET mice.

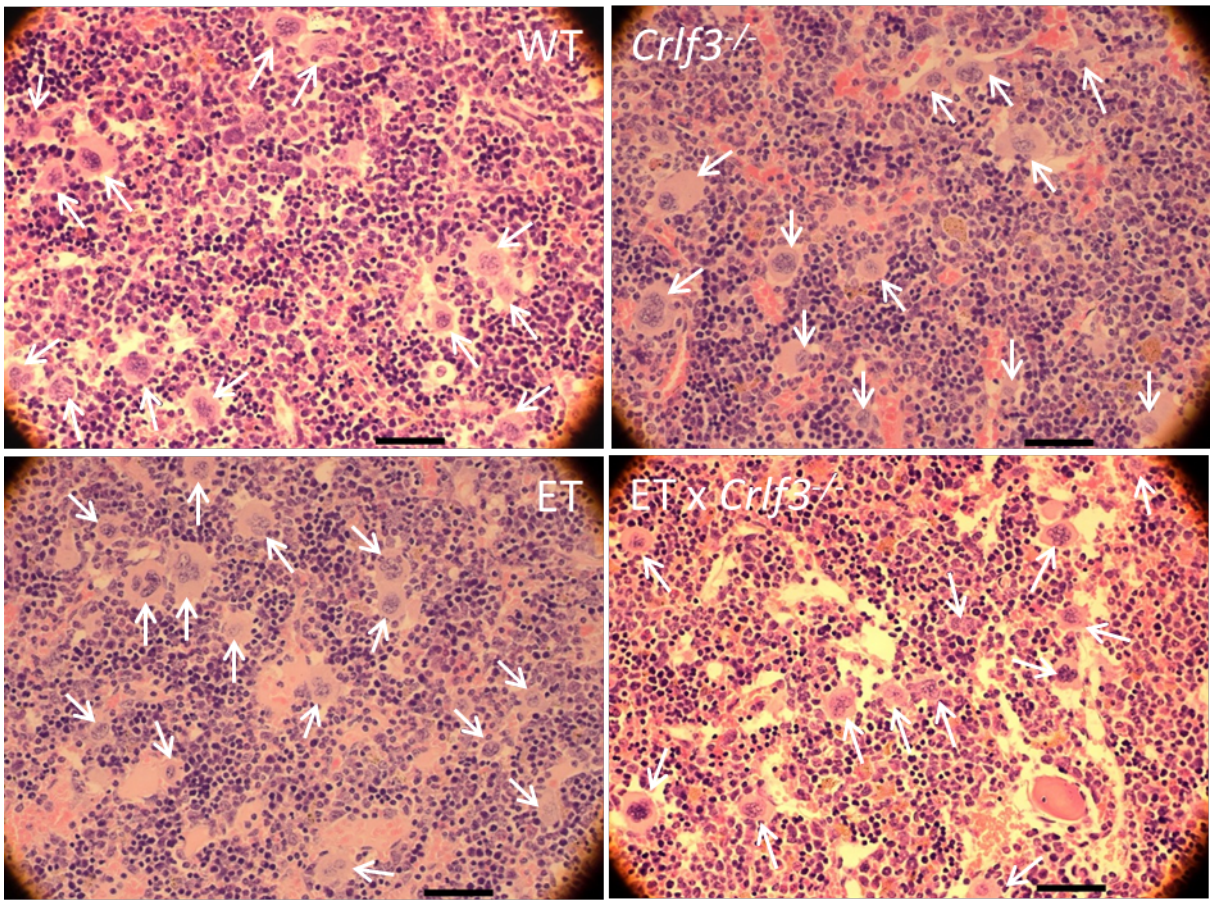

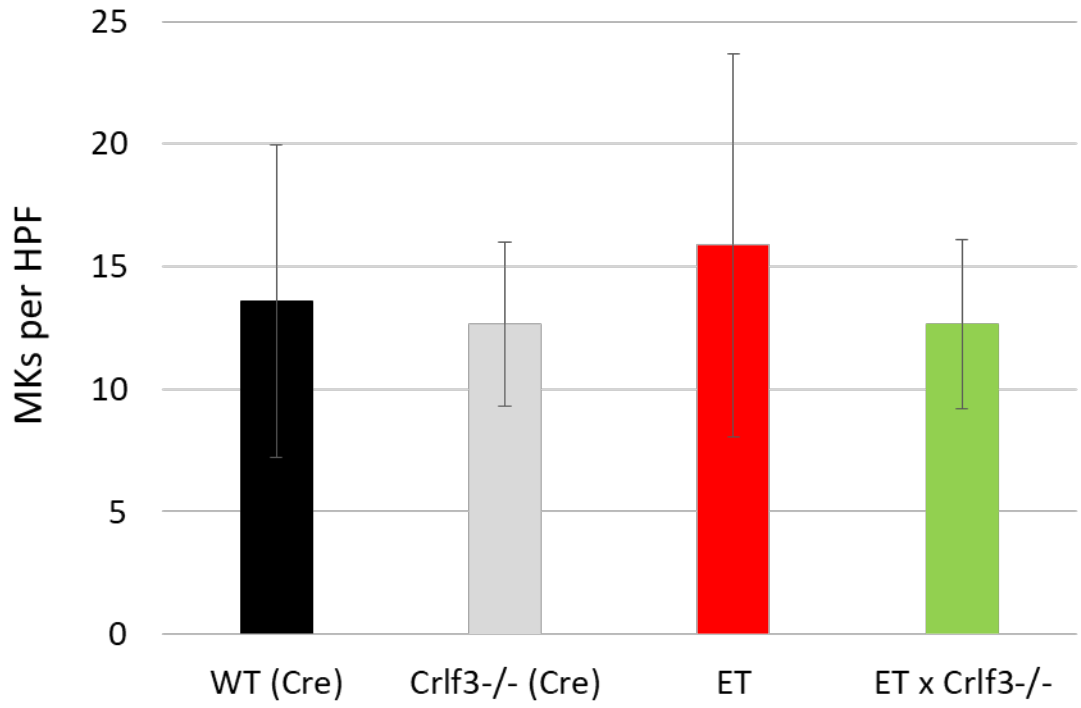

Figure 5.3 – MK hyperplasia is not exacerbated by ablation of *Crlf3* in ET mice. H&E staining performed on fixed and sectioned mice tibias. MKs blindly quantified by manual counting for WT (Cre) (black), *Crlf3*$^{-/-}$ (Cre) (grey), ET (red) and ET x *Crlf3-/-* (green) images (*n*=3). Images are representative of 12 month old mice and white arrows point to MKs. Scale bars are 50µm. HPF is high power field. Data represents mean ± SD. One-way ANOVA with Tukey's correction for multiple comparisons.

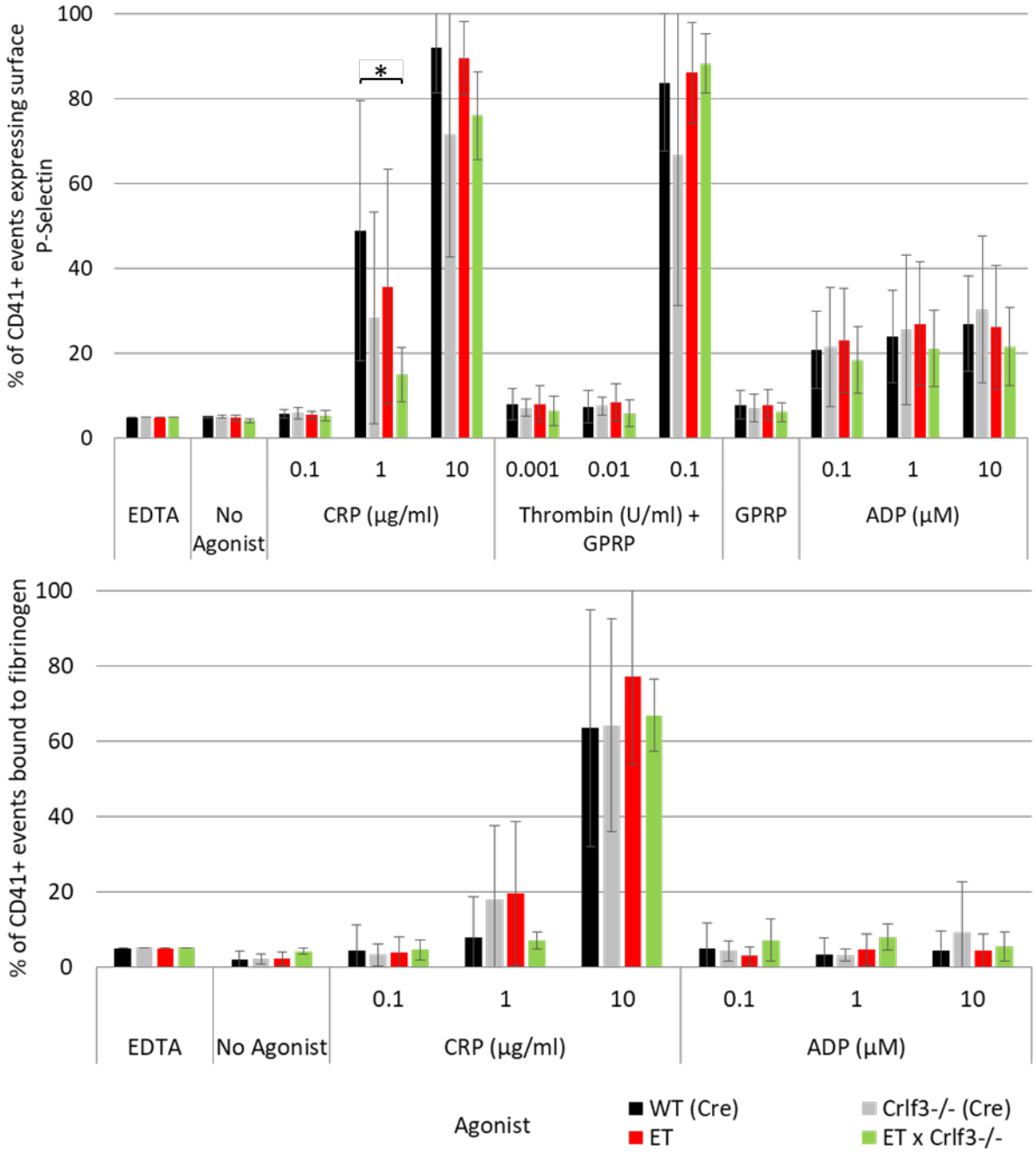

Figure 5.4 – Platelet activation is not grossly affected in ET x *Crlf3*$^{-/-}$ mice. WT (black), *Crlf3*$^{-/-}$ (grey), ET (red) and ET x *Crlf3*$^{-/-}$ (green) whole blood incubated with specific antibodies against CD41, P-Selectin and fibrinogen with or without addition of agonists. Percentage of CD41^{+} events expressing surface P-selectin (top panel) or bound to fibrinogen (bottom panel) was determined by flow cytometry. Data represents mean ± SD (*n*=3-4). Two-way ANOVA with Tukey's correction for multiple comparisons; * denotes $p<0.05$.

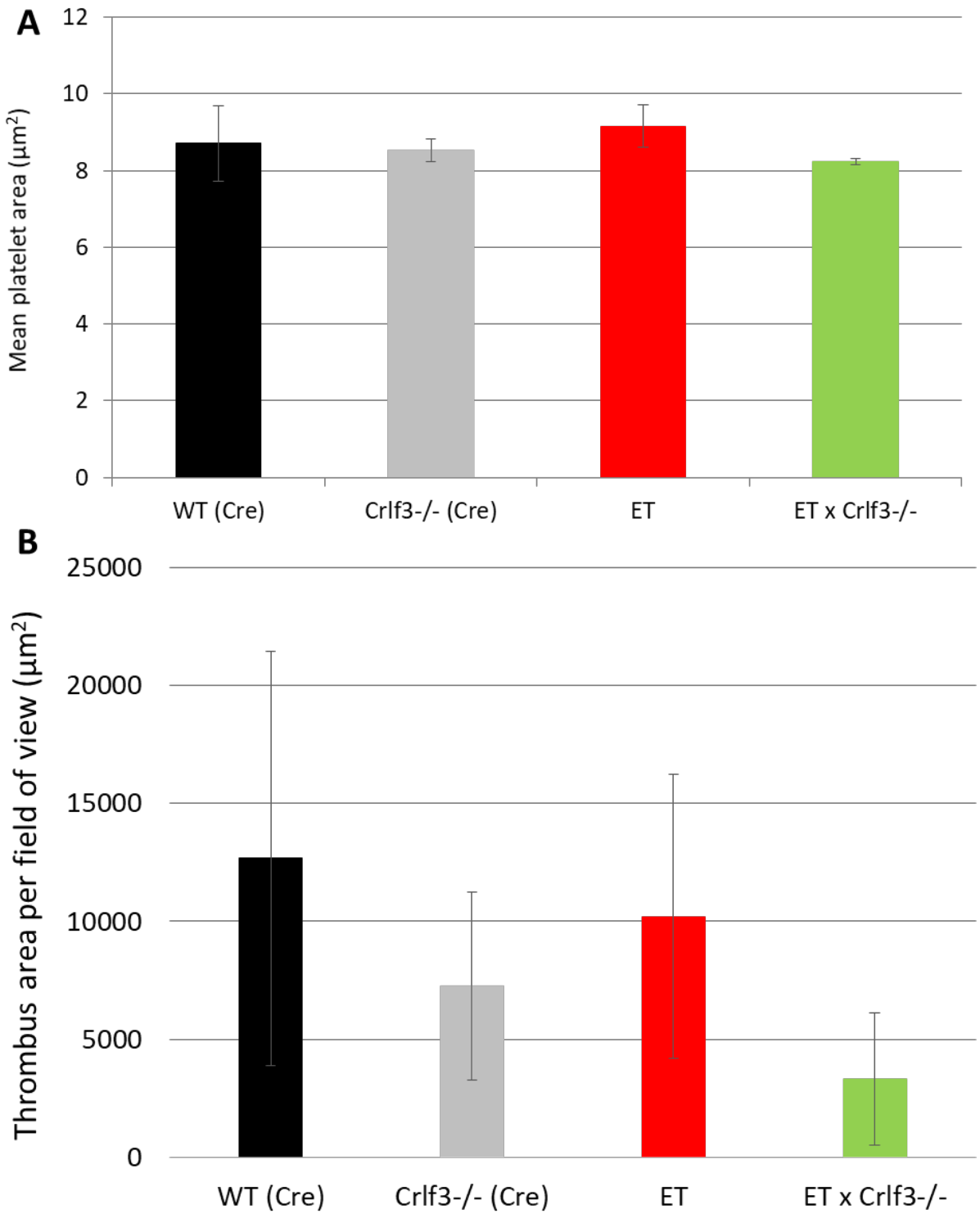

Figure 5.5 – Ability of ET platelets to spread and form stable thrombi is unaltered by ablation of *Crlf3*. (A) WT (Cre) (black), *Crlf3*$^{-/-}$ (Cre) (grey), ET (red) and ET x *Crlf3*$^{-/-}$ (green) washed platelets seeded onto fibrinogen coated coverslips and incubated for 30 mins at 37°C. Fixed samples stained with a fluorescently labelled F-actin probe and imaged by fluorescent microscopy. Platelet area determined by thresholding images on F-actin staining using ImageJ (*n*=3). (B) Heparinised whole blood flowed over fibrillar collagen and imaged by light microscopy. Thrombus area for 10 images for WT (Cre) (black), *Crlf3*$^{-/-}$ (Cre) (grey), ET (red) and ET x *Crlf3*$^{-/-}$ (green) mice determined by manually measuring the size of each thrombi using ImageJ (*n*=3). Data represents mean ± SD. One-way ANOVA with Tukey's correction for multiple comparisons.

5.5 Chapter conclusions

The aim of the chapter was to show that CRLF3 could be used as a novel therapeutic target for the treatment of ET. To this end, we cross breed *Crlf3*$^{-/-}$ mice with *Jak2*$^{fl/+}$ Cre^{+} ET mice heterozygous for the human JAK2 V617F mutation and have a phenotype similar to that seen in ET patients. Resultant pups were again crossbred to harbour ET mice with *Crlf3* ablated (ET x *Crlf3*$^{-/-}$), and appropriate controls (WT (Cre), *Crlf3*$^{-/-}$(Cre) and ET mice). Importantly, ET x *Crlf3*$^{-/-}$ platelet counts were similar to those of WT (Cre) control mice and significantly decreased from ET mice, suggesting removal of CRLF3 is able to normalise platelet counts in ET (fig. 5.2). This normalisation of platelet counts was without abnormalities in any other blood lineage (table 5.1), suggesting inhibitors of CRLF3 may have fewer haematological side effects than the cytoreductive agents currently used.

Beyond an increase in platelet numbers ET is associated with MK hyperplasia (Cervantes, 2011) and JAK2 V617F positive ET is associated with platelet hyper-reactivity (Hobbs et al, 2013). Bone marrow MK numbers were not increased in ET x *Crlf3*$^{-/-}$ mice compare to ET controls (fig. 5.3), suggesting inhibiting CRLF3 should not add to the burden of MK hyperplasia in ET. However, we were unable to recapitulate the MK hyperplasia which is a feature of these ET mice and of ET patients (Li et al, 2011) or the MK hyperplasia observed in *Crlf3*$^{-/-}$ mice (section 4.4.3) in the crossbred ET and *Crlf3*$^{-/-}$ (Cre) mice, respectively (fig. 5.3). The reasons for MK hyperplasia not being observed in the crossbred mice may be due to small *n* numbers used in experiments or due to the creation of an unsettled mouse background. *Crlf3*$^{-/-}$ mice are on a B6Brd;B6Dnk;B6N-Tyr background, whereas JAK2 V617F ET mice are on a B6J background. Crossbreeding of these two backgrounds may have caused an unsettled background strain, since background strain is known to have a major effect on haematopoietic cells (peters et al, 2002). The mice used in the experiments here represent pups from 1-4 inbred mating's of this mixed background strain. Therefore, it may be that more inbred mating's of this mixed background strain is required for the strain become settled.

The major cause of morbidity and mortality in ET patients is arterial and venous thrombotic events. JAK2 V617F positive ET patients have higher incidences of venous thrombotic events than JAK2 WT ET patients (Campbell et al., 2005), this may in part be accounted for by the hyper-reactive state of JAK2 V617F positive platelets. Therefore, it is important that any

therapeutic designed to treat ET does not exacerbate the hyper-reactive state of ET platelets. Ablation of *Crlf3* in an ET setting had little impact on the reactivity of platelets (it appears to decrease platelet activation at medium doses of CRP) and their ability to form stable thrombi (fig. 5.4 and 5.5B, respectively), suggesting that inhibitors of CRLF3 should not exacerbate the hyper-reactive state of platelets in JAK2 V617F positive ET. However, this must be put in the context that we were unable to recapitulate the hyper-reactive state of ET platelets in our crossbred ET mice, probably due to the reasons mentioned above.

6

Results 3

CRLF3 structure and function

6.1 Introduction

6.1.1 Protein structure

Proteins are composed of a chain of amino acids, known as a polypeptide chain, produced by translation of RNA by ribosomes. This polypeptide chain is termed the primary structure of a protein and is unique for each protein. Amino acids are organic molecules that contain amine (-NH2) and carboxyl (COOH) groups along with a side chain that is specific to each amino acid. Hydrogen bonds between amide and carbonyl groups of amino acids cause regular α-helical and β-sheet sub structures within the protein. These highly regular sub-structures of proteins are termed the secondary structure. Folding of the protein into a globular three-dimensional structure is driven by hydrophobic forces, hiding hydrophobic amino acids from external water. This 3D shape of a protein is termed the tertiary structure. Finally, some proteins have a quaternary structure, which refers to the aggregation of multiple globular polypeptide chains by non-covalent bonds into a single functional unit. For example, antibodies are composed of 2 light chain polypeptides and 2 heavy chain polypeptides.

The tertiary and quaternary 3D structure of a protein can be determined by a variety of different techniques. The most commonly used technique is X-ray crystallography, which is responsible for over 90% of solved 3D structures deposited in the Protein Data Bank (http://www.rcsb.org; (Berman et al., 2000)). X-ray crystallography involves exposing a crystal composed of purified protein of interest to a beam of X-rays, which creates a diffraction pattern. Computational processing of this diffraction pattern results in a 3D model of the protein (Smyth and Martin, 2000).

Determining the 3D structure of a protein is important for drug design. Structure based drug design relies on the structure of the binding site/s of a protein being known. Once the binding site/s is determined in the protein of interest, potential small inhibitors can be identified. This can be done in several ways, firstly, small inhibitors from existing libraries can be screened *in silico* for their ability to fit into the binding site. Secondly, known small inhibitors can be optimisation for the binding site of the protein of interest; or thirdly, new inhibitor molecules that fit the binding site can be designed using computational programs (Anderson, 2003; Klebe, 2000).

6.1.2 Protein interactome

The interactome of a protein refers to all the protein interactions that occur with a protein of interest within a cell. Understanding the interactome of a protein of unknown function can help determine its function, as proteins generally have similar functions to their interacting proteins (Schwikowski et al., 2000).

6.2 Chapter hypotheses and aims

We hypothesise that CRLF3 will contain domains that interact with other proteins and as such we aim to resolve the tertiary structure of CRLF3 using X-ray crystallography to discover these interacting domains. We also hypothesise that CRLF3 interacts with microtubules and/or proteins that themselves directly interact with microtubules and these CRLF3 dependent interactions affect microtubule stability. Therefore, we aim to uncover the interactome of CRLF3 in forward programmed human MKs.

6.3 Chapter overview

Firstly, this chapter will show how we were unable to resolve the tertiary structure of full length CRLF3 due to technical issues. We then show how different portions of CRLF3 were selected using freely available bioinformatics tools and how the portion corresponding to the second half of CRLF3 was produced from *E. coli* cells, purified, crystallised and its tertiary structure resolved by X-ray crystallography. We next show how we were able to attach a tandem affinity purification (TAP) tag to endogenous *CRLF3* in human induced pluripotent stem cells (iPSCs). We show the interactome of CRLF3 in iPSCs as determined by mass spectrometry after immunoprecipitation and finally, we show that TAP-tagged iPSCs are able to be forward programmed into MKs.

6.4 Results

6.4.1 CRLF3 crystal structure

Initially we intended to resolve the tertiary structure of full length murine CRLF3 (442 amino acids, longer splice variant). To do this, *Crlf3* was amplified from cDNA by PCR using specific primers (table 3.9 and 3.12). *Crlf3* was then ligated into pGEX-6P-2 vector (fig. 6.1), which generates glutathione-*S*-transferase (GST) fusion proteins when expressed in *E. coli* cells. *Crlf3* containing pGEX vectors were transformed into competent *E. coli* cells and CRLF3-GST was produced following the method described by Harper and Speicher (2008). GST was cleaved from CRLF3 with PreScission protease and CRLF3 purified by affinity chromatography. One litre of bacterial culture produced 0.6mg CRLF3 after GST cleavage and purification (n=1). Protein from 4 litres of bacterial culture was concentrated by centrifugation to ≈5mg/ml and used to set up crystallisation screen plates. However, despite producing enough concentrated CRLF3 to set up a number of crystallisation screenings using the vapour diffusion method, no crystals were formed (crystallisation screens performed by Giles Lewis, University of Cambridge, Cambridge UK).

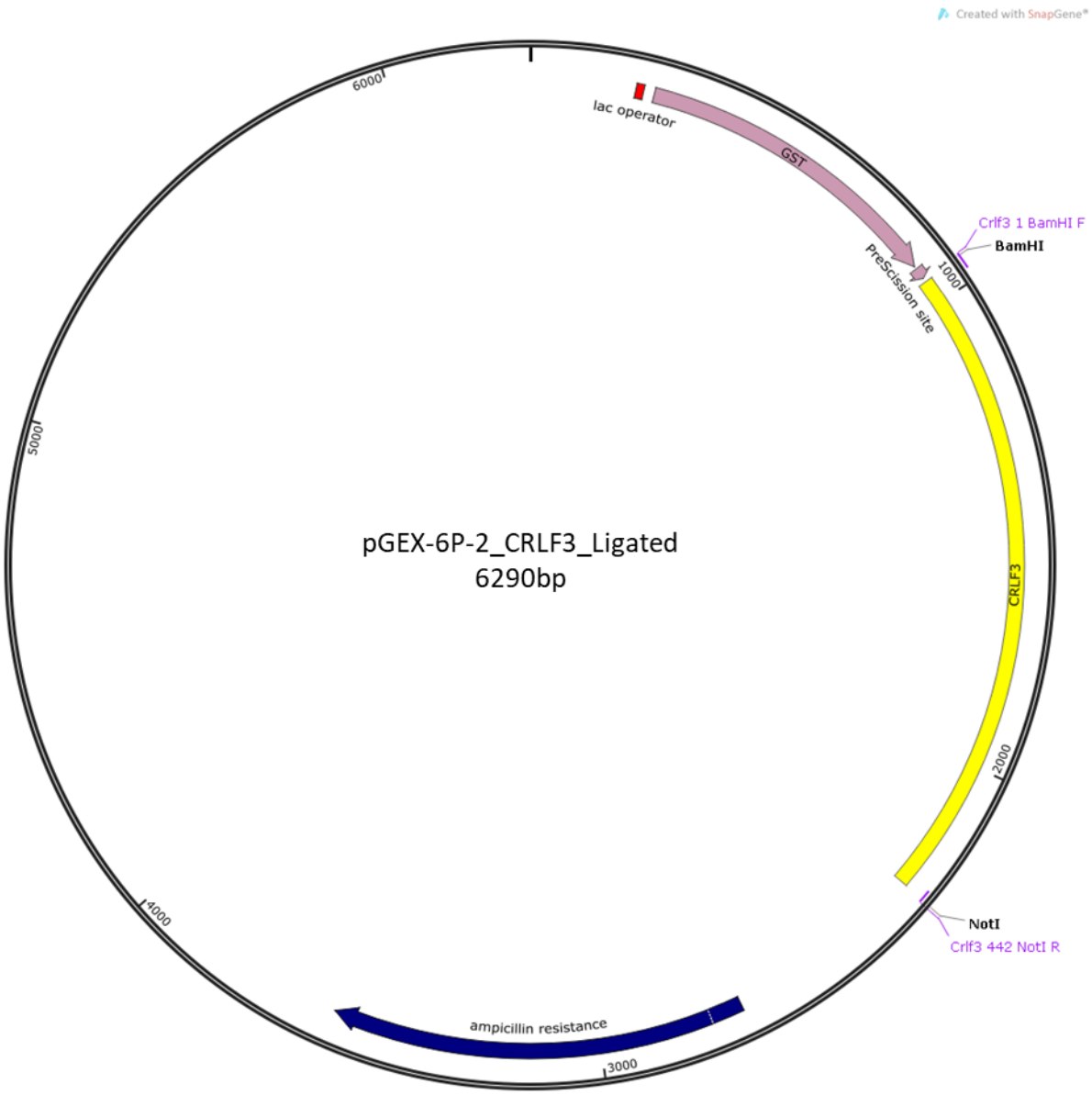

Figure 6.1 – Vector map of *Crlf3* ligated into pGEX-6P-2. *Crlf3* amplified from cDNA using primers shown (violet) ligated into BamHI and NotI restriction digested pGEX-6P-2 vector. Proteins produced from pGEX-6P-2 are fused to glutathione-*S*-transferase (GST; purple) which can be cleaved by PreScission protease at the site shown. Map created using SnapGene®.

6.4.1.1 Design of 4 CRLF3 constructs

Due to difficulties producing and crystallising the full length protein, we bioinformatically analysed murine CRLF3 to decide on portions of the protein that are more likely to crystallise (work done in collaboration with Randy Read and Richard Mifsud, University of Cambridge, Cambridge, UK). Figure 6.2A shows the 4 constructs that were decided upon based on a number of internet based tools. The first of these internet based tools, DISOPRED

(http://bioinf.cs.ucl.ac.uk/), predicts disorder within the primary sequence of a protein. The straight line (5% false positive rate (FPR)) is set as a cut off, and anything above this is predicted to be disordered. Disorder prediction is a valuable tool for identifying flexible regions in proteins that may hinder crystallisation (Bryson et al., 2005; Ward et al., 2004). As can be seen in figure 6.2D, the first 16 amino acids at the N-terminus are predicted to be highly disordered; therefore we decided to create a construct for the whole protein omitting the disordered N-terminus (construct 1 – amino acid 17 to 442).

We then used a tool that predicts the secondary structure of the protein, namely PSIPRED (http://bioinf.cs.ucl.ac.uk/; (Bryson et al., 2005)). As can be seen in figure 6.2B, CRLF3 is predicted to be composed of an α-helical section (purple cylinder) followed by a β-sheet section (yellow arrow). The α-helical section starts at amino acid 38; therefore we decided to create a construct from the start of this predicted α-helical section to the end of the protein (construct 2 – amino acid 38 to 442).

Finally, we used HHpred (https://toolkit.tuebingen.mpg.de/; (Alva et al., 2016)) to detect remote homologous proteins and predict structure (Soding et al., 2005). As can be seen in figure 6.2C, there are many predicted homologues of known structure for the second half of CRLF3, starting after the predicted α-helical section ends. However, the first half of the protein (amino acid 1-173) only had one predicted homologue (at the time of investigation, now currently has 4 predicted homologues). Based on these predictions, we decided to create a construct for the second half of the protein starting at amino acid 174, where the predicted α-helical section ends (construct 3 – amino acid 174 to 442). We have also decided to create a construct for the first half of the protein but still omitting the disordered N-terminus (construct 4 – amino acid 17-173) for completeness.

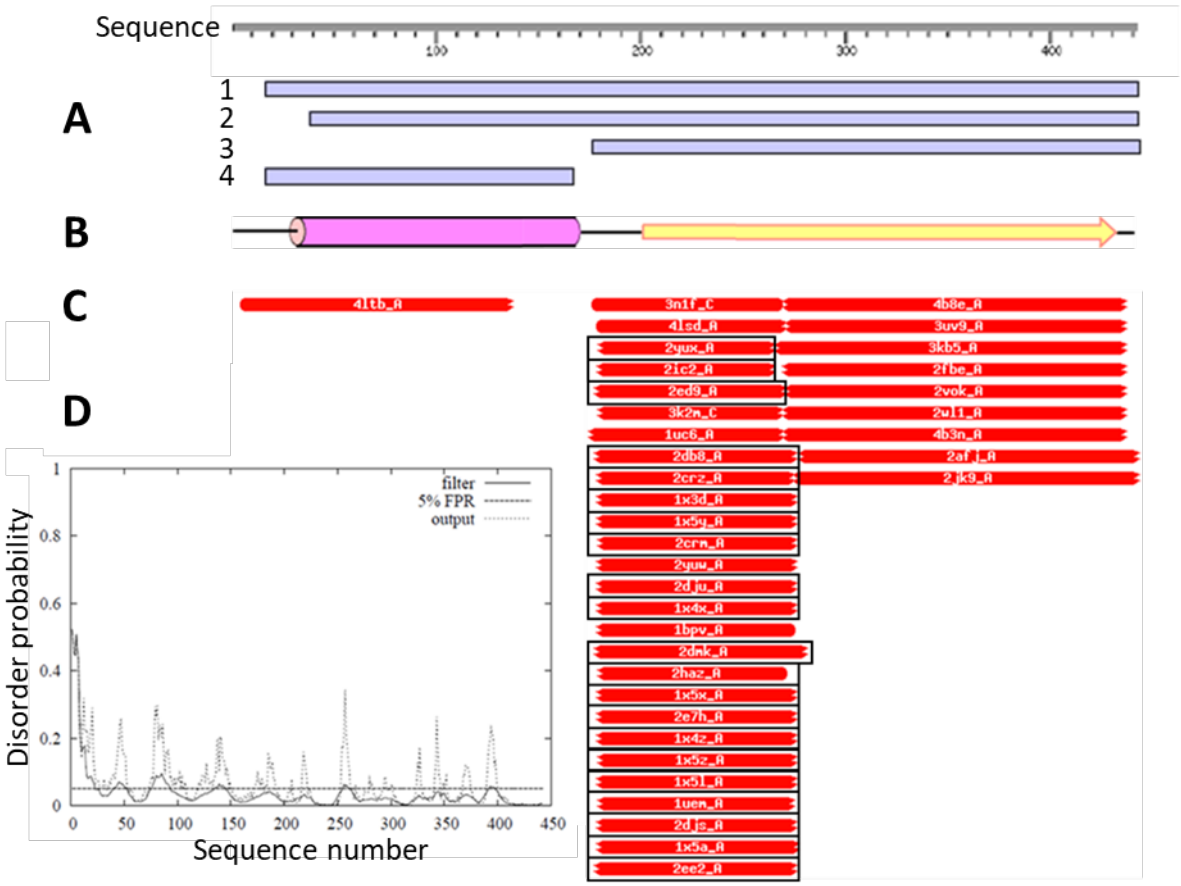

Figure 6.2 – Design of 4 CRLF3 constructs based on homology and disorder. (A) 4 constructs chosen after bioinformatic interrogation of murine CRLF3, aligned to full length CRLF3. Construct 1 – residue 16 to end (442); 2 – residue 38 to end; 3 – residue 174 to end and 4 – residue 16 to 173. (B) PSIPRED plot represents predicted α-helices (pink cylinder) and β-sheets (yellow arrow) within CRLF3's secondary structure. (C) HHpred result at time of interrogation. Homologous FN3 domains boxed. (D) Disorder in CRLF3 as assessed by DISOPRED. FPR is false positive rate.

6.4.1.2 Protein production and purification

After all 4 constructs were cloned in pGEX-6P-2 and transformed into *E. coli* cells, we produced protein from 1L of bacterial culture, removed GST with PreScission protease and purified by affinity chromatography. Only construct 3 produced significantly more protein than the full length protein (7.0mg construct 3 vs 0.6 construct 1, 0.7mg construct 2, 0.8mg construct 4 and 0.6mg full length; *n*=1). Due to its ability to produce vast amounts of protein, we decided to concentrate our efforts on construct 3.

We produced 13.6mg protein from 2L of bacterial culture, of which 8.2mg was retained after GST cleavage and purification by affinity chromatography; this was concentrated to 7.6mg/mL

in 1mL. The protein was further purified by ion exchange chromatography, which produced a large peak indicating pure protein (fig. 6.3A) that was confirmed to be CRLF3 (construct 3) by SDS-PAGE (fig 6.3B). The eluate collected during the large peak of ion exchange chromatography was again concentrated to 11.7mg/mL in 300µL.

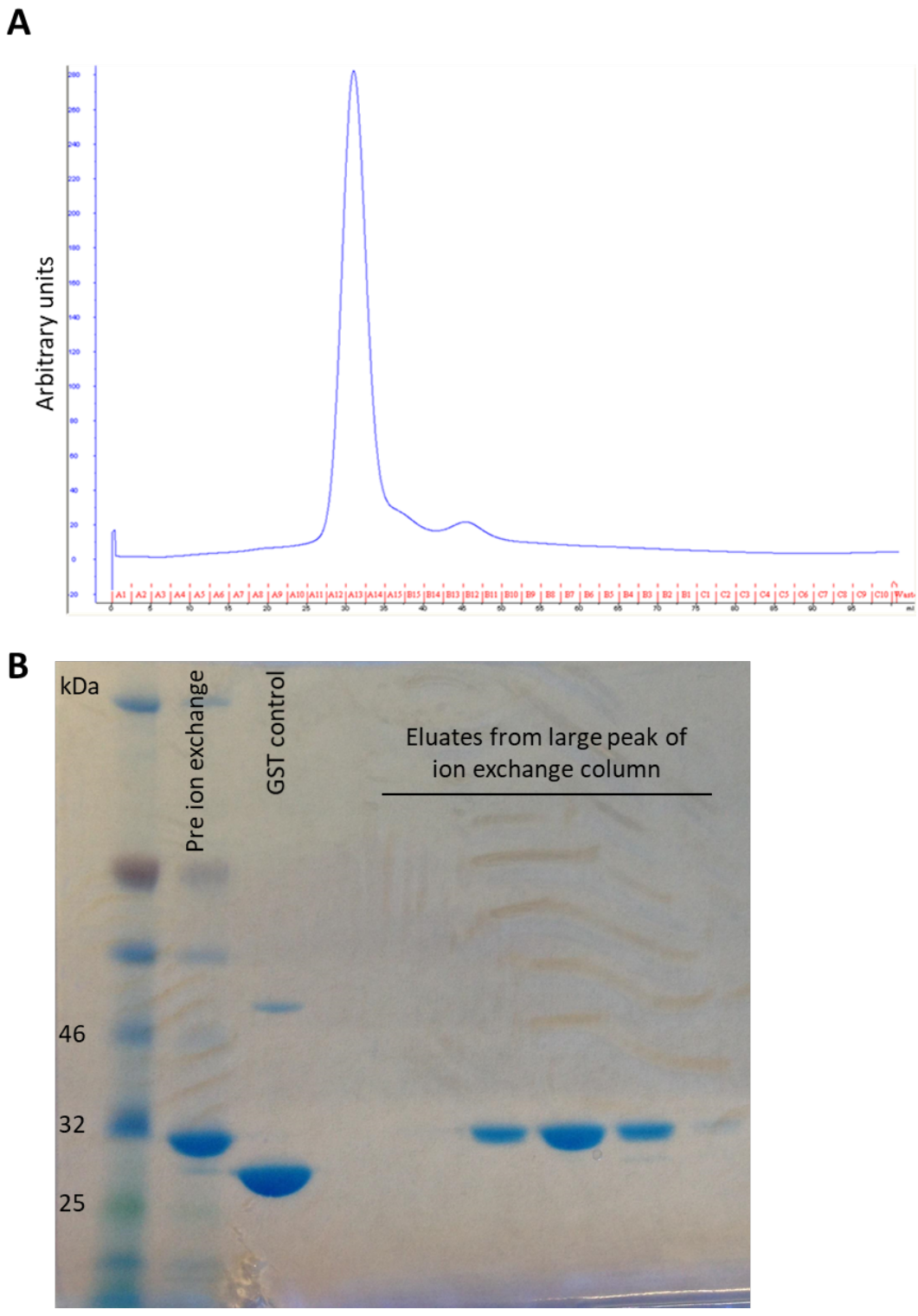

Figure 6.3 – Purification of CRLF3 construct 3 by ion exchange chromatography. (A) Protein of CRLF3 construct 3 produced from *E. coli* after initial purification and concentration, purified further by ion exchange chromatography. (B) Eluates from ion exchange chromatography resolved by SDS-PAGE.

6.4.1.3 Crystallisation of construct 3 and solving of 3D structure

Crystallisation was screened by the sitting drop vapour diffusion method using a variety of commercially available 96-well screen plates with the kind help of Yahui Yan (University of Cambridge, Cambridge, UK). Many conditions produced crystals of varying quality (table 6.1 and fig. 6.4A). Crystals grown in 20% PEG 3,350, 0.2M sodium formate, pH7.0 were soaked with the mercury (Hg) derivative thimerosal (10mM) overnight, then cryoprotected with 25% ethylene glycol. The data collection was recorded at Diamond Light Source beamline I04. A good 'peak' dataset was collected with redundancy of 6.7 at the peak wavelength which was determined experimentally by fluorescence scanning. Diffraction data were indexed, integrated, and scaled to 1.86Å using Mosflm (Leslie and Powell, 2007) and Aimless (Evans, 2011) via the xia2 (Winter, 2010) automated data processing pipeline. The Hg-single anomalous diffraction (SAD) phasing was solved using AutoSol-wizard (Terwilliger et al., 2009) which is an experimental phasing pipeline that combines Hybrid Substructure Search (HySS) for finding heavy-atom sites, Phaser for calculating experimental phases, and RESOLVE for density modification and model building. It found 14 mercury sites with the Figure of Merit (FOM; estimate of phase quality, ranging from 0 to 1) at 0.37 and the overall score (a standardised measure of how well the 3D model fits the electron density map which takes into account FOM, CC, R_{free} and R_{work}, ranging from 0-100) of 53.92 ± 7.90. The map-model correlation coefficient (CC; an estimate of how well the 3D model fits the electron density map, ranging from 0 to 1) was 0.78 after model building with R_{work} at 0.28 and R_{free} at 0.31 (both measures 3D model quality, where 0 would be perfect). The structure was further refined to a resolution of 1.7Å using Phenix.refine (Adams et al., 2010) and by manual building in Coot (Emsley et al., 2010) with a native dataset collected from crystals grown in 25% PEG 3,350, 0.2M ammonium acetate, 0.1M BIS-TRIS. This 3D structure revealed a fibronectin type III (FN3) domain at the N-terminus of construct 3 (fig 6.4B) that was predicted by HHpred (homologous proteins boxed in fig. 6.2C) and an SPRY domain at the C-terminus of construct 3 (fig 6.4B) (X-ray diffraction data collection and creation of 3D model done by Randy Read, Yahui Yan and Richard Mifsud, University of Cambridge, Cambridge, UK).

Company	Screen plate name	Well	Conditions
Hampton Research	PEG/Ion Screen	G4	20% PEG 3,350, 0.2M sodium formate
Molecular Dimensions	JCSG-plus	A5	20% PEG 3,350, 0.2M magnesium formate
Molecular Dimensions	JCSG-plus	E7	10% 2-propanol, 0.1M sodium cacodylate, 0.2M zinc acetate
Molecular Dimensions	JCSG-plus	D11	0.14M calcium chloride, 30% glycerol, 14% 2-propanol, 0.07M sodium acetate
Hampton Research	PEG/Ion Screen	C10	20% PEG 3,350, 0.2M potassium acetate
Hampton Research	PEG/Ion Screen	G2	20% PEG 3,350, 0.2M sodium acetate
Molecular Dimensions	JCSG-plus	C1	0.2M sodium chloride, 20% PEG 8,000, 0.1M sodium phosphate citrate
Molecular Dimensions	JCSG-plus	C10	2% 1,4-Dioxane, 10% PEG 20,000, 0.1M BICINE
Molecular Dimensions	JCSG-plus	E7	10% 2-propanol, 0.1M sodium cacodylate, 0.2M zinc acetate
Molecular Dimensions	JCSG-plus	H10	25% PEG 3,350, 0.2M ammonium acetate, 0.1M BIS-TRIS
Molecular Dimensions	Structure Screen 2	H6	25% Ethylene glycol
Emerald BioSystems	Wizard 2	G4	20% PEG 8,000, 0.2M calcium acetate 0.1M MES

Table 6.1 – Conditions in which CRLF3 construct 3 produced crystals

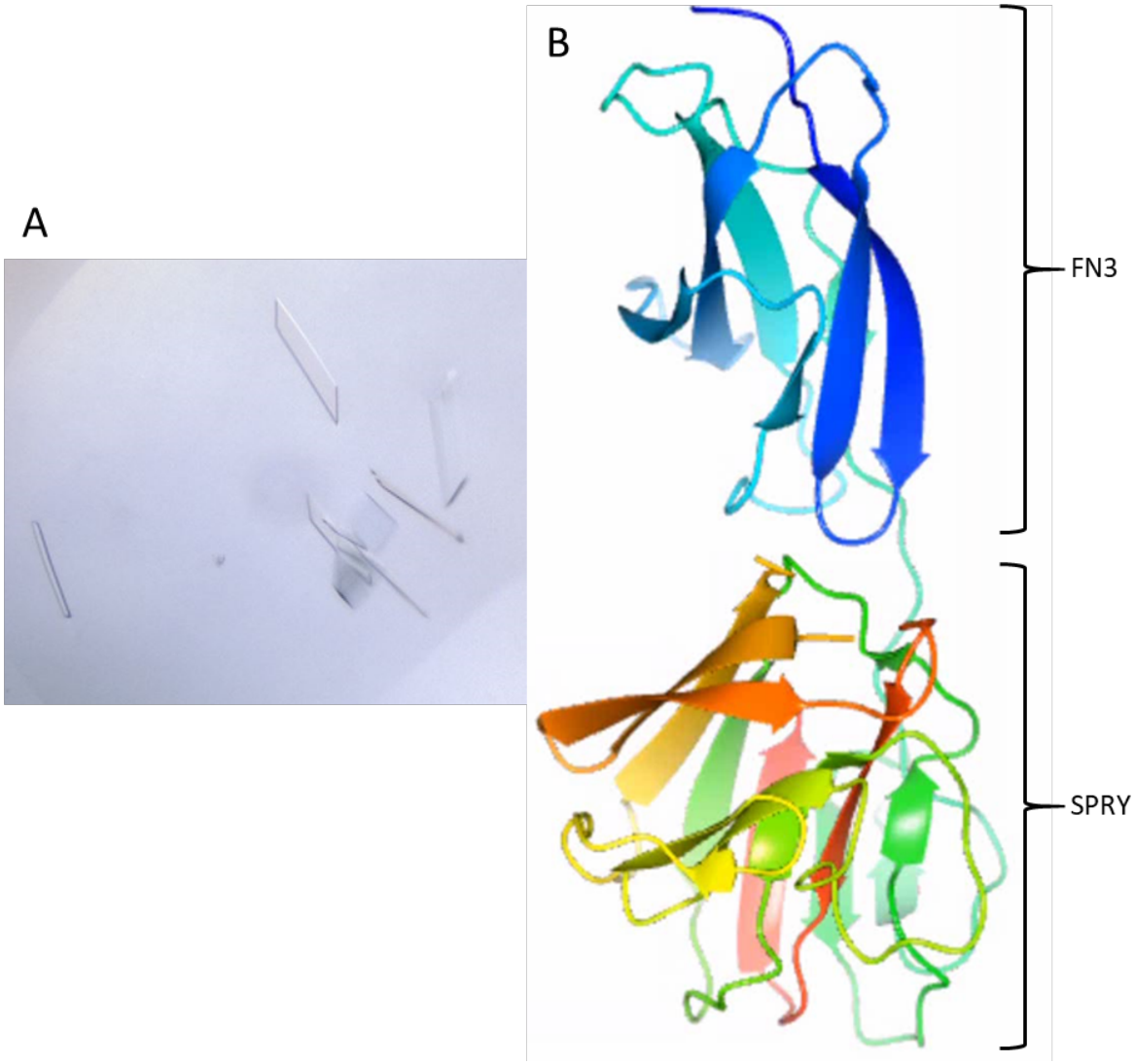

Figure 6.4 – 3D structure of CRLF3 construct 3. (A) Purified CRLF3 construct 3 protein was mixed with contents of well H10 of JCSG-plus by Molecular Dimensions and crystals allowed to form following the vapour diffusion method. (B) Crystals underwent X-ray diffraction and 3D structure solved by experimental phasing. Domains are labelled. FN3 is fibronectin type 3. Molecular graphics prepared using PyMOL.

6.4.2 Adding a Tandem Affinity Purification (TAP) tag to endogenous *CRLF3* in human iPSCs

To add the TAP tag, consisting of an N-terminal calmodulin binding domain and C-terminal 3x FLAG tag repeat separated by a TEV cleavage site, to endogenous *CRLF3* we used the CRISPR/Cas9 method Ran et al. (2013). Cas9 nuclease was guided by specific single-guided (sg) RNA's in a green fluorescent protein (GFP) expressing plasmid to introduce a double stranded break (DSB) in DNA close to the *CRLF3* stop codon (fig. 6.5A). A donor vector was then introduced to initiate homology directed repair (HDR) to add the TAP tag to the 3' end of *CRLF3* before the stop codon (fig 6.5B).

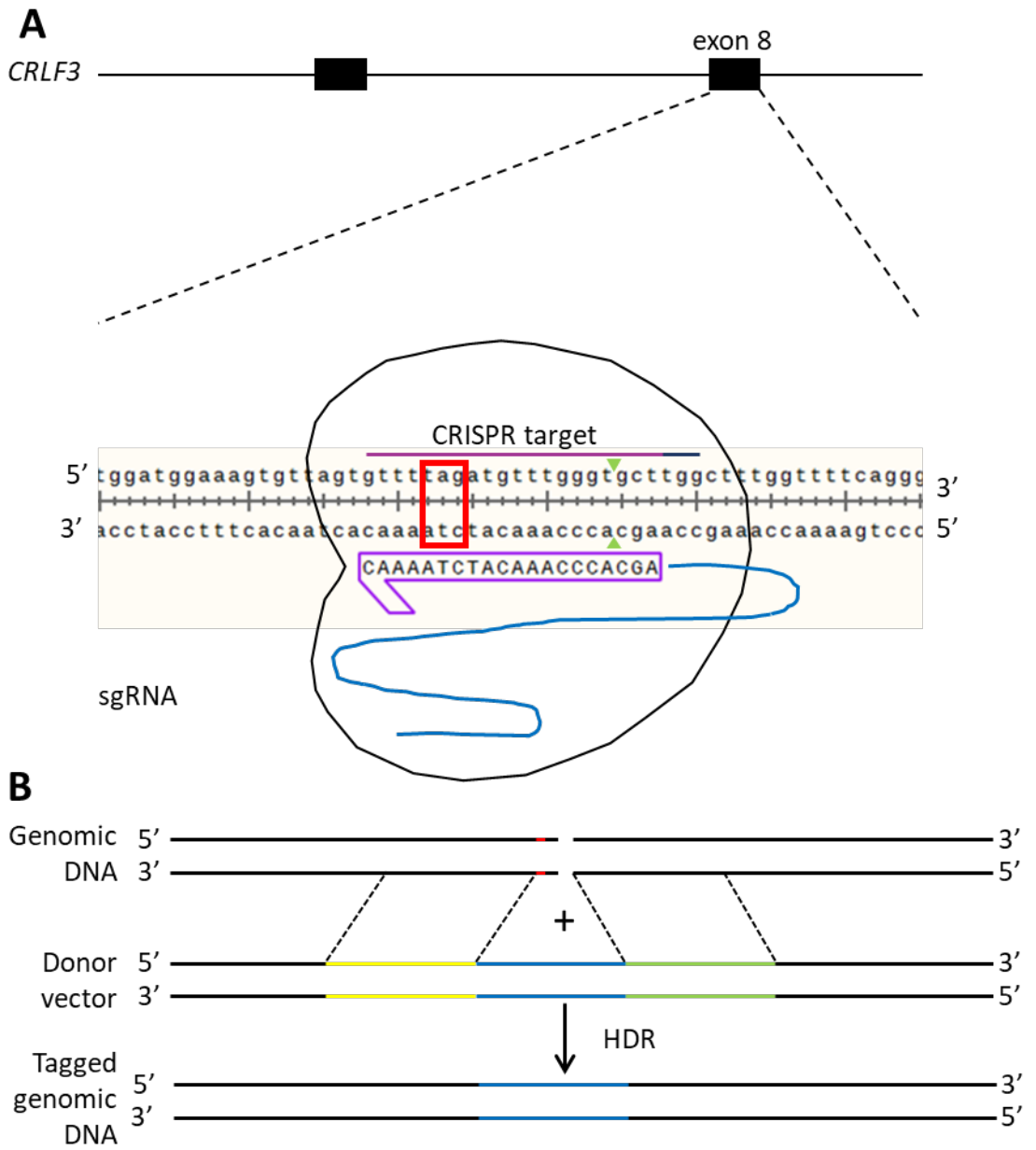

Figure 6.5 – Schematic diagram of adding a TAP-tag to *CRLF3* by CRISPR/Cas9. (A) Cas9 nuclease (black outline) is targeted to *CRLF3* exon 8 close its stop codon (red box) by an sgRNA consisting of a 20-nt guide sequence (CRISPR, purple) and a scaffold (light blue). The guide sequence pairs with the DNA target (purple bar on top strand), directly upstream of a 5’-NGG protospacer adjacent motif (PAM; dark blue). Cas9 mediates a double strand break (DSB) ~3 bp upstream of the PAM (green triangles). (B) The DSB caused by Cas9 close to *CRLF3*’s stop codon (red) in addition to the supplied donor vector leads to homology directed repair (HDR) and precise gene editing. The TAP tag (blue) is added directly before the stop codon of *CRLF3*, guided by 5’ and 3’ homology arms (yellow and green, respectively).

Originally, we intended to use the iPSC line FFDK1 as it was being cultured in-house and it was known to forward programme to MKs. The donor vector for HDR, was created by cloning of 1kb 3' and 5' *CRLF3* homology arms and TAP tag into linearized pBS KS vector by Gibson assembly (fig. 6.6). The donor vector was inserted into XL-10 Gold ultra-competent *E. coli* and vector DNA was extracted from liquid cultures using a commercially available kit. Sequencing of the donor vector using the M13F and M13R primers (table 3.12 and fig. 6.6) revealed multiple mutations in the 5' homology arm, with 3 mutations occurring in exons and one leading to an amino acid substitution (proline to leucine at amino acid 435). As we intended to tag wildtype *CRLF3*, as recorded at the National Centre for Biotechnology Information (https://www.ncbi.nlm.nih.gov/), we screened other in-house iPSC lines for mutations in *CRLF3*. To this end, *CRLF3* cDNA from iPSC lines BobC and Qolg was amplified by PCR using specific primers (table 3.11 and 3.12), cloned into TOPO vector by TOPO TA cloning and transformed into *E. coli* cells. Sequencing of DNA after extraction from liquid cultures revealed a 4bp deletion at amino acid 41 in BobC leading to a frameshift. However, no mutations were seen in Qolg *CRLF3*, therefore we continued with this line, creating a donor vector as above by Gibson assembly. The donor vector was confirmed to be correct by sequencing using M13F and M13R primers and restriction digestions. Restriction sites for EcoRI are found in the 5' and 3' homology arms (fig. 6.6) and digestion resulted in 4195bp and 869bp fragments as expected (fig. 6.7). Whereas, restrictions sites for XmnI are found in TAP tag and ampicillin resistance region of pBS KS (fig. 6.6) and digestion resulted in 3154bp and 1910bp fragments as expected (fig. 6.7).

Qolg TAP-tag donor vector and sgRNA/Cas9-GFP plasmid were inserted into Qolg iPSCs, in a single cell solution, by electroporation and then cells seeded onto vitronectin coated plates. Electroporated cells were maintained for 2 days then sorted by fluorescent-activated cell sorting (FACS) based on expression of GFP. Individual GFP-positive cells were sorted to individual wells of laminin coated 96 well plates (FACS sorting performed by staff of NIHR Cambridge BRC Cell Phenotyping Hub, University of Cambridge, Cambridge UK). Of the 96 GFP positive cells sorted, thirteen survived and formed colonies, which were expanded and gDNA isolated. PCR amplification of gDNA using specific primers (table 3.12 and fig. 6.6) revealed that only 6 of the 13 clones had the TAP tag-inserted onto *CRLF3* (fig. 6.8A). Protein expression of CRLF3-TAP in the positive clones was confirmed by western blot (fig. 6.8B) and flow cytometry (fig. 6.8C) using specific antibodies against the TAP tag.

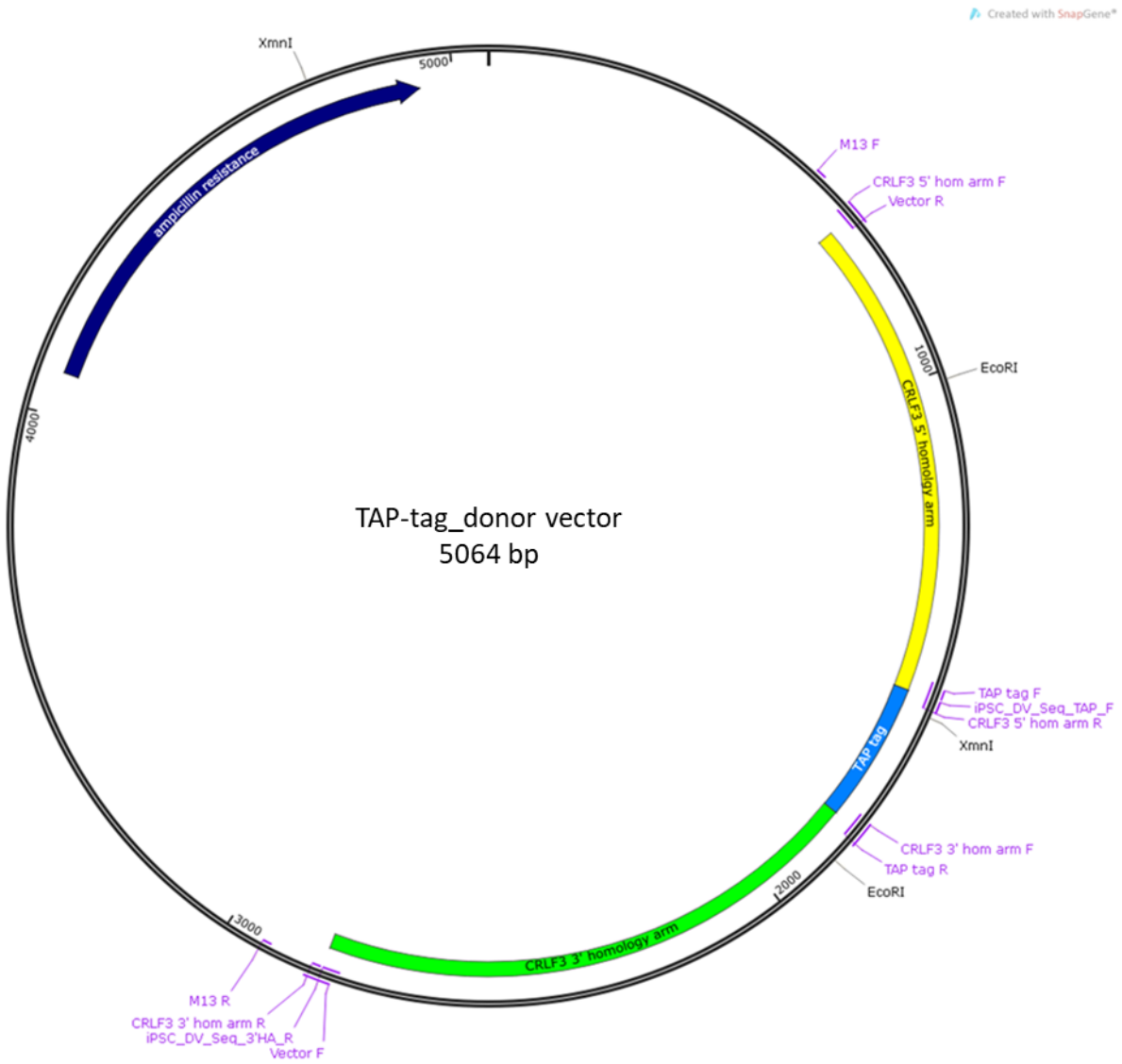

Figure 6.6 – Vector map of TAP-tag donor vector. 3' and 5' *CRLF3* homology arms (green and yellow, respectively) and TAP-tag (blue) cloned into linearised pBS KS vector by Gibson assembly. Homology arms and TAP-tag were amplified and pBS KS vector was linearised by PCR using the primers shown (light purple). Correct assembly of donor vectors was confirmed by sequencing using the M13F abd M13R primers (light purple) and by restriction digestion with EcoRI and XmnI (black). Map created using SnapGene®.

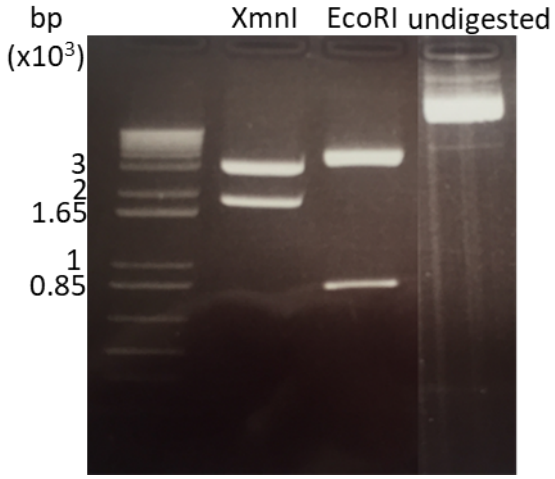

Figure 6.7 – Confirmation of TAP-tag donor vector by restriction digestion. Undigested donor vector DNA or DNA digested with XmnI or EcoRI resolved on a 1.5% agarose TBE gel supplemented with DNA SafeView.

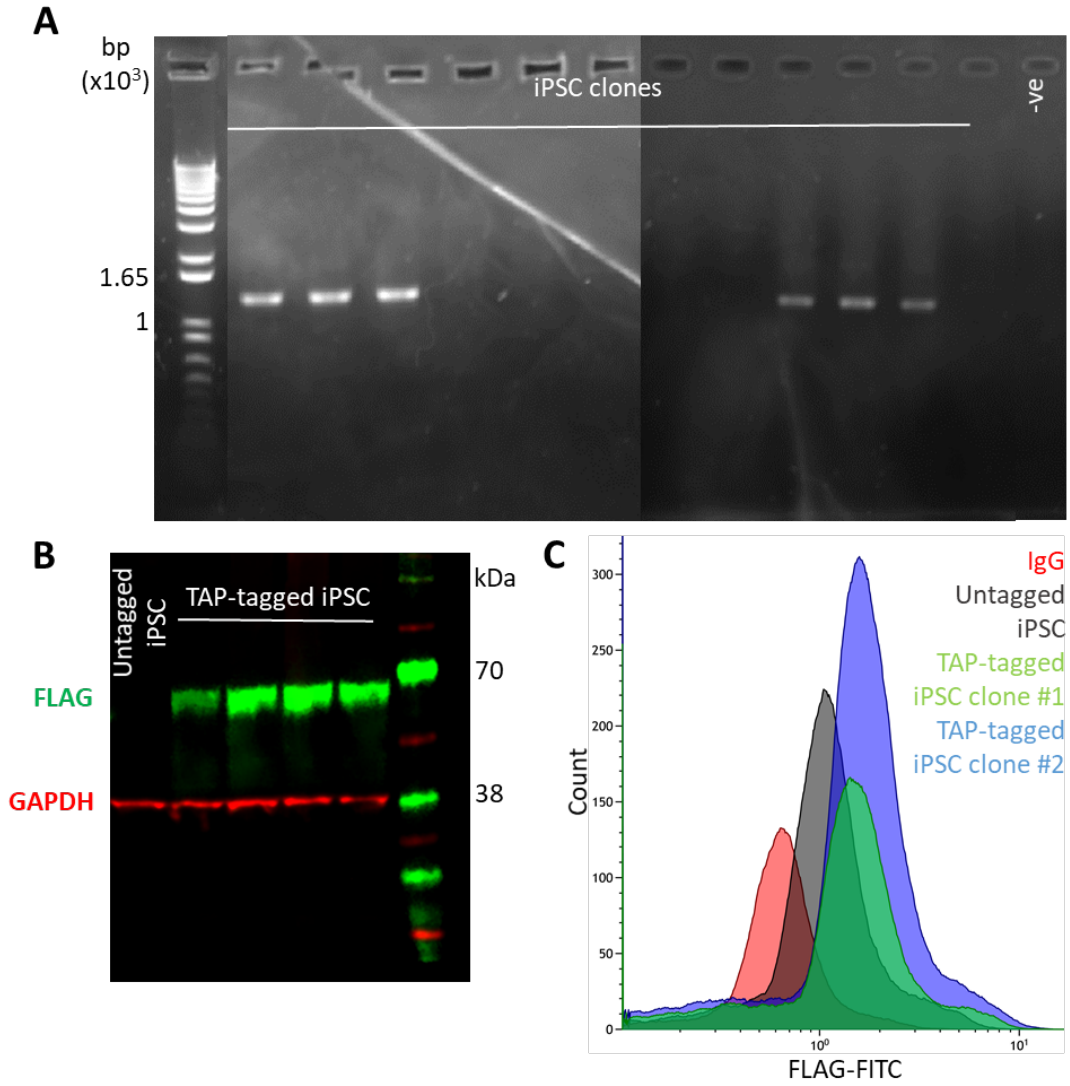

Figure 6.8 – Confirmation of CRLF3-TAP in iPSCs. (A) gDNA isolated from FACS sorted iPSC clones amplified by PCR with primers located in the TAP-tag and 3' homology arm (table 3.12 and fig. 6.6) and resolved on a 1.5% agarose TBE gel supplemented with DNA SafeView. (B) Western blot of TAP-tagged and untagged iPSCs using specific antibodies against FLAG and GAPDH. (C) Fixed and permeabilised TAP-tagged (green and blue) and untagged (grey) iPSCs stained with FITC conjugated antibody against FLAG and assessed by flow cytometry.

6.4.2.1 CRLF3's interactome in iPSCs

To determine the as yet unknown interactome of CRLF3, TAP-tagged and untagged WT iPSCs were lysed and CRLF3 and proteins bound to CRLF3 were immunoprecipitated with antibodies specific for the TAP tag. Mass spectrometry of the immunoprecipitated proteins revealed 18 proteins that were present in the TAP-tagged samples but not untagged samples (table 6.2) (Mass spectrometry performed by Renata Feret, Marco Chiapello and Mike Deery, Cambridge Centre for Proteomics, University of Cambridge, Cambridge, UK). CRLF3 was present in all TAP-tagged samples, but not untagged-samples, confirming CRLF3 was correctly tagged with the TAP-tag. Interestingly, four of these proteins (highlighted blue) are known to form desmosomes along with other proteins. Desmosomes are cell-to-cell adhesion molecules that bind cytoskeletal keratin filaments. Although numerous keratin isoforms were seen in both the TAP-tagged and untagged samples, 5 isoforms were only seen in the tagged samples (highlighted green).

UniProt ID	PROTEIN
J3QLS9	Cytokine receptor-like factor 3
Q08554	Desmocollin-1
Q02413	Desmoglein-1
P15924	Desmoplakin
Q13835	Plakophilin-1
P02533	Keratin, type I cytoskeletal 14
P08779	Keratin, type I cytoskeletal 16
P13647	Keratin, type II cytoskeletal 5
P02538	Keratin, type II cytoskeletal 6A
Q8N1N4	Keratin, type II cytoskeletal 78
A0A087WVD4	Arsenite methyltransferase
Q9NRM1	Enamelin
Q86YZ3	Hornerin
Q5T749	Keratinocyte proline-rich protein
H3BPJ9	NADH dehydrogenase [ubiquinone] 1 beta subcomplex subunit 10
A0A0A0MRQ5	Peroxiredoxin-1
Q7KZ85	Transcription elongation factor SPT6
O95625	Zinc finger and BTB domain-containing protein 11

Table 6.2 – Proteins identified in TAP-tagged but not untagged iPSC immunoprecipitation samples by mass spectrometry

6.4.2.2 Forward programming of tagged iPSCs

Finally, we wanted to forward programme TAP-tagged iPSCs into MKs to allow determination of CRLF3's interactome in MKs and visualisation of CRLF3 within MKs and during proplatelet formation. TAP-tagged iPSCs were forward programmed using the method developed by Moreau et al. (2016). We confirmed the presence of the TAP-tag in forward programmed TAP-tagged MKs by western blot (fig. 6.9A). The shift in size of the CRLF3 band in TAP-tagged MKs seen in figure 6.9B, results in a band with the same molecular weight as TAP-tagged MKs when blotted with antibodies against the TAP-tag; confirming that CRLF3 had been tagged with the TAP-tag. Based on immunoprecipitation experiments for mass spectrometry using forward programmed MKs performed previously by colleagues (unpublished data), large numbers of MKs (≈ 50 million) are needed for each sample. At the time of writing, we have not been able to produce this large quantity of MKs to perform immunoprecipitation and mass spectrometry assays, therefore the interactome of CRLF3 in MKs remains unknown.

Forward programmed MKs from TAP-tagged and untagged control iPSCs were seeded onto fibrinogen and allowed to form proplatelets. Samples were then fixed and stained with the nuclear stain DAPI and specific antibodies against the TAP-tag (anti-FLAG) to determine CRLF3 localisation during proplatelet formation. However, due to significant background staining with the anti-FLAG antibody in untagged forward programmed MKs, it was impossible to determine where CRLF3 was localised (fig. 6.10).

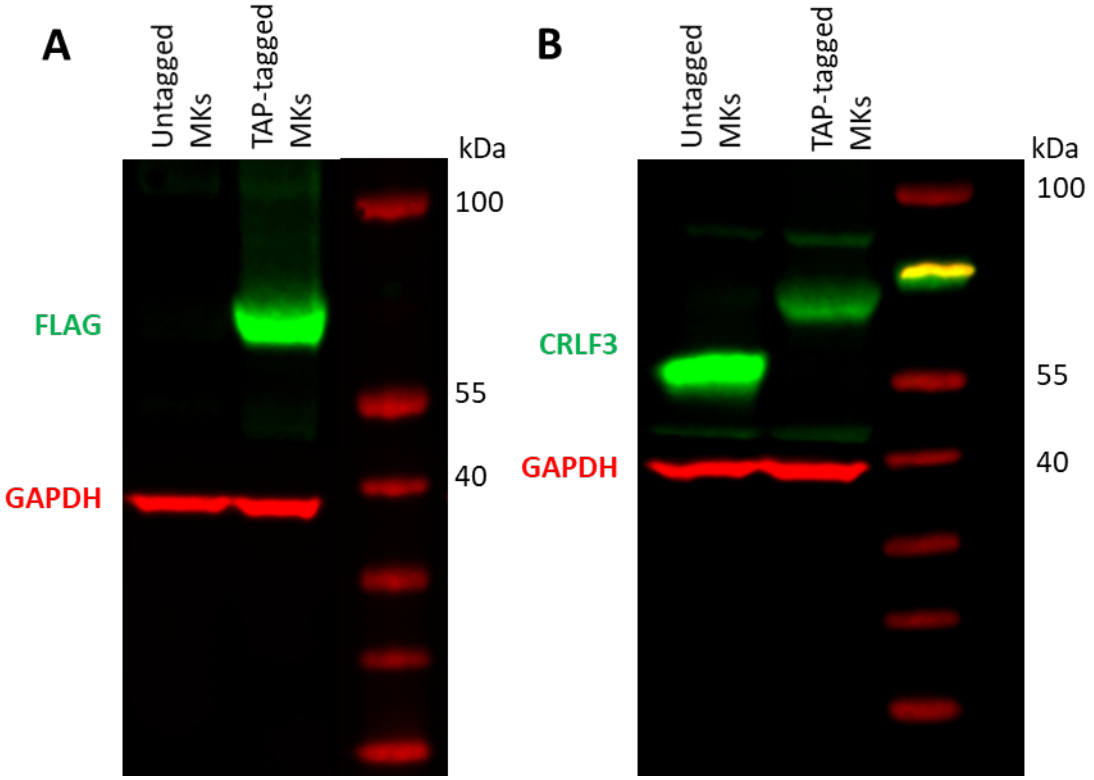

Figure 6.9 – Confirmation of CRLF3-TAP in forward programmed MKs. Western blot of TAP-tagged and untagged forward programmed MKs using specific antibodies against FLAG and GAPDH (A) and CRLF3 and GAPDH (B).

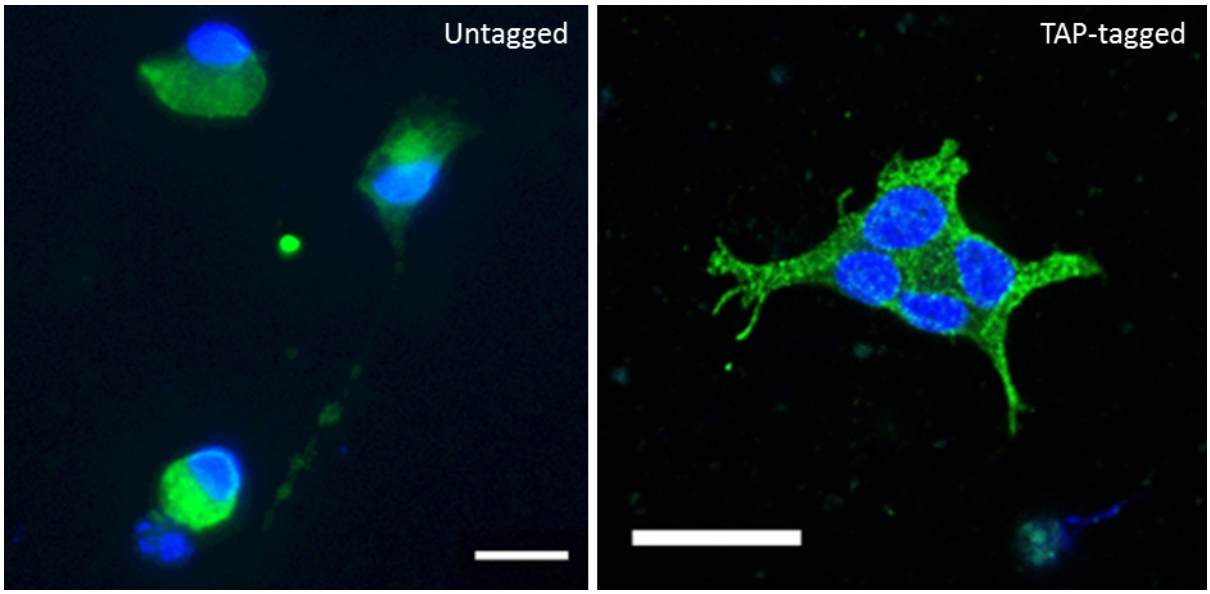

Figure 6.10 – High unspecific staining in proplatelet forming forward programmed MKs. Proplatelet forming untagged (left) and TAP-tagged (right) forward programmed MKs stained with antibodies against the TAP-tag (anti-FLAG; green) and the nuclear stain DAPI (blue). Scale bars are 20µm.

6.5 Chapter conclusions

The first aim of this chapter was to uncover the tertiary structure of CRLF3. We were unable to crystallise protein from full length CRLF3, therefore we were unable to determine the 3D structure of full length CRLF3. Using bioinformatic tools we chose 4 constructs covering different regions of the full length protein that were predicted to crystallise more readily. We concentrated our efforts on construct 3, which covers the predicted beta sheet region of CRLF3 (fig. 6.1), as it was produced in large quantities by *E.coli* cells compared to all other constructs. We were able to crystallise protein of CRLF3 construct 3 and its 3D structure was resolved at a resolution of 1.7Å by Hg-SAD and manual refinement. The 3D structure revealed both a FN3 domain at the N-terminus and a SPRY domain at the C-terminus of construct 3 (fig 6.4B). The FN3 domain was initially predicted by HHpred (homologous proteins boxed in fig. 6.2C).

The second aim of the chapter was to discover the interactome of CRLF3 in MKs. To this end, we were able to tag endogenous *CRLF3* with a TAP tag using CRISPR/Cas9 technology in human iPSCs (fig. 6.7-8). We were able to forward programme TAP-tagged iPSCs into MKs using the method of Moreau et al. (2016). However, due to the vast number of MKs needed to perform immunoprecipitation and mass spectrometry assays, we were unable to perform these experiments and therefore the interactome of CRLF3 remains unknown in MKs. We did however, perform immunoprecipitation and mass spectrometry assays on tagged and untagged iPSCs, which revealed 18 proteins in the tagged samples that were not present in the untagged samples (table 6.2). Interestingly, many of these are associated with desmosomes, which are involved in resisting shear forces.

Finally, we tried to discover the localisation of CRLF3 in MKs during proplatelet formation using fluorescent microscopy with antibodies against the TAP-tag (anti-FLAG). However, due to significant background staining caused by the anti-FLAG antibody in untagged forward programmed MKs (fig. 6.10), we were unable to determine CRLF3's localisation.

7

Discussion and future work

7.1 Ablation of *Crlf3* causes isolated chronic thrombocytopenia

In the first section of this thesis we showed that *Crlf3* knockout mice (*Crlf3*$^{-/-}$) developed by the Wellcome Trust Sanger Institute as part of an international consortium have a chronic and isolated thrombocytopenic phenotype (fig. 4.4 and table 4.1). There are currently over 20 known genes in which mutations lead to an inherited thrombocytopenias, *CRLF3* is not one of these genes. CRLF3 is 93% homologous between human and mice, suggesting both gene and protein are highly regulated. In keeping with this, predicted loss of function mutations in *CRLF3* are extremely rare, with only 31 mutations predicted to lead to a loss of function observed in 121,408 alleles genotyped as part of the Exome Aggregation Consortium (ExAC) (Lek et al., 2016). Furthermore, no individual out of 70,344 whose genome was sequenced in two studies were shown to have homozygous mutations in *CRLF3* (60,704 individuals in ExAC (Lek et al., 2016) and 9640 individuals as part of the BRIDGE Bleeding, thrombotic and Platelet Disorders (BPD) project (Westbury et al., 2015)) and no individual was shown to carry compound heterozygous mutations in the BPD study. It is also likely that mutations in *CRLF3* would cause an autosomal recessive disorder as heterozygous mice (*Crlf3*$^{+/-}$) are unaffected and individuals with heterozygous mutations in *CRLF3* did not have any platelet defects in the BPD study. These factors may be responsible for why *CRLF3*-related thrombocytopenias have not been observed in the human population.

We showed that despite the thrombocytopenia, *Crlf3*$^{-/-}$ platelets were still able to fulfil their primary haemostatic function. No incidence of bleeding was reported in *Crlf3*$^{-/-}$ mice and *Crlf3*$^{-/-}$ platelets: express the major surface receptors required for thrombus formation similarly to WT platelets (fig. 4.13A), are able to activate appropriately in response to a range of agonists (fig. 4.13B) and produce thrombi at arteriolar shear rates, similar to WT platelets (fig 4.14B).

We went on to show that the ablation of *Crlf3* causes preplatelets to be retained in the peripheral circulation (fig. 4.15A-D), suggesting terminal maturation of platelets is defective in *Crlf3*$^{-/-}$ mice. Under normal physiology, large preplatelets are released from proplatelet shafts into bone marrow sinusoids (Junt et al., 2007; Zhang et al., 2012). These preplatelets then rapidly undergo fission into mature discoid platelets by twisting of microtubules driven by the shear stress of the peripheral circulation (Thon et al., 2012a; Thon et al., 2010). Why a proportion of preplatelets are unable to mature into discoid platelets in *Crlf3*$^{-/-}$ mice in still not

fully understood. However, we have shown that microtubules are disorganised in *Crlf3*$^{-/-}$ platelets, especially in the preplatelet forms (fig. 4.16A-D). Disorganised microtubules is a feature of platelets from patients with WAS (Bender et al., 2014) and DIAPH1-related macrothrombocytopenia (Stritt et al., 2016) and profilin 1 knockout mice (Bender et al., 2014). In all cases, abnormal microtubule organisation is associated with increased tubulin stability. In agreement with this, depolymerisation of the microtubules is decreased in *Crlf3*$^{-/-}$ platelets incubated at 4^{o}C (fig. 4.16E-I). Also, post splenectomy there is a trend towards increased preplatelets in the peripheral circulation of *Crlf3*$^{-/-}$ mice compared to WT control mice (fig. 4.15E), suggesting that *Crlf3*$^{-/-}$ preplatelets survive longer in the peripheral circulation and may indicate increased stiffness of microtubules. However, increased tubulin stability is associated with increased levels of detyrosinated (Glu-) tubulin (Pan et al., 2014; Stritt et al., 2016), something that was not seen in *Crlf3*$^{-/-}$ platelets (fig. 4.16J-K). Therefore, more experimental data is needed to fully understand whether *Crlf3* ablation causes increased microtubule stability and whether this increased stability is the cause of decreased fission of *Crlf3*$^{-/-}$ preplatelets.

As the disorganised expression of tubulin is similar between *Crlf3*$^{-/-}$ platelets and that seen in patients with WAS and DIAPH1 mutations and profilin 1 knockout mice, it would be of interest to determine whether CRLF3 interacts with WAS, DIAPH1 or profilin1. If CRLF3 was found to interact with any of these proteins, it would help shed light on the function of CRLF3 in MKs and platelet genesis.

Myosin IIA has also been implicated in the fission of preplatelets. It is thought that the high shear force of the peripheral circulation causes dephosphorylation and activation of myosin IIA, which permits fission of preplatelets into mature discoid platelets. Patients with mutations in the gene that encodes myosin IIA, *MYH9*, have macrothrombocytopenia as a result of increased phosphorylation and inactivation of myosin IIA (Chen et al., 2013b; Spinler et al., 2015). However, very large preplatelets in the peripheral circulation, as seen in *Crlf3*$^{-/-}$ mice (fig. 4.15A-D), have not been recorded in patients with *MYH9* mutations (Chen et al., 2013b) or conditional *Myh9* knockout mice (Eckly et al., 2009), suggesting fission of large preplatelets to smaller preplatelets still occurs. Interestingly, proplatelet formation is up-regulated in *in vitro* cultured MKs from conditional *Myh9* knockout mice (Eckly et al., 2009), a feature that we observed in *in vitro* cultured *Crlf3*$^{-/-}$ MKs (fig. 4.9); although the opposite was seen in MKs

cultured from patients with *MYH9* mutations (Chen et al., 2013b). As phosphorylation of myosin IIA is implicated in the fission of platelets, it would be interesting to determine whether ablation of *Crlf3* has an effect on the level of phosphorylation of myosin IIA.

The thrombocytopenia seen in *Crlf3*$^{-/-}$ mice is a consequence of increased platelet clearance rather than decreased platelet production. We showed that megakaryopoiesis is upregulated in *Crlf3*$^{-/-}$ mice (fig. 4.5), maturation of *Crlf3*$^{-/-}$ MKs, as assessed by polyploidy, is unaffected *in vitro* (fig. 4.8) and proplatelet formation occurs quicker in *Crlf3*$^{-/-}$ MKs *in vitro* (fig. 4.9); all data that suggests platelet production from MKs is not decreased. Increased preplatelet clearance was confirmed in *Crlf3*$^{-/-}$ mice by performing splenectomies on young mice. Splenectomised *Crlf3*$^{-/-}$ mice showed restoration of platelet counts to WT levels within 7 days (fig. 4.11B), irrefutably linking the thrombocytopenia to splenic clearance. It is likely that rapid removal of preplatelets by the spleen is causing the thrombocytopenia in *Crlf3*$^{-/-}$ mice. Despite having the same percentage of circulating preplatelets before splenectomy, there was a trend towards increased circulating preplatelets in *Crlf3*$^{-/-}$ mice compared to WT controls post splenectomy (fig. 4.15E). This suggests that if the preplatelets are not rapidly removed by the spleen, they can eventually undergo fission into mature platelets.

7.2 CRLF3 as a novel therapeutic for the treatment of thrombocythaemia

Thrombocythaemia which occurs secondary to many conditions such as infection, cancer and inflammation. However, thrombocytopenia may also be genetically inherited and this is termed ET. ET is a rare inherited disease caused by mutations mainly in *JAK2*, *MPL* and *CALR* that results in a chronic increase in platelet counts (Cervantes, 2011). The major complications of ET are arterial and venous thrombotic events; therefore the focus of therapeutic treatment is primarily to prevent thrombotic events without increasing the risk of bleeding (Dombi et al., 2017). Patients at high risk of thrombotic or bleeding events are treated with low dose aspirin and cytoreductive agents. The cytoreductive agents are not MK and platelet specific and therefore are associated with a range of haematological side effects (Cervantes, 2011).

In the next section of this thesis we crossbred *Crlf3*$^{-/-}$ mice with JAK2 V617F knock in mice that have an ET phenotype (fig. 5.1), to determine whether CRLF3 may be a potential therapeutic target for the treatment of ET (and for the treatment of other thrombocythaemias).

Importantly, ablation of *Crlf3* in the setting of ET restored platelet counts to WT values (fig. 5.2 and table 5.1), suggesting therapeutics against CRLF3 could normalise platelet counts in ET patients. Interestingly, ablation of *Crlf3* in ET mice had no effect on any other blood lineage (table 5.1), suggesting therapeutics against CRLF3 may have less haematological side effects than the cytoreductive agents currently in use.

Beyond an increase in platelet numbers, ET also causes MK hyperplasia in the bone marrow (Cervantes, 2011). In our ET mice with *Crlf3* ablated (ET x *Crlf3*$^{-/-}$), we showed no increase in MK hyperplasia compared to WT (Cre) controls (fig. 5.3). However, this result must be put in the context that we did not observe MK hyperplasia in ET mice. One possibility for why MK hyperplasia was not observed in the ET mice may be due to an unsettled background strain created by cross breeding of *Crlf3*$^{-/-}$ mice with ET mice. *Crlf3*$^{-/-}$ animals are on a B6Brd;B6Dnk;B6N-Tyr background, whereas JAK2 V617F ET mice are on a B6J background. Mixing these two backgrounds may have caused an unsettled background, since background strain is known to have a major effect on haematopoietic cells (Peters et al., 2002). The crossbred mice used in these experiments represent pups from 1-4 inbred mating's of this mixed background strain. It may be that multiple more inbred mating's are required for the mixed background strain to become settled. Another possibility is that the numbers of animals used for each experiment was too small to determine significant differences. Therefore, whether ablation of CRLF3 effects MK numbers in an ET setting is yet to be determined. Repeating the quantification from bone marrow sections on mice crossbred at least 10 times should show any effect.

JAK2 V617F positive ET is also associated with platelet hyper-reactivity (Hobbs et al., 2013) and this hyper-reactivity may explain why JAK2 V617F positive ET patients have higher incidences of venous thrombotic events than JAK2 WT ET patients (Campbell et al., 2005). Similarly to MK hyperplasia, we show that ET x *Crlf3*$^{-/-}$ platelets are not hyper-reactive (fig. 5.4), but this is in the context that we failed to show the hyper-reactive nature of ET platelets.

7.3 Structure, function and localisation of CRLF3

In the final section of this thesis, we aimed to determine the tertiary structure of CRLF3, shed light on its function by determining its interactome and determine the localisation of CRLF3 in

MKs. We tried to determine the 3D structure of full length CRLF3 by X–ray crystallography, however due to technical difficulties in producing and crystallising full length CRLF3, we designed 4 partial constructs based on homology and disorder using freely available bioinformatic tools (fig. 6.2). Of these 4 constructs, only construct 3 which covers the predicted β-sheet region of the protein was able to be produced in greater quantities than the full length protein. After purification and concentration we were able to crystallise CRLF3 construct 3 protein in a range of conditions using the sitting drop vapour diffusion method (table 6.1 and fig 6.4A). The 3D structure was determined by Hg-SAD then further refined to a resolution of 1.7 Å (fig. 6.4B). The 3D structure uncovered a fibronectin type III (FN3) domain at the N-terminus and a SPRY domain at the C-terminus of construct 3 (fig 6.4B). FN3 is composed of 90-100 amino acids with a well-defined β-sandwich structure with seven β-strands. The FN3 domain is very common and expected to occur in approximately 2% of all animal proteins. Known proteins containing FN3 domains are all involved in molecular recognition and include cytokine receptors (e.g. erythropoietin receptor and interleukin 6 receptor), cell adhesion molecules (e.g. fibronectin and collagen XII) and protein kinases and phosphatases (e.g. insulin receptor and CD45 antigen) (Bork and Doolittle, 1992; Koide et al., 1998). The SPRY domain was first identified in a Dictyostelium discoidueum kinase splA and mammalian calcium-release channels ryanodine receptors and is a subgroup of the B30.2 domain, which contains a SPRY domain preceded by a shorter PRY domain. Approximately 150 human proteins contain B30.2 (PRY-SPRY) or SPRY only domains and experimental data suggest these SPRY containing domains facilitates protein interactions (Woo et al., 2006). For example, Zhai *et al*, showed that the B30.2 domain was responsible for the interaction between TRIM7 and glycogenin (Zhai et al., 2004). This suggests that CRLF3 recognises another protein/s in MKs/platelets and interaction of CRLF3 with this protein/s allows proper fission of preplatelets in the peripheral circulation. However, it may be that FN3 and SPRY are not the only binding domains of CRLF3, therefore it would be of interest to uncover the 3D structure of the full length protein. This could be done using the full length protein or by determining the 3D structure of the unknown α-helical portion of CRLF3 and joining the two portions computationally.

Determining the interactome of a protein of unknown function can help determine its function, as proteins generally have similar functions to their interacting proteins (Schwikowski et al., 2000). Therefore to help shed light on the function of CRLF3, we aimed to

uncover its interactome. We tagged endogenous *CRLF3* with a tandem affinity purification (TAP) tag, consisting of an N-terminal calmodulin binding domain and C-terminal 3x FLAG tag repeat separated by a TEV cleavage site, by CRISPR/Cas9 in human iPSCs (fig. 6.8). We intended to determine CRLF3's interactome in MKs. To produce TAP-tagged MKs, we forward programme TAP-tagged iPSCs into MKs using the method of Moreau et al. (2016); however, we have been so far unable to produce enough MKs to perform immunoprecipitation and mass spectrometry assays. Therefore, we performed immunoprecipitation and mass spectrometry experiments on TAP-tagged and untagged control iPSCs. Results revealed 18 proteins that were present in the TAP-tagged samples but not untagged samples (table 6.2). Interestingly, four of these proteins are known to form desmosomes along with other proteins. Desmosomes are cell-to-cell adhesion molecules are important for resisting shear forces (Garrod and Chidgey, 2008). Although desmosomes are not known to exist in platelets or preplatelets, unsurprisingly as platelets are not in physically contact in their resting state, it is interesting that platelet maturation is driven by shear forces. It may be possible that CRLF3 is involved in resisting shear forces in many cell types. In platelets it is possible that binding of CRLF3 to unknown protein/s is important for permitting shear forces to drive cytoplasmic rearrangement and/or myosin IIA dephosphorylation and therefore fission into mature platelets.

CRLF3 has has been shown to interact with proteins of the DOCK and LRCH family (Couzens et al., 2013), however no DOCK or LRCH family proteins were shown to interact with CRLF3 by us (table 6.2). These conflicting results in CRLF3's interactome may be due to the differing cell type used in the immunoprecipitation experiments. It may be that CRLF3 interacts with different proteins in different cell types. This would explain why, despite CRLF3 being ubiquitously expressed in the haematopoietic system (fig. 4.1), *Crlf3*$^{-/-}$ mice have a platelet isolated phenotype. Therefore, it is important to uncover the interactome of CRLF3 in MKs or platelets.

CRLF3 is known to be localised in the cytoplasm in human cell lines (Yang et al., 2009). However, as *Crlf3*$^{-/-}$ mice have an isolated platelet phenotype it would be interesting to determine the localisation of CRLF3 in MKs, especially during proplatelet formation. As commercially available antibodies against CRLF3 are not specific enough to perform immunohistochemistry, we intended to determine the localisation of CRLF3 in TAP-tagged

CRLF3. However, we have shown that proplatelet forming forward programmed MKs have high autofluorescence (fig. 6.10), therefore we were unable to determine the localisation of CRLF3. It would be of interest to optimise the fixation and staining protocol to decrease the autofluorescence in forward programmed MKs, to allow the localisation of CRLF3 to be determined.

7.4 Towards a therapeutic against CRLF3

Many steps would need to be taken before a therapeutic against CRLF3 could be trailed in humans. Firstly, it would be important to determine whether a therapeutic against CRLF3 would be tolerated. Apart from thrombocytopenia, *Crlf3*$^{-/-}$ mice are otherwise unaffected, however these mice have not had CRLF3 since embryogenesis. Inhibition of CRLF3 in animals that have had working CRLF3 could have drastically different effects and this is currently unknown. It would be interesting to create an inducible *Crlf3* knockout mouse, as ablation of *Crlf3* post gestation would mimic treatment with an inhibitor of CRLF3.

Secondly, the binding site/s of CRLF3 would need to be determined. To do this, the 3D structure of CRLF3 would need to be resolved as mentioned above. Once the binding site/s are known, existing small inhibitors can be screened *in silico* and optimised or new inhibitors can be designed computationally. Thirdly, the interactome and downstream pathways of CRLF3 would need to be determined, as this would allow high throughput screening of the potential inhibitors in cell lines. Knowledge of the downstream pathways of CRLF3 would allow for determination of whether the inhibitor was able prevent CRLF3 having an effect on its downstream interacting proteins and would show any off target effects of the inhibitor. Once highly selective inhibitors have been identifies in high throughput screenings, these molecules would need to be tested in animal models to determine whether they could lower platelet counts and to assess any off target effects.

7.5 Final Remarks

Current treatments of high risk ET patients relies on cytoreductive agents and despite being effective at decreasing platelet counts, these cytoreductive agents have a range of

haematological side effects. An ideal therapy would decrease platelet counts to normal values with minimal side effects. We have shown that CRLF3 has a role specific to controlling platelet numbers in mice. *Crlf3*$^{-/-}$ mice have a chronic and isolated thrombocytopenic phenotype caused by rapid removal of large preplatelets from the peripheral circulation. It appears that CRLF3 affects the fission of preplatelets into mature platelets in the peripheral circulation, potentially due to affecting tubulin stability.

We have shown the rational for continued research of CRLF3 as a therapeutic target for the treatment of ET, ET mice with *Crlf3* ablated show restoration of platelet counts to WT numbers. Also, ablation of CRLF3 does not seem to add to other burdens of ET, such as MK hyperplasia and platelet hyper-reactivity. Despite these initial positive results suggesting CRLF3 could be a novel therapeutic target for the treatment of ET, much work needs to be done to confirm pharmacological inhibition of CRLF3 would be a more effective treatment of ET than current cytoreductive therapies.

8

Bibliography

Abbonante, V., Gruppi, C., Rubel, D., Gross, O., Moratti, R., and Balduini, A. (2013). Discoidin domain receptor 1 protein is a novel modulator of megakaryocyte-collagen interactions. The Journal of biological chemistry *288*, 16738-16746.

Adams, P.D., Afonine, P.V., Bunkoczi, G., Chen, V.B., Davis, I.W., Echols, N., Headd, J.J., Hung, L.W., Kapral, G.J., Grosse-Kunstleve, R.W.*, et al.* (2010). PHENIX: a comprehensive Python-based system for macromolecular structure solution. Acta crystallographica Section D, Biological crystallography *66*, 213-221.

Adolfsson, J., Mansson, R., Buza-Vidas, N., Hultquist, A., Liuba, K., Jensen, C.T., Bryder, D., Yang, L., Borge, O.J., Thoren, L.A.*, et al.* (2005). Identification of Flt3+ lympho-myeloid stem cells lacking erythro-megakaryocytic potential a revised road map for adult blood lineage commitment. Cell *121*, 295-306.

Albers, C.A., Paul, D.S., Schulze, H., Freson, K., Stephens, J.C., Smethurst, P.A., Jolley, J.D., Cvejic, A., Kostadima, M., Bertone, P.*, et al.* (2012). Compound inheritance of a low-frequency regulatory SNP and a rare null mutation in exon-junction complex subunit RBM8A causes TAR syndrome. Nature genetics *44*, 435-439, s431-432.

Alva, V., Nam, S.Z., Soding, J., and Lupas, A.N. (2016). The MPI bioinformatics Toolkit as an integrative platform for advanced protein sequence and structure analysis. Nucleic acids research *44*, W410-415.

Alvarez-Larran, A., Pereira, A., Guglielmelli, P., Hernandez-Boluda, J.C., Arellano-Rodrigo, E., Ferrer-Marin, F., Samah, A., Griesshammer, M., Kerguelen, A., Andreasson, B.*, et al.* (2016). Antiplatelet therapy versus observation in low-risk essential thrombocythemia with a CALR mutation. Haematologica *101*, 926-931.

Anderson, A.C. (2003). The process of structure-based drug design. Chemistry & biology *10*, 787-797.

Araki, M., Yang, Y., Masubuchi, N., Hironaka, Y., Takei, H., Morishita, S., Mizukami, Y., Kan, S., Shirane, S., Edahiro, Y.*, et al.* (2016). Activation of the thrombopoietin receptor by mutant calreticulin in CALR-mutant myeloproliferative neoplasms. Blood *127*, 1307-1316.

Avecilla, S.T., Hattori, K., Heissig, B., Tejada, R., Liao, F., Shido, K., Jin, D.K., Dias, S., Zhang, F., Hartman, T.E.*, et al.* (2004). Chemokine-mediated interaction of hematopoietic progenitors

with the bone marrow vascular niche is required for thrombopoiesis. Nature medicine *10*, 64-71.

Balduini, A., Malara, A., Balduini, C.L., and Noris, P. (2011). Megakaryocytes derived from patients with the classical form of Bernard-Soulier syndrome show no ability to extend proplatelets in vitro. Platelets *22*, 308-311.

Bartley, T.D., Bogenberger, J., Hunt, P., Li, Y.S., Lu, H.S., Martin, F., Chang, M.S., Samal, B., Nichol, J.L., Swift, S.*, et al.* (1994). Identification and cloning of a megakaryocyte growth and development factor that is a ligand for the cytokine receptor Mpl. Cell *77*, 1117-1124.

Baxter, E.J., Scott, L.M., Campbell, P.J., East, C., Fourouclas, N., Swanton, S., Vassiliou, G.S., Bench, A.J., Boyd, E.M., Curtin, N.*, et al.* (2005). Acquired mutation of the tyrosine kinase JAK2 in human myeloproliferative disorders. Lancet (London, England) *365*, 1054-1061.

Becker, R.P., and De Bruyn, P.P. (1976). The transmural passage of blood cells into myeloid sinusoids and the entry of platelets into the sinusoidal circulation; a scanning electron microscopic investigation. The American journal of anatomy *145*, 183-205.

Begonja, A.J., Hoffmeister, K.M., Hartwig, J.H., and Falet, H. (2011). FlnA-null megakaryocytes prematurely release large and fragile platelets that circulate poorly. Blood *118*, 2285-2295.

Behnke, O. (1968). An electron microscope study of the megacaryocyte of the rat bone marrow. I. The development of the demarcation membrane system and the platelet surface coat. Journal of ultrastructure research *24*, 412-433.

Behnke, O., and Forer, A. (1998). From megakaryocytes to platelets: platelet morphogenesis takes place in the bloodstream. European journal of haematology Supplementum *61*, 3-23.

Bender, M., Eckly, A., Hartwig, J.H., Elvers, M., Pleines, I., Gupta, S., Krohne, G., Jeanclos, E., Gohla, A., Gurniak, C.*, et al.* (2010). ADF/n-cofilin-dependent actin turnover determines platelet formation and sizing. Blood *116*, 1767-1775.

Bender, M., Stritt, S., Nurden, P., van Eeuwijk, J.M., Zieger, B., Kentouche, K., Schulze, H., Morbach, H., Stegner, D., Heinze, K.*, et al.* (2014). Megakaryocyte-specific Profilin1-

deficiency alters microtubule stability and causes a Wiskott-Aldrich syndrome-like platelet defect. Nat Commun *5*, 4746.

Bender, M., Thon, J.N., Ehrlicher, A.J., Wu, S., Mazutis, L., Deschmann, E., Sola-Visner, M., Italiano, J.E., and Hartwig, J.H. (2015). Microtubule sliding drives proplatelet elongation and is dependent on cytoplasmic dynein. Blood *125*, 860-868.

Berge, K.E., Tian, H., Graf, G.A., Yu, L., Grishin, N.V., Schultz, J., Kwiterovich, P., Shan, B., Barnes, R., and Hobbs, H.H. (2000). Accumulation of Dietary Cholesterol in Sitosterolemia Caused by Mutations in Adjacent ABC Transporters. Science (New York, NY) *290*, 1771.

Berman, H.M., Westbrook, J., Feng, Z., Gilliland, G., Bhat, T.N., Weissig, H., Shindyalov, I.N., and Bourne, P.E. (2000). The Protein Data Bank. Nucleic acids research *28*, 235-242.

Birgegard, G. (2016). The Use of Anagrelide in Myeloproliferative Neoplasms, with Focus on Essential Thrombocythemia. Current hematologic malignancy reports *11*, 348-355.

Blair, P., and Flaumenhaft, R. (2009). Platelet alpha-granules: basic biology and clinical correlates. Blood reviews *23*, 177-189.

Bork, P., and Doolittle, R.F. (1992). Proposed acquisition of an animal protein domain by bacteria. Proceedings of the National Academy of Sciences of the United States of America *89*, 8990-8994.

Bovill, E.G., and van der Vliet, A. (2011). Venous valvular stasis-associated hypoxia and thrombosis: what is the link? Annu Rev Physiol *73*, 527-545.

Briddell, R.A., Brandt, J.E., Straneva, J.E., Srour, E.F., and Hoffman, R. (1989). Characterization of the human burst-forming unit-megakaryocyte. Blood *74*, 145-151.

Briere, J.B. (2007). Essential thrombocythemia. Orphanet journal of rare diseases *2*, 3.

Brinkmann, V., Reichard, U., Goosmann, C., Fauler, B., Uhlemann, Y., Weiss, D.S., Weinrauch, Y., and Zychlinsky, A. (2004). Neutrophil extracellular traps kill bacteria. Science (New York, NY) *303*, 1532-1535.

Brinkmann, V., and Zychlinsky, A. (2012). Neutrophil extracellular traps: Is immunity the second function of chromatin? The Journal of cell biology *198*, 773.

Brizzi, M.F., Dentelli, P., Lanfrancone, L., Rosso, A., Pelicci, P.G., and Pegoraro, L. (1996). Discrete protein interactions with the Grb2/c-Cbl complex in SCF- and TPO-mediated myeloid cell proliferation. Oncogene *13*, 2067-2076.

Browse, N.L., and Thomas, M.L. (1974). Source of non-lethal pulmonary emboli. Lancet (London, England) *1*, 258-259.

Bryder, D., Rossi, D.J., and Weissman, I.L. (2006). Hematopoietic stem cells: the paradigmatic tissue-specific stem cell. The American journal of pathology *169*, 338-346.

Bryson, K., McGuffin, L.J., Marsden, R.L., Ward, J.J., Sodhi, J.S., and Jones, D.T. (2005). Protein structure prediction servers at University College London. Nucleic acids research *33*, W36-38.

Budarf, M.L., Konkle, B.A., Ludlow, L.B., Michaud, D., Li, M., Yamashiro, D.J., McDonald-McGinn, D., Zackai, E.H., and Driscoll, D.A. (1995). Identification of a patient with Bernard-Soulier syndrome and a deletion in the DiGeorge/velo-cardio-facial chromosomal region in 22q11.2. Human molecular genetics *4*, 763-766.

Bunting, S., Widmer, R., Lipari, T., Rangell, L., Steinmetz, H., Carver-Moore, K., Moore, M.W., Keller, G.A., and de Sauvage, F.J. (1997). Normal platelets and megakaryocytes are produced in vivo in the absence of thrombopoietin. Blood *90*, 3423-3429.

Burk, C.D., Newman, P.J., Lyman, S., Gill, J., Coller, B.S., and Poncz, M. (1991). A deletion in the gene for glycoprotein IIb associated with Glanzmann's thrombasthenia. The Journal of clinical investigation *87*, 270-276.

Burstein, S.A., Mei, R.L., Henthorn, J., Friese, P., and Turner, K. (1992). Leukemia inhibitory factor and interleukin-11 promote maturation of murine and human megakaryocytes in vitro. Journal of cellular physiology *153*, 305-312.

Campbell, P.J., Scott, L.M., Buck, G., Wheatley, K., East, C.L., Marsden, J.T., Duffy, A., Boyd, E.M., Bench, A.J., Scott, M.A*., et al.* (2005). Definition of subtypes of essential thrombocythaemia and relation to polycythaemia vera based on JAK2 V617F mutation status: a prospective study. Lancet (London, England) *366*, 1945-1953.

Cervantes, F. (2011). Management of essential thrombocythemia. Hematology / the Education Program of the American Society of Hematology American Society of Hematology Education Program *2011*, 215-221.

Chang, Y., Bluteau, D., Debili, N., and Vainchenker, W. (2007). From hematopoietic stem cells to platelets. Journal of thrombosis and haemostasis : JTH *5 Suppl 1*, 318-327.

Chen, L., Kostadima, M., Martens, J.H.A., Canu, G., Garcia, S.P., Turro, E., Downes, K., Macaulay, I.C., Bielczyk-Maczynska, E., Coe, S.*, et al.* (2014). Transcriptional diversity during lineage commitment of human blood progenitors. Science (New York, NY) *345*, 1251033.

Chen, Y., Aardema, J., Kale, S., Whichard, Z.L., Awomolo, A., Blanchard, E., Chang, B., Myers, D.R., Ju, L., Tran, R.*, et al.* (2013a). Loss of the F-BAR protein CIP4 reduces platelet production by impairing membrane-cytoskeleton remodeling. Blood *122*, 1695-1706.

Chen, Y., Boukour, S., Milloud, R., Favier, R., Saposnik, B., Schlegel, N., Nurden, A., Raslova, H., Vainchenker, W., Balland, M.*, et al.* (2013b). The abnormal proplatelet formation in MYH9-related macrothrombocytopenia results from an increased actomyosin contractility and is rescued by myosin IIA inhibition. Journal of thrombosis and haemostasis : JTH *11*, 2163-2175.

Cho, J., Furie, B.C., Coughlin, S.R., and Furie, B. (2008). A critical role for extracellular protein disulfide isomerase during thrombus formation in mice. The Journal of clinical investigation *118*, 1123-1131.

Choi, E.S., Nichol, J.L., Hokom, M.M., Hornkohl, A.C., and Hunt, P. (1995). Platelets generated in vitro from proplatelet-displaying human megakaryocytes are functional. Blood *85*, 402-413.

Chott, A., Gisslinger, H., Thiele, J., Fritz, E., Linkesch, W., Radaszkiewicz, T., and Ludwig, H. (1990). Interferon-alpha-induced morphological changes of megakaryocytes: a histomorphometrical study on bone marrow biopsies in chronic myeloproliferative disorders with excessive thrombocytosis. British journal of haematology *74*, 10-16.

Cimmino, G., and Golino, P. (2013). Platelet biology and receptor pathways. Journal of cardiovascular translational research *6*, 299-309.

Cooney, K.A., Nichols, W.C., Bruck, M.E., Bahou, W.F., Shapiro, A.D., Bowie, E.J., Gralnick, H.R., and Ginsburg, D. (1991). The molecular defect in type IIB von Willebrand disease. Identification of four potential missense mutations within the putative GpIb binding domain. The Journal of clinical investigation *87*, 1227-1233.

Cooper, N., and Bussel, J. (2006). The pathogenesis of immune thrombocytopaenic purpura. British journal of haematology *133*, 364-374.

Cortelazzo, S., Finazzi, G., Ruggeri, M., Vestri, O., Galli, M., Rodeghiero, F., and Barbui, T. (1995). Hydroxyurea for patients with essential thrombocythemia and a high risk of thrombosis. The New England journal of medicine *332*, 1132-1136.

Cotton, L.T., and Clark, C. (1965). ANATOMICAL LOCALIZATION OF VENOUS THROMBOSIS. Annals of the Royal College of Surgeons of England *36*, 214-224.

Couzens, A.L., Knight, J.D., Kean, M.J., Teo, G., Weiss, A., Dunham, W.H., Lin, Z.Y., Bagshaw, R.D., Sicheri, F., Pawson, T.*, et al.* (2013). Protein interaction network of the mammalian Hippo pathway reveals mechanisms of kinase-phosphatase interactions. Science signaling *6*, rs15.

Croker, B.A., Kiu, H., and Nicholson, S.E. (2008). SOCS regulation of the JAK/STAT signalling pathway. Seminars in cell & developmental biology *19*, 414-422.

Cruz, M.A., Yuan, H., Lee, J.R., Wise, R.J., and Handin, R.I. (1995). Interaction of the von Willebrand factor (vWF) with collagen. Localization of the primary collagen-binding site by analysis of recombinant vWF A domain polypeptides. The Journal of biological chemistry *270*, 19668.

Cserhati, I., Tanos, B., and Kelemen, E. (1958). [Acute prolonged thrombocytosis in mice induced by the serum of patients having thrombocythemia; postulated human thrombopoietin]. Orvosi hetilap *99*, 540-541.

Dasouki, M.J., Rafi, S.K., Olm-Shipman, A.J., Wilson, N.R., Abhyankar, S., Ganter, B., Furness, L.M., Fang, J., Calado, R.T., and Saadi, I. (2013). Exome sequencing reveals a thrombopoietin ligand mutation in a Micronesian family with autosomal recessive aplastic anemia. Blood *122*, 3440-3449.

Datta, N.S., Williams, J.L., Caldwell, J., Curry, A.M., Ashcraft, E.K., and Long, M.W. (1996). Novel alterations in CDK1/cyclin B1 kinase complex formation occur during the acquisition of a polyploid DNA content. Molecular biology of the cell *7*, 209-223.

Debrincat, M.A., Pleines, I., Lebois, M., Lane, R.M., Holmes, M.L., Corbin, J., Vandenberg, C.J., Alexander, W.S., Ng, A.P., Strasser, A.*, et al.* (2015). BCL-2 is dispensable for thrombopoiesis and platelet survival. Cell death & disease *6*, e1721.

Deppermann, C., and Kubes, P. (2016). Platelets and infection. Seminars in immunology *28*, 536-545.

Derry, J.M., Ochs, H.D., and Francke, U. (1994). Isolation of a novel gene mutated in Wiskott-Aldrich syndrome. Cell *78*, 635-644.

Dombi, P., Illes, A., Demeter, J., Homor, L., Simon, Z., Karadi, E., Udvardy, M., and Egyed, M. (2017). Anagrelide reduces thrombotic risk in essential thrombocythaemia vs. hydroxyurea plus aspirin. European journal of haematology *98*, 106-111.

Douglas, J., Cilliers, D., Coleman, K., Tatton-Brown, K., Barker, K., Bernhard, B., Burn, J., Huson, S., Josifova, D., Lacombe, D.*, et al.* (2007). Mutations in RNF135, a gene within the NF1 microdeletion region, cause phenotypic abnormalities including overgrowth. Nature genetics *39*, 963-965.

Dutting, S., Gaits-Iacovoni, F., Stegner, D., Popp, M., Antkowiak, A., van Eeuwijk, J.M.M., Nurden, P., Stritt, S., Heib, T., Aurbach, K.*, et al.* (2017). A Cdc42/RhoA regulatory circuit downstream of glycoprotein Ib guides transendothelial platelet biogenesis. Nat Commun *8*, 15838.

Eckly, A., Heijnen, H., Pertuy, F., Geerts, W., Proamer, F., Rinckel, J.Y., Leon, C., Lanza, F., and Gachet, C. (2014). Biogenesis of the demarcation membrane system (DMS) in megakaryocytes. Blood *123*, 921-930.

Eckly, A., Strassel, C., Freund, M., Cazenave, J.P., Lanza, F., Gachet, C., and Leon, C. (2009). Abnormal megakaryocyte morphology and proplatelet formation in mice with megakaryocyte-restricted MYH9 inactivation. Blood *113*, 3182-3189.

Elliott, M.A., and Tefferi, A. (2005). Thrombosis and haemorrhage in polycythaemia vera and essential thrombocythaemia. British journal of haematology *128*, 275-290.

Emsley, P., Lohkamp, B., Scott, W.G., and Cowtan, K. (2010). Features and development of Coot. Acta crystallographica Section D, Biological crystallography *66*, 486-501.

Espasandin, Y.R., Glembotsky, A.C., Grodzielski, M., Lev, P.R., Goette, N.P., Molinas, F.C., Marta, R.F., and Heller, P.G. (2015). Anagrelide platelet-lowering effect is due to inhibition of both megakaryocyte maturation and proplatelet formation: insight into potential mechanisms. Journal of thrombosis and haemostasis : JTH *13*, 631-642.

Eto, K., Murphy, R., Kerrigan, S.W., Bertoni, A., Stuhlmann, H., Nakano, T., Leavitt, A.D., and Shattil, S.J. (2002). Megakaryocytes derived from embryonic stem cells implicate CalDAG-GEFI in integrin signaling. Proceedings of the National Academy of Sciences of the United States of America *99*, 12819-12824.

Evans, P.R. (2011). An introduction to data reduction: space-group determination, scaling and intensity statistics. Acta crystallographica Section D, Biological crystallography *67*, 282-292.

Falet, H., Marchetti, M.P., Hoffmeister, K.M., Massaad, M.J., Geha, R.S., and Hartwig, J.H. (2009). Platelet-associated IgAs and impaired GPVI responses in platelets lacking WIP. Blood *114*, 4729-4737.

Fichelson, S., Freyssinier, J.M., Picard, F., Fontenay-Roupie, M., Guesnu, M., Cherai, M., Gisselbrecht, S., and Porteu, F. (1999). Megakaryocyte growth and development factor-induced proliferation and differentiation are regulated by the mitogen-activated protein kinase pathway in primitive cord blood hematopoietic progenitors. Blood *94*, 1601-1613.

Fletcher, S.J., Johnson, B., Lowe, G.C., Bem, D., Drake, S., Lordkipanidze, M., Guiu, I.S., Dawood, B., Rivera, J., Simpson, M.A*., et al.* (2015). SLFN14 mutations underlie thrombocytopenia with excessive bleeding and platelet secretion defects. The Journal of clinical investigation *125*, 3600-3605.

Fogelson, A.L., and Neeves, K.B. (2015). Fluid Mechanics of Blood Clot Formation. Annual review of fluid mechanics *47*, 377-403.

Fujiwara, Y., Browne, C.P., Cunniff, K., Goff, S.C., and Orkin, S.H. (1996). Arrested development of embryonic red cell precursors in mouse embryos lacking transcription factor GATA-1. Proceedings of the National Academy of Sciences of the United States of America *93*, 12355-12358.

Furie, B., and Furie, B.C. (2008). Mechanisms of thrombus formation. The New England journal of medicine *359*, 938-949.

Gao, Y., Smith, E., Ker, E., Campbell, P., Cheng, E.C., Zou, S., Lin, S., Wang, L., Halene, S., and Krause, D.S. (2012). Role of RhoA-specific guanine exchange factors in regulation of endomitosis in megakaryocytes. Developmental cell *22*, 573-584.

Garrod, D., and Chidgey, M. (2008). Desmosome structure, composition and function. Biochimica et biophysica acta *1778*, 572-587.

Gawaz, M., and Vogel, S. (2013). Platelets in tissue repair: control of apoptosis and interactions with regenerative cells. Blood *122*, 2550-2554.

Geddis, A.E. (2010). Megakaryopoiesis. Seminars in hematology *47*, 212-219.

Geddis, A.E., Fox, N.E., and Kaushansky, K. (2001). Phosphatidylinositol 3-kinase is necessary but not sufficient for thrombopoietin-induced proliferation in engineered Mpl-bearing cell lines as well as in primary megakaryocytic progenitors. The Journal of biological chemistry *276*, 34473-34479.

Geddis, A.E., Fox, N.E., Tkachenko, E., and Kaushansky, K. (2007). Endomitotic megakaryocytes that form a bipolar spindle exhibit cleavage furrow ingression followed by furrow regression. Cell cycle (Georgetown, Tex) *6*, 455-460.

Geddis, A.E., Linden, H.M., and Kaushansky, K. (2002). Thrombopoietin: a pan-hematopoietic cytokine. Cytokine & growth factor reviews *13*, 61-73.

Geng, Y., Yu, Q., Sicinska, E., Das, M., Schneider, J.E., Bhattacharya, S., Rideout, W.M., Bronson, R.T., Gardner, H., and Sicinski, P. (2003). Cyclin E ablation in the mouse. Cell *114*, 431-443.

Grozovsky, R., Begonja, A.J., Liu, K., Visner, G., Hartwig, J.H., Falet, H., and Hoffmeister, K.M. (2015a). The Ashwell-Morell receptor regulates hepatic thrombopoietin production via JAK2-STAT3 signaling. Nature medicine *21*, 47-54.

Grozovsky, R., Giannini, S., Falet, H., and Hoffmeister, K.M. (2015b). Regulating billions of blood platelets: glycans and beyond. Blood *126*, 1877-1884.

Grozovsky, R., Hoffmeister, K.M., and Falet, H. (2010). Novel clearance mechanisms of platelets. Current opinion in hematology *17*, 585-589.

Guerrero, J.A., Bennett, C., van der Weyden, L., McKinney, H., Chin, M., Nurden, P., McIntyre, Z., Cambridge, E.L., Estabel, J., Wardle-Jones, H.*, et al.* (2014). Gray platelet syndrome: proinflammatory megakaryocytes and alpha-granule loss cause myelofibrosis and confer metastasis resistance in mice. Blood *124*, 3624-3635.

Gunay-Aygun, M., Falik-Zaccai, T.C., Vilboux, T., Zivony-Elboum, Y., Gumruk, F., Cetin, M., Khayat, M., Boerkoel, C.F., Kfir, N., Huang, Y.*, et al.* (2011). NBEAL2 is mutated in gray platelet syndrome and is required for biogenesis of platelet alpha-granules. Nature genetics *43*, 732-734.

Gurney, A.L., Carver-Moore, K., de Sauvage, F.J., and Moore, M.W. (1994). Thrombocytopenia in c-mpl-deficient mice. Science (New York, NY) *265*, 1445-1447.

Hall, M.A., Curtis, D.J., Metcalf, D., Elefanty, A.G., Sourris, K., Robb, L., Gothert, J.R., Jane, S.M., and Begley, C.G. (2003). The critical regulator of embryonic hematopoiesis, SCL, is vital in the adult for megakaryopoiesis, erythropoiesis, and lineage choice in CFU-S12. Proceedings of the National Academy of Sciences of the United States of America *100*, 992-997.

Hamer, J.D., Malone, P.C., and Silver, I.A. (1981). The PO2 in venous valve pockets: its possible bearing on thrombogenesis. The British journal of surgery *68*, 166-170.

Handagama, P.J., Feldman, B.F., Jain, N.C., Farver, T.B., and Kono, C.S. (1987). Circulating proplatelets: isolation and quantitation in healthy rats and in rats with induced acute blood loss. American journal of veterinary research *48*, 962-965.

Harper, M.T., and Poole, A.W. (2010). Diverse functions of protein kinase C isoforms in platelet activation and thrombus formation. Journal of thrombosis and haemostasis : JTH *8*, 454-462.

Harper, S., and Speicher, D.W. (2008). Expression and purification of GST fusion proteins. Current protocols in protein science / editorial board, John E Coligan [et al] *Chapter 6*, Unit 6.6.

Hart, A., Melet, F., Grossfeld, P., Chien, K., Jones, C., Tunnacliffe, A., Favier, R., and Bernstein, A. (2000). Fli-1 is required for murine vascular and megakaryocytic development and is hemizygously deleted in patients with thrombocytopenia. Immunity *13*, 167-177.

Heijnen, H., and van der Sluijs, P. (2015). Platelet secretory behaviour: as diverse as the granules ... or not? Journal of thrombosis and haemostasis : JTH *13*, 2141-2151.

Heijnen, H.F., Debili, N., Vainchencker, W., Breton-Gorius, J., Geuze, H.J., and Sixma, J.J. (1998). Multivesicular bodies are an intermediate stage in the formation of platelet alpha-granules. Blood *91*, 2313-2325.

Hitchcock, I.S., and Kaushansky, K. (2014). Thrombopoietin from beginning to end. British journal of haematology *165*, 259-268.

Hobbs, C.M., Manning, H., Bennett, C., Vasquez, L., Severin, S., Brain, L., Mazharian, A., Guerrero, J.A., Li, J., Soranzo, N.*, et al.* (2013). JAK2V617F leads to intrinsic changes in platelet formation and reactivity in a knock-in mouse model of essential thrombocythemia. Blood *122*, 3787-3797.

Hock, H., Meade, E., Medeiros, S., Schindler, J.W., Valk, P.J., Fujiwara, Y., and Orkin, S.H. (2004). Tel/Etv6 is an essential and selective regulator of adult hematopoietic stem cell survival. Genes & development *18*, 2336-2341.

Hodgkins, A., Farne, A., Perera, S., Grego, T., Parry-Smith, D.J., Skarnes, W.C., and Iyer, V. (2015). WGE: a CRISPR database for genome engineering. Bioinformatics (Oxford, England) *31*, 3078-3080.

Huang, N., Lou, M., Liu, H., Avila, C., and Ma, Y. (2016). Identification of a potent small molecule capable of regulating polyploidization, megakaryocyte maturation, and platelet production. Journal of hematology & oncology *9*, 136.

Humphrey, J.H. (1955). Origin of blood platelets. Nature *176*, 38.

Ihara, K., Ishii, E., Eguchi, M., Takada, H., Suminoe, A., Good, R.A., and Hara, T. (1999). Identification of mutations in the c-mpl gene in congenital amegakaryocytic thrombocytopenia. Proceedings of the National Academy of Sciences of the United States of America *96*, 3132-3136.

Isaacs, A., and Lindenmann, J. (1957). Virus interference. I. The interferon. Proceedings of the Royal Society of London Series B, Biological sciences *147*, 258-267.

Israels, S.J., Gerrard, J.M., Jacques, Y.V., McNicol, A., Cham, B., Nishibori, M., and Bainton, D.F. (1992). Platelet dense granule membranes contain both granulophysin and P-selectin (GMP-140). Blood *80*, 143-152.

Italiano, J.E., Jr., Lecine, P., Shivdasani, R.A., and Hartwig, J.H. (1999). Blood platelets are assembled principally at the ends of proplatelet processes produced by differentiated megakaryocytes. The Journal of cell biology *147*, 1299-1312.

Izumi, R., Niihori, T., Suzuki, N., Sasahara, Y., Rikiishi, T., Nishiyama, A., Nishiyama, S., Endo, K., Kato, M., Warita, H.*, et al.* (2014). GNE myopathy associated with congenital thrombocytopenia: A report of two siblings. Neuromuscular Disorders *24*, 1068-1072.

James, C., Ugo, V., Le Couedic, J.P., Staerk, J., Delhommeau, F., Lacout, C., Garcon, L., Raslova, H., Berger, R., Bennaceur-Griscelli, A.*, et al.* (2005). A unique clonal JAK2 mutation leading to constitutive signalling causes polycythaemia vera. Nature *434*, 1144-1148.

Jensvoll, H., Blix, K., Braekkan, S.K., and Hansen, J.B. (2014). Platelet count measured prior to cancer development is a risk factor for future symptomatic venous thromboembolism: the Tromso Study. PloS one *9*, e92011.

Junt, T., Schulze, H., Chen, Z., Massberg, S., Goerge, T., Krueger, A., Wagner, D.D., Graf, T., Italiano, J.E., Jr., Shivdasani, R.A.*, et al.* (2007). Dynamic visualization of thrombopoiesis within bone marrow. Science (New York, NY) *317*, 1767-1770.

Kaushansky, K. (2016). Thrombopoietin and its receptor in normal and neoplastic hematopoiesis. Thrombosis journal *14*, 40.

Kaushansky, K., Lok, S., Holly, R.D., Broudy, V.C., Lin, N., Bailey, M.C., Forstrom, J.W., Buddle, M.M., Oort, P.J., Hagen, F.S*., et al.* (1994). Promotion of megakaryocyte progenitor expansion and differentiation by the c-Mpl ligand thrombopoietin. Nature *369*, 568-571.

Kelemen, E., Cserhati, I., and Tanos, B. (1958). Demonstration and some properties of human thrombopoietin in thrombocythaemic sera. Acta haematologica *20*, 350-355.

Kelly, P.N., White, M.J., Goschnick, M.W., Fairfax, K.A., Tarlinton, D.M., Kinkel, S.A., Bouillet, P., Adams, J.M., Kile, B.T., and Strasser, A. (2010). Individual and overlapping roles of BH3-only proteins Bim and Bad in apoptosis of lymphocytes and platelets and in suppression of thymic lymphoma development. Cell death and differentiation *17*, 1655-1664.

Kiladjian, J.J., Chomienne, C., and Fenaux, P. (2008). Interferon-alpha therapy in bcr-abl-negative myeloproliferative neoplasms. Leukemia *22*, 1990-1998.

Kile, B.T. (2015). Aging platelets stimulate TPO production. Nature medicine *21*, 11-12.

Klampfl, T., Gisslinger, H., Harutyunyan, A.S., Nivarthi, H., Rumi, E., Milosevic, J.D., Them, N.C., Berg, T., Gisslinger, B., Pietra, D*., et al.* (2013). Somatic mutations of calreticulin in myeloproliferative neoplasms. The New England journal of medicine *369*, 2379-2390.

Klebe, G. (2000). Recent developments in structure-based drug design. Journal of molecular medicine (Berlin, Germany) *78*, 269-281.

Kodaki, T., Woscholski, R., Hallberg, B., Rodriguez-Viciana, P., Downward, J., and Parker, P.J. (1994). The activation of phosphatidylinositol 3-kinase by Ras. Current biology : CB *4*, 798-806.

Koide, A., Bailey, C.W., Huang, X., and Koide, S. (1998). The fibronectin type III domain as a scaffold for novel binding proteins. Journal of molecular biology *284*, 1141-1151.

Kosoff, R.E., Aslan, J.E., Kostyak, J.C., Dulaimi, E., Chow, H.Y., Prudnikova, T.Y., Radu, M., Kunapuli, S.P., McCarty, O.J., and Chernoff, J. (2015). Pak2 restrains endomitosis during megakaryopoiesis and alters cytoskeleton organization. Blood *125*, 2995-3005.

Kralovics, R., Passamonti, F., Buser, A.S., Teo, S.S., Tiedt, R., Passweg, J.R., Tichelli, A., Cazzola, M., and Skoda, R.C. (2005). A gain-of-function mutation of JAK2 in myeloproliferative disorders. The New England journal of medicine *352*, 1779-1790.

Kunishima, S., Kobayashi, R., Itoh, T.J., Hamaguchi, M., and Saito, H. (2009). Mutation of the beta1-tubulin gene associated with congenital macrothrombocytopenia affecting microtubule assembly. Blood *113*, 458-461.

Kunishima, S., Nishimura, S., Suzuki, H., Imaizumi, M., and Saito, H. (2014). TUBB1 mutation disrupting microtubule assembly impairs proplatelet formation and results in congenital macrothrombocytopenia. European journal of haematology *92*, 276-282.

Kwiatkowski, B.A., Zielinska-Kwiatkowska, A.G., Bauer, T.R., Jr., and Hickstein, D.D. (2000). The ETS family member Tel antagonizes the Fli-1 phenotype in hematopoietic cells. Blood cells, molecules & diseases *26*, 84-90.

Lacout, C., Pisani, D.F., Tulliez, M., Gachelin, F.M., Vainchenker, W., and Villeval, J.L. (2006). JAK2V617F expression in murine hematopoietic cells leads to MPD mimicking human PV with secondary myelofibrosis. Blood *108*, 1652-1660.

Larson, M.K., and Watson, S.P. (2006). Regulation of proplatelet formation and platelet release by integrin alpha IIb beta3. Blood *108*, 1509-1514.

Laurenti, E., and Dick, J.E. (2012). Molecular and functional characterization of early human hematopoiesis. Annals of the New York Academy of Sciences *1266*, 68-71.

Leblanc, R., and Peyruchaud, O. (2016). Metastasis: new functional implications of platelets and megakaryocytes. Blood *128*, 24-31.

Leeksma, C.H., and Cohen, J.A. (1955). Determination of the life of human blood platelets using labelled diisopropylfluorophosphanate. Nature *175*, 552-553.

Lefrancais, E., Ortiz-Munoz, G., Caudrillier, A., Mallavia, B., Liu, F., Sayah, D.M., Thornton, E.E., Headley, M.B., David, T., Coughlin, S.R.*, et al.* (2017). The lung is a site of platelet biogenesis and a reservoir for haematopoietic progenitors. Nature.

Lek, M., Karczewski, K.J., Minikel, E.V., Samocha, K.E., Banks, E., Fennell, T., O'Donnell-Luria, A.H., Ware, J.S., Hill, A.J., Cummings, B.B*., et al.* (2016). Analysis of protein-coding genetic variation in 60,706 humans. Nature *536*, 285-291.

Lentz, B.R. (2003). Exposure of platelet membrane phosphatidylserine regulates blood coagulation. Progress in lipid research *42*, 423-438.

Leslie, A.G.W., and Powell, H.R. (2007). Processing diffraction data with mosflm. In Evolving Methods for Macromolecular Crystallography: The Structural Path to the Understanding of the Mechanismof Action of CBRN Agents, R.J. Read, and J.L. Sussman, eds. (Dordrecht: Springer Netherlands), pp. 41-51.

Levin, C., Koren, A., Pretorius, E., Rosenberg, N., Shenkman, B., Hauschner, H., Zalman, L., Khayat, M., Salama, I., Elpeleg, O*., et al.* (2015). Deleterious mutation in the FYB gene is associated with congenital autosomal recessive small-platelet thrombocytopenia. Journal of Thrombosis and Haemostasis *13*, 1285-1292.

Levine, R.L., Wadleigh, M., Cools, J., Ebert, B.L., Wernig, G., Huntly, B.J., Boggon, T.J., Wlodarska, I., Clark, J.J., Moore, S*., et al.* (2005). Activating mutation in the tyrosine kinase JAK2 in polycythemia vera, essential thrombocythemia, and myeloid metaplasia with myelofibrosis. Cancer cell *7*, 387-397.

Levy, G.G., Nichols, W.C., Lian, E.C., Foroud, T., McClintick, J.N., McGee, B.M., Yang, A.Y., Siemieniak, D.R., Stark, K.R., Gruppo, R*., et al.* (2001). Mutations in a member of the ADAMTS gene family cause thrombotic thrombocytopenic purpura. Nature *413*, 488-494.

Li, J., Kim, K., Barazia, A., Tseng, A., and Cho, J. (2015). Platelet–neutrophil interactions under thromboinflammatory conditions. Cellular and molecular life sciences : CMLS *72*, 2627-2643.

Li, J., Spensberger, D., Ahn, J.S., Anand, S., Beer, P.A., Ghevaert, C., Chen, E., Forrai, A., Scott, L.M., Ferreira, R*., et al.* (2010). JAK2 V617F impairs hematopoietic stem cell function in a conditional knock-in mouse model of JAK2 V617F-positive essential thrombocythemia. Blood *116*, 1528-1538.

Liu, G.C., Ferris, E.J., Reifsteck, J.R., and Baker, M.E. (1986). Effect of anatomic variations on deep venous thrombosis of the lower extremity. AJR American journal of roentgenology *146*, 845-848.

Loftus, J., O'Toole, T., Plow, E., Glass, A., Frelinger, A., and Ginsberg, M. (1990). A beta 3 integrin mutation abolishes ligand binding and alters divalent cation-dependent conformation. Science (New York, NY) *249*, 915-918.

Lok, S., Kaushansky, K., Holly, R.D., Kuijper, J.L., Lofton-Day, C.E., Oort, P.J., Grant, F.J., Heipel, M.D., Burkhead, S.K., Kramer, J.M.*, et al.* (1994). Cloning and expression of murine thrombopoietin cDNA and stimulation of platelet production in vivo. Nature *369*, 565-568.

Long, M.W., Gragowski, L.L., Heffner, C.H., and Boxer, L.A. (1985). Phorbol diesters stimulate the development of an early murine progenitor cell. The burst-forming unit-megakaryocyte. The Journal of clinical investigation *76*, 431-438.

Lordier, L., Jalil, A., Aurade, F., Larbret, F., Larghero, J., Debili, N., Vainchenker, W., and Chang, Y. (2008). Megakaryocyte endomitosis is a failure of late cytokinesis related to defects in the contractile ring and Rho/Rock signaling. Blood *112*, 3164-3174.

Luoh, S.M., Stefanich, E., Solar, G., Steinmetz, H., Lipari, T., Pestina, T.I., Jackson, C.W., and de Sauvage, F.J. (2000). Role of the distal half of the c-Mpl intracellular domain in control of platelet production by thrombopoietin in vivo. Molecular and cellular biology *20*, 507-515.

Ma, A.D., and Key, N.S. (2009). Chapter 15 - Molecular Basis of Hemostatic and Thrombotic Diseases A2 - Coleman, William B. In Molecular Pathology, G.J. Tsongalis, ed. (San Diego: Academic Press), pp. 247-264.

Machlus, K.R., and Italiano, J.E., Jr. (2013). The incredible journey: From megakaryocyte development to platelet formation. The Journal of cell biology *201*, 785-796.

Mackman, N. (2012). New insights into the mechanisms of venous thrombosis. The Journal of clinical investigation *122*, 2331-2336.

Manchev, V.T., Hilpert, M., Berrou, E., Elaib, Z., Aouba, A., Boukour, S., Souquere, S., Pierron, G., Rameau, P., Andrews, R.*, et al.* (2014). A new form of macrothrombocytopenia induced by a germ-line mutation in the PRKACG gene. Blood *124*, 2554-2563.

Mason, K.D., Carpinelli, M.R., Fletcher, J.I., Collinge, J.E., Hilton, A.A., Ellis, S., Kelly, P.N., Ekert, P.G., Metcalf, D., Roberts, A.W.*, et al.* (2007). Programmed anuclear cell death delimits platelet life span. Cell *128*, 1173-1186.

Matsunaga, T., Fukai, F., Kameda, T., Shide, K., Shimoda, H., Torii, E., Kamiunten, A., Sekine, M., Yamamoto, S., Hidaka, T.*, et al.* (2012). Potentiated activation of VLA-4 and VLA-5 accelerates proplatelet-like formation. Annals of hematology *91*, 1633-1643.

Maugeri, N., Campana, L., Gavina, M., Covino, C., De Metrio, M., Panciroli, C., Maiuri, L., Maseri, A., D'Angelo, A., Bianchi, M.E.*, et al.* (2014). Activated platelets present high mobility group box 1 to neutrophils, inducing autophagy and promoting the extrusion of neutrophil extracellular traps. Journal of thrombosis and haemostasis : JTH *12*, 2074-2088.

Mazharian, A., and Senis, Y.A. (2016). Signalling Pathways Regulating Platelet Biogenesis. In Molecular and Cellular Biology of Platelet Formation: Implications in Health and Disease, H. Schulze, and J. Italiano, eds. (Cham: Springer International Publishing), pp. 153-173.

Mazharian, A., Thomas, S.G., Dhanjal, T.S., Buckley, C.D., and Watson, S.P. (2010). Critical role of Src-Syk-PLC{gamma}2 signaling in megakaryocyte migration and thrombopoiesis. Blood *116*, 793-800.

Mazzarello, P., Calligaro, A.L., and Calligaro, A. (2001). Giulio Bizzozero: a pioneer of cell biology. Nat Rev Mol Cell Biol *2*, 776-784.

McArthur, K., Chappaz, S., and Kile, B.T. (2018). Apoptosis in megakaryocytes and platelets: the life and death of a lineage. Blood *131*, 605-610.

McLachlin, A.D., McLachlin, J.A., Jory, T.A., and Rawling, E.G. (1960). Venous stasis in the lower extremities. Annals of surgery *152*, 678-685.

McPherson, S., McMullin, M.F., and Mills, K. (2017). Epigenetics in Myeloproliferative Neoplasms. Journal of cellular and molecular medicine *21*, 1660-1667.

Metzler, Kathleen D., Goosmann, C., Lubojemska, A., Zychlinsky, A., and Papayannopoulos, V. (2014). A Myeloperoxidase-Containing Complex Regulates Neutrophil Elastase Release and Actin Dynamics during NETosis. Cell Reports *8*, 883-896.

Moreau, T., Evans, A.L., Vasquez, L., Tijssen, M.R., Yan, Y., Trotter, M.W., Howard, D., Colzani, M., Arumugam, M., Wu, W.H.*, et al.* (2016). Large-scale production of megakaryocytes from human pluripotent stem cells by chemically defined forward programming. Nat Commun *7*, 11208.

Morison, I.M., Cramer Borde, E.M., Cheesman, E.J., Cheong, P.L., Holyoake, A.J., Fichelson, S., Weeks, R.J., Lo, A., Davies, S.M., Wilbanks, S.M*., et al.* (2008). A mutation of human cytochrome c enhances the intrinsic apoptotic pathway but causes only thrombocytopenia. Nature genetics *40*, 387-389.

Murphy, A.C., Lindsay, A.J., McCaffrey, M.W., Djinovic-Carugo, K., and Young, P.W. (2016). Congenital macrothrombocytopenia-linked mutations in the actin-binding domain of alpha-actinin-1 enhance F-actin association. FEBS letters *590*, 685-695.

Nangalia, J., Massie, C.E., Baxter, E.J., Nice, F.L., Gundem, G., Wedge, D.C., Avezov, E., Li, J., Kollmann, K., Kent, D.G*., et al.* (2013). Somatic CALR mutations in myeloproliferative neoplasms with nonmutated JAK2. The New England journal of medicine *369*, 2391-2405.

Nichols, K.E., Crispino, J.D., Poncz, M., White, J.G., Orkin, S.H., Maris, J.M., and Weiss, M.J. (2000). Familial dyserythropoietic anaemia and thrombocytopenia due to an inherited mutation in GATA1. Nature genetics *24*, 266-270.

Nishimura, S., Nagasaki, M., Kunishima, S., Sawaguchi, A., Sakata, A., Sakaguchi, H., Ohmori, T., Manabe, I., Italiano, J.E., Jr., Ryu, T*., et al.* (2015). IL-1alpha induces thrombopoiesis through megakaryocyte rupture in response to acute platelet needs. The Journal of cell biology *209*, 453-466.

Noris, P., Perrotta, S., Seri, M., Pecci, A., Gnan, C., Loffredo, G., Pujol-Moix, N., Zecca, M., Scognamiglio, F., De Rocco, D*., et al.* (2011). Mutations in ANKRD26 are responsible for a frequent form of inherited thrombocytopenia: analysis of 78 patients from 21 families. Blood *117*, 6673-6680.

Norris, R., and Neale, R. (1882). THE NEW BLOOD-CORPUSCLE. The Lancet *119*, 163.

Nurden, P., Debili, N., Coupry, I., Bryckaert, M., Youlyouz-Marfak, I., Sole, G., Pons, A.C., Berrou, E., Adam, F., Kauskot, A*., et al.* (2011). Thrombocytopenia resulting from mutations in filamin A can be expressed as an isolated syndrome. Blood *118*, 5928-5937.

Orkin, S.H., and Zon, L.I. (2008). Hematopoiesis: an evolving paradigm for stem cell biology. Cell *132*, 631-644.

Osler, W. (1873). An Account of Certain Organisms Occurring in the Liquor Sanguinis. Proceedings of the Royal Society of London *22*, 391-398.

Palazzo, A., Bluteau, O., Messaoudi, K., Marangoni, F., Chang, Y., Souquere, S., Pierron, G., Lapierre, V., Zheng, Y., Vainchenker, W.*, et al.* (2016). The cell division control protein 42-Src family kinase-neural Wiskott-Aldrich syndrome protein pathway regulates human proplatelet formation. Journal of thrombosis and haemostasis : JTH *14*, 2524-2535.

Pan, J., Lordier, L., Meyran, D., Rameau, P., Lecluse, Y., Kitchen-Goosen, S., Badirou, I., Mokrani, H., Narumiya, S., Alberts, A.S.*, et al.* (2014). The formin DIAPH1 (mDia1) regulates megakaryocyte proplatelet formation by remodeling the actin and microtubule cytoskeletons. Blood *124*, 3967-3977.

Pang, L., Xue, H.H., Szalai, G., Wang, X., Wang, Y., Watson, D.K., Leonard, W.J., Blobel, G.A., and Poncz, M. (2006). Maturation stage-specific regulation of megakaryopoiesis by pointed-domain Ets proteins. Blood *108*, 2198-2206.

Pardanani, A.D., Levine, R.L., Lasho, T., Pikman, Y., Mesa, R.A., Wadleigh, M., Steensma, D.P., Elliott, M.A., Wolanskyj, A.P., Hogan, W.J.*, et al.* (2006). MPL515 mutations in myeloproliferative and other myeloid disorders: a study of 1182 patients. Blood *108*, 3472-3476.

Patel, S.R., Richardson, J.L., Schulze, H., Kahle, E., Galjart, N., Drabek, K., Shivdasani, R.A., Hartwig, J.H., and Italiano, J.E., Jr. (2005). Differential roles of microtubule assembly and sliding in proplatelet formation by megakaryocytes. Blood *106*, 4076-4085.

Patel-Hett, S., Richardson, J.L., Schulze, H., Drabek, K., Isaac, N.A., Hoffmeister, K., Shivdasani, R.A., Bulinski, J.C., Galjart, N., Hartwig, J.H.*, et al.* (2008). Visualization of microtubule growth in living platelets reveals a dynamic marginal band with multiple microtubules. Blood *111*, 4605-4616.

Patel-Hett, S., Wang, H., Begonja, A.J., Thon, J.N., Alden, E.C., Wandersee, N.J., An, X., Mohandas, N., Hartwig, J.H., and Italiano, J.E., Jr. (2011). The spectrin-based membrane skeleton stabilizes mouse megakaryocyte membrane systems and is essential for proplatelet and platelet formation. Blood *118*, 1641-1652.

Patrignani, P., Filabozzi, P., and Patrono, C. (1982). Selective cumulative inhibition of platelet thromboxane production by low-dose aspirin in healthy subjects. The Journal of clinical investigation *69*, 1366-1372.

Peters, L.L., Cheever, E.M., Ellis, H.R., Magnani, P.A., Svenson, K.L., Von Smith, R., and Bogue, M.A. (2002). Large-scale, high-throughput screening for coagulation and hematologic phenotypes in mice. Physiological genomics *11*, 185-193.

Picard, C., McCarl, C.A., Papolos, A., Khalil, S., Luthy, K., Hivroz, C., LeDeist, F., Rieux-Laucat, F., Rechavi, G., Rao, A.*, et al.* (2009). STIM1 mutation associated with a syndrome of immunodeficiency and autoimmunity. The New England journal of medicine *360*, 1971-1980.

Pikman, Y., Lee, B.H., Mercher, T., McDowell, E., Ebert, B.L., Gozo, M., Cuker, A., Wernig, G., Moore, S., Galinsky, I.*, et al.* (2006). MPLW515L is a novel somatic activating mutation in myelofibrosis with myeloid metaplasia. PLoS medicine *3*, e270.

Pleines, I., Woods, J., Chappaz, S., Kew, V., Foad, N., Ballester-Beltran, J., Aurbach, K., Lincetto, C., Lane, R.M., Schevzov, G.*, et al.* (2017). Mutations in tropomyosin 4 underlie a rare form of human macrothrombocytopenia. The Journal of clinical investigation *127*, 814-829.

Poujol, C., Ware, J., Nieswandt, B., Nurden, A.T., and Nurden, P. (2002). Absence of GPIbalpha is responsible for aberrant membrane development during megakaryocyte maturation: ultrastructural study using a transgenic model. Experimental hematology *30*, 352-360.

Psaila, B., Lyden, D., and Roberts, I. (2012). Megakaryocytes, malignancy and bone marrow vascular niches. Journal of thrombosis and haemostasis : JTH *10*, 177-188.

Ran, F.A., Hsu, P.D., Wright, J., Agarwala, V., Scott, D.A., and Zhang, F. (2013). Genome engineering using the CRISPR-Cas9 system. Nature protocols *8*, 2281-2308.

Raslova, H., Roy, L., Vourc'h, C., Le Couedic, J.P., Brison, O., Metivier, D., Feunteun, J., Kroemer, G., Debili, N., and Vainchenker, W. (2003). Megakaryocyte polyploidization is associated with a functional gene amplification. Blood *101*, 541-544.

Record, J., Malinova, D., Zenner, H.L., Plagnol, V., Nowak, K., Syed, F., Bouma, G., Curtis, J., Gilmour, K., Cale, C.*, et al.* (2015). Immunodeficiency and severe susceptibility to bacterial infection associated with a loss-of-function homozygous mutation of MKL1. Blood *126*, 1527-1535.

Richardson, J.L., Shivdasani, R.A., Boers, C., Hartwig, J.H., and Italiano, J.E., Jr. (2005). Mechanisms of organelle transport and capture along proplatelets during platelet production. Blood *106*, 4066-4075.

Rivera, J., Lozano, M.L., Navarro-Nunez, L., and Vicente, V. (2009). Platelet receptors and signaling in the dynamics of thrombus formation. Haematologica *94*, 700-711.

Robb, L., Lyons, I., Li, R., Hartley, L., Kontgen, F., Harvey, R.P., Metcalf, D., and Begley, C.G. (1995). Absence of yolk sac hematopoiesis from mice with a targeted disruption of the scl gene. Proceedings of the National Academy of Sciences of the United States of America *92*, 7075-7079.

Rodriguez, V., Nichols, W.L., Charlesworth, J.E., and White, J.G. Sebastian Platelet Syndrome: A Hereditary Macrothrombocytopenia. Mayo Clinic Proceedings *78*, 1416-1421.

Rodriguez, V., Nichols, W.L., Charlesworth, J.E., and White, J.G. (2013). Sebastian Platelet Syndrome: A Hereditary Macrothrombocytopenia. Mayo Clinic Proceedings *78*, 1416-1421.

Ru, Y.X., Dong, S.X., Liang, H.Y., and Zhao, S.X. (2016). Platelet production of megakaryocyte: A review with original observations on human in vivo cells and bone marrow. Ultrastructural pathology *40*, 163-170.

Rumbaut, R.E., and Thiagarajan, P. (2010). Platelet Adhesion to Vascular Walls. In Platelet-Vessel Wall Interactions in Hemostasis and Thrombosis, D.N.G.J. Granger, ed. (San Rafael (CA): Morgan & Calypool Life Sciences).

Rumi, E., and Cazzola, M. (2016). How I treat essential thrombocythemia. Blood *128*, 2403-2414.

Ryder, E., Gleeson, D., Sethi, D., Vyas, S., Miklejewska, E., Dalvi, P., Habib, B., Cook, R., Hardy, M., Jhaveri, K.*, et al.* (2013). Molecular characterization of mutant mouse strains generated

from the EUCOMM/KOMP-CSD ES cell resource. Mammalian genome : official journal of the International Mammalian Genome Society *24*, 286-294.

Sabri, S., Foudi, A., Boukour, S., Franc, B., Charrier, S., Jandrot-Perrus, M., Farndale, R.W., Jalil, A., Blundell, M.P., Cramer, E.M.*, et al.* (2006). Deficiency in the Wiskott-Aldrich protein induces premature proplatelet formation and platelet production in the bone marrow compartment. Blood *108*, 134-140.

Sabri, S., Jandrot-Perrus, M., Bertoglio, J., Farndale, R.W., Mas, V.M., Debili, N., and Vainchenker, W. (2004). Differential regulation of actin stress fiber assembly and proplatelet formation by alpha2beta1 integrin and GPVI in human megakaryocytes. Blood *104*, 3117-3125.

Sakurai, T., Yamada, T., Kihara-Negishi, F., Teramoto, S., Sato, Y., Izawa, T., and Oikawa, T. (2003). Effects of overexpression of the Ets family transcription factor TEL on cell growth and differentiation of K562 cells. International journal of oncology *22*, 1327-1333.

Sarratt, K.L., Chen, H., Zutter, M.M., Santoro, S.A., Hammer, D.A., and Kahn, M.L. (2005). GPVI and alpha2beta1 play independent critical roles during platelet adhesion and aggregate formation to collagen under flow. Blood *106*, 1268-1277.

Sasaki, H., Hirabayashi, Y., Ishibashi, T., Inoue, T., Matsuda, M., Kai, S., Ikuta, K., Yokoyama, K., Yokota, T., Maruyama, Y.*, et al.* (1995). Effects of erythropoietin, IL-3, IL-6 and LIF on a murine megakaryoblastic cell line: growth enhancement and expression of receptor mRNAs. Leukemia research *19*, 95-102.

Schafer, A.I. (2004). Thrombocytosis. The New England journal of medicine *350*, 1211-1219.

Schulze, H., Korpal, M., Hurov, J., Kim, S.W., Zhang, J., Cantley, L.C., Graf, T., and Shivdasani, R.A. (2006). Characterization of the megakaryocyte demarcation membrane system and its role in thrombopoiesis. Blood *107*, 3868-3875.

Schwer, H.D., Lecine, P., Tiwari, S., Italiano, J.E., Jr., Hartwig, J.H., and Shivdasani, R.A. (2001). A lineage-restricted and divergent beta-tubulin isoform is essential for the biogenesis, structure and function of blood platelets. Current biology : CB *11*, 579-586.

Schwertz, H., Koster, S., Kahr, W.H., Michetti, N., Kraemer, B.F., Weitz, D.A., Blaylock, R.C., Kraiss, L.W., Greinacher, A., Zimmerman, G.A*., et al.* (2010). Anucleate platelets generate progeny. Blood *115*, 3801-3809.

Schwikowski, B., Uetz, P., and Fields, S. (2000). A network of protein-protein interactions in yeast. Nature biotechnology *18*, 1257-1261.

Scott, L.M., Scott, M.A., Campbell, P.J., and Green, A.R. (2006). Progenitors homozygous for the V617F mutation occur in most patients with polycythemia vera, but not essential thrombocythemia. Blood *108*, 2435-2437.

Semple, J.W., Italiano, J.E., Jr., and Freedman, J. (2011). Platelets and the immune continuum. Nature reviews Immunology *11*, 264-274.

Sevitt, S. (1974). The structure and growth of valve-pocket thrombi in femoral veins. Journal of clinical pathology *27*, 517-528.

Shivdasani, R.A., Fujiwara, Y., McDevitt, M.A., and Orkin, S.H. (1997). A lineage-selective knockout establishes the critical role of transcription factor GATA-1 in megakaryocyte growth and platelet development. The EMBO journal *16*, 3965-3973.

Shivdasani, R.A., Mayer, E.L., and Orkin, S.H. (1995). Absence of blood formation in mice lacking the T-cell leukaemia oncoprotein tal-1/SCL. Nature *373*, 432-434.

Skarnes, W.C., Rosen, B., West, A.P., Koutsourakis, M., Bushell, W., Iyer, V., Mujica, A.O., Thomas, M., Harrow, J., Cox, T*., et al.* (2011). A conditional knockout resource for the genome-wide study of mouse gene function. Nature *474*, 337-342.

Smyth, M.S., and Martin, J.H. (2000). x ray crystallography. Molecular pathology : MP *53*, 8-14.

Soding, J., Biegert, A., and Lupas, A.N. (2005). The HHpred interactive server for protein homology detection and structure prediction. Nucleic acids research *33*, W244-248.

Sohma, Y., Akahori, H., Seki, N., Hori, T., Ogami, K., Kato, T., Shimada, Y., Kawamura, K., and Miyazaki, H. (1994). Molecular cloning and chromosomal localization of the human thrombopoietin gene. FEBS letters *353*, 57-61.

Song, W.J., Sullivan, M.G., Legare, R.D., Hutchings, S., Tan, X., Kufrin, D., Ratajczak, J., Resende, I.C., Haworth, C., Hock, R.*, et al.* (1999). Haploinsufficiency of CBFA2 causes familial thrombocytopenia with propensity to develop acute myelogenous leukaemia. Nature genetics *23*, 166-175.

Sorensen, A.L., Rumjantseva, V., Nayeb-Hashemi, S., Clausen, H., Hartwig, J.H., Wandall, H.H., and Hoffmeister, K.M. (2009). Role of sialic acid for platelet life span: exposure of beta-galactose results in the rapid clearance of platelets from the circulation by asialoglycoprotein receptor-expressing liver macrophages and hepatocytes. Blood *114*, 1645-1654.

Spinler, K.R., Shin, J.W., Lambert, M.P., and Discher, D.E. (2015). Myosin-II repression favors pre/proplatelets but shear activation generates platelets and fails in macrothrombocytopenia. Blood *125*, 525-533.

Spivak, J.L. (2017). Myeloproliferative Neoplasms. The New England journal of medicine *376*, 2168-2181.

Sreeramkumar, V., Adrover, J.M., Ballesteros, I., Cuartero, M.I., Rossaint, J., Bilbao, I., Nácher, M., Pitaval, C., Radovanovic, I., Fukui, Y.*, et al.* (2014). Neutrophils scan for activated platelets to initiate inflammation. Science (New York, NY) *346*, 1234.

Stritt, S., Beck, S., Becker, I.C., Vogtle, T., Hakala, M., Heinze, K.G., Du, X., Bender, M., Braun, A., Lappalainen, P.*, et al.* (2017). Twinfilin 2a regulates platelet reactivity and turnover in mice. Blood *130*, 1746-1756.

Stritt, S., Nurden, P., Turro, E., Greene, D., Jansen, S.B., Westbury, S.K., Petersen, R., Astle, W.J., Marlin, S., Bariana, T.K.*, et al.* (2016). A gain-of-function variant in DIAPH1 causes dominant macrothrombocytopenia and hearing loss. Blood.

Sugiyama, T., Kohara, H., Noda, M., and Nagasawa, T. (2006). Maintenance of the hematopoietic stem cell pool by CXCL12-CXCR4 chemokine signaling in bone marrow stromal cell niches. Immunity *25*, 977-988.

Sungaran, R., Markovic, B., and Chong, B.H. (1997). Localization and regulation of thrombopoietin mRNa expression in human kidney, liver, bone marrow, and spleen using in situ hybridization. Blood *89*, 101-107.

Suzuki, A., Shin, J.W., Wang, Y., Min, S.H., Poncz, M., Choi, J.K., Discher, D.E., Carpenter, C.L., Lian, L., Zhao, L.*, et al.* (2013). RhoA is essential for maintaining normal megakaryocyte ploidy and platelet generation. PloS one *8*, e69315.

Tefferi, A., Elliott, M.A., Kao, P.C., Yoon, S., El-Hemaidi, I., and Pearson, T.C. (2000). Hydroxyurea-induced marked oscillations of platelet counts in patients with polycythemia vera. Blood *96*, 1582-1584.

Terwilliger, T.C., Adams, P.D., Read, R.J., McCoy, A.J., Moriarty, N.W., Grosse-Kunstleve, R.W., Afonine, P.V., Zwart, P.H., and Hung, L.W. (2009). Decision-making in structure solution using Bayesian estimates of map quality: the PHENIX AutoSol wizard. Acta crystallographica Section D, Biological crystallography *65*, 582-601.

Teviotdale, B.M., and Gwynne, J.F. (1967). Deep calf vein thrombosis and pulmonary embolism: a necropsy study. The New Zealand medical journal *66*, 530-534.

Thompson, A.A., and Nguyen, L.T. (2000). Amegakaryocytic thrombocytopenia and radio-ulnar synostosis are associated with HOXA11 mutation. Nature genetics *26*, 397-398.

Thon, J.N., Macleod, H., Begonja, A.J., Zhu, J., Lee, K.C., Mogilner, A., Hartwig, J.H., and Italiano, J.E., Jr. (2012a). Microtubule and cortical forces determine platelet size during vascular platelet production. Nat Commun *3*, 852.

Thon, J.N., Montalvo, A., Patel-Hett, S., Devine, M.T., Richardson, J.L., Ehrlicher, A., Larson, M.K., Hoffmeister, K., Hartwig, J.H., and Italiano, J.E., Jr. (2010). Cytoskeletal mechanics of proplatelet maturation and platelet release. The Journal of cell biology *191*, 861-874.

Thon, J.N., Peters, C.G., Machlus, K.R., Aslam, R., Rowley, J., Macleod, H., Devine, M.T., Fuchs, T.A., Weyrich, A.S., Semple, J.W.*, et al.* (2012b). T granules in human platelets function in TLR9 organization and signaling. The Journal of cell biology *198*, 561-574.

Tiedt, R., Hao-Shen, H., Sobas, M.A., Looser, R., Dirnhofer, S., Schwaller, J., and Skoda, R.C. (2008). Ratio of mutant JAK2-V617F to wild-type Jak2 determines the MPD phenotypes in transgenic mice. Blood *111*, 3931-3940.

Tijssen, M.R., and Ghevaert, C. (2013). Transcription factors in late megakaryopoiesis and related platelet disorders. Journal of thrombosis and haemostasis : JTH *11*, 593-604.

Tijssen, M.R., Moreau, T., and Ghevaert, C. (2016). Transcriptional Regulation of Platelet Formation: Harnessing the Complexity for Efficient Platelet Production In Vitro. In Molecular and Cellular Biology of Platelet Formation: Implications in Health and Disease, H. Schulze, and J. Italiano, eds. (Cham: Springer International Publishing), pp. 23-60.

Tsang, A.P., Fujiwara, Y., Hom, D.B., and Orkin, S.H. (1998). Failure of megakaryopoiesis and arrested erythropoiesis in mice lacking the GATA-1 transcriptional cofactor FOG. Genes & development *12*, 1176-1188.

Tunnacliffe, A., Jones, C., Le Paslier, D., Todd, R., Cherif, D., Birdsall, M., Devenish, L., Yousry, C., Cotter, F.E., and James, M.R. (1999). Localization of Jacobsen syndrome breakpoints on a 40-Mb physical map of distal chromosome 11q. Genome research *9*, 44-52.

van Genderen, P.J., van Vliet, H.H., Prins, F.J., van de Moesdijk, D., van Strik, R., Zijlstra, F.J., Budde, U., and Michiels, J.J. (1997). Excessive prolongation of the bleeding time by aspirin in essential thrombocythemia is related to a decrease of large von Willebrand factor multimers in plasma. Annals of hematology *75*, 215-220.

Vigon, I., Mornon, J.P., Cocault, L., Mitjavila, M.T., Tambourin, P., Gisselbrecht, S., and Souyri, M. (1992). Molecular cloning and characterization of MPL, the human homolog of the v-mpl oncogene: identification of a member of the hematopoietic growth factor receptor superfamily. Proceedings of the National Academy of Sciences of the United States of America *89*, 5640-5644.

von Bruhl, M.L., Stark, K., Steinhart, A., Chandraratne, S., Konrad, I., Lorenz, M., Khandoga, A., Tirniceriu, A., Coletti, R., Kollnberger, M.*, et al.* (2012). Monocytes, neutrophils, and platelets cooperate to initiate and propagate venous thrombosis in mice in vivo. The Journal of experimental medicine *209*, 819-835.

Ward, J.J., McGuffin, L.J., Bryson, K., Buxton, B.F., and Jones, D.T. (2004). The DISOPRED server for the prediction of protein disorder. Bioinformatics (Oxford, England) *20*, 2138-2139.

Ware, J., Russell, S.R., Vicente, V., Scharf, R.E., Tomer, A., McMillan, R., and Ruggeri, Z.M. (1990). Nonsense mutation in the glycoprotein Ib alpha coding sequence associated with

Bernard-Soulier syndrome. Proceedings of the National Academy of Sciences of the United States of America *87*, 2026-2030.

Wernig, G., Mercher, T., Okabe, R., Levine, R.L., Lee, B.H., and Gilliland, D.G. (2006). Expression of Jak2V617F causes a polycythemia vera-like disease with associated myelofibrosis in a murine bone marrow transplant model. Blood *107*, 4274-4281.

Westbury, S.K., Turro, E., Greene, D., Lentaigne, C., Kelly, A.M., Bariana, T.K., Simeoni, I., Pillois, X., Attwood, A., Austin, S*., et al.* (2015). Human phenotype ontology annotation and cluster analysis to unravel genetic defects in 707 cases with unexplained bleeding and platelet disorders. Genome medicine *7*, 36.

White, J.K., Gerdin, A.K., Karp, N.A., Ryder, E., Buljan, M., Bussell, J.N., Salisbury, J., Clare, S., Ingham, N.J., Podrini, C*., et al.* (2013). Genome-wide generation and systematic phenotyping of knockout mice reveals new roles for many genes. Cell *154*, 452-464.

Winter, G. (2010). xia2: an expert system for macromolecular crystallography data reduction. Journal of Applied Crystallography *43*, 186-190.

Woo, J.S., Imm, J.H., Min, C.K., Kim, K.J., Cha, S.S., and Oh, B.H. (2006). Structural and functional insights into the B30.2/SPRY domain. The EMBO journal *25*, 1353-1363.

Wright, J.H. (1906). The origin and nature of the blood plates. Boston Med Surg J *154*, 643-645.

Wright, S.D., Michaelides, K., Johnson, D.J., West, N.C., and Tuddenham, E.G. (1993). Double heterozygosity for mutations in the platelet glycoprotein IX gene in three siblings with Bernard-Soulier syndrome. Blood *81*, 2339-2347.

Yang, F., Xu, Y.P., Li, J., Duan, S.S., Fu, Y.J., Zhang, Y., Zhao, Y., Qiao, W.T., Chen, Q.M., Geng, Y.Q*., et al.* (2009). Cloning and characterization of a novel intracellular protein p48.2 that negatively regulates cell cycle progression. The international journal of biochemistry & cell biology *41*, 2240-2250.

Youssefian, T., and Cramer, E.M. (2000). Megakaryocyte dense granule components are sorted in multivesicular bodies. Blood *95*, 4004-4007.

Zhai, L., Dietrich, A., Skurat, A.V., and Roach, P.J. (2004). Structure-function analysis of GNIP, the glycogenin-interacting protein. Archives of biochemistry and biophysics *421*, 236-242.

Zhang, L., Orban, M., Lorenz, M., Barocke, V., Braun, D., Urtz, N., Schulz, C., von Bruhl, M.L., Tirniceriu, A., Gaertner, F.*, et al.* (2012). A novel role of sphingosine 1-phosphate receptor S1pr1 in mouse thrombopoiesis. The Journal of experimental medicine *209*, 2165-2181.

Zhang, M.Y., Churpek, J.E., Keel, S.B., Walsh, T., Lee, M.K., Loeb, K.R., Gulsuner, S., Pritchard, C.C., Sanchez-Bonilla, M., Delrow, J.J.*, et al.* (2015). Germline ETV6 mutations in familial thrombocytopenia and hematologic malignancy. Nature genetics *47*, 180-185.

Zhang, Y., Wang, Z., and Ravid, K. (1996). The cell cycle in polyploid megakaryocytes is associated with reduced activity of cyclin B1-dependent cdc2 kinase. The Journal of biological chemistry *271*, 4266-4272.

Zheng, C., Yang, R., Han, Z., Zhou, B., Liang, L., and Lu, M. (2008). TPO-independent megakaryocytopoiesis. Critical reviews in oncology/hematology *65*, 212-222.